Nuclear Science
NEA/NSC/R(2023)8
September 2023
www.oecd-nea.org

Benchmark on Dose Rate Calculations for Irradiated Assembly

OECD
BETTER POLICIES FOR BETTER LIVES

NEA
NUCLEAR ENERGY AGENCY

Organisation for Economic Co-operation and Development

NEA/NSC/R(2023)8

Unclassified English text only

Benchmark on Dose Rate Calculations for Irradiated Assembly

ORGANISATION FOR ECONOMIC CO-OPERATION AND DEVELOPMENT

The OECD is a unique forum where the governments of 38 democracies work together to address the economic, social and environmental challenges of globalisation. The OECD is also at the forefront of efforts to understand and to help governments respond to new developments and concerns, such as corporate governance, the information economy and the challenges of an ageing population. The Organisation provides a setting where governments can compare policy experiences, seek answers to common problems, identify good practice and work to co-ordinate domestic and international policies.

The OECD member countries are: Australia, Austria, Belgium, Canada, Chile, Colombia, Costa Rica, the Czech Republic, Denmark, Estonia, Finland, France, Germany, Greece, Hungary, Iceland, Ireland, Israel, Italy, Japan, Korea, Latvia, Lithuania, Luxembourg, Mexico, the Netherlands, New Zealand, Norway, Poland, Portugal, the Slovak Republic, Slovenia, Spain, Sweden, Switzerland, Türkiye, the United Kingdom and the United States. The European Commission takes part in the work of the OECD.

OECD Publishing disseminates widely the results of the Organisation's statistics gathering and research on economic, social and environmental issues, as well as the conventions, guidelines and standards agreed by its members.

NUCLEAR ENERGY AGENCY

The OECD Nuclear Energy Agency (NEA) was established on 1 February 1958. Current NEA membership consists of 34 countries: Argentina, Australia, Austria, Belgium, Bulgaria, Canada, the Czech Republic, Denmark, Finland, France, Germany, Greece, Hungary, Iceland, Ireland, Italy, Japan, Korea, Luxembourg, Mexico, the Netherlands, Norway, Poland, Portugal, Romania, Russia (suspended), the Slovak Republic, Slovenia, Spain, Sweden, Switzerland, Türkiye, the United Kingdom and the United States. The European Commission and the International Atomic Energy Agency also take part in the work of the Agency.

The mission of the NEA is:

– to assist its member countries in maintaining and further developing, through international co-operation, the scientific, technological and legal bases required for a safe, environmentally sound and economical use of nuclear energy for peaceful purposes;

– to provide authoritative assessments and to forge common understandings on key issues as input to government decisions on nuclear energy policy and to broader OECD analyses in areas such as energy and the sustainable development of low-carbon economies.

Specific areas of competence of the NEA include the safety and regulation of nuclear activities, radioactive waste management and decommissioning, radiological protection, nuclear science, economic and technical analyses of the nuclear fuel cycle, nuclear law and liability, and public information. The NEA Data Bank provides nuclear data and computer program services for participating countries.

Foreword

Under the auspices of the Nuclear Energy Agency (NEA) Nuclear Science Committee (NSC), the Working Party on the Scientific Issues of Advanced Fuel Cycles (WPFC) has been established to co-ordinate scientific activities regarding various existing and advanced nuclear fuel cycles, including fuel cycle scenarios, innovative fuels and materials, separation chemistry, waste disposal and coolant technologies. Various expert groups were established to cover these topics.

The Expert Group on Advanced Fuel Cycle Scenarios (EGAFCS) was created in 2010 to study research and development (R&D) needs associated with the transition from current to future advanced nuclear fuel cycles. Since then, the members of the Expert Group have been conducting a series of benchmark studies to compare existing codes in terms of capabilities, modelling and results.

The Task Force on Dose Rate Calculations for Irradiated Fuel Assembly was launched in 2015 to assess code predictions of dose rates from bare spent fuel assemblies and to benchmark multiple codes and validate them against available experimental data. This report provides details of the benchmark specifications, method and code characteristics, as well as a comparison and analysis of the calculation results.

Acknowledgements

The NEA expresses its sincere gratitude to the members of the Expert Group on Advanced Fuel Cycle Scenarios (EGAFCS) for contributing to this report. The collaboration of R. Eschbach (CEA, France) who led this task force and B. Dixon (INL, United States), former chair of the EGAFCS, is gratefully acknowledged. Special thanks also go to E. Malambu (SCK CEN, Belgium) for all his efforts in summarising the results of calculations in Chapter 7 of this report.

List of contributing authors

BELGIUM

Edouard Mbala MALAMBU (SCK CEN)

CANADA

Geoffrey EDWARDS (CNL)

FINLAND

Silja HÄKKINEN (VTT)

FRANCE

Romain ESCHBACH (CEA), Task Force Leader

Vincent LEGER (ORANO TN)

Yannick PENELIAU (CEA)

GERMANY

Fabrizio GABRIELLI (KIT)

ITALY

Federico ROCCHI (ENEA)

SPAIN

Francisco ÁLVAREZ VELARDE (CIEMAT), Chair of the EGAFCS

UNITED STATES

Yan CAO (ANL)

Brent DIXON (INL), former Chair of the EGAFCS (until November 2021)

Bo FENG (ANL, United States)

NEA

Stéphanie CORNET, former Technical Secretariat (until October 2020)

Gabriele GRASSI, Technical Secretariat

Table of contents

List of figures

List of tables

List of abbreviations and acronyms

ACAB	Activation Abacus Code
ACE	A Compact ENDF
ANSI	American National Standards Institute (United States)
ANL	Argonne National Laboratory (United States)
ANS	American Nuclear Society
ARP	Automatic rapid processing
BISTRO	Bidimensionel Sn TRansport Optimise
BWR	Boiling water reactor
C/E	Calculation/experiment
CEA	Commissariat à l'énergie atomique et aux énergies alternatives (French Alternative Energies and Atomic Energy Commission)
CIEMAT	Centre for Energy, Environment and Technology (Spain)
CNL	Canadian National Laboratory (Canada)
CSG	Constructive solid geometry
CSEWG	Cross Section Evaluation Working Group
CRAM	Chebyshev Rational Approximation Method
DBRC	Doppler broadening rejection correction
DOE	Department of Energy (United States)
EADL	Evaluated Atomic Data Library (United States)
ECCO	European cell code
EDF	Electricité de France (France)
EDR	Equivalent dose rate
EFPD	Effective full power days
EGAFCS	Expert Group on Advanced Fuel Cycle Scenarios (NEA)
ENEA	National Agency for New Technologies, Energy and Sustainable Economic Development (Italy)
ENDF	Evaluated Nuclear Data File
EoL	End of Life
EPLD	Evaluated Photon Data Library
ERANOS	European Reactor Analysis Optimised System
FA	Fuel assembly
FBR	Fast breeder reactor
FP	Fission product

GWd/MTIHM	Gigawatt-days per metric tonne of initial heavy metal
HM	Heavy metal
IAEA	International Atomic Energy Agency
ICRP	International Commission on Radiological Protection
INL	Idaho National Laboratory (United States)
JEFF	Joint Evaluated Fission and Fusion
KIT	Karlsruhe Institute of Technology (Germany)
LANL	Los Alamos National Laboratory (United States)
LLNL	Lawrence Livermore National Laboratory (United States)
LWR	Light water reactor
MOX	Mixed oxide
NAS	National Academy of Science (United States)
NEA	Nuclear Energy Agency
NEWT	New ESC-based weighting transport code
NRC	Nuclear Regulatory Commission (United States)
NSC	Nuclear Science Committee (NEA)
ORNL	Oak Ridge National Laboratory (United States)
PWR	Pressurised water reactor
R&D	Research and development
RSD	Relative standard deviation
SCK CEN	Studiecentrum Voor Kernergie – Belgian Nuclear Research Centre (Belgium)
SD	Standard deviation
Sv/h	Sievert per hour
TENDL	TALYS Evaluated Nuclear Data Library
TLD	Thermoluminescent dosimeter
US	United States
UOX	Uranium oxide
VTT	Technical Research Centre of Finland (Finland)
WPFC	Working Party on Scientific Issues of Advanced Fuel Cycles (NEA)

Executive summary

The dose rate from a spent fuel assembly (FA) is an important attribute for two reasons. The first is to determine shielding and handling requirements to protect personnel working with spent fuel, while the second is related to non-proliferation aspects; the gamma and neutron radiation may serve as a self-protecting deterrent to theft for decades after the fuel is discharged. The United States Nuclear Regulatory Commission (US NRC) and the International Atomic Energy Agency (IAEA) consider the "self-protecting" dose rate to be 1 Sv/h at 1 m from the FA. The uncertainty inherent in dose rate calculations can be addressed by using conservative estimates. For personnel protection, an overestimation of the dose is conservative while for self-protection, an underestimation is conservative.

A comparative study on dose rate calculations for pressurised water reactor (PWR) uranium oxide (UOX) and mixed oxide (MOX) spent FAs was performed in 2014 by the Argonne National Laboratory (ANL) and the French Alternative Energies and Atomic Energy Commission (CEA). This joint effort was undertaken to improve confidence in each organisation's dose rate calculation methodology, especially for cases in which quantitative measurements of proliferation resistance are desired.

For the UOX case, which was intended to benchmark a frequently-cited reference study[1], 30-year dose rates calculated by the CEA and ANL were roughly three times lower than that of the reference study. This finding brings into question commonly held beliefs regarding the levels of self-protection exhibited by spent PWR fuels. Furthermore, the dose rates were estimated using MicroShield, a point-kernel code that is typically used for shielding design, and high gamma transport build-up factors for air were intentionally selected to provide more conservative values for shielding purposes, i.e. higher dose rates.

Given these discrepancies, it seems important to be able to define a reference calculation for the dose rate from a spent FA, to validate this calculation by a code-to-code comparison, to analyse the sensitivity of the calculation results to different hypotheses, and finally to be able to validate this calculation by comparison with experimental measurements.

Under the framework of the Nuclear Energy Agency (NEA) Expert Group on Advanced Fuel Cycle Scenarios (EGAFCS), an international benchmark on dose rate calculations for PWR spent FA was conducted. The objectives of the benchmark were to verify updated dose rate calculation procedures (new modelling approaches, new nuclear data, new versions of codes) and to share the benchmark results at the international level. The benchmark was divided into two parts, verification (comparison of results with different codes/methodologies, sensitivity studies) and validation (comparison of results with experimental data).

Nine institutes participated in this benchmark: Argonne National Laboratory (ANL, United States), French Alternative Energies and Atomic Energy Commission (CEA, France), Centre for Energy, Environment and Technology (CIEMAT, Spain), Canadian National Laboratory (CNL, Canada), National Agency for New Technologies, Energy and Sustainable Economic Development, (ENEA, Italy), Karlsruhe Institute of Technology (KIT, Germany), ORANO TN (France), Belgian Nuclear Research Centre (SCK CEN, Belgium), and Technical Research Centre of Finland (VTT, Finland).

[1] Lloyd, W.R, M.K. Sheaffer and W.G. Sutcliffe (1994), *Dose Rate Estimates from Irradiated Light Water Reactor Fuel Assemblies in Air*, Lawrence Livermore National Laboratory Livermore, CA, United States, https://doi.org/10.2172/10137382.

Chapter 1 provides an overall introduction to the benchmarking exercise.

Chapter 2 presents the specifications of the verification benchmark.

Chapter 3 gives a general description of the approaches (codes and nuclear data) used by the participants to estimate the dose rate emitted by an irradiated PWR FA after some years of decay. The methodology is based on the following calculations steps:

- Depletion: Given the FA description and irradiation history conditions, the discharge composition is calculated.
- Decay: A period of decay after discharge is simulated to obtain the isotopic composition of the photon source. Also, the isotopic photon release rates that are discretised into multiple gamma energy groups have been estimated.
- Radiation: The multi-group gamma source is applied to a heterogeneous three-dimensional (3D) transport model of the FA and the gamma flux away from the assembly is estimated, calculating the corresponding dose rate using flux-to-dose rate conversion factors.

Chapter 4 is dedicated to the verification step. The participants conducted a code-to-code benchmark comparing nuclide masses, photon release rates and gamma dose rates at 1 m distance from a PWR UOX and a PWR MOX fuel assembly (a 15x15 PWR UOX at 33 GWd/MTIHM burn-up and a 17x17 PWR MOX at 60 GWd/MTIHM burn-up, respectively). The benchmark looked at two time frames, at discharge and 30 years after discharge. It included 46 heavy-metal (HM) nuclides and 30 fission products (FPs) at discharge and 20 HMs and 8 FPs at 30 years when some nuclides and FPs had decayed away. The agreement between nuclide masses was good, especially for the examined FPs. The largest discrepancies between participants occurred in some HM nuclides with small concentrations.

Gamma dose rates were calculated at 3.7 and 30 years after discharge using two different photon flux-to-dose rate conversion factors (the time of 3.7 years was calculated to correspond to the experimental measurements, see Chapter 7). The agreement between participants was quite good, with relative standard deviations (RSD) from 7 to 15%. The calculated dose rate for the PWR MOX FA is two times greater than that for the PWR UOX FA, in accordance with a higher gamma release rate. For the American National Standards Institute (ANSI) conversion factor ANSI (1977) and 30 years of cooling, the average calculated dose rates are 5.8 Sv/h (UOX) and 11.1 Sv/h (MOX). It should be noted that these dose rates are 20 to 25% lower using the ANSI (1991) conversion factor because of the differences in the weighting factors.

The previous 1994 reference study for a similar UOX FA calculated the 30-year dose rates to be 13.0 to 15.2 Sv/h (at 30 or 35 GWd/MTIHM), using the point-kernal code MicroShield, which may yield higher values out of conservatism with respect to worker protection. The approach used in this verification study did not add conservatism regarding worker protection or non-proliferation. Thus, this verification step shows that, in a best-estimate description of the dose rate calculation, the calculated values can be two to three times lower than previous conservative reference calculations. Dose rates estimated using MicroShield were conservative for shielding purposes (higher dose rates) while dose rates calculated in this benchmark according to an advanced methodology did not intentionally use conservative assumptions one way or the other.

It is interesting to note that in this best-estimate approach the self-protection capability of the PWR UOX spent FA after 30 years of cooling time is confirmed ($\cong$ 5 Sv/h at 1 m), and

this self-protection is guaranteed for about a century (1 Sv/h at 100 years of cooling time – CEA calculations).

At 3.7 years of cooling, the average dose rates were calculated to be 32.2 Sv/h and 65.8 Sv/h for UOX and MOX, respectively, with the ANSI (1977) conversion factor, with an RSD from 7 to 11%.

Chapter 5 presents the various sensitivity studies carried out to assess the impact of the calculation scheme on the calculated dose rate. The calculation parameters that all participants contributed to analysing are:

- the assembly geometry, homogeneous vs heterogeneous;
- the radial burn-up distribution (uniform or not);
- the irradiation history (with or without decay periods);
- the Rim effect (increased burn-up in the external ring of the pellet);
- the gamma source group structure (different energy groups from 18 to 62, or explicit gamma rays);
- the bremsstrahlung effect;
- the cross-sections effects;
- the modelling assumptions (tally geometry description, flux-to-dose conversion factors, interpolation factors…);
- the neutron dose rate contribution.

None of these parameters exceeds 20% of the impact on the final calculated dose rates. Most of them have an impact lower than 2%, except:

- flux-to-dose conversion factor (≈ 20%);
- gamma source group structure (≈ 20%);
- axial burn-up distribution (10 to 15%).

From these results, some recommendations for dose rate calculation models in the air can be derived:

- a homogeneous model of the assembly is convenient;
- non-uniform pin-by-pin gamma source distribution is not necessary;
- simple irradiation histories are convenient;
- very detailed gamma source distribution in the pin is not necessary;
- a realistic axial burn-up distribution is necessary;
- use of a relevant gamma energy mesh is necessary;
- bremsstrahlung in the gamma sources mesh is necessary;
- for the tested cross-section (neutron and photon) the impact is low;
- the impact of tally geometry is low;
- the neutron dose rate contribution is negligible.

These recommendations apply only to the cases considered in this benchmark (PWR, fuel, burn-up, cooling time).

After demonstrating, by using a code-to-code benchmark, a satisfactory agreement between the institutes for the calculation of the dose rate on different fuels and at different cooling times, Chapter 6 and Chapter 7 deal with the experimental validation of these calculations by comparing them against different dose rate measurements carried out on spent FAs in the air.

The Morris experiments (1981) were a series of gamma dose rate measurements completed in the General Electric spent fuel storage facility at Morris Operation. In these experiments, the gamma dose rates were measured in the vicinity of the discharged spent nuclear fuel bundles. A wide range of fuel types, power levels and burn-ups were selected in the experiments. Particularly among the 38 FAs selected, four PWR fuel bundles have gamma dose rates measured in the air (Westinghouse 14x14 PWR). Their fuel burn-up ranged from 26.4 GWd/MTIHM to 40.2 GWd/MTIHM, and the FA cooling time before measurement ranged from 2.5 years to 6.9 years. Two institutes, the ANL (US) and CEA (France), have modelled this experiment.

Experimental data on dose rates in air, carried out in the 1980s using irradiated FA of the Turkey Point Unit 3 reactor, were used for comparison to the calculated dose rates. The Turkey Point Unit 3 is a conventional 3-loop PWR, designed by Westinghouse Electric Corp. and operated by Florida Power and Light Co. Two spent FAs, serial numbers B03 and D04, discharged from the reactor core after an irradiation period of, respectively, 827 and 851 effective full power days (EFPDs) and under cooling periods of 3.7 and 1.8 years, were used for the measurements. Eight institutes have contributed to the experimental validation: ANL, CIEMAT, CEA, ENEA, KIT, ORANO TN, SCK CEN and VTT.

For the Morris experiments, compared with the measured gamma dose rates, both the CEA and ANL numerical approaches underestimate the measured gamma dose rates. Both institutions showed calculated dose rates that are lower than the measured values by about 10 to 25%. ANL's calculated values are generally about 7% higher than CEA's. In numerical simulations, CEA and ANL used slightly different assumptions on the experimental setup geometry. They also used slightly different source axial distributions. Another difference is that the CEA calculation did not consider the gamma dose rate contributions from the ^{60}Co impurities, which ANL found to increase the total dose rate by 13% (for assembly 1A). Despite all these modelling differences, the dose rate from the CEA calculation at each detector location is still very close to the ANL values. Both CEA and ANL studies demonstrated that the numerically calculated gamma dose rates from the spent nuclear fuel are on the conservative side to determine the nuclear fuel self-protection.

For the Turkey Point experiments, the study has shown that the delayed gamma source term is dominated by the signature of gammas-rays from a few FPs. In addition, there are the two signature gamma rays of ^{60}Co, an activation product of ^{59}Co, found as an impurity component of the spacer grids and gas plenum spring, both consisting of Inconel-718 alloy. The calculated dose rate value is highly dependent on the photon-fluence-to-dose conversion function. The dose rate values calculated using the American Nuclear Society (ANS) conversion function ANS-6.1.1 (1977) are 24-25% higher compared to values obtained with the ANS-6.1.1 (1991) conversion function, in agreement with the statement quoted from the literature. A critical review of the experimental data has highlighted the disagreement between some of the dose rate distribution curves and the available experimental burn-up and the gamma source scan profiles. For the D04 spent FA, the calculated dose rates appear to overestimate the dose distribution through the axial detector holder tube 30.48 cm above the spent fuel. However, the situation is reversed for the dose rates through the vertical axis, where the calculated dose rates yield a better agreement, with an average underestimation of ≅ 30%. For the B03 spent fuel, the detail modelling approach adopted by SCK CEN including cobalt impurity has been proven to be effective

in achieving the lower discrepancy (underestimation of ≅ 20%) where the experiment dose rate curves sound reliable. Another item likely to influence the dose rate calculation is the radiation backscattering due to various materials surrounding the experimental setup, mainly the hot cell walls and the FA support table.

Calculation/measurement deviations are within a range of ± 30% on average.

To conclude, this benchmark made it possible to establish the recommendations for the calculations of dose rate in the air for PWR UOX and MOX spent FAs for self-protection determination. These reference calculations have been validated by comparison with two experiments (Morris, Turkey Point). The experimental validation exercise showed the need for accurate and complete measurements (knowledge of the level of impurities in the components in particular). The benchmark study also confirmed that calculations with MicroShield are conservative for shielding determination, but should not be used for self-protection determination.

In the future, the dose rate could be an additional relevant parameter for the scenario studies, in particular in the framework of proliferation resistance evaluations, by comparing the self-protection capabilities of different reactors or fuel cycles. Thus, it would be interesting to complete the calculations carried out here on PWR UOX and MOX with calculations on other types of fuels and reactors, such as boiling water reactors (BWRs) or fast reactors, and to complete and consolidate the experimental validation with quality measurements, subject to availability.

1. Introduction

The dose rate emitted from a spent fuel assembly (FA) holds significance due to two factors. Firstly, it is used to establish the required shielding and handling protocols to ensure the safety of personnel working with spent fuel. Secondly, it is associated with non-proliferation considerations, since the gamma and neutron radiation act as a self-protecting deterrent to theft for decades following fuel discharge. The United States Nuclear Regulatory Commission (US NRC) and the International Atomic Energy Agency (IAEA) consider that an FA is "self-protecting" if the dose rate is at least 1 Sv/h at 1 m from it [1]. Conservative estimates can be used to account for the inherent uncertainty in dose rate calculations. An overestimation of the dose is conservative for personnel protection, while an underestimation is conservative for self-protection.

In 2014, the Argonne National Laboratory (ANL) and the French Alternative Energies and Atomic Energy Commission (CEA) carried out a comparative study on dose rate calculations for uranium oxide (UOX) and mixed oxide (MOX) spent FAs from pressurised water reactor (PWR) [2]. This joint endeavour was initiated to improve confidence in the dose rate calculation methodology employed by each organisation, specifically in situations requiring quantitative measurements of proliferation resistance.

The 30-year dose rates calculated by CEA and ANL for the UOX case [2] were roughly three times lower than that of a frequently-cited reference study [3]. This finding brings into question commonly held beliefs regarding the levels of self-protection exhibited by spent PWR fuels. It is worth noting that the methodology adopted for the reference study included the point-kernel code MicroShield, which is typically used for shielding design, and a conservative approach to worker protection, leading to higher dose rates.

In this context, the Nuclear Energy Agency (NEA) Expert Group on Advanced Fuel Cycle Scenarios (EGAFCS) launched an international benchmark on dose rate calculations for PWR spent FA. The objectives were to verify updated dose rate calculation procedures (new modelling approaches, new nuclear data, new versions of the codes) and share the benchmark results at the international level.

The benchmark was divided into two parts:

- verification (comparison of results with different codes/methodologies);
- validation (comparison of results with experimental data).

Two sets of representative experimental data were considered:

- Morris experiments, a series of gamma dose rate measurements completed in the General Electrical spent fuel storage facility at Morris Operation;
- Turkey Point experiments, with dose rate measurements from different assemblies.

In both cases, dose rates were measured in the vicinity of the discharged spent fuel bundles, with a wide range of fuel types, power levels, burn-ups and cooling times.

References

[1] DOE (1997), *Non-proliferation and Arms Control Assessment of Weapons Usable Fissile Material Storage and Excess Plutonium Disposition Alternatives*, DOE/NN-0007, www.osti.gov/scitech/biblio/425259, US Department of Energy, United States.

[2] Feng, B, R. Hill, R. Girieud and R. Eschbach (2014), "Comparison of gamma dose rate calculations for PWR spent fuel assemblies", *Proceedings of PHYSOR 2014*, Kyoto, Japan, 28 September-3 October.

[3] Lloyd, W.R, M.K. Sheaffer, and W.G. Sutcliffe (1994), *Dose Rate Estimates from Irradiated Light Water Reactor Fuel Assemblies in Air*, Lawrence Livermore National Laboratory Livermore, CA, United States, https://doi.org/10.2172/10137382.

2. Specification of the benchmark

2.1. Motivation

The ANL and the CEA conducted a comparative study on dose rate calculations for typical PWR spent FAs (with UOX and MOX fuels) [1]. The goal was to verify each organisation's gamma dose rate calculation methodology, especially for cases in which quantitative measurements of proliferation resistance are desired. The goal of this benchmark is to expand on that work by including more international participants to verify the dose rate results for the UOX and MOX cases and by potentially including validation efforts if appropriate experimental data is available.

2.2. Background

The plutonium that is created in UOX fuel during irradiation and sometimes recycled in the form of MOX fuel could potentially be diverted to weapons use. If the UOX and MOX FAs were recently discharged after normal residence times from civilian reactors, the significant amount of gamma radiation from the FAs makes them unattractive to theft, thereby providing an inherent barrier of self-protection. The US NRC and the IAEA consider the "self-protecting" dose rate to be 1 Sv/h at 1 m from the FA [2]. This dose rate would help a MOX FA meet the National Academy of Science's (NAS) "spent fuel standard", a condition in which the Pu becomes roughly as inaccessible and unattractive for weapons use as the Pu that exists in conventional commercial spent fuel (UOX).

The dose rate from a spent FA decreases with time after discharge due to the radioactive decay of the gamma-emitting isotopes. Table 2.1 shows calculated neutron, gamma, and total dose rates from a standard PWR MOX FA at 1 m away through the air (for both fresh and irradiated fuels – 45 GWd/MTIHM) after different cooling times. The gamma dose rate is 3-4 orders of magnitude higher than the neutron dose rate for irradiated fuels. So for the purpose of this study, the total dose rate can be approximated by just the gamma dose rate.

Accurate predictions of this dose rate after decades of cooling depend on factors such as the assembly's power history, composition and geometry as well as the calculated gamma source and radiation deposited on the target. Therefore, in addition to gamma transport calculations, the depletion, decay and gamma source calculation approaches need to be precisely carried out.

For the UOX case, which intended to benchmark a frequently-cited reference study [3], the 30-year dose rates calculated by CEA and ANL [1] were roughly three times lower than that of the reference study. It was shown that the reference dose rate calculations were performed by a point-kernel code typically used for shielding design (MicroShield) with high gamma transport build-up factors for air that were intentionally selected to provide more conservative values for shielding purposes. This can partially explain the large differences between the new calculations and the reference ones, but additional verification and analysis are necessary.

Table 2.1. Dose rate for a standard PWR MOX fuel at 1 m in air

	Fresh assembly	Irradiated PWR MOX assembly			
Cooling time (y)	N/A	0.5	3	10	30
Neutron dose rate (µSv/h)	1.62E+02	2.75E+04	2.05E+04	1.56E+04	7.43E+03
Gamma dose rate (µSv/h)	5.48E+01	2.37E+08	4.91E+07	1.44E+07	6.37E+06
Total dose rate (µSv/h)	2.17E+02	2.37E+08	4.92E+07	1.44E+07	6.38E+06

2.3. Objective of the benchmark

The objectives of the benchmark are to verify updated dose rate calculation procedures (new modelling approaches, new nuclear data, new versions of the codes) and to share the benchmark results at the international level. The benchmark is divided into two parts:

- verification (comparison of results with different codes/methodologies);
- validation (comparison of results with experimental data, if available).

The verification part is divided into three calculation steps:

- Depletion: Given the FA description and power conditions, simulate the depletion (burn-up) of a FA to obtain the discharge composition.
- Decay: Simulate a 30-year period of decay for this discharge composition, and calculate the isotopic photon release rates that are discretised into multiple gamma energy groups.
- Radiation: Apply the multi-group gamma source uniformly (axially and radially) to a heterogeneous 3D transport model of the FA and tally the gamma flux at 1 m away from the midpoint. Calculate the corresponding dose rate using flux-to-dose rate conversion factors.

Figure 2.1 illustrates the comprehensive calculation approach to predicting a FA dose rate. The primary goal is to benchmark dose rate calculations for PWR spent fuel elements (bare assemblies) for both UOX and MOX fuels. However, dose rate calculations involving different assembly designs, such as those for fast reactors, may also be included.

Regarding the second part (validation), a comparison with experimental results is always very interesting. This greatly improves confidence in each organisation's dose rate calculation methodology. Of course, the experiments should be representative of dose rate measurements on a single bare assembly in the air from commercial PWR spent fuel elements (UOX and/or MOX).

Figure 2.1. Comprehensive calculation approach to predicting a FA dose rate

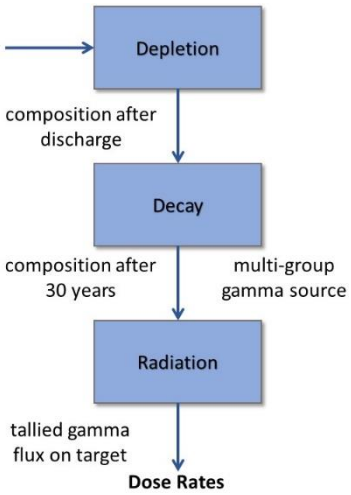

Source: NEA EGAFCS data, 2020.

2.4. Specification of the verification benchmark

For the verification part of the benchmark, two spent FA models were proposed: a 15x15 PWR assembly with UOX fuel and a 17x17 PWR assembly with MOX fuel. At the very minimum, all participants were asked to model these two assemblies and calculate their dose rates. For the UOX FA, they performed depletion, decay and radiation calculations. For the MOX FA, they were provided with the depleted compositions and perform the decay and radiation calculations only. This was to remove any additional source of discrepancy and help pinpoint any major differences. Lastly, a few optional calculations were suggested as described in Section 2.4.5 to provide more insights on modelling impacts.

2.4.1. Model description

The 15x15 UOX PWR FA is shown in Figure 2.2. and described in Table 2.2. All 208 fuel pins have a uniform initial enrichment of 3.11 wt% ^{235}U, and the assembly is irradiated to 33 GWd/MTIHM. These properties are consistent with the PWR assembly model described in [3]. For simplicity, the 17 water tubes can be approximated as fuel pins filled with water instead of fuel. There are no assembly cans or sleeves surrounding the assembly; for the depletion calculations, the pins are only surrounded by water (assuming infinite lattice), and after the 30-year cooling period, there is only air between the radiation target and the outermost row of fuel pins. Nominal/typical conditions have been assumed for all other parameters that are not specified (power level, temperatures, water densities, etc.). As an example, the values that CEA used to perform calculations are detailed below (benchmark participants could either use these values or different ones):

- ^{234}U init: 303 ppm;
- fuel temperature: 821°C;
- clad temperature: 342°C;
- water temperature: 305.6°C;
- pressure: 155 bar;

- boron: 456 ppm;
- specific power: 48 W/g;
- guide tube inner/outer diameter: 1.242 mm / 1.382 mm.

Figure 2.2. 15x15 UOX FA (with 17 water tubes)

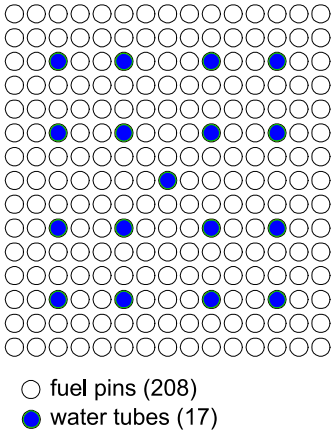

Source: NEA EGAFCS data, 2020.

Table 2.2. Assumed model parameters for 15x15 PWR assembly with UOX fuel

Parameter	Value
Fuel pellet diameter [cm]	0.925
Cladding inner diameter [cm]	0.9398
Cladding outer diameter [cm]	1.0668
Pin pitch [cm]	1.4224
Active height [cm]	365.76
Assembly pitch [cm]	21.4 (gap water: 0.064)
Fuel pins per assembly	208
Water tubes per assembly	17
UO_2 fuel density [g/cm^3]	10.412
HM mass [kgHM]	469.22
^{235}U Enrichment [wt%]	3.11
Burn-up [GWd/MTIHM]	33

The 17x17 PWR MOX assembly has three zones with different plutonium contents (see Figure 2.3.): 12 pins with low enrichment, 68 pins with intermediate enrichment and 184 pins with high enrichment. This information was needed for the burn-up calculation, which is not required for the benchmark since the lumped discharge composition for the MOX assembly is provided. However, participants could use their calculated compositions. For ANL and CEA calculations, the FA's total gamma source and lumped fuel composition were spread uniformly in the axial and radial directions within all of the fuel inside the cladding. The fresh fuel has an assembly average of 8.65 wt% Pu recovered from reprocessed UOX fuel (originally at 3.7 wt% ^{235}U enrichment, discharged at 45 GWd/MTIHM, and with five years of cooling and then two years of ageing years of cooling) and mixed with depleted uranium (0.25 wt% ^{235}U). This plutonium vector in fresh MOX fuel is shown in Table 2.3. The assumed model parameters for the 17x17 PWR MOX assembly are shown in Table 2.4. All other modelling assumptions are the same as those

for the PWR UOX model. As an example, the nominal conditions used by CEA are given below:

- ^{234}U init.: 0 ppm;
- fuel temperature: 620°C;
- clad temperature: 342°C;
- water temperature: 309°C;
- pressure: 155 bar;
- boron: 600 ppm;
- specific power: 41 W/g;
- guide tube inner/outer diameter: 1.142 mm/1.226 mm.

2.4.2. Depletion

Participants were free to use their preferred codes and procedures for all calculations. The codes and procedures used by CEA and ANL from [1] are described below the benchmark proposal and were given in the benchmark proposal only to serve as a guide.

For the UOX and MOX assembly depletion calculations, the CEA used APOLLO2.8, the reference neutronics code package used in France for light water reactors (LWRs). The CEA also used the CEA2005V4 multi-group cross-section library derived from recent the Joint Evaluated Fission and Fusion (JEFF) version 3.1.1 [10] evaluations. APOLLO2.8 provides the neutronics data (self-shielded cross sections and neutron spectra) to DARWIN2.3, the French reference package for fuel cycle calculations, which re-calculates the compositions of the discharged FA.

For the UOX fuel, the ANL used discharged compositions from a previous study that were calculated using CASMO-4, a multi-group 2D transport code based on the method of characteristics that is used by utilities in the United States and worldwide. The microscopic cross sections are based on the Evaluated Nuclear Data File (ENDF), version ENDF/B-V and were divided into 70 energy groups. The discharged composition was taken directly from CASMO-4 for the next calculation step. For the MOX fuel, the DARWIN2.3-calculated composition used by CEA was also used by ANL to remove a potential source of discrepancy.

Figure 2.3. 17x17 MOX FA

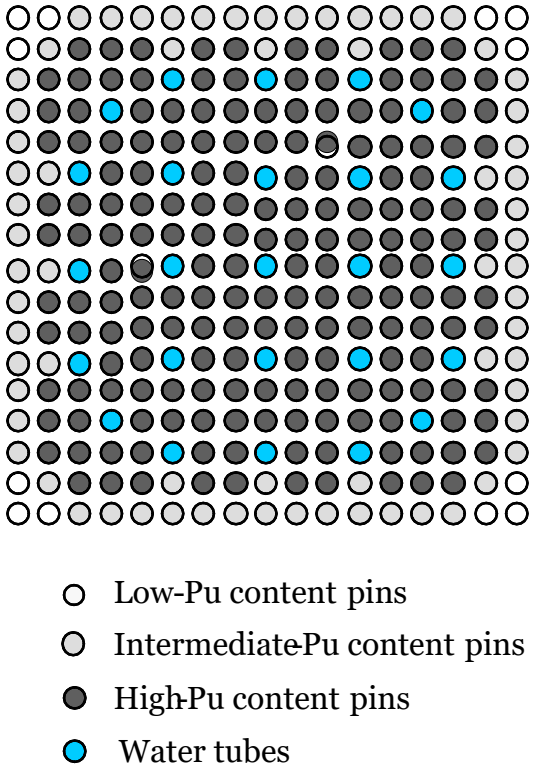

Source: NEA EGAFCS data, 2020.

Table 2.3. Plutonium vector in fresh MOX fuel

Isotope	Weight per cent
^{238}Pu	2.62%
^{239}Pu	52.67%
^{240}Pu	25.45%
^{241}Pu	10.65%
^{242}Pu	7.54%
^{241}Am	1.07%

As mentioned, APOLLO2.8/DARWIN2.3 and CASMO-4 were used by the CEA and ANL, respectively, for the assembly depletion calculations to obtain the fuel composition at discharge. Due to slight modelling variations, not all parameters in Table 2.2 were matched exactly. However, all results from the calculations were scaled to the reference 469 kgHM mass, which is one of the most important parameters with respect to the gamma source. Both codes calculated a ^{238}U mass of 434.594 g. Table 2.5 summarises the codes and libraries used.

Table 2.4. Assumed model parameters for 17x17 PWR assembly with MOX fuel

Parameter	Value
Fuel pellet diameter [cm]	0.8192
Cladding inner diameter [cm]	0.836
Cladding outer diameter [cm]	0.950
Pin pitch [cm]	1.26
Active height [cm]	365.76
Assembly pitch [cm]	21.58
Fuel pins per assembly	264
Water tubes per assembly	25
MOX fuel density [g/cm^3]	11.3
HM mass [kgHM]	454
Low-content Pu/HM [wt%]	3.65
Intermediate-content Pu/HM [wt%]	6.49
High-content Pu/HM [wt%]	9.77
Burn-up [GWd/MTIHM]	60

Table 2.5. Codes for depletion

Institutes	Codes for depletion	Nuclear Data Library
CEA	APOLLO2.8/DARWIN2.3	JEFF3.1.1
ANL	For UOX: CASMO-4 For MOX: used results from CEA	ENDF/B-V

Comparison at discharge for UOX fuel

Tables 2.6 and 2.7 show the masses in grams of the HM and FP, respectively, in the 469 kgHM spent UOX assembly, calculated by CEA and ANL. The benchmark participants were asked to produce these compositions with their codes/procedures in the same format and units (normalised to the 469 kgHM total mass).

Table 2.6. Calculated HM masses [g] in PWR/UOX assembly at discharge (469 kg of total initial HM)

	CEA	ANL
U-234	8.29E+01	6.27E+01
U-235	3.82E+03	3.41E+03
U-236	1.80E+03	1.68E+03
U-237	5.84E+00	5.67E+00
U-238	4.42E+05	4.35E+05
Np-236	1.41E-04	7.18E-04
Np-236m	7.28E-06	-
Np-237	1.84E+02	1.72E+02
Np-238	8.22E-01	6.19E-01
Np-239	5.93E+01	4.53E+01
Pu-236	4.71E-04	-
Pu-237	1.35E-04	-
Pu-238	6.04E+01	5.58E+01
Pu-239	2.55E+03	2.36E+03
Pu-240	1.10E+03	9.91E+02
Pu-241	6.35E+02	5.89E+02
Pu-242	2.44E+02	2.28E+02
Pu-243	8.98E-02	6.08E-02
Pu-244	1.46E-02	-
Am-241	1.18E+01	1.44E+01
Am-242	5.09E-02	4.63E-02
Am-242m	2.39E-01	1.97E-01
Am-243	4.52E+01	3.91E+01
Am-244	3.69E-03	4.19E-02
Cm-242	5.54E+00	5.59E+00
Cm-243	1.13E-01	1.21E-01
Cm-244	1.35E+01	1.20E+01
Cm-245	6.91E-01	5.55E-01
Cm-246	5.88E-02	5.22E-02
Cm-247	6.35E-04	4.51E-04
Cm-248	3.31E-05	2.34E-05
Bk-249	3.36E-07	3.23E-10
Cf-249	3.05E-08	2.40E-07
Cf-250	1.81E-07	3.40E-10
Cf-251	3.89E-08	-
Cf-252	1.93E-08	6.27E+01

Table 2.7. Calculated FP masses [g] in PWR/UOX assembly at discharge (469 kg of total initial HM)

	CEA	ANL
Kr-83	1.88E+01	1.84E+01
Rh-103	2.05E+02	1.95E+02
Rh-105	8.38E-01	6.56E-01
Ag-109	3.64E+01	3.49E+01
I-135	3.30E-01	2.56E-01
Xe-131	1.98E+02	1.92E+02
Xe-135	8.85E-02	7.78E-02
Cs-133	5.14E+02	4.96E+02
Cs-134	6.11E+01	6.18E+01
Cs-135	1.28E+02	1.42E+02
Cs-137	5.73E+02	5.55E+02
Ba-137m	8.80E-05	-
Ba-140	1.43E+01	1.10E+01
La-140	1.93E+00	1.49E+00
Nd-143	3.59E+02	3.51E+02
Nd-145	3.14E+02	3.08E+02
Nd-148	1.77E+02	-
Pm-147	9.51E+01	8.18E+01
Pm-148	7.80E-01	5.33E-01
Pm-149	8.64E-01	7.36E-01
Sm-147	2.38E+01	2.76E+01
Sm-149	9.92E-01	1.02E+00
Sm-150	1.39E+02	1.36E+02
Sm-151	5.37E+00	5.90E+00
Sm-152	5.06E+01	5.75E+01
Eu-153	5.45E+01	5.57E+01
Eu-154	1.12E+01	1.64E+01
Eu-155	3.71E+00	2.26E+00
Eu-156	2.59E+00	1.91E+00
Gd-155	1.85E-02	1.53E-02

Comparison at discharge for MOX fuel

Tables 2.8 and 2.9 show the masses in grams of the HM and FP, respectively, in the 454 kgHM spent MOX assembly, calculated by CEA and ANL. The benchmark participants were free to use these calculated compositions or produce them with their codes/procedures in the same format and units (normalised to the 454 kgHM total mass).

Table 2.8. Calculated HM masses [g] in PWR/MOX assembly at discharge (454 kg of total initial HM)

	CEA	ANL
U-234	2.29E+01	3.90E+01
U-235	4.31E+02	4.54E+02
U-236	1.32E+02	1.28E+02
U-237	1.10E+00	1.52E-04
U-238	3.96E+05	3.94E+05
Np-236	2.55E-04	1.89E-04
Np-236M	3.46E-06	0.00E+00
Np-237	9.44E+01	8.52E+01
Np-238	2.07E-01	2.83E-06
Np-239	3.67E+01	8.83E-04
Pu-236	4.86E-04	3.43E-04
Pu-237	3.21E-03	2.03E-04
Pu-238	1.04E+03	1.23E+03
Pu-239	9.39E+03	9.83E+03
Pu-240	8.24E+03	9.22E+03
Pu-241	4.66E+03	4.86E+03
Pu-242	3.64E+03	4.12E+03
Pu-243	4.38E-01	5.49E-12
Pu-244	4.53E-01	4.26E-01
Am-241	4.25E+02	5.97E+02
Am-242	5.85E-01	1.95E-04
Am-242M	1.39E+01	1.51E+01
Am-243	9.85E+02	1.03E+03
Am-244	4.07E-02	0.00E+00
Cm-242	1.13E+02	5.96E+01
Cm-243	6.13E+00	6.09E+00
Cm-244	6.92E+02	6.50E+02
Cm-245	9.37E+01	7.88E+01
Cm-246	8.57E+00	8.26E+00
Cm-247	2.25E-01	1.58E-01
Cm-248	1.77E-02	1.14E-02
Bk-249	4.19E-04	1.61E-04
Cf-249	1.22E-04	1.39E-04
Cf-250	2.01E-04	1.13E-04
Cf-251	3.75E-05	2.06E-05
Cf-252	1.30E-05	6.28E-06

Table 2.9. Calculated FP masses [g] in PWR/MOX assembly at discharge (454 kg of total initial HM)

	CEA	ANL
Kr-83	2.13E+01	2.15E+01
Rh-103	5.51E+02	5.97E+02
Ag-109	1.43E+02	1.51E+02
I-135	2.64E-01	0.00E+00
Xe-131	3.47E+02	3.69E+02
Xe-135	2.15E-01	0.00E+00
Cs-133	8.52E+02	8.80E+02
Cs-134	1.23E+02	9.69E+01
Cs-135	6.57E+02	6.32E+02
Cs-137	9.74E+02	9.69E+02
Ba-137m	1.49E-04	1.48E-04
Ba-140	1.09E+01	6.04E-04
La-140	1.47E+00	5.71E+05
Nd-143	6.07E+02	6.22E+02
Nd-145	4.59E+02	4.66E+02
Nd-148	3.02E+02	2.99E+02
Pm-147	1.13E+02	1.11E+02
Pm-148	6.29E-01	6.28E-04
Pm-149	6.57E-01	9.33E-26
Sm-147	5.88E+01	7.77E+01
Sm-149	3.85E+00	4.66E+00
Sm-150	2.49E+02	2.48E+02
Sm-151	2.07E+01	2.11E+01
Sm-152	9.05E+01	9.87E+01
Eu-153	1.25E+02	1.28E+02
Eu-154	4.62E+01	4.06E+01
Eu-155	1.06E+01	9.51E+00
Eu-156	3.07E+00	7.71E-04
Gd-155	3.07E-01	9.76E-01

2.4.3. Decay and gamma source

For the CEA approach, DARWIN2.3 was also used for the decay calculation to provide the assembly's lumped fuel inventory, decay heat, activity, neutron, gamma/alpha/beta sources, and spectrum for up to 30 years after discharge. For the ANL approach, the discharged fuel composition from CASMO-4 (for UOX) or DARWIN2.3 (for MOX) were lumped into a single mass as input into ORIGEN2 to provide the same parameters after 30 years of decay. The main parameter provided by these codes is the multi-group gamma photon release rate from the FA after 30 years.

Comparison for UOX fuel after 30 years of decay

Tables 2.10 and 2.11 show the masses in grams of HM and FP, respectively, in the spent UOX assembly after 30 years of cooling. The benchmark participants were asked to produce these compositions with their codes/procedures in the same format and units (normalised to the 469 kgHM total mass).

Table 2.10. Calculated HM masses [g] in PWR/UOX after 30 years (469 kg of total initial HM)

	CEA	ANL
U-234	9.66E+01	7.55E+01
U-235	3.82E+03	3.41E+03
U-236	1.80E+03	1.68E+03
U-237	4.64E-06	4.30E-06
U-238	4.42E+05	4.35E+05
Np-237	2.04E+02	1.91E+02
Pu-238	5.25E+01	4.89E+01
Pu-239	2.61E+03	2.40E+03
Pu-240	1.11E+03	9.96E+02
Pu-241	1.49E+02	1.39E+02
Pu-242	2.43E+02	2.28E+02
Am-241	4.83E+02	4.50E+02
Am-242	2.66E-06	1.72E-01
Am-242M	2.06E-01	2.06E-06
Am-243	4.51E+01	3.91E+01
Am-244	1.10E-17	0.00E+00
Cm-244	4.26E+00	3.83E+00
Cm-245	6.89E-01	5.53E-01
Cf-251	3.80E-08	2.50E-08
Cf-252	7.46E-12	5.08E-12

Table 2.11. Calculated FP masses [g] in PWR/UOX after 30 years (469 kg of total initial HM)

	CEA	ANL
Sr-90	1.19E+02	-
Y-90	3.02E-02	-
Cs-137	2.87E+02	2.77E+02
Ba-137m	4.37E-05	4.24E-05
Sm-154	1.79E+01	-
Eu-153	5.49E+01	5.57E+01
Eu-154	9.99E-01	1.46E+00
Eu-155	4.67E-02	3.42E-02

Comparison for MOX fuel after 30 years of decay

Tables 2.12 and 2.13 show the masses, in grams, of HM and FP, respectively, in the spent MOX assembly after 30 years of cooling. The benchmark participants were asked to produce these compositions with their codes/procedures in the same format and units (normalised to the 454 kgHM total mass).

Table 2.12. Calculated HM masses [g] in PWR/MOX assembly after 30 years (454 kg of total initial HM)

	CEA	ANL
U-234	2.61E+02	3.02E+02
U-235	4.39E+02	4.62E+02
U-236	1.59E+02	1.57E+02
U-237	3.41E-05	3.64E-05
U-238	3.96E+05	3.94E+05
Np-237	2.17E+02	2.16E+02
Pu-238	9.09E+02	1.02E+03
Pu-239	9.42E+03	9.83E+03
Pu-240	8.68E+03	9.63E+03
Pu-241	1.09E+03	1.18E+03
Pu-242	3.64E+03	4.12E+03
Am-241	3.87E+03	4.15E+03
Am-242	1.54E-04	1.58E-04
Am-242m	1.20E+01	1.32E+01
Am-243	9.83E+02	1.02E+03
Am-244	3.97E-14	0.00E+00
Cm-244	2.18E+02	2.10E+02
Cm-245	9.35E+01	7.86E+01
Cf-251	3.66E-05	2.01E-05
Cf-252	5.01E-09	2.70E-09

Table 2.13. Calculated FP masses [g] in PWR/MOX assembly after 30 years (454 kg of total initial HM)

	CEA	ANL
Sr-90	9.74E+01	9.80E+01
Y-90	2.47E-02	2.46E-02
Cs-137	4.88E+02	4.90E+02
Ba-137	5.34E+02	5.36E+02
Ba-137m	7.43E-05	7.50E-05
Sm-154	5.29E+01	5.33E+01
Eu-153	1.26E+02	1.28E+02
Eu-154	4.11E+00	3.77E+00
Eu-155	1.33E-01	1.50E-01

Comparison of gamma sources

The energy discretisation is different for each code and the release rates from ORIGEN2 were artificially adjusted to preserve the total gamma energy, so there is no direct way to compare the two release rates. Table 2.14 summarises the codes and libraries used for the decay calculations. Tables 2.15 and 2.16 give the calculated 30-year gamma release rates and contributions from each energy group for PWR assembly with UOX and MOX fuels, respectively. Both CEA and ANL results include bremsstrahlung in the gamma source.

Table 2.14. Codes for decay and gamma source

Institutes	Codes for depletion	Nuclear Data Library
CEA	DARWIN2.3	JEFF3.1.1
ANL	ORIGEN2	gxuo2brm.lib (ORIGEN photon library)

Table 2.15. Calculated 30-year gamma release rates and contributions from each energy group for PWR assembly with UOX fuel (number of energy groups and group structure can be different)

CEA				ANL			
E_{low} [MeV]	E_{high} [MeV]	Gamma release rate [photons/sec]	Percent of total gammas	E_{low} [MeV]	E_{high} [MeV]	Gamma release rate [photons/sec]	Percent of total gammas
0	0.0482	1.09E+14	11.71%	0	0.02	1.17E+14	10.16%
0.0482	0.0713	2.26E+13	2.42%	0.02	0.03	1.86E+13	1.62%
0.0713	0.106	9.04E+11	0.10%	0.03	0.045	6.91E+13	6.02%
0.106	0.156	4.20E+12	0.45%	0.045	0.07	3.53E+13	3.07%
0.156	0.231	1.08E+11	0.01%	0.07	0.1	7.09E+12	0.62%
0.231	0.342	8.02E+11	0.09%	0.1	0.15	9.61E+12	0.84%
0.342	0.507	1.70E+11	0.02%	0.15	0.3	4.05E+12	0.35%
0.507	0.75	7.87E+14	84.27%	0.3	0.45	6.11E+11	0.05%
0.75	1.25	5.10E+12	0.55%	0.45	0.7	8.72E+14	75.96%
1.25	1.75	3.77E+12	0.40%	0.7	1	7.05E+12	0.61%
1.75	2.25	1.94E+08	0.00%	1	1.5	7.69E+12	0.67%
2.25	2.75	1.34E+08	0.00%	1.5	2	2.30E+11	0.02%
2.75	3.5	9.12E+05	0.00%	2	2.5	8.86E+06	0.00%
3.5	4.5	2.25E+05	0.00%	2.5	3	5.13E+06	0.00%
4.5	5.5	3.99E+04	0.00%	3	4	4.61E+06	0.00%
5.5	6.5	1.27E+04	0.00%	4	6	1.97E+06	0.00%
6.5	7.5	1.72E+02	0.00%	6	8	2.27E+05	0.00%
7.5	8.65	0.00E+00	0.00%	8	11	2.61E+04	0.00%
8.65	20	0.00E+00	0.00%	**Total**		1.15E+15	100%
Total		9.34E+14	100%				

Table 2.16. Calculated 30-year gamma release rates and contributions from each energy group for PWR assembly with MOX fuel (number of energy groups and group structure can be different)

CEA				ANL			
E_{low} [MeV]	E_{high} [MeV]	Gamma release rate [photons/sec]	Percent of total gammas	E_{low} [MeV]	E_{high} [MeV]	Gamma release rate [photons/sec]	Percent of total gammas
0	0.0482	5.02E+14	23.88%	0	0.02	8.57E+14	26.70%
0.0482	0.0713	1.79E+14	8.51%	0.02	0.03	1.16E+14	3.61%
0.0713	0.106	1.24E+13	0.59%	0.03	0.045	1.74E+14	5.42%
0.106	0.156	2.05E+13	0.97%	0.045	0.07	2.89E+14	9.00%
0.156	0.231	2.09E+12	0.10%	0.07	0.1	6.08E+13	1.89%
0.231	0.342	5.17E+12	0.25%	0.1	0.15	5.46E+13	1.70%
0.342	0.507	6.55E+11	0.03%	0.15	0.3	4.85E+13	1.51%
0.507	0.75	1.35E+15	63.96%	0.3	0.45	1.76E+13	0.55%
0.75	1.25	2.08E+13	0.99%	0.45	0.7	1.55E+15	48.29%
1.25	1.75	1.55E+13	0.74%	0.7	1	2.08E+13	0.65%
1.75	2.25	9.20E+08	0.00%	1	1.5	2.08E+13	0.65%
2.25	2.75	2.13E+08	0.00%	1.5	2	6.63E+11	0.02%
2.75	3.5	4.67E+07	0.00%	2	2.5	4.85E+08	0.00%
3.5	4.5	1.15E+07	0.00%	2.5	3	3.86E+08	0.00%
4.5	5.5	2.05E+06	0.00%	3	4	2.49E+08	0.00%
5.5	6.5	6.53E+05	0.00%	4	6	1.07E+08	0.00%
6.5	7.5	8.78E+03	0.00%	6	8	1.23E+07	0.00%
7.5	8.65	0.00E+00	0.00%	8	11	1.41E+06	0.00%
8.65	20	0.00E+00	0.00%	**Total**		3.21E+15	100%
Total		2.11E+15	100%				

2.4.4. Radiation and dose rate

Once the multi-group gamma source and 30-year fuel composition were obtained, a heterogeneous 3D assembly model was created with this information and the geometry of PWR 15x15 for UOX, and PWR 17x17 for MOX. Stochastic transport codes (TRIPOLI-4 and MCNP5) were then used to calculate the gamma flux on a target 1 m away from the axial midpoint. Figure 2.4 shows a schematic of this model and where the gamma photon flux is tallied. The assembly was assumed to be unshielded and surrounded by air at room temperature. No axial burn-up distribution was taken into account. The fuel composition and gamma source were spread uniformly across each pin radially and axially.

Table 2.17 summarises the codes and libraries used for the radiation transport calculations.

Figure 2.4. Schematic of gamma photon flux calculation

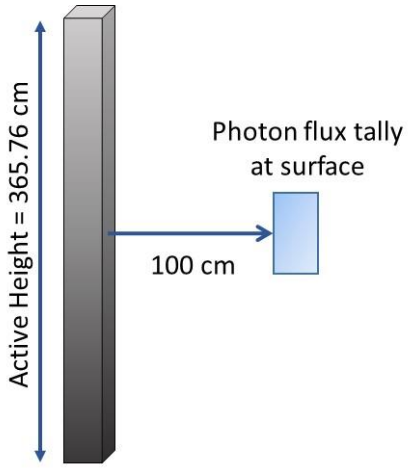

Source: NEA EGAFCS data, 2020.

Table 2.17. Codes for gamma transport

Institutes	Codes for depletion	Nuclear Data Library
CEA	TRIPOLI-4	JEFF3.1.1
ANL	MCNP-5	ENDF/B-VII.0

The tallied flux in units of photons/cm^2-s is converted to a dose rate in units of Sv/h with flux-to-dose-rate conversion factors that are energy dependent (see Figure 2.5).

Table 2.18 shows the conversion factors and these values can be used to linearly interpolate values between data points. The energy of each gamma particle at the tally surface was used to find the conversion factor to calculate that particle's contribution to the dose rate. Two conversion factor models were used for this study: one from the 1977 ANSI/ANS report [4] and the other from the 1991 ANSI/ANS report [5], as shown in Figure 2.5. The 1977 version was based on the maximum dose equivalent on a tissue-equivalent cylinder (30 cm diameter and 60 cm height) whereas the 1991 version considers the effective dose equivalent based on a more realistic representation of the human body and organ weighting factors [6]. Another major difference is that the 1991 conversion factor indicates that there is no significant contribution to the dose from gammas with low energies (< 0.1 MeV) whereas, for the 1977 conversion factor, there is a significant increase as the photon energy decreases below 0.1 MeV. Although ANSI believes that the information contained in the 1991 standard is correct, a formal ANS review to determine its accuracy was not performed in the allotted time. Therefore, it was officially withdrawn by ANSI as an American national standard in 2001 [6]. For this study, the dose rate results from both conversion factor models are shown to determine the range of potential values and help highlight potential sources of discrepancy between different code calculation approaches. The calculated dose rates are shown in Tables 2.19 and 2.20 for the UOX and MOX fuels, respectively.

Figure 2.5. Flux-to-dose-rate conversion factors

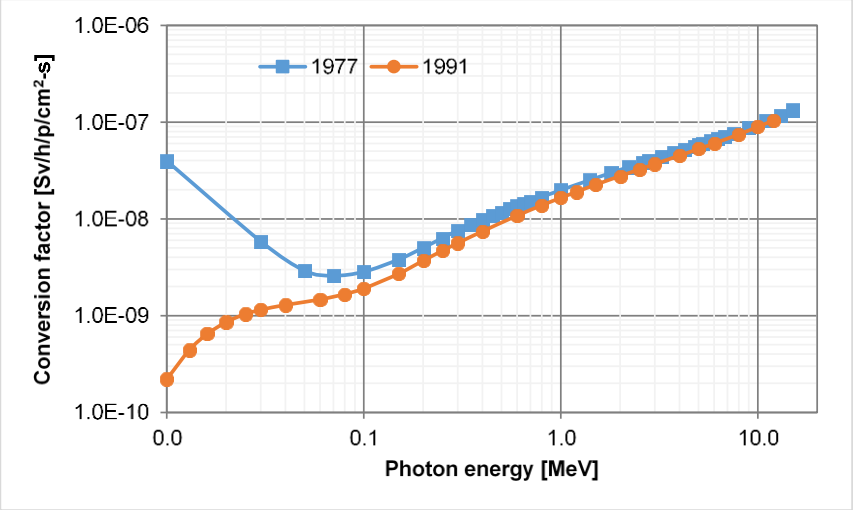

Source: NEA EGAFCS, 2020 – using data from ANSI/ANS (1977) and ANSI/ANS (1991).

Table 2.18. Photon flux-to-dose rate conversion factors (values shown in Figure 2.5) in units of [Rem/hr/flux]

	ANSI/ANS 1977			ANSI/ANS 1991
E, MeV	factor		E, MeV	factor
1.00E-02	3.96E-06		1.00E-02	2.21E-08
3.00E-02	5.82E-07		1.30E-02	4.41E-08
5.00E-02	2.90E-07		1.60E-02	6.45E-08
7.00E-02	2.58E-07		2.00E-02	8.58E-08
1.00E-01	2.83E-07		2.50E-02	1.04E-07
1.50E-01	3.79E-07		3.00E-02	1.15E-07
2.00E-01	5.01E-07		4.00E-02	1.29E-07
2.50E-01	6.31E-07		6.00E-02	1.47E-07
3.00E-01	7.59E-07		8.00E-02	1.67E-07
3.50E-01	8.78E-07		1.00E-01	1.91E-07
4.00E-01	9.85E-07		1.50E-01	2.71E-07
4.50E-01	1.08E-06		2.00E-01	3.70E-07
5.00E-01	1.17E-06		2.50E-01	4.68E-07
5.50E-01	1.27E-06		3.00E-01	5.63E-07
6.00E-01	1.36E-06		4.00E-01	7.44E-07
6.50E-01	1.44E-06		6.00E-01	1.08E-06
7.00E-01	1.52E-06		8.00E-01	1.38E-06
8.00E-01	1.68E-06		1.00E+00	1.65E-06
1.00E+00	1.98E-06		1.20E+00	1.90E-06
1.40E+00	2.51E-06		1.50E+00	2.25E-06
1.80E+00	2.99E-06		2.00E+00	2.77E-06
2.20E+00	3.42E-06		2.50E+00	3.24E-06
2.60E+00	3.82E-06		3.00E+00	3.69E-06
2.80E+00	4.01E-06		4.00E+00	4.50E-06
3.25E+00	4.41E-06		5.00E+00	5.27E-06

Table 2.18. Photon flux-to-dose rate conversion factors (values shown in Figure 2.5) in units of [Rem/hr/flux] (Continued)

	ANSI/ANS 1977			ANSI/ANS 1991
E, MeV	factor		E, MeV	factor
3.75E+00	4.83E-06		6.00E+00	6.01E-06
4.25E+00	5.23E-06		8.00E+00	7.46E-06
4.75E+00	5.60E-06		1.00E+01	8.92E-06
5.00E+00	5.80E-06		1.20E+01	1.04E-05
5.25E+00	6.01E-06			
5.75E+00	6.37E-06			
6.25E+00	6.74E-06			
6.75E+00	7.11E-06			
7.50E+00	7.66E-06			
9.00E+00	8.77E-06			
1.10E+01	1.03E-05			
1.30E+01	1.18E-05			
1.50E+01	1.33E-05			

Table 2.19. Calculated 30-year dose rates [Sv/h] at 1 m from the midpoint for a PWR with UOX fuel with a uniform gamma source

Conversion factor	CEA	ANL
1977	5.21	5.79
1991	4.76	4.56

Table 2.20. Calculated 30-year dose rates [Sv/h] at 1 m from the midpoint for a PWR with MOX fuel with a uniform gamma source

Conversion factor	CEA	ANL
1977	9.46	10.96
1991	8.64	8.62

2.4.5. Optional calculations

Participants were free to provide additional calculations that may help explain different results and/or show the impacts of various assumptions. A few suggestions were provided:

- impact of homogeneous/heterogeneous geometry;
- impact of axial burn-up distribution;
- impact of gamma source group structure;
- impact of pin-by-pin depletion instead of radially smearing out compositions;
- impact of using pin-by-pin gamma source distribution instead of radially smearing out gamma source.

2.4.6. Validation benchmark

As mentioned above, the possibility of a comparison with experimental results would be very interesting. According to the available data from the institutes participating in the benchmark, a new phase could be considered, including the description of the experiment and a comparison between measurements and calculated values. The same modelling approach described in Section 2.4 would be used but with specifications corresponding to the experiment. One report [7] has been found so far that describes measured dose rates from commercial spent fuel through the air, but only after a few years of cooling. Additional details on these measured dose rates may be found in the technical reports [8,9]. A more extensive literature review is required to obtain more experimental data.

References

[1] Feng, B., R. Hill, R. Girieud and R. Eschbach (2014), "Comparison of gamma dose rate calculations for PWR spent fuel assemblies", *PHYSOR 2014*, Kyoto, Japan, 28 September-3 October.

[2] DOE (1997), *Non-proliferation and Arms Control Assessment of Weapons-Usable Fissile Material Storage and Excess Plutonium Disposition Alternatives*, DOE/NN-007, United States, https://doi.org/10.2172/425259.

[3] Lloyd, W.R., M.K. Sheaffer and W.G. Sutcliffe (1994), *Dose Rate Estimates from Irradiated Light-Water Reactor Fuel Assemblies in Air*, Lawrence Livermore National Laboratory, Livermore, CA, United States, https://doi.org/10.2172/10137382.

[4] ANS (1977), *American National Standard for Neutron and Gamma-Ray Flux-to-Dose-Rate Factors*, ANSI/ANS-6.1.1 (1977), American Nuclear Society, United States.

[5] ANS, (1991), *American National Standard for Neutron and Gamma-Ray Flux-to-Dose-Rate Factors*, ANSI/ANS-6.1.1-1991.

[6] ANS (2004), "Responses to inquiries on standards", *Nuclear News*, Vol. 47(11), p.79, American Nuclear Society, United States, www.ans.org/file/374/6.1.1-1991-clarification-nn-1004.pdf.

[7] Willingham, C.E., (1981), *Radiation Dose Rates from Commercial PWR and BWR Spent Fuel Elements*, PNL-3954, Pacific Northwest Laboratory, October, https://doi.org/10.2172/6052779.

[8] Davis, R.B. (1980), *Data Report for the Nondestructive Examination of Turkey Point Spent Fuel Assemblies B02, B03, B17, B41 and B43, HEDL-TME-79-68*, Hanford Engineering Development Laboratory, Richland, Washington, www.osti.gov/scitech/servlets/purl/5445903.

[9] Davis, R.B. (1980), *Pre-Test Nondestructive Examination Data Summary Report on Turkey Point Spent Fuel Assemblies 001, 004 and 006 for the Climax-Spent Fuel Test, HEDL-TME-80-83*, Hanford Engineering Development Laboratory, Richland, Washington, www.osti.gov/scitech/servlets/purl/971850.

[10] NEA (2009), *The JEFF-3.1.1 Nuclear Data Library: JEFF Report 22*, OECD publishing, Paris, www.oecd-nea.org/jcms/pl_14470.

[11] Cao, Y. and B. Feng (2019), *Validation of Gamma Dose Rate Calculation Methodology using the Morris and Turkey Point Measurements*, ANL-19/06, Argonne National Laboratory, United States.

3. Description of approaches (codes and nuclear data)

3.1. General procedure

The objective of this work was to estimate the dose rate emitted by an irradiated PWR FA after some years of decay, at one or more points from the FA through the air. The methodology for the performance of this work was divided into three calculation steps:

- Depletion: Given the FA description and irradiation history conditions, the discharge composition is to be calculated.
- Decay: A period of decay after discharge is to be simulated to obtain the isotopic composition of the photon source. Also, the isotopic photon release rates that are discretised into multiple gamma energy groups have to be estimated.
- Radiation: The multi-group gamma source is applied to a heterogeneous 3D transport model of the FA and the gamma flux away from the assembly is estimated, calculating the corresponding dose rate using flux-to-dose rate conversion factors.

The comprehensive calculation approach to predicting the dose rate of an assembly is illustrated in Figure 2.1. Differences may appear between the verification, sensitivity and validation phases, since they involve different FA materials, irradiations, decay periods and detector locations, according to the specifications. However, as these parameters do not alter the methodology procedure, the approach will be described as follows in a general way.

3.2. Description of the codes used

Different simulation codes have been used by the participants to simulate the three calculation steps (depletion, decay and radiation transport) needed to finally estimate the dose rate. Table 3.1 shows the codes and the cross-section libraries used in the simulations, divided into these three steps. Proper referencing can be found in the following subsections.

The depletion step contains a large variety of choices. Deterministic (APOLLO, BISTRO, ERANOS, NEWT, ORIGEN-ARP) and Monte Carlo (ALEPH, EVOLCODE, KENO, MCODE, SERPENT, TRIPOLI) codes have been chosen with different libraries and versions. The decay calculation step also includes a significant variety of codes. For the photon transport step, all the participants have chosen different Monte Carlo codes. Two flux-to-dose conversion factor models were given as reference data for the benchmark: the 1977 ANSI/ANS conversion factors [1] and the 1991 ANSI/ANS conversion factors [2]. Additionally, the response function H*(10), based on the International Commission on Radiological Protection (ICRP) ICRP-74 recommendations [3], has also been used by CEA. A brief description of the codes and libraries can be found in the next subsections.

Table 3.1. Codes and libraries used by the participants for the three calculation steps

Institution	Depletion code	Decay code	Photon transport code	Cross-section library	Photon library	Comments
ANL	MCODE	ORIGEN2	MCNP	ENDF/B-VII.0	MCPLIB04	-
ANL	SERPENT	ORIGEN-S	MCNP	ENDF/B-VII.0	MCPLIB04	-
CEA	APOLLO	DARWIN	TRIPOLI	JEFF-3.1.1	EPDL-97	For verification
CEA	TRIPOLI	TRIPOLI	TRIPOLI	JEFF-3.1.1	EPDL-97	For validation
CNL	SERPENT	SERPENT	MCNP	ENDF/B-VII.0		
CIEMAT	EVOLCODE	ACAB	MCNP	JEFF-3.2	MCPLIB84	-
ENEA	APOLLO	ORIGEN-S	MCNPX	JEFF-3.1.1	MCPLIB04	-
ENEA	NEWT	ORIGEN-S	MCNPX	ENDF/B-VII.0	MCPLIB04	-
ENEA	SERPENT	ORIGEN-S	MCNPX	ENDF/B-VII.0	MCPLIB04	-
ENEA	KENO	ORIGEN-S	MCNPX	ENDF/B-VII.0	MCPLIB04	-
ENEA	ORIGEN-ARP	ORIGEN-ARP	MCNPX	ENDF/B-V	MCPLIB04	-
KIT	ERANOS-ECCO	ORIGEN	MCNPX	JEFF-3.1	TENDL-2014/ MCPLIB04	For UOX
KIT	BISTRO-ECCO	ORIGEN	MCNPX	JEFF-3.1	TENDL-2014/ MCPLIB04	For MOX
ORANO TN	ORIGEN-ARP	ORIGEN-ARP	TRIPOLI	JEFF-3.1.1	JEFF-3.1.1	-
SCK CEN	ALEPH	ALEPH	MCNP	JEFF-3.2	MCPLIB04	-
VTT	SERPENT	SERPENT	SERPENT	JEFF-3.1.2	MCPLIB02/ ENDF/B-VII.1	-

3.2.1. ACAB

The Activation Abacus (ACAB) code [4] is a computer program designed to perform activation and transmutation calculations for nuclear applications. The main computational algorithm is based on that of the ORIGEN2 code [5].

ACAB can perform space-dependent inventory calculations allowing for a very flexible geometry and neutron flux description. The code solves the general nuclear transmutation chains for multidimensional neutron flux distributions. One- and two-dimensional multi-group neutron fluxes generated by discrete-ordinates transport codes can be used. In addition, ACAB can use three-dimensional neutron fluxes generated by Monte Carlo neutron transport codes allowing inventory calculations to be performed for complex geometries. The multi-group neutron fluxes may be given in an arbitrary group structure.

3.2.2. ALEPH

ALEPH is a coupled neutronics and material evolution simulation system under continuous development at SCK CEN since 2004. The current version, ALEPH v2 [6], couples any version of the MCNP/MCNPX Monte Carlo code with a "deterministic" depletion equations module based on a Radau IIA implicit Runge-Kutta method (three stages, accuracy order 5) as implemented in RADAU5 solver [7]. This algorithm, hard coded in ALEPH v2, has shown reasonable performance and excellent stability when solving the system containing up to ~4 000 equations for all known nuclides. A typical step of the

ALEPH v2 simulation consists of an MCNP steady-state calculation to obtain the transported particle fluxes and spectra that are used to prepare spectrum-average data to be eventually used in a depletion solver to update the material compositions for the next irradiation step. In the present case, the steady-state calculations have been carried out using the MCNP5 version 1.60 [8].

Amongst the key features of the ALEPH v2, the full consistency in the nuclear data used should be highlighted both for the steady-state Monte Carlo and for time-dependent depletion calculations. ALEPH is capable of using almost all data supplied in basic libraries, namely radioactive decay data (e.g. JEFF-3.2 radioactive decay file contains information for 3 851 nuclides), total recoverable energy per fission of fissile nuclides, spontaneous fission product yields, direct neutron and proton fission product yields, and heating numbers (kerma) due to neutron and photon irradiation of materials. For the present calculations, the continuous pointwise nuclear data were used from JEFF.3.2.

3.2.3. ***APOLLO***

The APOLLO2 [9,10] is a neutron transport code using deterministic methods. It is designed as a modular structure, providing the users with specific tools to solve dedicated problems. APOLLO2 offers thus the possibility to perform reference calculations, with the maximum precision allowed by the available computers, as well as project routine calculations that run faster and require less precision. Physical, numerical and structural functions are built into the code as modules that perform specific tasks (geometry, self-shielding, flux solver, etc.) and can be viewed as operators that act on input objects to create output objects. This specific structure of the code also allows an easy implementation of new methods and models. The multi-group isotopic library used in the code is obtained by processing the most recent nuclear evaluations, without any cross-section adjustment, making it fully application-independent.

3.2.4. ***BISTRO***

The discrete ordinate module (*Bidimensionel Sn TRansport Optimise*, i.e. optimised two-dimensional Sn transport) BISTRO [11] in ERANOS [12] uses the Sn approximation to solve the neutron transport solution.

3.2.5. ***DARWIN***

DARWIN [13,14] is the French reference calculation package for the fuel cycle of all types of reactors. It has been developed by the CEA and its French partners such as AREVA and Electricité de France (EDF) to estimate the physical quantities characterising the spent fuels from reactors: material balance, decay heat, activity, neutron, α, β, γ sources and spectrum, and radiotoxicity. DARWIN is devoted to all cycle studies, with current fuels (UOX, MOX) or innovative fuels and for every nuclear road such as PWR, fast breeder reactor (FBR), BWR, advanced reactor, etc. DARWIN is also used in the back-end cycle for actinide incineration or long-term interim storage studies.

3.2.6. ***ECCO***

The European cell code (ECCO) cell/lattice code [15] included in the ERANOS3 package uses the subgroup method to treat resonance self-shielding effects in 1D, 2D or 3D calculations. This method is particularly suitable for calculations involving complex heterogeneous structures. ECCO prepares self-shielded cross sections and matrices by combining a slowing-down treatment in many groups (1968 groups) with the subgroup method within each fine group. The subgroup method takes into account the resonance

structure of cross sections using probability tables and by assuming that the neutron source is uniform in lethargy within a given fine group. Flux calculations in heterogeneous geometry are performed using the collision probability method.

Self-shielded cross sections and matrices are condensed and smeared to provide effective cross sections and matrices in the user-required broad group scheme. The neutron balance is preserved in ECCO after condensation and smearing. The effective cross sections and matrices produced by ECCO are subsequently used in full-core ERANOS calculations.

The user can chain several calculation steps to produce design (less accurate, faster) or reference (more accurate, slower) calculations, or even to use specific capabilities, according to the needs of a given study.

3.2.7. *ERANOS*

The European Reactor ANalysis Optimised calculation System (ERANOS) [12], has been developed and validated to provide a suitable basis for reliable neutronics calculations of current as well as advanced fast reactor cores. It consists of data libraries, deterministic codes and calculation procedures which have been developed within the European Collaboration on Fast Reactors over the past 20 years to answer the needs of both industrial and R&D organisations.

The main contents of the ERANOS package are nuclear data libraries (multi-group cross sections), a cell and lattice code (ECCO), reactor flux solvers (diffusion, Sn transport, nodal variational transport), a burn-up module, various processing modules (material and neutron balance, breeding gains, etc.), tools related to perturbation theory and sensitivity analysis, core follow-up modules, a fine burn-up analysis subset (mass balances, activities, decay heat, dose rates). Coupled neutron/gamma calculations are also possible using specific libraries.

3.2.8. *EVOLCODE*

EVOLCODE 2.0 [16] is a combined neutronics and burn-up evolution simulation system. Developed at CIEMAT, it is aimed at describing the burn-up evolution of current and future reactors in any range of operations and providing detailed spatial distribution and time evolution of the isotopic composition of fuels and activated materials. The code can estimate a great variety of nuclear reactor parameters. In particular, the capability of making simulations of isotopic evolution in the fuel for nuclear systems with very diverse characteristics and reaching long fuel burn-ups was focused. For these reasons, the present version of the EVOLCODE system is based upon the MCNP/X code [17,18] for the neutronics transport simulation and the ORIGEN code for the depletion calculations. Any version of these codes can be implemented in EVOLCODE 2.0. Alternatively, the user has the option of using the ACAB code for depletion instead of ORIGEN to gain additional capabilities.

Burn-up problems are solved by EVOLCODE 2.0 using a time interval method consisting of the successive calculation of first the neutron flux for fixed material densities at a given time and later the depletion of these densities, using the hypothesis of constant neutron flux. Given that the validity of the hypotheses of constant properties is limited in the irradiation time, several calculations are needed to solve the system for the whole irradiation period.

3.2.9. ***KENO***

KENO [19] is a 3D Monte Carlo program developed and maintained for use as part of the SCALE code package [20] for criticality safety analyses. It can be used as part of a sequence or as a standalone program. Its features include the ability to calculate the problem-dependent neutron lifetime and generation time, energy-dependent leakages, fission densities, and energy- and region-dependent absorptions, fission, and fluxes. A problem can be solved using either multi-group cross sections or continuous energy cross sections.

3.2.10. ***MCNP/X***

MCNP/X [18,17,21] is a multipurpose Monte Carlo radiation transport code that tracks numerous particles (neutron, photon, electron, etc., and coupled transport) at different energies in a general 3D geometry. This code has been developed at Los Alamos National Laboratory (LANL) over nearly sixty years. Specific areas of application include, but are not limited to, radiological protection and dosimetry, radiation shielding, radiography, medical physics, nuclear criticality safety, detector design and analysis, nuclear oil well logging, accelerator target design, fission and fusion reactor design, decontamination and decommissioning.

Pointwise cross-section data typically are used, although group-wise data also are available. For neutrons, all reactions given in a particular cross-section evaluation are accounted for. Thermal neutrons are described by both the free gas and S(α,β) models. For photons, the code accounts for incoherent and coherent scattering, the possibility of fluorescent emission after photoelectric absorption, absorption in pair production with local emission of annihilation radiation, and bremsstrahlung. Important standard features that make MCNP very versatile and easy to use include a powerful general source, criticality source and surface source, both geometry and output tally plotters, a rich collection of variance reduction techniques, a flexible tally structure, and an extensive collection of cross-section data.

3.2.11. MCODE

MCODE Version 2.2 is a linkage program that combines the continuous-energy Monte Carlo code, MCNP-4C, and the one-group depletion code, ORIGEN2, to perform burn-up calculations for nuclear fission reactor systems [22]. MCNP is used as the advanced physics modelling tool providing the neutron flux solution and detailed reaction rates in the predefined spatial burn-up zones. ORIGEN, in turn, carries out multi-nuclide depletion calculations in each region and updates the corresponding material composition in the MCNP model. The MCNP/ORIGEN coupling follows the predictor-corrector approach.

As a standalone code written in ANSI C, MCODE-2.2 is portable between Windows personal computers (PC's) and UNIX/Linux machines. There are three utility programs in MCODE-2.2: (1) preproc to pre-process MCNP/ORIGEN libraries; (2) mcode as the console to run steady-state burn-up/decay calculations; and (3) mcodeout to collect results from scattered data files under temporary directory and produce a detailed output. Further, there is an auxiliary program called mcnpxs, which is to prepare a nuclide summary table of continuous energy MCNP cross-section libraries. The routine usage of MCODE-2.2 only requires a tandem running of the three utility codes. The auxiliary code, mcnpxs, is intended to help users during the code installation/setup. Compared to other similar linkage codes, MCODE-2.2 emphasises functionality, versatility and usability.

3.2.12. *NEWT*

The New ESC-based weighting transport code (NEWT) [23] is a multi-group discrete-ordinates radiation transport computer code with flexible meshing capabilities that allow two-dimensional 2D neutron transport calculations using complex geometric models. It is included in the SCALE code package. The differencing scheme employed by NEWT, the extended step characteristic approach, allows a computational mesh based on arbitrary polygons. Such a mesh can be used to closely approximate curved or irregular surfaces to provide the capability to model problems that were formerly difficult or impractical to model directly with discrete-ordinates methods. Automated grid generation capabilities provide a simplified user input specification in which elementary bodies can be defined and placed within a problem domain. NEWT can be used for eigenvalue, critical-buckling correction and source calculations, and it can be used to prepare collapsed weighted cross sections in AMPX working library format. Like other SCALE modules, NEWT can be run as a standalone module or as part of a SCALE sequence.

3.2.13. *ORIGEN2/S/ARP*

ORIGEN2 [24] is a versatile point-depletion and radioactive-decay computer code for use in simulating nuclear fuel cycles and calculating the nuclide compositions and characteristics of materials contained therein. It was developed at the Oak Ridge National Laboratory (ORNL) and distributed worldwide beginning in the early 1970s. Included in ORIGEN2 are provisions for incorporating data generated by more sophisticated reactor physics codes, a free-format input, and a highly flexible and controllable output; with these features, ORIGEN2 has the capability for simulating a wide variety of fuel cycle flow sheets.

The decay, cross-section, fission product yield and photon emission databases employed by ORIGEN2 have been extensively updated, and the list of reactors that can be simulated includes pressurised water reactors, boiling water reactors, liquid-metal fast breeder reactors and Canada deuterium uranium reactors.

ORIGEN-ARP [25] is a SCALE depletion analysis sequence used to perform point-depletion calculations with the ORIGEN-S code [26] using problem-dependent cross sections. Problem-dependent cross-section libraries are generated using the automatic rapid processing (ARP) module using an interpolation algorithm that operates on pre-generated libraries created for a range of fuel properties and operating conditions. Methods are provided in SCALE to generate these libraries using one-, two- and three-dimensional transport codes.

3.2.14. SERPENT

SERPENT [27] is a multipurpose three-dimensional continuous-energy Monte Carlo particle transport code that has been developed at VTT since 2004. The code is capable of reactor physics modelling, multi-physics simulations and neutron, photon and coupled neutron/photon transport calculations for various purposes.

The basic geometry description in SERPENT relies on a universe-based constructive solid geometry (CSG) model, which allows the description of practically any two- or three-dimensional fuel or reactor configuration. Complicated irregular systems can be modelled using CAD- and unstructured mesh-based geometry types.

Particle transport in SERPENT is based on the combination of conventional surface-tracking and the Woodcock delta-tracking method. A weight-window based variance

reduction scheme supports the MCNP WWINP mesh format. SERPENT also has a built-in importance solver based on the response matrix method.

SERPENT has built-in state-of-the-art routines for depletion calculations and no coupling to external solvers is needed. The primary method used for solving the Bateman depletion equations is based on the Chebyshev Rational Approximation Method (CRAM), an advanced matrix exponential solution developed for SERPENT at VTT.

Photon physics routines in SERPENT [28] cover the basic interactions from 1 keV to 100 MeV. In SERPENT 2.1.30 and prior, photoatomic reaction cross sections, which determine mean free paths and reaction probabilities, are read from a user-defined A Compact ENDF (ACE) format library, whereas form factors, incoherent scattering functions, fluorescence data and photoionisation shell probabilities are from ENDF/B-VII.1, which is derived from the Evaluated Photon Data Library (EPDL) EPDL97 and Evaluated Atomic Data Library (EADL91) [29]. SERPENT also uses Compton profile data [30] for Doppler broadening of Compton-scattered photons. The photon source generation can be obtained from a radioactive decay source or combined with a burn-up or activation calculation performed using built-in automated calculation routines.

3.2.15. *TRIPOLI*

TRIPOLI-4® [31] solves the linear Boltzmann equation for neutrons, photons, electrons and positrons, with the Monte Carlo method, in any 3D geometry. TRIPOLI-4® has its native geometry package, allowing for both a pure surface-based representation and a combinatorial representation with predefined shapes and Boolean operators (any combination of these two kinds of representations can be adopted).

3.3. Description of the nuclear data libraries

Participants used different nuclear data libraries to obtain the dose rate. These nuclear data libraries, shown in Table 3.1, can be divided into neutron cross-section libraries for the depletion step and photon libraries for the final photon transport.

The neutron cross-section libraries contain several data types, including neutron and proton interaction data, radioactive decay data, fission yield data, and thermal scattering law data. In this work, participants have mainly chosen the JEFF Nuclear Data Library (developed within the NEA) and the ENDF/B Nuclear Data Library, which is co-ordinated by the Cross Section Evaluation Working Group (CSEWG)[2].

For the case of the JEFF library, different versions have been used, including JEFF-3.1 [32], JEFF-3.1.1 [33] , JEFF-3.1.2 [34] (these three versions with incident neutron data for 381 isotopes) and JEFF-3.2 [35] (with incident neutron data for 472 nuclides or elements). Different versions of the ENDF/B library have also been used, including versions ENDF/B-V [36] and ENDF/B-VII.0 [37], with information about 295 and 393 targets or materials, respectively.

The Evaluated Photon Data Library [38], 1997 version (EPDL97), and derived libraries were the most frequently chosen photon library in this work. It was designed for use in photon transport calculations at Lawrence Livermore National Laboratory (LLNL). This library includes photon interaction data for all elements with an atomic number between Z = 1 (hydrogen) and 100 (fermium), including photoionisation, photoexcitation, coherent

[2] Co-operative effort by Canada and the United States.

and incoherent scattering, and pair and triplet production cross sections. For use in applications, data is provided for all elements over the energy range of 1 eV to 100 GeV.

The photoatomic data library MCPLIB04 [39] contains a set of data taken from ENDF/B-VI release 8, including cross-section, form factor, scattering function and fluorescence data. These data are derived from EPDL97. The photoatomic data library MCPLIB84 [40] is identical to the MCPLIB04 data except for the array given for the Compton broadening, where it uses a cumulative distribution function instead of a probability distribution function, with impact only on the calculations of detector efficiency curves for photon measurements, which are not applicable to this work.

Finally, another library used by the participants is the TALYS Evaluated Nuclear Data Library (TENDL) [41], created from the nuclear model code TALYS [42]. This library consists of a complete set of nuclear reaction data for incident neutrons, photons and other particles for 2 430 isotopes.

References

[1] ANS (1977), *American National Standard for Neutron and Gamma-Ray Flux-to-Dose-Rate Factors*, ANSI/ANS-6.1.1 (1977), United States.

[2] ANS (1991), *American National Standard for Neutron and Gamma-Ray Flux-to-Dose-Rate Factors*, ANSI-ANS-6.1.1 (1991), United States.

[3] ICRP (1996), *Conversion Coefficients for use in Radiological Protection against External Radiation*, ICRP Publication 74, https://doi.org/10.1016/S0146-6453(96)90001-9.

[4] NEA (2008), *ACAB-2008: Activation Abacus Code V2008*, NEA Data Bank NEA-1839.

[5] Croff, A.G. (1980), *A User's Manual for the ORIGEN2 Computer Code*, ORNL/TM-7175.

[6] Stankovskiy, A. and G. Van Den Eynde, (2012), "Advanced method for calculations of core burnup, activation of structural materials, and spallation products accumulation in accelerator-driven systems", *Sci. Technol. Nucl. Install.* Vol. 2012, https://doi.org/10.1155/2012/545103.

[7] Hairer, E. and G. Wanner, (1996), *Solving Ordinary Differential Equations. Stiff and Differential-Algebraic Problems*, Vol. 14 of Springer Series in Computational Mathematics, 2nd edition, ISBN 978-3-642-05221-7.

[8] LANL (2008), *MCNP - A General Monte Carlo N-Particle Transport Code*, Version 5, Vol. 2: User's Guide, X-5 Monte Carlo Team, Los Alamos National Laboratory, LA-CP-03-0245., United States.

[9] Sanchez, R.,I. Zmijarevic, M. Coste-Delclaux, E. Masiello, S. Santandrea, E. Martinolli, L Villate, N. Schwartz and N. Guler, (2010), "APOLLO-2 year 2010", *Nucl. Eng. Technol*. Vol. 42, http://dx.doi.org/10.5516/NET.2010.42.5.474.

[10] Santamarina, A., D. Bernard, P. Blaise and P. Leconte (2009), "APOLLO2.8: A validated code package for PWR neutronics calculations", Advances in Nuclear Fuel Management IV (ANFM 2009), Hilton Head Island, South Carolina, United States.

[11] Palmiotti, G., J.M. Rieunier, C. Gho and M. Salvatores (1990), "Optimized two-dimensional Sn transport (BISTRO)", *Nucl. Sci. Eng.* Vol. 104, 26, pp. 26-33, https://doi.org/10.13182/NSE90-1.

[12] Doriath, J.Y., C.W. McCallien, E. Kiefhaber, U. Wehmann and J.M. Rieunier, (1993), "ERANOS1: The Advanced European System of Codes for Reactor Physics Analysis", *Int. Conf. on Mathematical Methods and Supercomputing for Nuclear Application*, Karlsruhe, Germany.

[13] San-Felice, L., R. Eschbach and P Bourdot (2013), "Experimental validation of the DARWIN2.3 package for fuel cycle applications", *Nucl. Technol.*, Vol. 184, pp. 217-232, https://doi.org/10.13182/NT12-121.

[14] Tsilanizara, A., C.M. Diop, B. Nimal, M. Detoc, L. Lunéville, M. Chiron, T.D. Huynh, I. Brésard,

M. Eid, J.C. Klein, B. Roque, P. Marimbeau, C. Garzenne, J.M. Parize and C. Vergne (2000), "DARWIN: An evolution code system for a large range of applications", *Nucl. Sci. Technol.* Vol. 37, pp. 845–849, http://dx.doi.org/10.1080/00223131.2000.10875009.

[15] Rimpault, R. (1995), "Algorithmic features of the ECCO cell code for treating heterogeneous reactor subassemblies", *Int. Topical Meeting on Reactor Physics and Computations*, Portland, OR, United States, 30 April-4 May.

[16] Alvarez-Velarde F., E.M. González-Romero and I.M. Rodríguez (2014), "Validation of the burnup code EVOLCODE 2.0 with PWR experimental data and with a sensitivity/uncertainty analysis", *Annals of Nuclear Energy* Vol. 73, pp. 175–188, Elsevier, Amsterdam, https://doi.org/10.1016/j.anucene.2014.06.049.

[17] Pelowitz, D.B. (2011), *MCNPX User's Manual*, Version 2.7.0. LA-CP-11-00438, Los Alamos National Laboratory, United States.

[18] Pelowitz, D.B (2014), *MCNP6 User's Manual*, Code Version 6.1.1beta, LA-CP-14-00745, Los Alamos National Laboratory, United States.

[19] Petrie, L.M., N.F. Landers, D.F. Hollenbach, B.T. Rearden, M.E. Dunn and S. Goluoglu (2009), *KENO V.a: An Improved Monte Carlo Criticality Program*, SCALE 6 Manual, Vol. II, Sect. F11, ORNL/TM-2005/39, Oak Ridge National Laboratory, United States.

[20] Rearden, B.T. and M.A. Jessee (2016), *SCALE Code System*, ORNL/TM-2005/39, Version 6.2.1, Oak Ridge National Laboratory, United States.

[21] Pelowitz, D.B. (2011), *MCNP6-TM User's Manual*, LA-CP-11-01708, December 2011, Los Alamos National Laboratory, United States.

[22] Xu, Z. and P. Hejzlar (2006), *MCODE, Version 2.2 – An MCNP-ORIGEN Depletion Program*, MIT NFC-TR-104, Massachusetts Institute of Technology, United States.

[23] Jessee, M.A. and M.D. DeHart (2011), *NEWT: A New Transport Algorithm for Two-dimensional Discrete-ordinates Analysis in Non-orthogonal Geometries*, SCALE 6.1 Manual, Sect. F21, ORNL/TM-2005/39, Oak Ridge National Laboratory, United States.

[24] Croff, A.G. (1983), "ORIGEN2: A versatile computer code for calculating the nuclide compositions and characteristics of nuclear materials", *Nucl. Technol.* Vol. 62, pp. 335-352, https://doi.org/10.13182/NT83-1.

[25] Gault I.C., S.M. Bowman and J.E. Horwedel (2011), *ORIGEN-ARP: Automatic Rapid Processing for Spent Fuel Depletion, Decay, and Source Term Analysis, SCALE 6.1 Manual*, Sect. D1, ORNL/TM-2005/39, Oak Ridge National Laboratory, United States.

[26] Hermann O.W. and R.M. Westfall (1984), *ORIGEN-S: SCALE System Module to Calculate Fuel Depletion, Actinide Transmutation, Fission Product Buildup and Decay, and Associated Radiation Source Terms*, NUREG/CR--0200-VOL.2, Nuclear Regulatory Commission, United States.

[27] Leppänen, J., M. Pusa, T. Viitanen, V. Valtavirta and T. Kaltiasenaho (2015), "The Serpent Monte Carlo code: Status, development and applications in 2013", *Annals of Nuclear Energy*, Vol. 82, pp. 142–150, Elsevier, Amsterdam.

[28] Kaltiaisenaho, T. (2016), *Implementing a Photon Physics Model in Serpent 2*, M.Sc. Thesis, Aalto University, Finland.

[29] Perkins, S.T., M.H. Chen, D.E. Cullen and J.H. Hubbell (1991), *Tables and Graphs of Atomic Subshell and Relaxation Data Derived from the LLNL Evaluated Atomic Data Library (EADL), Z=1-100*, UCRL-50400, Vol. 30, Lawrence Livermore National Laboratory, United States.

[30] Biggs, F., L.B. Mendelsohn and J.B. Mann (1975), "Hartree-Fock Compton profiles for the elements", *Atomic and Nuclear Data Tables*, Vol. 16, pp. 201-309, Elsevier, Amsterdam, https://doi.org/10.1016/0092-640X(75)90030-3.

[31] Brun, E., F. Damian, C.M. Diop, E. Dumonteil, F.X. Hugot, C. Jouanne, Y.K. Lee, F. Malvagi, A. Mazzolo, O. Petit, J.C. Trama, T. Visonneau and A. Zoia (2015), "Tripoli-4®, CEA, EDF and AREVA reference Monte Carlo code", *Annals of Nuclear Energy*, Vol.82, pp. 151-160, Elsevier, Amsterdam, https://doi.org/10.1016/j.anucene.2014.07.053.

[32] NEA (2006), *The JEFF-3.1 Nuclear Data Library. JEFF Report 21*, OECD Publishing, Paris, www.oecd-nea.org/dbdata/nds_jefreports/jefreport-21/jeff21.pdf.

[33] NEA (2009), *The JEFF-3.1.1 nuclear data library, JEFF Report 22*, OECD Publishing, Paris, www.oecd-nea.org/upload/docs/application/pdf/2020-08/jefreport-22.pdf.

[34] Koning, A.J., E. Bauge, C.J. Dean, E. Dupont, U. Fischer, R.A. Forrest, R. Jacqmin, H. Leeb, M.A. Kellett, R.W. Mills, C. Nordborg, M. Pescarini, Y. Rugama and P. Rullhusen (2011), "Status of the JEFF Nuclear Data Library", *Journal of the Korean Physical Society* 59 (2), pp. 1057-1062, doi: 10.3938/jkps.59.1057.

[35] NEA (2014), *JEFF-3.2 Evaluated Data Library – Neutron data*, OECD Publishing, Paris, www.oecd-nea.org/dbforms/data/eva/evatapes/jeff_32/.

[36] Kinsey, R. (1979), *ENDF-201, ENDF/B-VI summary documentation*, BNL-NCS-17541 (ENDF-201), 3rd Edition (ENDFA-V), UC-80, Brookhaven National Laboratory, United States.

[37] Chadwick, M.B. et al. (2006), "ENDF/B-VII.0: Next generation evaluated nuclear data library for nuclear science and technology", *Nucl. Data Sheets*, Vol. 107, pp. 2931–3060.

[38] Cullen, D.E., J.H. Hubbell and L. Kissel (1997), *EPDL97: The Evaluated Photon Data Library*, '97 Version, *UCRL-LR-50400* Vol. 6, Rev. 5, Lawrence Livermore National Laboratory, United States, https://doi.org/10.2172/295438.

[39] White, M.C. (2003), *Photoatomic Data Library MCPLIB04: A New Photoatomic Library based on Data from ENDF/B-VI Release 8*, LA-UR-03-1019, Los Alamos National Laboratory, United States.

[40] White, M.C. (2012), *Further Notes on MCNPLIB03/04 and New MCPLIB63/84 Compton Broadening Data for All Versions of MCNP5*, LA-UR-12-00018, Los Alamos National Laboratory, United States.

[41] Koning, A.J. and D. Rochman (2012), "Modern nuclear data evaluation with the TALYS code system", *Nucl. Data Sheets*, Vol. 113, pp. 2841-2934, https://doi.org/10.1016/j.nds.2012.11.002.

[42] Koning, A.J., M.C. Duijvestijn and S. Hilaire (2007), "TALYS-1.0", *International Conference on Nuclear Data for Science and Technology*, Nice, France.

4. Verification step

This chapter is a summary of the different contributions. More details about each participant's contribution can be found in Appendix A.

4.1. Abstract

A code-to-code benchmark comparing nuclide masses, photon release rates and gamma dose rates at a 1 m distance from a PWR UOX and PWR MOX was conducted with nine participants. The benchmark included 46/20 HM nuclides and 30/8 FPs at discharge/30 years after discharge. The agreement between nuclide masses was good, especially for the examined FPs. The largest discrepancies between participants occurred in some HM nuclides with small concentrations. Gamma dose rates were calculated at 3.7 and 30 years after discharge using two different photon flux-to-dose rate conversion factors. The agreement between participants was quite good with relative standard deviations (RSD) from 7 to 15%.

4.2. Introduction

The purpose of the code-to-code benchmark is to verify modern calculation methods and to examine the self-protection properties of spent PWR UOX and PWR MOX fuel after 30 years of cooling. The self-protection dose rate is considered by the IAEA and US NRC to be 1 Sv/h at 1 m from the assembly [1]. The benchmark includes a comparison of a fixed set of HM and FP masses at discharge and 30 years after discharge, total gamma release rates, and calculated equivalent dose rates (EDR) 30 and 3.7 years after discharge. These values are reported for each participant along with the average of all participants ($\bar{x}$), standard deviation (SD) and the RSD. The RSD indicates a degree of consistency between the results calculated by the participants. A small RSD indicates good agreement and a big RSD indicates poor agreement.

$$\bar{x} = \frac{\sum_{n=1}^{N} x_n}{N}$$

$$SD = \sqrt{\frac{\sum_{n=1}^{N}(x_n - \bar{x})^2}{N-1}}$$

$$RDS = \frac{SD}{\bar{x}} \times 100\ \%$$

Two different conversion factor models were used in the study to convert the calculated photon flux [photon/cm^2-s] into dose rates [Sv/h]: a conversion factor from the 1977 ANSI standard [2] and a conversion factor from the 1991 ANSI standard [3]. The conversion factors are presented in Figure 2.5. The figure indicates that the conversion factors are quite similar except in low energies (< 0.1 MeV). The 1977 conversion factor emphasises the low-energy region whereas the 1991 conversion factor gives it less weight than the higher energies.

4.3. Nuclide masses at discharge and after 30 years of decay

This section presents nuclide masses calculated for both PWR UOX and PWR MOX assemblies. The masses are presented as grams in the whole assembly of 469 kg of initial HM (UOX) or 454 kg of initial HM (MOX).

HM and FP masses for the UOX assembly are presented in Tables 4.1 to 4.4. The average values of all participants together with the RSD after 30 years of decay for the UOX assembly are also presented in Figures 4.1 and 4.2.

Generally, a quite good agreement was found in the calculated HM masses for the UOX assembly, with the RSDs remaining mostly below 30%. The RSDs for uranium and plutonium isotopes 30 years after discharge were below 11%. The RSD in the ^{238}U mass was 0.5 %. Large RSDs around 100% were found for ^{236M}Np, ^{236}Pu (at discharge), ^{244}Am, ^{249}Cf and ^{251}Cf. The largest RSD, over 250% was found in ^{252}Cf mass. All these nuclides had very small masses, which naturally makes their tracking more prone to errors.

Quite good agreement was found also in the calculated FP masses. The largest RSDs from 20 to 30% at discharge were found for ^{148}Pm, ^{149}Pm and ^{155}Gd. The largest RSDs in the masses of the nuclides studied after 30 years of decay were 13% for ^{154}Eu and 19% for ^{155}Eu. The RSDs of all other nuclides after 30 years of decay were less than 2.2%. The main contributor to the gamma dose rate after 30 years of decay is ^{137}Cs/^{137M}Ba (661.657 keV). The RSD of these nuclides was around 1%.

Table 4.1. UOX HM masses [g] at discharge

Nuclide	CEA	ANL	KIT	CNL	ENEA	ENEA	ENEA	ENEA	SCK CEN	VTT	ORANOTN	CIEMAT			
	APOLLO	CASMO-4E	ERANOS-ECCO	SERPENT	APOLLO	NEWT	SERPENT	KENO	ALEPH	SERPENT	ORIGEN-ARP	EVOLCODE	$\bar{x}$	SD	RSD [%]
U-234	8.29E+01	6.27E+01	7.87E+01	8.23E+01	8.14E+01	8.38E+01	8.31E+01	8.26E+01	8.26E+01	9.35E+01	8.21E+01	8.32E+01	**8.16E+01**	**6.60E+00**	**8.1**
U-235	3.82E+03	3.41E+03	3.41E+03	3.80E+03	3.69E+03	3.83E+03	3.64E+03	3.93E+03	3.66E+03	3.79E+03	3.81E+03	3.73E+03	3.71E+03	**1.53E+02**	**4.1**
U-236	1.80E+03	1.68E+03	1.85E+03	1.81E+03	1.80E+03	1.81E+03	1.81E+03	1.80E+03	1.83E+03	1.78E+03	1.80E+03	1.88E+03	1.80E+03	**4.63E+01**	**2.6**
U-237	5.84E+00	5.67E+00	6.69E+00	6.01E+00	5.49E+00	5.77E+00	5.81E+00	5.90E+00	6.04E+00	3.33E+00	6.01E+00	6.47E+00	4.97E+00	**5.69E+00**	**8.24E-01**	**14**
U-238	4.42E+05	4.35E+05	4.41E+05	4.43E+05	4.43E+05	4.42E+05	4.43E+05	4.42E+05	4.43E+05	4.42E+05	4.43E+05	4.43E+05	4.43E+05	**4.42E+05**	**2.18E+03**	**0.49**
Np-236	1.41E-04	7.18E-04		7.76E-04	5.24E-04	1.62E-04	6.88E-04	1.76E-04	7.91E-05	4.58E-04	5.81E-04	8.18E-05	5.49E-04	**4.11E-04**	**2.66E-04**	**65**
Np-236m	7.28E-06			3.20E-09		1.06E-05	2.86E-09	1.11E-05	4.05E-06	1.84E-06	5.23E-09	4.01E-06		**4.32E-06**	**4.42E-06**	**102**
Np-237	1.84E+02	1.72E+02	2.08E+02	1.90E+02	1.75E+02	1.85E+02	1.84E+02	1.90E+02	1.88E+02	1.96E+02	1.87E+02	2.00E+02	1.86E+02	**1.88E+02**	**9.66E+00**	**5.1**
Np-238	8.22E-01	6.19E-01	9.76E-01	8.26E-01	7.83E-01	7.80E-01	7.78E-01	8.00E-01	8.42E-01	4.96E-01	8.38E-01	8.93E-01	7.00E-01	**7.81E-01**	**1.21E-01**	**15**
Np-239	5.93E+01	4.53E+01	6.63E+01	6.09E+01	5.92E+01	6.01E+01	5.94E+01	6.11E+01	5.90E+01	3.12E+01	6.04E+01	5.70E+01	4.91E+01	**5.60E+01**	**9.19E+00**	**16**
Pu-236	4.71E-04			1.27E-05	4.50E-04	6.96E-04	1.12E-05	7.31E-04	2.67E-04	2.15E-04	3.40E-06	2.78E-04	2.81E-06	**2.85E-04**	**2.73E-04**	**96**
Pu-237	1.35E-04			1.81E-04	1.29E-04	1.79E-04	1.56E-04	1.93E-04	1.55E-04	1.26E-04	1.41E-04	1.59E-04	1.23E-04	**1.52E-04**	**2.41E-05**	**16**
Pu-238	6.04E+01	5.58E+01	7.13E+01	5.98E+01	5.80E+01	5.73E+01	5.49E+01	5.97E+01	6.00E+01	7.67E+01	6.14E+01	6.51E+01	6.22E+01	**6.17E+01**	**6.16E+00**	**10**
Pu-239	2.55E+03	2.36E+03	2.71E+03	2.62E+03	2.51E+03	2.65E+03	2.45E+03	2.80E+03	2.52E+03	2.44E+03	2.62E+03	2.45E+03	2.50E+03	**2.55E+03**	**1.24E+02**	**4.9**
Pu-240	1.10E+03	9.91E+02	1.18E+03	1.09E+03	1.10E+03	1.11E+03	1.11E+03	1.13E+03	1.10E+03	1.01E+03	1.10E+03	9.69E+02	1.09E+03	**1.08E+03**	**5.80E+01**	**5.4**
Pu-241	6.35E+02	5.89E+02	7.02E+02	6.47E+02	6.32E+02	6.44E+02	5.98E+02	6.71E+02	6.06E+02	6.59E+02	6.45E+02	6.97E+02	6.13E+02	**6.42E+02**	**3.52E+01**	**5.5**
Pu-242	2.44E+02	2.28E+02	2.85E+02	2.37E+02	2.49E+02	2.35E+02	2.33E+02	2.33E+02	2.41E+02	2.71E+02	2.42E+02	2.58E+02	2.40E+02	**2.46E+02**	**1.66E+01**	**6.7**
Pu-243	8.98E-02	6.08E-02	1.14E-01	9.96E-02	8.77E-02	9.74E-02	9.29E-02	9.78E-02	9.88E-02	5.99E-02	9.03E-02	1.14E-01	7.33E-02	**9.05E-02**	**1.71E-02**	**19**
Pu-244	1.46E-02		1.29E-02	1.56E-02	8.99E-03	1.52E-02	1.40E-02	1.54E-02	9.72E-03	9.61E-03	1.47E-02	1.03E-02	7.32E-03	**1.24E-02**	**2.97E-03**	**24**
Am-241	1.18E+01	1.44E+01	1.25E+01	1.30E+01	1.17E+01	1.31E+01	1.20E+01	1.37E+01	1.22E+01	2.02E+01	1.19E+01	1.35E+01	1.27E+01	**1.33E+01**	**2.23E+00**	**17**
Am-242	5.09E-02	4.63E-02	5.85E-02	5.07E-02	5.06E-02	4.90E-02	4.73E-02	5.00E-02	4.36E-02	5.65E-02	5.30E-02	4.85E-02	5.13E-02	**5.05E-02**	**3.99E-03**	**7.9**
Am-242m	2.39E-01	1.97E-01	1.99E-01	1.43E-01	2.36E-01	1.82E-01	1.24E-01	1.96E-01	2.44E-01	3.79E-01	1.51E-01	2.78E-01	2.69E-01	**2.18E-01**	**6.78E-02**	**31**
Am-243	4.52E+01	3.91E+01	5.70E+01	4.95E+01	4.48E+01	4.94E+01	4.62E+01	4.97E+01	5.08E+01	5.70E+01	4.52E+01	5.45E+01	4.43E+01	**4.87E+01**	**5.27E+00**	**11**
Am-244	3.69E-03	4.19E-02		4.16E-03	5.84E-02	4.05E-03	3.69E-03	4.12E-03	6.18E-02	2.98E-02	3.72E-03	6.86E-02	4.80E-02	**2.77E-02**	**2.66E-02**	**96**
Cm-242	5.54E+00	5.59E+00	6.50E+00	5.42E+00	5.60E+00	5.26E+00	5.03E+00	5.36E+00	4.63E+00	8.31E+00	5.78E+00	4.98E+00	6.16E+00	**5.70E+00**	**9.23E-01**	**16**
Cm-243	1.13E-01	1.21E-01	1.43E-01	1.12E-01	1.15E-01	1.08E-01	1.00E-01	1.12E-01	1.16E-01	2.29E-01	1.16E-01	1.18E-01	1.57E-01	**1.28E-01**	**3.39E-02**	**27**
Cm-244	1.35E+01	1.20E+01	1.95E+01	1.51E+01	1.36E+01	1.49E+01	1.32E+01	1.53E+01	1.44E+01	1.92E+01	1.36E+01	1.48E+01	1.29E+01	**1.48E+01**	**2.25E+00**	**15**
Cm-245	6.91E-01	5.55E-01	1.01E+00	9.00E-01	6.94E-01	8.38E-01	7.26E-01	8.99E-01	5.37E-01	1.19E+00	7.10E-01	5.24E-01	7.26E-01	**7.69E-01**	**1.94E-01**	**25**
Cm-246	5.88E-02	5.22E-02	9.23E-02	7.51E-02	6.05E-02	7.03E-02	6.39E-02	7.19E-02	4.70E-02	1.07E-01	5.87E-02	4.19E-02	5.93E-02	**6.61E-02**	**1.78E-02**	**27**
Cm-247	6.35E-04	4.51E-04	1.13E-03	8.08E-04	6.52E-04	7.50E-04	6.49E-04	7.94E-04	4.45E-04	1.26E-03	6.51E-04	3.75E-04	6.05E-04	**7.08E-04**	**2.54E-04**	**36**
Cm-248	3.31E-05	2.34E-05	6.65E-05	4.53E-05	3.41E-05	4.14E-05	3.47E-05	4.44E-05	2.40E-05	7.53E-05	3.37E-05	2.00E-05	3.06E-05	**3.90E-05**	**1.62E-05**	**42**
Bk-249	3.36E-07	3.23E-10	5.66E-07	8.09E-07	3.42E-07	4.20E-07	3.25E-07	4.74E-07	2.44E-07	7.82E-07	6.10E-07	1.94E-07	3.12E-07	**4.16E-07**	**2.30E-07**	**55**
Cf-249	3.05E-08	2.40E-07	2.10E-07	1.02E-07	3.09E-08	3.82E-08	2.78E-08	4.37E-08	2.17E-08	1.34E-07	7.91E-08	1.70E-08	3.36E-08	**7.76E-08**	**7.41E-08**	**96**
Cf-250	1.81E-07	3.40E-10	3.56E-07	4.96E-18	1.84E-07	1.73E-07	1.46E-07	1.86E-07	5.54E-08	4.73E-07		4.28E-08	1.69E-07	**1.64E-07**	**1.39E-07**	**85**
Cf-251	3.89E-08		1.92E-07	1.48E-13	4.03E-08	6.67E-08	5.26E-08	7.39E-08	2.96E-08	1.15E-07	1.60E-13	2.34E-08	3.71E-08	**5.58E-08**	**5.33E-08**	**96**
Cf-252	1.93E-08		1.09E-06		2.07E-08	3.33E-08	2.73E-08	3.53E-08	1.53E-08	6.38E-08		1.16E-08	1.88E-08	**1.33E-07**	**3.35E-07**	**252**
Total	4.53E+05	4.44E+05	4.52E+05	4.53E+05	4.53E+05	4.53E+05	4.53E+05	4.53E+05	4.53E+05	4.52E+05	4.53E+05	4.53E+05	4.53E+05	4.52E+05	2.43E+03	0.54

Table 4.2. UOX FP masses [g] at discharge

Nuclide	CEA	ANL	KIT	CNL	ENEA	ENEA	ENEA	ENEA	SCK CEN	VTT	ORANO TN	CIEMAT	$\bar{x}$	SD	RSD [%]
	APOLLO	CASMO-4E	ERANOS-ECCO	SERPENT	APOLLO	NEWT	SERPENT	KENO	ORIGEN-ARP	ALEPH	SERPENT	ORIGEN-ARP	EVOLCODE			
Kr-83	1.88E+01	1.84E+01	1.84E+01	1.94E+01	1.87E+01	1.92E+01	1.94E+01	1.92E+01	1.92E+01	1.94E+01	1.93E+01	1.93E+01	2.04E+01	1.92E+01	5.06E-01	2.6
Rh-103	2.05E+02	1.95E+02	1.90E+02	2.03E+02	2.05E+02	2.05E+02	2.03E+02	2.05E+02	2.04E+02	2.13E+02	2.06E+02	2.04E+02	2.04E+02	2.03E+02	5.52E+00	2.7
Rh-105	8.38E-01	6.56E-01		8.04E-01	8.45E-01	7.66E-01	7.91E-01	7.67E-01	7.55E-01	4.56E-01	8.16E-01	7.89E-01	6.60E-01	7.45E-01	1.09E-01	15
Ag-109	3.64E+01	3.49E+01	4.30E+01	3.77E+01	3.67E+01	3.76E+01	3.70E+01	3.76E+01	3.67E+01	4.30E+01	4.17E+01	3.74E+01	4.40E+01	3.87E+01	3.03E+00	7.8
I-135	3.30E-01	2.56E-01	3.24E-01	3.39E-01	3.29E-01	3.36E-01	3.38E-01	3.36E-01	3.38E-01	1.72E-01	3.30E-01	3.33E-01	2.72E-01	3.10E-01	4.92E-02	16
Xe-131	1.98E+02	1.92E+02	1.85E+02	1.99E+02	1.92E+02	2.00E+02	2.01E+02	2.00E+02	1.96E+02	1.99E+02	1.97E+02	1.96E+02	1.99E+02	1.96E+02	4.51E+00	2.3
Xe-135	8.85E-02	7.78E-02	7.86E-02	9.23E-02	8.68E-02	9.22E-02	8.47E-02	9.26E-02	8.83E-02	7.65E-02	9.04E-02	9.07E-02	8.17E-02	8.62E-02	5.81E-03	6.7
Cs-133	5.14E+02	4.96E+02	5.07E+02	5.20E+02	5.15E+02	5.24E+02	5.22E+02	5.24E+02	5.28E+02	5.23E+02	5.14E+02	5.34E+02	5.12E+02	5.18E+02	9.90E+00	1.9
Cs-134	6.11E+01	6.18E+01	6.49E+01	6.27E+01	6.13E+01	6.15E+01	6.08E+01	6.15E+01	5.57E+01	5.76E+01	6.20E+01	5.73E+01	5.92E+01	6.06E+01	2.48E+00	4.1
Cs-135	1.28E+02	1.42E+02	1.15E+02	1.30E+02	1.26E+02	1.31E+02	1.23E+02	1.30E+02	1.33E+02	1.87E+02	1.29E+02	1.30E+02	1.45E+02	1.35E+02	1.74E+01	13
Cs-137	5.73E+02	5.55E+02	5.73E+02	5.75E+02	5.67E+02	5.72E+02	5.74E+02	5.72E+02	5.78E+02	5.74E+02	5.73E+02	5.80E+02	5.62E+02	5.71E+02	6.68E+00	1.2
Ba-137m	8.80E-05			8.83E-05	8.82E-05	8.82E-05	8.82E-05	8.82E-05	8.91E-05	8.83E-05	8.81E-05	8.94E-05	8.62E-05	8.82E-05	8.50E-07	1
Ba-140	1.43E+01	1.10E+01	1.38E+01	1.43E+01		1.42E+01	1.43E+01	1.42E+01	1.43E+01	7.46E+00	1.43E+01	1.42E+01	1.17E+01	1.32E+01	2.12E+00	16
La-140	1.93E+00	1.49E+00	1.88E+00	1.94E+00	1.93E+00	1.92E+00	1.94E+00	1.92E+00	1.94E+00	1.01E+00	1.94E+00	1.93E+00	1.59E+00	1.80E+00	2.78E-01	15
Nd-143	3.59E+02	3.51E+02	3.50E+02	3.62E+02	3.58E+02	3.63E+02	3.58E+02	3.63E+02	3.62E+02	3.62E+02	3.59E+02	3.65E+02	3.56E+02	3.59E+02	4.64E+00	1.3
Nd-145	3.14E+02	3.08E+02	3.05E+02	3.10E+02	3.15E+02	3.10E+02	3.11E+02	3.10E+02	3.15E+02	3.18E+02	3.15E+02	3.16E+02	3.12E+02	3.12E+02	3.55E+00	1.1
Nd-148	1.77E+02		1.71E+02	1.75E+02	1.77E+02	1.75E+02	1.74E+02	1.75E+02	1.73E+02	1.77E+02	1.75E+02	1.73E+02	1.70E+02	1.74E+02	2.23E+00	1.3
Pm-147	9.51E+01	8.18E+01	8.26E+01	9.29E+01	9.53E+01	9.22E+01	9.38E+01	9.42E+01	8.95E+01	8.18E+01	9.45E+01	8.95E+01	9.08E+01	9.03E+01	5.07E+00	5.6
Pm-148	7.80E-01	5.33E-01	7.22E-01	7.95E-01	7.75E-01	8.02E-01	7.92E-01	7.80E-01	6.53E-01	4.80E-01	7.91E-01	6.63E-01	1.19E+00	7.50E-01	1.68E-01	22
Pm-149	8.64E-01	7.36E-01	9.12E-01	8.66E-01	8.63E-01	8.51E-01	8.66E-01	8.43E-01	9.67E-01	4.00E-01	8.66E-01	9.81E-01	5.03E-01	8.09E-01	1.71E-01	21
Sm-147	2.38E+01	2.76E+01	2.11E+01	2.33E+01	2.39E+01	2.34E+01	2.37E+01	2.37E+01	2.31E+01	3.99E+01	2.35E+01	2.34E+01	2.77E+01	2.52E+01	4.75E+00	19
Sm-149	9.92E-01	1.02E+00	9.98E-01	1.08E+00	9.70E-01	1.08E+00	9.78E-01	1.07E+00	1.13E+00	8.76E-01	1.01E+00	1.19E+00	6.82E-01	1.01E+00	1.26E-01	13
Sm-150	1.39E+02	1.36E+02	1.38E+02	1.40E+02	1.39E+02	1.38E+02	1.39E+02	1.39E+02	1.45E+02	1.30E+02	1.39E+02	1.48E+02	1.09E+02	1.37E+02	9.41E+00	6.9
Sm-151	5.37E+00	5.90E+00	5.97E+00	5.47E+00	5.29E+00	5.61E+00	5.09E+00	5.45E+00	7.05E+00	5.46E+00	5.55E+00	7.37E+00	4.90E+00	5.73E+00	7.18E-01	13
Sm-152	5.06E+01	5.75E+01	5.01E+01	4.94E+01	5.13E+01	5.13E+01	5.05E+01	5.02E+01	6.11E+01	5.00E+01	5.04E+01	6.16E+01	4.92E+01	5.26E+01	4.42E+00	8.4
Eu-153	5.45E+01	5.57E+01	5.64E+01	5.44E+01	5.43E+01	5.49E+01	5.37E+01	5.42E+01	5.38E+01	5.58E+01	5.44E+01	5.51E+01	5.34E+01	5.47E+01	8.82E-01	16
Eu-154	1.12E+01	1.64E+01	1.06E+01	1.14E+01	1.11E+01	1.14E+01	1.07E+01	1.14E+01	1.06E+01	1.13E+01	1.12E+01	1.07E+01	1.08E+01	1.14E+01	1.51E+00	13
Eu-155	3.71E+00	2.26E+00	4.00E+00	3.74E+00	3.71E+00	3.75E+00	3.84E+00	3.74E+00	2.56E+00	3.68E+00	3.70E+00	2.53E+00	3.65E+00	3.45E+00	5.81E-01	17
Eu-156	2.59E+00	1.91E+00	2.98E+00	2.70E+00	2.61E+00	2.65E+00	2.69E+00	2.64E+00	2.59E+00	1.57E+00	2.65E+00	2.60E+00	2.24E+00	2.49E+00	3.75E-01	15
Gd-155	1.85E-02	1.53E-02	1.86E-02	1.89E-02	1.81E-02	1.88E-02	1.74E-02	1.88E-02	1.32E-02	3.60E-02	1.89E-02	1.39E-02	2.13E-02	1.90E-02	5.56E-03	29
Total	2.99E+03	2.75E+03	2.91E+03	3.00E+03	2.96E+03	3.00E+03	2.99E+03	3.00E+03	3.01E+03	3.06E+03	3.00E+03	3.03E+03	2.95E+03	2.97E+03	7.56E+01	2.5

Table 4.3. UOX HM masses [g] after 30 years of decay

Nuclide	CEA	ANL	KIT	CNL	ENEA	ENEA	ENEA	ENEA	SCK CEN	VTT	ORANO TN	CIEMAT			
	DARWIN	ORIGEN-II	ORIGEN	SERPENT	ORIGEN-S	ORIGEN-S	ORIGEN-S	ORIGEN-S	ORIGEN-ARP	ALEPH	SERPENT	ORIGEN-ARP	ACAB	$\bar{x}$	SD	RSD [%]
U-234	9.66E+01	7.55E+01	9.50E+01	9.60E+01	9.48E+01	9.69E+01	9.57E+01	9.57E+01	9.55E+01	1.00E+02	1.08E+02	9.68E+01	9.75E+01	9.57E+01	6.94E+00	7.3
U-235	3.82E+03	3.41E+03	3.41E+03	3.80E+03	3.70E+03	3.84E+03	3.65E+03	3.83E+03	3.66E+03	3.80E+03	3.81E+03	3.73E+03	3.71E+03	3.70E+03	1.45E+02	3.9
U-236	1.80E+03	1.68E+03	1.85E+03	1.81E+03	1.80E+03	1.81E+03	1.82E+03	1.81E+03	1.83E+03	1.78E+03	1.80E+03	1.88E+03	1.81E+03	1.81E+03	4.61E+01	2.5
U-237	4.64E-06	4.30E-06	5.13E-06	4.71E-06	4.60E-06	4.69E-06	4.35E-06	4.71E-06	4.31E-06	4.83E-06	4.72E-06	4.96E-06	4.49E-06	4.65E-06	2.45E-07	5.3
U-238	4.42E+05	4.35E+05	4.41E+05	4.43E+05	4.43E+05	4.42E+05	4.43E+05	4.42E+05	4.43E+05	4.42E+05	4.43E+05	4.43E+05	4.43E+05	4.42E+05	2.12E+03	0.48
Np-237	2.04E+02	1.91E+02	2.31E+02	2.11E+02	1.94E+02	2.06E+02	2.03E+02	2.06E+02	2.08E+02	2.15E+02	2.08E+02	2.22E+02	2.05E+02	2.08E+02	1.04E+01	5
Pu-238	5.25E+01	4.89E+01	6.22E+01	5.21E+01	5.08E+01	5.00E+01	4.79E+01	4.79E+01	5.17E+01	6.75E+01	5.37E+01	5.60E+01	5.45E+01	5.35E+01	5.68E+00	11
Pu-239	2.61E+03	2.40E+03	2.77E+03	2.68E+03	2.57E+03	2.71E+03	2.51E+03	2.73E+03	2.58E+03	2.47E+03	2.68E+03	2.50E+03	2.55E+03	2.60E+03	1.13E+02	4.3
Pu-240	1.11E+03	9.96E+02	1.19E+03	1.10E+03	1.10E+03	1.12E+03	1.11E+03	1.12E+03	1.11E+03	1.02E+03	1.11E+03	9.76E+02	1.09E+03	1.09E+03	5.77E+01	5.3
Pu-241	1.49E+02	1.39E+02	1.66E+02	1.51E+02	1.48E+02	1.50E+02	1.40E+02	1.51E+02	1.42E+02	1.54E+02	1.51E+02	1.64E+02	1.44E+02	1.50E+02	8.12E+00	5.4
Pu-242	2.43E+02	2.28E+02	2.85E+02	2.37E+02	2.49E+02	2.35E+02	2.33E+02	2.34E+02	2.41E+02	2.71E+02	2.42E+02	2.58E+02	2.40E+02	2.46E+02	1.64E+01	6.7
Am-241	4.83E+02	4.50E+02	5.33E+02	4.94E+02	4.82E+02	4.92E+02	4.57E+02	4.95E+02	4.62E+02	5.09E+02	4.91E+02	5.31E+02	4.68E+02	4.88E+02	2.57E+01	5.3
Am-242	2.66E-06	2.06E-06	2.08E-06	1.59E-06	2.63E-06	2.03E-06	1.34E-06	2.04E-06	2.72E-06	4.23E-06	1.68E-06	3.10E-06	2.99E-06	2.39E-06	7.74E-07	32
Am-242M	2.06E-01	1.72E-01	1.74E-01	1.23E-01	2.04E-01	1.57E-01	1.04E-01	1.58E-01	2.11E-01	3.27E-01	1.30E-01	2.40E-01	2.32E-01	1.87E-01	5.92E-02	32
Am-243	4.51E+01	3.91E+01	5.70E+01	4.95E+01	4.48E+01	4.93E+01	4.62E+01	4.85E+01	5.07E+01	5.69E+01	4.51E+01	5.44E+01	4.43E+01	4.85E+01	5.26E+00	11
Am-244	1.10E-17									4.20E-17			1.47E-17	2.26E-17	1.69E-17	75
Cm-244	4.26E+00	3.83E+00	6.19E+00	4.78E+00	4.32E+00	4.71E+00	4.18E+00	2.21E+00	4.59E+00	6.07E+00	4.28E+00	4.71E+00	4.09E+00	4.48E+00	9.83E-01	22
Cm-245	6.89E-01	5.53E-01	1.01E+00	8.98E-01	6.92E-01	8.36E-01	7.24E-01	3.99E-01	5.36E-01	1.19E+00	7.08E-01	5.23E-01	7.25E-01	7.29E-01	2.14E-01	29
Cf-251	3.80E-08	2.50E-08	1.88E-07	1.44E-13	3.94E-08	6.52E-08	5.18E-08	6.20E-08	2.89E-08	1.12E-07	1.57E-13	2.29E-08	3.63E-08	5.15E-08	5.03E-08	98
Cf-252	7.46E-12	5.08E-12	4.11E-10		7.98E-12	1.28E-11	1.05E-11	1.20E-11	5.87E-12	2.47E-11		4.47E-12	7.22E-12	4.63E-11	1.21E-10	262
Total	4.53E+05	4.45E+05	4.52E+05	4.53E+05	4.53E+05	4.53E+05	4.53E+05	4.53E+05	4.53E+05	4.53E+05	4.53E+05	4.53E+05	4.53E+05	4.52E+05	2.35E+03	0.52

Table 4.4. UOX FP masses [g] after 30 years of decay

Nuclide	CEA	ANL	KIT	CNL	ENEA	ENEA	ENEA	ENEA	SCK CEN	VTT	ORANO TN	CIEMAT	$\bar{x}$	SD	RSD [%]
	DARWIN	ORIGEN-II	ORIGEN	SERPENT	ORIGEN-S	ORIGEN-S	ORIGEN-S	ORIGEN-ARP	ALEPH	SERPENT	ORIGEN-ARP	ACAB			
Sr-90	1.19E+02		1.19E+02	1.21E+02	1.19E+02	1.21E+02	1.22E+02	1.20E+02	1.17E+02	1.19E+02	1.20E+02	1.19E+02	1.20E+02	1.48E+00	1.2
Y-90	3.02E-02		2.98E-02	3.08E-02	3.01E-02	3.07E-02	3.10E-02	3.12E-02	2.97E-02	3.02E-02	3.11E-02	3.03E-02	3.05E-02	5.00E-04	1.6
Cs-137	2.87E+02	2.77E+02	2.87E+02	2.88E+02	2.84E+02	2.86E+02	2.87E+02	2.89E+02	2.85E+02	2.87E+02	2.90E+02	2.81E+02	2.86E+02	3.42E+00	1.2
Ba-137m	4.37E-05	4.24E-05	4.38E-05	4.38E-05	4.34E-05	4.37E-05	4.39E-05	4.41E-05	4.34E-05	4.38E-05	4.43E-05	4.29E-05	4.36E-05	5.05E-07	1.2
Sm-154	1.79E+01		1.78E+01	1.80E+01	1.79E+01	1.79E+01	1.77E+01	1.72E+01		1.86E+01	1.74E+01	1.83E+01	1.79E+01	3.88E-01	2.2
Eu-153	5.49E+01	5.57E+01	5.71E+01	5.51E+01	5.43E+01	5.49E+01	5.37E+01	5.45E+01	5.55E+01	5.50E+01	5.58E+01	5.39E+01	5.50E+01	9.14E-01	1.7
Eu-154	9.99E-01	1.46E+00	9.45E-01	1.01E+00	9.89E-01	1.02E+00	9.53E-01	9.38E-01	9.91E-01	1.00E+00	9.54E-01	9.59E-01	1.02E+00	1.36E-01	13
Eu-155	4.67E-02	3.42E-02	6.04E-02	4.71E-02	4.67E-02	4.72E-02	4.83E-02	3.01E-02	4.58E-02	4.68E-02	2.98E-02	4.60E-02	4.43E-02	8.35E-03	19
Total	4.80E+02	3.34E+02	4.81E+02	4.83E+02	4.76E+02	4.81E+02	4.82E+02	4.82E+02	4.58E+02	4.81E+02	4.84E+02	4.73E+02	4.67E+02	4.06E+01	8.7

Figure 4.1. UOX HM masses after 30 years of decay

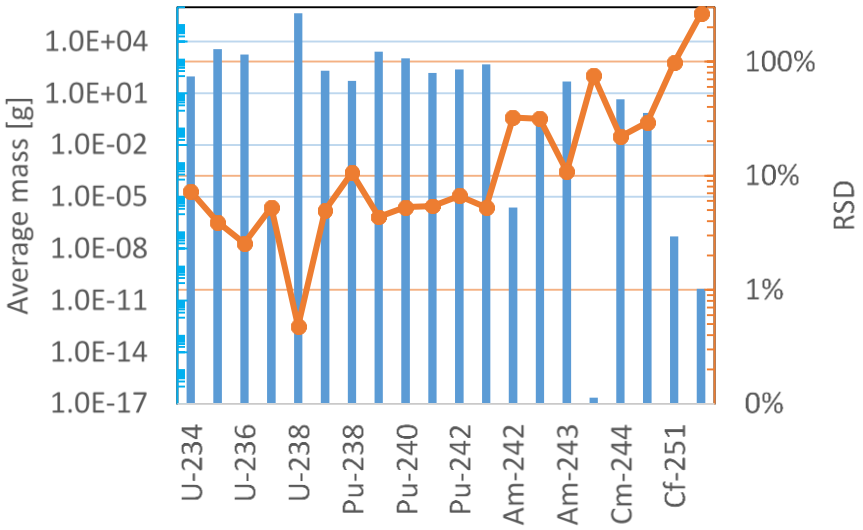

Note: The vertical axes are in a logarithmic scale.
Source: NEA EGAFCS data, 2020.

Figure 4.2. UOX FP masses after 30 years of decay

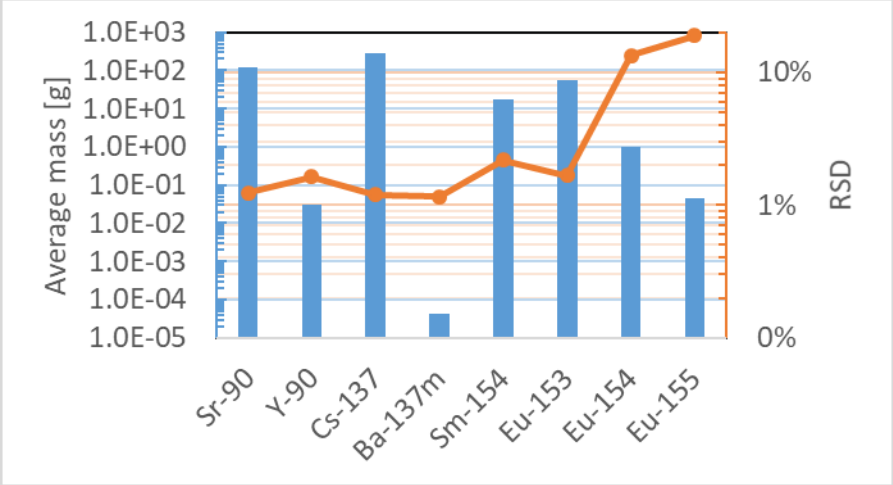

Note: The vertical axes are in a logarithmic scale.
Source: NEA EGAFCS data, 2020.

HM and FP masses in grams for the MOX assembly are presented in Tables 4.5 to 4.8. The average values of all participants together with the RSD after 30 years of decay for the MOX assembly are also presented in Figures 4.3 and 4.4.

A good agreement was found in the calculated HM masses. The largest RSDs around 100% were found for ^{236M}Np, ^{244}Am and ^{250}Cf. For most HM nuclides, the RSDs were below 30%. For uranium and plutonium nuclides 30 years after discharge, the RSDs were less than 12%. The RSD for ^{238}U was 3.5%.

A good agreement was found also for the calculated FP masses. At discharge, the largest RSDs between 10-27% were found for ^{134}Cs, ^{151}Sm, ^{156}Eu, ^{155}Eu and ^{155}Gd in order of

increasing RSD. The largest RSD 30 years after discharge was 20% for ^{155}Eu and all other RSDs were below 6%. The RSDs for ^{137}Cs and ^{137M}Ba were always below 3%.

Table 4.5. MOX HM masses [g] at discharge

Nuclide	CEA	KIT	CNL	ENEA	ENEA	ENEA	ENEA	SCK CEN	VTT	ORANO TN	$\bar{x}$	SD	RSD [%]
	APOLLO	BISTRO-ECCO	SERPENT	APOLLO	NEWT	SERPENT	KENO	ORIGEN-ARP	ALEPH	SERPENT	ORIGEN-ARP			
U234	2.29E+01	2.10E+01	2.22E+01	2.19E+01	2.23E+01	2.21E+01	2.23E+01	2.11E+01	3.03E+01	2.24E+01	8.14E+01	2.82E+01	1.78E+01	63
U235	4.31E+02	2.99E+02	4.21E+02	4.33E+02	4.29E+02	4.25E+02	4.31E+02	4.38E+02	4.98E+02	4.26E+02	4.80E+02	4.28E+02	4.93E+01	12
U236	1.32E+02	1.12E+02	1.33E+02	1.31E+02	1.32E+02	1.33E+02	1.32E+02	1.31E+02	1.44E+02	1.32E+02	1.36E+02	1.32E+02	7.57E+00	5.7
U237	1.10E+00	1.30E+00	1.20E+00	1.13E+00	1.19E+00	1.21E+00	1.19E+00	1.15E+00	1.14E+00	1.15E+00	1.23E+00	1.18E+00	5.62E-02	4.8
U238	3.96E+05	3.93E+05	3.96E+05	3.97E+05	3.96E+05	3.96E+05	3.96E+05	3.96E+05	4.42E+05	3.95E+05	3.96E+05	4.00E+05	1.39E+04	3.5
Np-236	2.55E-04		1.30E-03	9.77E-04	2.93E-04	1.38E-03	2.95E-04	3.66E-04	1.10E-03	1.02E-03	3.73E-04	7.36E-04	4.60E-04	62
Np-236M	3.46E-06		1.70E-09	-	5.37E-06	1.69E-09	5.38E-06	1.95E-06	1.77E-06	2.60E-09	2.06E-06	2.22E-06	2.14E-06	96
Np-237	9.44E-01	9.99E-01	9.91E-01	9.25E-01	1.00E+02	1.02E+02	1.00E+02	9.44E-01	1.13E+02	9.43E+01	9.53E+01	9.87E+01	5.79E+00	5.9
Np-238	2.07E-01	2.68E-01	2.21E-01	2.10E-01	2.18E-01	2.19E-01	2.18E-01	2.11E-01	2.22E-01	2.13E-01	2.21E-01	2.21E-01	1.64E-02	7.4
Np-239	3.67E+01	4.69E+01	3.81E+01	3.82E+01	3.81E+01	3.93E+01	3.82E+01	3.88E+01	3.47E+01	3.87E+01	4.05E+01	3.89E+01	3.03E+00	7.8
Pu-236	4.86E-04		8.22E-04	4.76E-04	1.54E-03	8.27E-04	1.55E-03	1.10E-03	4.87E-04	2.05E-04	1.11E-03	8.61E-04	4.62E-04	54
Pu-237	3.21E-03		4.18E-03	3.24E-03	4.19E-03	4.24E-03	4.21E-03	3.72E-03	3.79E-03	3.42E-03	3.90E-03	3.81E-03	4.08E-04	11
Pu-238	1.04E+03	1.04E+03	1.03E+03	1.03E+03	1.02E+03	1.02E+03	1.02E+03	1.00E+03	1.26E+03	1.05E+03	1.00E+03	1.05E+03	7.09E+01	6.8
Pu-239	9.38E+03	8.97E+03	8.99E+03	9.20E+03	9.30E+03	9.43E+03	9.35E+03	9.77E+03	1.18E+04	9.26E+03	9.84E+03	9.58E+03	7.93E+02	8.3
Pu-240	8.24E+03	7.62E+03	7.97E+03	8.18E+03	8.21E+03	8.23E+03	8.17E+03	8.10E+03	9.01E+03	8.07E+03	8.06E+03	8.17E+03	3.30E+02	4
Pu-241	4.66E+03	4.87E+03	4.75E+03	4.69E+03	4.68E+03	4.73E+03	4.71E+03	4.83E+03	5.29E+03	4.78E+03	4.84E+03	4.80E+03	1.76E+02	3.7
Pu-242	3.64E+03	3.82E+03	3.68E+03	3.84E+03	3.64E+03	3.59E+03	3.63E+03	3.65E+03	3.87E+03	3.67E+03	3.63E+03	3.70E+03	9.86E+01	2.7
Pu-243	4.38E-01	5.60E-01	4.62E-01	4.20E-01	4.53E-01	4.63E-01	4.56E-01	4.67E-01	4.28E-01	4.54E-01	5.03E-01	4.64E-01	3.85E-02	8.3
Pu-244	4.53E-01	1.83E-01	4.21E-01	1.14E-01	4.11E-01	4.24E-01	4.14E-01	1.28E-01	2.86E-01	4.58E-01	1.30E-01	3.11E-01	1.45E-01	47
Am-241	4.25E+02	3.64E+02	4.65E+02	4.14E+02	4.68E+02	4.75E+02	4.71E+02	4.71E+02	5.31E+02	4.19E+02	4.69E+02	4.52E+02	4.37E+01	10
Am-242	5.85E-01	6.41E-01	6.26E-01	5.97E-01	5.97E-01	6.12E-01	5.99E-01	5.60E-01	5.79E-01	6.31E-01	5.63E-01	5.99E-01	2.66E-02	4.4
Am-242M	1.39E+01	9.48E+00	8.05E+00	1.32E+01	1.06E+01	8.04E+00	1.08E+01	1.57E+01	1.66E+01	8.39E+00	1.61E+01	1.19E+01	3.33E+00	28
Am-243	9.85E+02	1.09E+03	1.00E+03	9.06E+02	1.00E+03	1.03E+03	1.01E+03	1.03E+03	1.08E+03	9.94E+02	1.04E+03	1.02E+03	5.06E+01	5
Am-244	4.07E-02		4.23E-02	6.11E-01	4.16E-02	4.24E-02	4.19E-02	6.97E-01	4.63E-01	4.18E-02	7.46E-01	2.77E-01	3.12E-01	113
Cm-242	1.13E+02	1.24E+02	1.19E+02	1.14E+02	1.13E+02	1.16E+02	1.13E+02	1.05E+02	1.14E+02	1.21E+02	1.06E+02	1.14E+02	5.65E+00	4.9
Cm-243	6.13E+00	7.12E+00	6.17E+00	6.06E+00	5.84E+00	6.13E+00	5.87E+00	6.32E+00	8.37E+00	6.36E+00	6.39E+00	6.43E+00	7.28E-01	11
Cm-244	6.92E+02	9.16E+02	6.89E+02	6.23E+02	6.81E+02	6.95E+02	6.85E+02	7.32E+02	8.23E+02	6.96E+02	7.39E+02	7.25E+02	8.03E+01	11
Cm-245	9.37E+01	1.20E+02	1.00E+02	8.01E+01	9.82E+01	1.02E+02	9.94E+01	9.47E+01	1.40E+02	9.39E+01	9.86E+01	1.02E+02	1.57E+01	15
Cm-246	8.57E+00	1.29E+01	9.46E+00	7.42E+00	9.28E+00	9.30E+00	9.30E+00	8.35E+00	1.27E+01	8.56E+00	8.36E+00	9.49E+00	1.76E+00	19
Cm-247	2.25E-01	4.14E-01	2.23E-01	1.89E-01	2.35E-01	2.33E-01	2.36E-01	1.99E-01	3.82E-01	2.28E-01	2.02E-01	2.52E-01	7.43E-02	29
Cm-248	1.77E-02	3.91E-02	2.07E-02	1.48E-02	2.12E-02	2.04E-02	2.12E-02	1.41E-02	3.93E-02	1.75E-02	1.42E-02	2.18E-02	9.01E-03	41
Bk-249	4.19E-04	6.31E-04	7.16E-04	3.38E-04	4.59E-04	4.73E-04	4.61E-04	3.08E-04	1.22E-03	6.29E-04	3.19E-04	5.43E-04	2.63E-04	48
Cf-249	1.22E-04	2.45E-04	2.87E-04	9.38E-05	1.30E-04	1.31E-04	1.31E-04	8.86E-05	3.75E-04	2.60E-04	8.90E-05	1.77E-04	9.72E-05	55
Cf-250	2.01E-04	3.43E-04	1.19E-14	1.56E-04	1.39E-04	1.44E-04	1.39E-04	7.51E-05	6.39E-04		7.71E-05	1.93E-04	1.87E-04	97
Cf-251	3.75E-05	1.26E-04	1.94E-10	3.04E-05	7.78E-05	7.83E-05	7.80E-05	6.37E-05	1.32E-04	2.48E-10	6.62E-05	6.27E-05	4.37E-05	70
Cf-252	1.30E-05	4.91E-05		1.15E-05	3.03E-05	2.92E-05	3.00E-05	2.26E-05	5.79E-05		2.26E-05	2.96E-05	1.53E-05	52
Total	4.26E+05	4.23E+05	4.25E+05	4.26E+05	4.26E+05	4.26E+05	4.26E+05	4.26E+05	4.77E+05	4.25E+05	4.26E+05	4.30E+05	1.54E+04	3.6

Table 4.6. MOX FP masses [g] at discharge

Nuclide	CEA	KIT	CNL	ENEA	ENEA	ENEA	ENEA	SCK CEN	VTT	ORANO TN	$\bar{x}$	SD	RSD [%]
	APOLLO	BISTRO-ECCO	SERPENT	APOLLO	NEWT	SERPENT	KENO	ALEPH	SERPENT	ORIGEN-ARP			
Kr-83	2.13E+01	2.11E+01	2.32E+01	2.13E+01	2.28E+01	2.33E+01	2.29E+01	2.43E+01	2.21E+01	2.24E+01	2.25E+01	9.99E-01	4.4
Rh-103	5.51E+02	5.35E+02	5.57E+02	5.49E+02	5.56E+02	5.65E+02	5.56E+02	5.92E+02	5.54E+02	5.28E+02	5.52E+02	1.80E+01	3.3
Ag-109	1.43E+02	1.60E+02	1.44E+02	1.43E+02	1.43E+02	1.44E+02	1.43E+02	1.65E+02	1.58E+02	1.32E+02	1.46E+02	1.05E+01	7.2
I-135	2.64E-01	2.86E-01	2.82E-01	2.76E-01	2.78E-01	2.81E-01	2.78E-01	2.22E-01	2.72E-01	2.67E-01	2.71E-01	1.73E-02	6.4
Xe-131	3.47E+02	3.17E+02	3.61E+02	3.38E+02	3.59E+02	3.61E+02	3.58E+02	3.69E+02	3.51E+02	3.19E+02	3.46E+02	1.88E+01	5.4
Xe-135	2.15E-01	2.00E-01	2.18E-01	2.15E-01	2.18E-01	2.21E-01	2.20E-01	2.12E-01	2.17E-01	2.29E-01	2.17E-01	7.62E-03	3.5
Cs-133	8.52E+02	8.62E+02	8.70E+02	8.56E+02	8.69E+02	8.71E+02	8.69E+02	9.16E+02	8.62E+02	8.54E+02	8.67E+02	1.77E+01	2
Cs-134	1.23E+02	1.50E+02	1.23E+02	1.22E+02	1.21E+02	1.24E+02	1.21E+02	1.44E+02	1.25E+02	1.09E+02	1.24E+02	1.27E+01	10
Cs-135	6.57E+02	6.00E+02	6.62E+02	6.40E+02	6.59E+02	6.64E+02	6.62E+02	7.67E+02	6.55E+02	6.78E+02	6.66E+02	3.98E+01	6
Cs-137	9.74E+02	1.03E+03	1.00E+03	9.75E+02	9.92E+02	1.00E+03	9.92E+02	1.06E+03	9.84E+02	9.97E+02	1.00E+03	2.56E+01	2.6
Ba-137m	1.49E-04		1.53E-04		1.53E-04	1.53E-04	1.53E-04	1.64E-04	1.51E-04	1.53E-04	1.54E-04	4.33E-06	2.8
Ba-140	1.09E-01	1.16E-01	1.13E+01		1.12E+01	1.13E+01	1.12E+01	9.21E+00	1.13E+01	1.13E+01	1.11E+01	6.69E-01	6.1
La-140	1.47E+00	1.57E+00	1.53E+00	1.54E+00	1.51E+00	1.52E+00	1.51E+00	1.25E+00	1.52E+00	1.53E+00	1.50E+00	8.86E-02	5.8
Nd-143	6.07E+02	6.16E+02	6.13E+02	6.07E+02	6.10E+02	6.16E+02	6.10E+02	6.68E+02	6.11E+02	6.09E+02	6.16E+02	1.76E+01	2.9
Nd-145	4.59E+02	4.55E+02	4.60E+02	4.60E+02	4.57E+02	4.60E+02	4.57E+02	4.99E+02	4.64E+02	4.51E+02	4.61E+02	1.33E+01	2.9
Nd-148	3.02E+02	3.07E+02	3.03E+02	3.02E+02	3.01E+02	3.03E+02	3.01E+02	3.30E+02	3.02E+02	2.94E+02	3.03E+02	9.55E+00	3.1
Pm-147	1.13E+02	1.02E+02	1.13E+02	1.16E+02	1.12E+02	1.13E+02	1.12E+02	1.08E+02	1.15E+02	1.06E+02	1.11E+02	4.41E+00	4
Pm-148	6.29E-01	7.04E-01	6.56E-01	6.54E-01	6.50E-01	6.55E-01	6.50E-01	7.02E-01	6.57E-01	6.09E-01	6.50E-01	3.61E-02	5.6
Pm-149	6.57E-01	7.47E-01	6.78E-01	6.90E-01	6.60E-01	6.73E-01	6.60E-01	5.29E-01	6.81E-01	7.03E-01	6.70E-01	5.32E-02	7.9
Sm-147	5.88E+01	4.95E+01	5.76E+01	5.82E+01	5.79E+01	5.76E+01	5.79E+01	6.84E+01	5.78E+01	5.58E+01	5.78E+01	4.35E+00	7.5
Sm-149	3.85E+00	3.72E+00	3.87E+00	3.73E+00	3.89E+00	3.96E+00	3.95E+00	4.87E+00	3.85E+00	4.54E+00	4.06E+00	3.81E-01	9.4
Sm-150	2.49E+02	2.47E+02	2.49E+02	2.50E+02	2.40E+02	2.50E+02	2.40E+02	2.64E+02	2.52E+02	2.48E+02	2.49E+02	6.36E+00	2.6
Sm-151	2.07E+01	2.36E+01	2.02E+01	2.03E+01	2.08E+01	2.04E+01	2.10E+01	2.59E+01	2.10E+01	2.73E+01	2.26E+01	2.85E+00	13
Sm-152	9.05E+01	9.49E+01	9.14E+01	9.29E+01	9.15E+01	9.10E+01	9.14E+01	9.07E+01	9.17E+01	9.28E+01	9.21E+01	1.48E+00	1.6
Eu-153	1.25E+02	1.33E+02	1.28E+02	1.25E+02	1.30E+02	1.27E+02	1.30E+02	1.32E+02	1.26E+02	1.27E+02	1.28E+02	2.82E+00	2.2
Eu-154	4.62E+01	4.82E+01	4.58E+01	4.52E+01	4.65E+01	4.65E+01	4.66E+01	5.39E+01	4.61E+01	4.75E+01	4.71E+01	2.39E+00	5.1
Eu-155	1.06E+01	1.20E+01	1.08E+01	1.05E+01	1.09E+01	1.14E+01	1.09E+01	1.14E+01	1.06E+01	7.33E+00	1.03E+01	1.55E+00	15
Eu-156	3.07E+00	4.20E+00	3.28E+00	3.17E+00	3.23E+00	3.24E+00	3.22E+00	2.95E+00	3.20E+00	3.14E+00	3.25E+00	3.28E-01	10
Gd-155	3.07E-01	3.03E-01	2.81E-01	2.79E-01	2.82E-01	2.99E-01	2.87E-01	5.51E-01	2.98E-01	2.55E-01	3.08E-01	8.31E-02	27
Total	5.77E+03	5.78E+03	5.86E+03	5.44E+03	5.82E+03	5.87E+03	5.82E+03	6.31E+03	5.83E+03	5.73E+03	5.84E+03	1.64E+02	2.8

Table 4.7. MOX HM masses [g] after 30 years of decay

Nuclide	CEA	KIT	CNL	ENEA	ENEA	ENEA	ENEA	SCK CEN	VTT	ORANO TN	$\bar{x}$	SD	RSD [%]
	DARWIN	ORIGEN	SERPENT	ORIGEN-S	ORIGEN-S	ORIGEN-S	ORIGEN-ARP	ALEPH	SERPENT	ORIGEN-ARP			
U-234	2.61E+02	2.62E+02	2.59E+02	2.59E+02	2.57E+02	2.57E+02	2.51E+02	3.14E+02	2.66E+02	3.11E+02	2.68E+02	2.24E+01	8.3
U-235	4.39E+02	3.07E+02	4.29E+02	4.41E+02	4.37E+02	4.33E+02	4.46E+02	5.08E+02	4.34E+02	4.89E+02	4.37E+02	4.98E+01	11
U-236	1.59E+02	1.37E+02	1.58E+02	1.57E+02	1.58E+02	1.59E+02	2.00E+02	1.73E+02	1.58E+02	1.62E+02	1.62E+02	1.51E+01	9.3
U-237	3.41E-05	3.56E-05	3.46E-05	3.41E-05	3.41E-05	3.45E-05	3.51E-05	3.43E-05	3.88E-05	3.51E-05	3.44E-05	3.50E-05	1.36E-06	3.9
U-238	3.96E+05	3.93E+05	3.96E+05	3.97E+05	3.96E+05	3.96E+05	3.96E+05	3.96E+05	4.42E+05	3.95E+05	3.96E+05	4.00E+05	1.39E+04	3.5
Np-237	2.17E+02	2.25E+02	2.26E+02	2.16E+02	2.26E+02	2.29E+02	1.29E+02	2.23E+02	2.55E+02	2.20E+02	2.24E+02	2.17E+02	3.11E+01	14
Pu-238	9.09E+02	9.20E+02	9.05E+02	9.03E+02	8.94E+02	8.97E+02	8.76E+02	8.76E+02	1.08E+03	9.28E+02	8.77E+02	9.15E+02	5.77E+01	6.3
Pu-239	9.42E+03	9.02E+03	9.03E+03	9.24E+03	9.34E+03	9.47E+03	9.80E+03	9.81E+03	1.19E+04	9.30E+03	9.88E+03	9.65E+03	7.89E+02	8.2
Pu-240	8.68E+03	8.21E+03	8.40E+03	8.57E+03	8.64E+03	8.67E+03	8.56E+03	8.56E+03	9.54E+03	8.51E+03	8.54E+03	8.63E+03	3.30E+02	3.8
Pu-241	1.09E+03	1.15E+03	1.11E+03	1.09E+03	1.09E+03	1.10E+03	1.13E+03	1.13E+03	1.24E+03	1.12E+03	1.14E+03	1.13E+03	4.28E+01	3.8
Pu-242	3.64E+03	3.82E+03	3.68E+03	3.84E+03	3.64E+03	3.59E+03	3.65E+03	3.65E+03	3.87E+03	3.67E+03	3.63E+03	3.70E+03	9.76E+01	2.6
Am-241	3.87E+03	3.96E+03	3.98E+03	3.89E+03	3.93E+03	3.98E+03	4.04E+03	4.03E+03	4.44E+03	3.95E+03	4.04E+03	4.01E+03	1.54E+02	3.8
Am-242	1.54E-04	9.89E-05	8.96E-05	1.47E-04	1.18E-04	8.95E-05	1.75E-04	1.75E-04	1.85E-04	9.36E-05	1.79E-04	1.37E-04	3.94E-05	29
Am-242m	1.20E+01	8.26E+00	6.95E+00	1.14E+01	9.15E+00	6.94E+00	1.36E+01	1.36E+01	1.43E+01	7.24E+00	1.39E+01	1.07E+01	3.00E+00	28
Am-243	9.83E+02	1.09E+03	1.00E+03	9.04E+02	9.98E+02	1.03E+03	1.01E+03	1.03E+03	1.08E+03	9.91E+02	1.04E+03	1.01E+03	5.05E+01	5
Am-244	3.97E-14							2.44E-13				1.42E-13	1.44E-13	102
Cm-244	2.18E+02	2.91E+02	2.18E+02	1.98E+02	2.16E+02	2.20E+02	2.32E+02	2.32E+02	2.59E+02	2.19E+02	2.34E+02	2.31E+02	2.51E+01	11
Cm-245	9.35E+01	1.20E+02	9.98E+01	7.99E+01	9.80E+01	1.02E+02	9.45E+01	9.45E+01	1.40E+02	9.37E+01	9.84E+01	1.01E+02	1.58E+01	16
Cf-251	3.66E-05	1.23E-04	1.90E-10	2.97E-05	7.60E-05	7.66E-05	6.22E-05	6.22E-05	1.29E-04	2.42E-10	6.47E-05	6.00E-05	4.24E-05	71
Cf-252	5.01E-09	1.85E-08		4.43E-09	1.17E-08	1.12E-08	8.71E-09	8.71E-09	2.24E-08		8.69E-09	1.10E-08	5.94E-09	54
Total	4.26E+05	4.23E+05	4.25E+05	4.27E+05	4.26E+05	4.26E+05	4.25E+05	4.26E+05	4.77E+05	4.25E+05	4.26E+05	4.30E+05	1.54E+04	3.6

Table 4.8. MOX FP masses [g] after 30 years of decay

Nuclide	CEA	KIT	CNL	ENEA	ENEA	ENEA	ENEA	SCK CEN	VTT	ORANO TN	$\bar{x}$	SD	RSD [%]
	DARWIN	ORIGEN	SERPENT	ORIGEN-S	ORIGEN-S	ORIGEN-S	ORIGEN-ARP	ALEPH	SERPENT	ORIGEN-ARP			
Sr-90	9.74E+01	9.73E+01	1.02E+02	9.74E+01	1.01E+02	1.02E+02	1.01E+02	1.07E+02	9.84E+01	9.81E+01	1.00E+02	3.07E+00	3.1
Y-90	2.47E-02	2.44E-02	2.59E-02	2.47E-02	2.56E-02	2.59E-02	2.56E-02	2.72E-02	2.50E-02	2.55E-02	2.54E-02	7.76E-04	3.1
Cs-137	4.88E+02	5.14E+02	5.01E+02	4.88E+02	4.97E+02	5.01E+02	4.97E+02	5.33E+02	4.93E+02	4.98E+02	5.01E+02	1.27E+01	2.5
Ba-137	5.34E+02	5.62E+02	5.47E+02	4.87E+02	5.43E+02	5.47E+02	5.43E+02	5.46E+02	5.38E+02	5.46E+02	5.39E+02	1.98E+01	3.7
Ba-137m	7.43E-05	7.86E-05	7.63E-05	7.46E-05	7.59E-05	7.66E-05	7.59E-05	8.12E-05	7.51E-05	7.61E-05	7.64E-05	1.95E-06	2.6
Sm-154	5.29E+01	5.65E+01	5.30E+01	5.29E+01	5.25E+01	5.29E+01	5.25E+01		5.45E+01	5.17E+01	5.31E+01	1.42E+00	2.7
Eu-153	1.26E+02	1.34E+02	1.29E+02	1.25E+02	1.30E+02	1.27E+02	1.30E+02	1.33E+02	1.27E+02	1.28E+02	1.29E+02	2.83E+00	2.2
Eu-154	4.11E+00	4.30E+00	4.07E+00	4.03E+00	4.14E+00	4.14E+00	4.16E+00	4.80E+00	4.11E+00	4.22E+00	4.20E+00	2.14E-01	5.1
Eu-155	1.33E-01	1.82E-01	1.35E-01	1.32E-01	1.37E-01	1.43E-01	1.37E-01	1.43E-01	1.34E-01	8.61E-02	1.32E-01	2.64E-02	20
Total	1.30E+03	1.37E+03	1.34E+03	1.25E+03	1.33E+03	1.34E+03	1.33E+03	1.32E+03	1.31E+03	1.33E+03	1.27E+03	1.66E+02	13

Figure 4.3. MOX HM masses after 30 years of decay

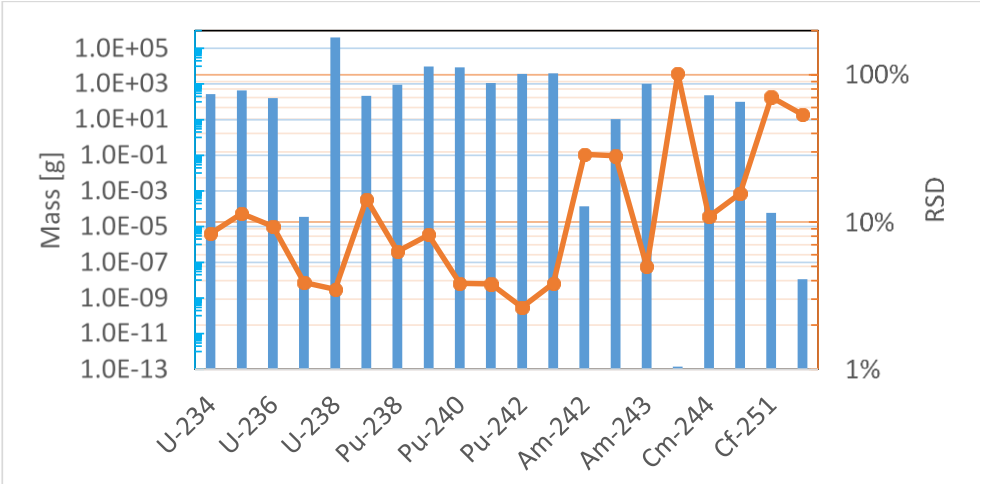

Note: The vertical axes are in a logarithmic scale.
Source: NEA EGAFCS data, 2020.

Figure 4.4. MOX FP masses after 30 years of decay

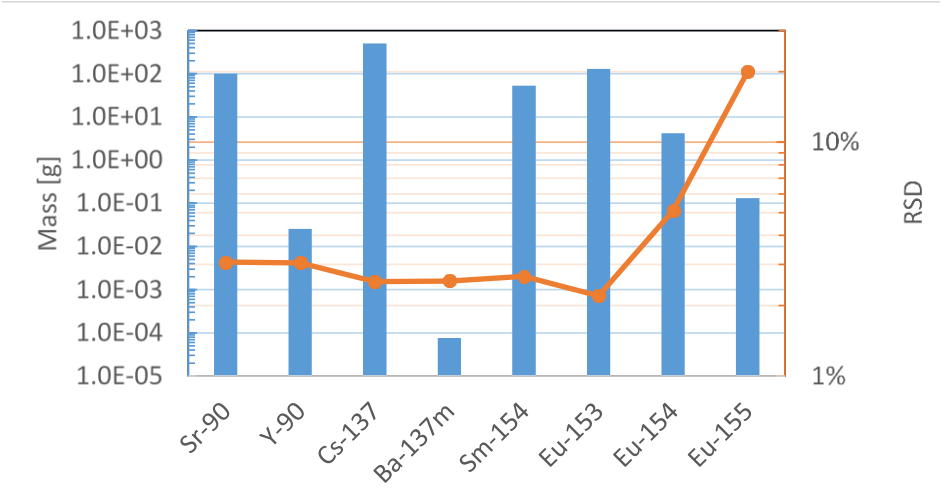

Note: The vertical axes are in a logarithmic scale.
Source: NEA EGAFCS data, 2020.

4.4. Gamma release rates after 30 years of decay

The gamma release rates [photons/s] calculated by the participants are presented in Figure 4.5 for UOX and in Figure 4.6 for MOX. Different energy meshes have been used in the calculation: 18 groups (ANL, ENEA, ORANO-TN, KIT), 19 groups (CEA), 45 groups (CNL), 62 groups (ORANO-TN) and 1 800 groups (CIEMAT). In these calculations, the number of photons in an energy group was adjusted so that the total gamma energy of the group was conserved, resulting in effective dose rates. This adjustment of the number of photons, which was performed by many of the participants, is dependent on the group structure used. In other words, the number of gammas in Figures 4.5 and 4.6 illustrate the effective total number of gammas and therefore the numbers between the participants are

quite different with an RSD of 32% for UOX and 23% for MOX. For SCK CEN and VTT, the gamma source was obtained ray by ray and the number of gammas in Figure 4.5 and Figure 4.6 for SCK CEN and VTT are the actual numbers without adjustments.

Figure 4.5. Comparison of total gamma release rate for PWR UOX at 30 years

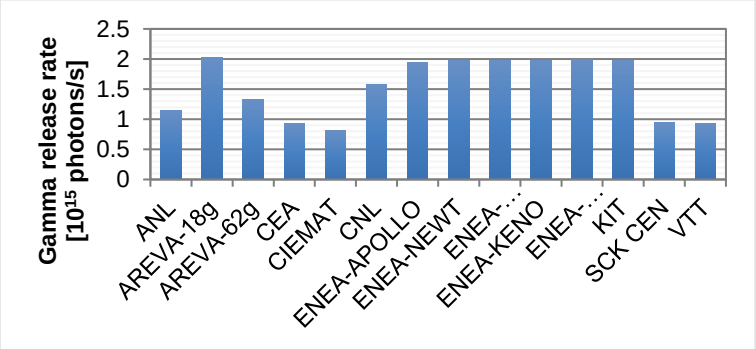

Source: NEA EGAFCS data, 2020.

Figure 4.6. Comparison of total gamma release rate for PWR MOX at 30 years

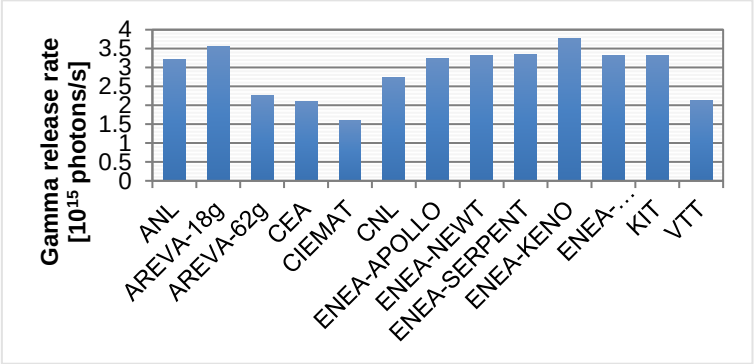

Source: NEA EGAFCS data, 2020.

The average effective gamma release rates at 3.7 years of cooling are $6.4 \cdot 10^{15}$ photons/s for the UOX assembly and $1.3 \cdot 10^{16}$ photons/s for the MOX assembly. The corresponding RSDs are 41% and 28% for UOX and MOX, respectively. These release rates are more than four times larger than at 30 years of cooling.

4.5. Dose rates after 30 years of decay

The calculated EDRs for both UOX and MOX assemblies are presented in Table 4.9, in Figure 4.7 and in Figure 4.8. The blue bars in the figures present results calculated using the 1977 ANSI conversion factor and the orange bars are obtained with the 1991 conversion factor. The average EDR for the UOX FA is 5.8 or 4.6 Sv/h with conversion factors from 1977 and 1991, respectively. For the MOX FA, the corresponding average EDR values are 11.1 and 8.9 Sv/h. The EDRs for the MOX FA are approximately two times higher than for the UOX FA in accordance with a greater gamma release rate ($2.9 \cdot 10^{15}$ photons/s for MOX, $1.5 \cdot 10^{15}$ photons/s for UOX).

Table 4.9. EDR comparison at 30 years [Sv/h]

Institute	PWR - UOX 30 years		PWR - MOX 30 years	
	Conversion factor		Conversion factor	
	1977	1991	1977	1991
ANL	5.8	4.6	11.0	8.6
ORANO TN-18g	5.8	4.6	10.2	8.1
ORANO TN-62g	6.6	5.3	11.7	9.4
CEA	5.2	4.8	9.5	8.6
CIEMAT	5.2	4.2	9.3	7.4
CNL	7.9	6.3	13.7	10.9
ENEA-1	5.3	4.1	11.4	9.0
ENEA-2	5.3	4.2	11.6	9.2
ENEA-3	5.2	4.1	11.7	9.3
ENEA-4	5.2	4.1	11.8	9.3
ENEA-5	5.2	4.1	11.7	9.2
KIT	5.5	4.3	11.5	9.1
SCK CEN	7.0	5.6	-	-
VTT	5.7	4.5	10.1	7.9
$\bar{x}$	**5.8**	**4.6**	**11.1**	**8.9**
SD	0.8	0.7	1.2	0.8
RSD	14 %	15 %	10 %	10 %

The calculated EDRs are only slightly lower with the 1991 conversion factors than with the 1977 conversion factors, which indicates that there is no significant contribution to the gamma doses with low energies (< 0.1 MeV). The required self-protection limit of 1 Sv/h at a 1 m distance from the assembly is well satisfied. Also, the different calculation codes give consistent results with RSDs of the order of 15% and 10% for UOX and MOX assemblies, respectively.

Figure 4.7. EDR comparison PWR - UOX at 30 years [Sv/h]

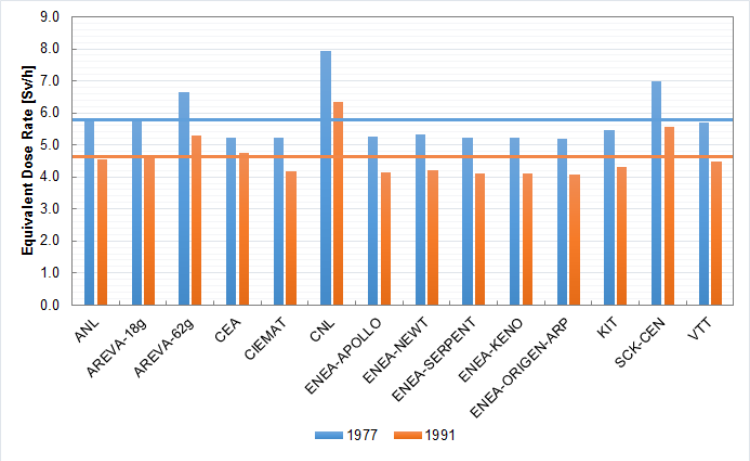

Source: NEA EGAFCS data, 2020.

Figure 4.8. EDR comparison PWR - MOX at 30 years [Sv/h]

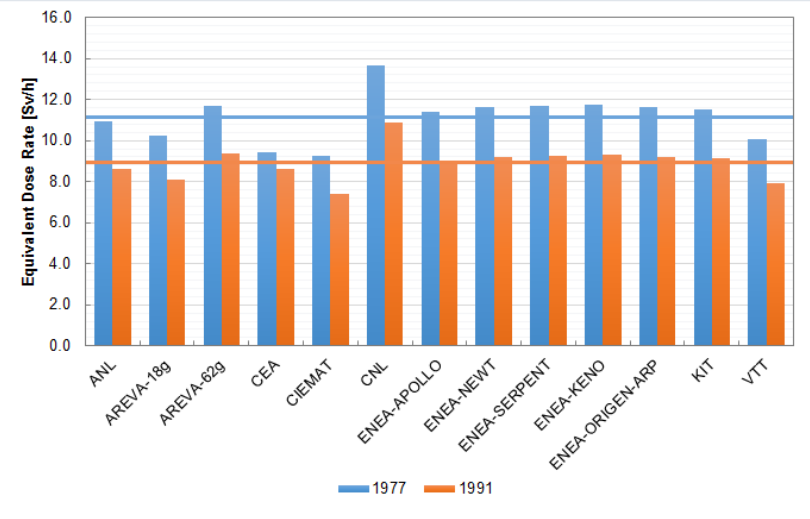

Source: NEA EGAFCS data, 2020.

4.6. Dose rates after 3.7 years of decay

Table 4.10 and Figures 4.9 and 4.10 present the calculated EDRs at 3.7 years after discharge. The values are nearly six times greater than the EDRs at 30 years. The average value for the UOX FA is 32 Sv/h and 26 Sv/h with the 1977 or 1991 conversion factors, respectively. For the MOX FA, these values are 66 Sv/h and 53 Sv/h, respectively. There is a good agreement between participants with RSDs ranging from 7% to 11%.

No impurities were considered in these calculations. For example, the activation of ^{59}Co into ^{60}Co ($T_{1/2}$ = 5.3 years) was not taken into account. Cobalt is commonly present in small amounts e.g. in Zircaloy, Inconel and stainless steel. Depending on the concentration of cobalt in these materials, it could affect the absolute dose rates with short decay times, but this effect was not considered here.

Table 4.10. EDR comparison at 3.7 years [Sv/h]

	PWR - UOX 3.7 years		**PWR - MOX 3.7 years**	
	Conversion factor		Conversion factor	
Institute	1977	1991	1977	1991
ANL	32.1	25.7		
ORANO TN-18g	33.9	27.2	67.2	54.1
ORANO TN-62g	35.2	28.3	69.1	55.7
CEA	34.3	31.7		
CIEMAT	29.9	24.0		
KIT	30.8	24.6	69.8	55.9
VTT	29.4	23.1	57.1	47.5
$\bar{x}$	**32.2**	**26.4**	**65.8**	**53.3**
SD	2.3	2.9	5.9	4.0
RSD	7 %	11 %	9 %	7 %

Figure 4.9. EDR comparison PWR - UOX at 3.7 years [Sv/h]

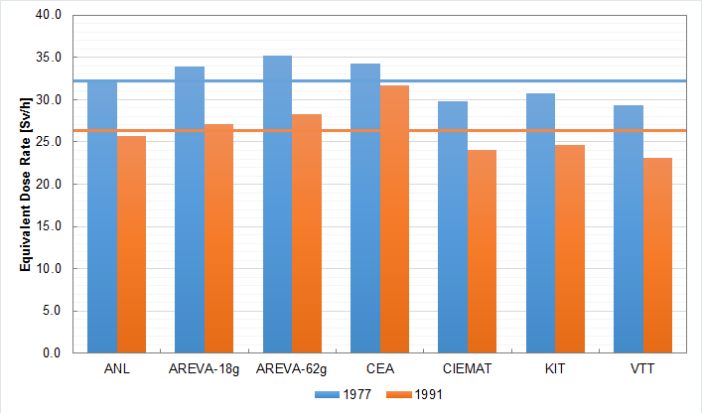

Source: NEA EGAFCS data, 2020.

Figure 4.10. EDR comparison PWR - MOX at 3.7 years [Sv/h]

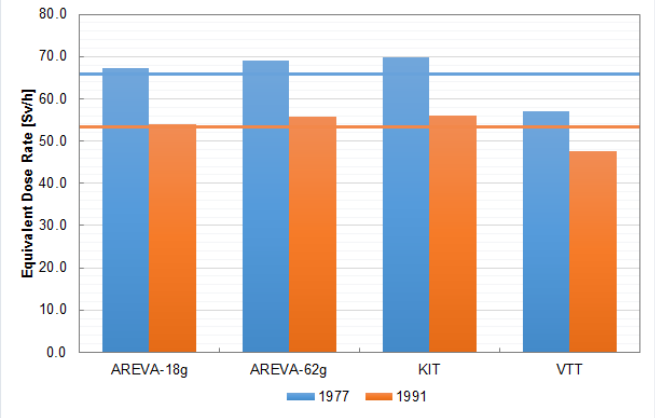

Source: NEA EGAFCS data, 2020.

References

[1] DOE (1997), *Non-proliferation and Arms Control Assessment of Weapons-Usable Fissile Material Storage And Excess Plutonium Disposition Alternatives*, DOE/NN-007, US Department of Energy, United States, https://doi.org/10.2172/425259.

[2] ANS (1977), *American National Standard for Neutron and Gamma-Ray Flux-to-Dose-Rate Factors*, ANSI/ANS-6.1.1 (1977), United States.

[3] ANS (1991), *American National Standard for Neutron and Gamma-Ray Flux-to-Dose-Rate Factors*, ANSI/ANS-6.1.1 (1991), United States.

5. Sensitivity studies

This chapter is a synthesis of the different contributions which can be found in Appendix B.

5.1. Context

Under the auspices of the NEA EGAFCS, a benchmark on dose rate calculations for PWR spent FA was completed. This multinational effort was first proposed by CEA and ANL after conducting their bilateral comparative study on dose rate calculations for typical UOX and MOX spent FAs [1]. The goals of this benchmark are to expand on that work by including more international participants, verify the dose rate results and potentially include validation efforts depending on the availability of appropriate experimental data.

5.2. Calculations cases

This benchmark involves two reference cases [2]:

- a 15x15 PWR spent FA with UOX fuel at 33 GWd/MTIHM burn-up;
- a 17x17 PWR spent FA with MOX fuel at 60 GWd/MTIHM burn-up.

Two different cooling times were chosen: 30 years and 3.7 years to differentiate the short-lived and long-lived fission product contributions to the dose rate.

5.3. Sensitivity studies

Different sensitivity studies were carried out to assess the impact of the calculation scheme on calculated EDRs. The calculation parameters that all participants contributed to analysing are:

- the assembly geometry, homogeneous vs heterogeneous;
- the radial burn-up distribution (uniform or not);
- the irradiation history (with or without decay periods);
- the Rim effect (increased burn-up in the external ring of the pellet);
- the gamma source group structure (different energy groups from 18 to 62, or explicit gamma rays);
- the bremsstrahlung effect;
- the cross-sections effects;
- the modelling assumptions (tally geometry description, flux-to-dose conversion factors, interpolation factors…);
- the neutron dose rate contribution, etc.

5.3.1. Assembly geometry – Radiation calculation

For the radiation step, all the participants chose different Monte Carlo codes involving 3D models with two different assumptions concerning the FA geometry in the XY scale:

- pin-by-pin model;
- or a homogeneous model.

The obtained results show that, to tally the gamma flux at 1 m away from the FA radial external surface, a homogeneous model is convenient by using the relevant equivalent FA density.

5.3.2. Radial burn-up distribution

Some calculations were performed with the assumption of a radial burn-up distribution in the FA XY scale. The obtained results show that, to tally the gamma flux at 1 m away from the FA radial external surface, the use of a non-uniform pin-by-pin gamma source distribution is not necessary.

5.3.3. Irradiation history

Simple irradiation histories were tested to check the impact of intermediate decay periods during irradiation. Using these irradiation histories, the isotopic inventory shows some differences regarding the reference calculation, mainly for those isotopes being generated via decay from their radioactive parents, such as ^{241}Am, ^{242}Am, ^{242M}Am, ^{242}Cm and ^{243}Cm. These sensitivity calculations also provide values of the photon emission 2% to 5% larger than the reference calculation, providing values of the dose rate also 2% to 5% larger.

5.3.4. Rim effect

Some calculations were performed with the assumption of a non-uniform gamma source distribution inside each pin. The obtained results show that, to tally the gamma flux at 1 m away from the FA radial external surface, the use of such a very detailed gamma source distribution is not necessary.

5.3.5. Gamma group structure

Different energy meshes were used to calculate the gamma release rate: 18 groups (ANL, ENEA, ORANO TN, KIT), 19 groups (CEA), 45 groups (CNL) or 62 groups (ORANO TN). For these calculations, the number of gamma photons released from each energy group is adjusted to conserve energy, thereby resulting in EDR. This adjustment of the number of photons is dependent on the group structure used. Different large energy group structures were also used by CIEMAT (1 800 groups) and CEA (≈19 000 groups). For other participants, the gamma source was obtained ray by ray and no adjustments were needed. Such differences in the gamma energy mesh lead to a maximum effect of 20% on the calculated EDR.

So, to tally the gamma flux at 1 m away from the FA radial external surface, the use of a relevant gamma energy mesh is necessary.

5.3.6. Bremsstrahlung effect

For the depletion step, most participants used a decay code taking bremsstrahlung in the gamma sources. ^{106}Rh and ^{90}Y isotopes are the main contributor to these gamma sources and generate less than 10% of the total dose rate, a small but not negligible contribution.

So, to tally the gamma flux at 1 m away from the FA radial external surface, taking bremsstrahlung in the gamma sources mesh is necessary.

5.3.7. Cross-sections effect

Some participants performed radiation calculations using different cross-section libraries (while other parameters were fixed). The obtained results show that, to tally the gamma flux at 1 m away from the FA radial external surface, cross-section libraries issued from JEFF, ENDF/B and TENDL evaluations lead to equivalent dose rates.

5.3.8. Modelling assumptions

A set of calculations were performed to study the impact of the statistics in the radiation transport calculation, using different detector sizes (spheres with a radius of 1 cm, 2 cm, 5 cm and 10 cm, centred at 1 m of the FA at mid-plane). The different values of the dose rate obtained for different detector sizes range within a relatively small interval of 3% with no clear tendency. These differences are probably caused by the statistical uncertainty of the different Monte Carlo calculations.

Furthermore, LIN-LIN/-LOG or LOG-LIN/-LOG interpolation schemes for the flux-to-dose rate conversion factors were considered. These different interpolation schemes provide only a maximum of 1% difference in the final values of the dose rate whatever the conversion factor evaluation used (ANSI/ANS, ICRP).

5.3.9. Neutron dose rate contribution

The obtained results show that the neutron contribution to the total dose rate, at 1 m away from the FA radial external surface, is negligible.

References

[1] Feng, B., R. Hill, R. Girieud and R. Eschbach (2014), "Comparison of gamma dose rate calculations for PWR spent fuel assemblies", *PHYSOR 2014*, Kyoto, Japan, 28 September-3 October 2014.

[2] Eschbach, R. et al. (2017), "Verification of dose rate calculations for PWR spent fuel assemblies", Paper A-081, *GLOBAL2017*, Seoul, Korea, 24-29 September 2017.

6. Experimental validation: Morris experiment

Two institutes, ANL and CEA, modelled this experiment. The following chapter summarises the results.

6.1. Description of the experimental setup

The Morris experiments were a series of gamma dose rate measurements completed in the General Electric spent fuel storage facility at Morris Operation and the details were documented in the NEDG-24922 report [1]. The measurements were performed to support the programme of developing a potential US Department of Energy (DOE) site for spent nuclear fuel storage at the Morris Operation. In these experiments, the gamma dose rates were measured in the vicinity of the discharged spent nuclear fuel bundles. A wide range of fuel types, power levels and burn-ups was selected in the experiments. Particularly among the 38 fuel bundles selected, four PWR fuel bundles have gamma dose rates measured in the air. Their fuel bundles were designated as 1A, 2A, 2B and 2D, and were all Westinghouse 14X14 PWR fuel bundles irradiated at unidentified utilities (either Utility #1 or #2 as indicated in the fuel bundle names). Their fuel burn-up ranged from 26.4 GWd/MTIHM to 40.2 GWd/MTIHM, and the FA cooling time before measurement ranged from 30 months to 83 months. The main characteristics of the FAs are listed in Table 6.1 with their fuel burn-up and decay histories.

To measure the gamma dose rates for each FA, the FAs were moved underwater from the fuel storage to the place where the experimental pit was installed. Figure 6.1 (a) shows the Morris experimental setup. It was composed of two main parts, with the lower vessel to support the fuel bundle and an upper diving bell. The lower vessel was on a stainless steel support plate and had a tube welded on top of the plate. The tube was a 9-inch square with internal spacers on the four sides to house the fuel bundles. For the PWR fuel, the bundles were 7.8 x 7.8 inches (presumably the dimensions of the grid spacers). The tube wall was 12 feet tall. It had a slot cut in the upper part and had two adjacent sides removed to form an open corner to allow most of the radiation to be measured without obstructions. The open slot was 7.7 feet down from the top.

Figure 6.1 (c) shows an X-Y cut-off view of the experimental setup. As shown in the figure, the tube was on one side of the support plate leaving room to house the detectors. Lead blocks were added to balance the lower vessel as shown in Figure 6.1 (a). The whole experimental lower vessel with detectors was submerged underwater. To measure the dose rate in the air environment, a “diving bell” which was the main upper part of the experimental setup was equipped to cover both the fuel bundles and the detectors, as shown in Figure 6.1 (a) and Figure 6.1 (c). Compressed air was added to the bell to expel the water out of the bell for measuring gamma dose rates in the air.

The gamma dose rates were measured by the dose monitor unit’s ion chambers with locations indicated in Figure 6.1 (b) and Figure 6.1 (c). The FAs from Utilities 1 and 2 used FAs with different lengths: 144 and 120 inches, respectively. In measurements, the top of the FA was always the reference zero point for the axial detector locations as shown in Table 6.2. Detectors were movable along three fixed axial lines A-1, B-1 and E-1. The dose rates were measured with detectors at the top, ¾, and halfway points of the axial height of the fuel bundles. For convenience, Table 6.2 names each of these detector locations using two characters, with the numbers to represent the detector axial location, and the letter “A”, “B” and “E” to represent the fixed axial line along which the detector moved. In particular,

for the axial direction, "0" represents the detector lined up with the top of the FA. "1" represents the detector at the ¾ height of FA, and "2" represents the detector at the middle plane of the FA [1]. In addition, measurements were taken at a detector located above the top of the standing FAs. The description of these two top detector locations is inconsistent in the reference [1]. Due to these ambiguities, these two points were ignored in the rest of the discussions.

Table 6.1. Specifications of the Morris fuel bundles 1A, 2A, 2B and 2D and Turkey Point FAs B03 and D04

Experimental fuel bundle	Morris/1A	Morris/2A	Morris/2B	Morris/2D	Turkey Point /B03	Turkey Point /D04
Fuel type (array)	14 X 14	14 X 14	14 X 14	14 X 14	15 X 15	15 X15
Fuel ^{235}U (%)	3.397	3.865	3.865	3.996	2.55	2.55
Fuel density (g/cm^3)	9.908	10.10	10.10	10.379	10.08	10.08
Cladding material	Zircaloy-4	SS304	SS304	SS304	Zircaloyr-4	Zircaloy-4
Pellet D (Inch.)	0.365	0.3835	0.3835	0.3835	0.365	0.365
Rod D (Inch.)	0.422	0.422	0.422	0.422	0.422	0.422
Pitch (Inch.)	0.556	0.556	0.556	0.556	0.5617	0.5617
Rod length (Inch.)	144	120	120	120	144	144
Fuel mass (kgHM)	386	362	362	372	448	448
Power (MW/tU)	31.8	23.5	23.5	23.5	31.16	31.2
Burn-up (GWd/MTIHM)	40.2	32.4	26.4	30.4	25.77*	26.55
Burn-up time (d)	1 264	1 379	1 123	1 294	827	851
Decay time (month)	48	83	83	30	46	21.6

*This number is calculated using the specified average thermal power per assembly, the fuel mass per assembly and the irradiation full power days from Table 6.1 and Table 6.2 of the reference [2]. It is slightly different from the value listed in Table 6.2.

When measuring the gamma dose rates, the detectors were placed at those positions near the open corner of the fuel bundles. The other three corners of the FAs were covered by the tube. The measured dose rates were found to be significantly different by placing different corners facing the open slot. These variations were thought mainly due to the variation of the neutron fluxes across the fuel bundles while they were irradiated. The final experimental measurements at each detector location were the average values with different corners facing the open slot. It was stated that within a confidence limit of 95%, the true gamma exposure rates were within 8% of the average values among the measurements taken from the different corners. Table 6.3 lists all the averaged gamma dose rates for each detector location and each FA [1]. Gamma dose rates are given in kilo-rem per hour (kR/hr), with 100 rem of absorbed gamma dose rates equivalent to 1 Sv.

Table 6.2. Locations of the ion chambers for FAs from Utilities 1 and 2

Detector	Utility 1 Assemblies (1A)			Utility 2 Assemblies (2A, 2B, 2D)		
	X (inch)	Y (inch)	Z (inch)	X(inch)	Y (inch)	Z(inch)
0.B	1.6	-1.6	0	1.6	-1.6	0
0.A	7	-7	0	7	-7	0
0.E	-3.9	-10	0	-3.9	-10	0
1.B	1.6	-1.6	-36	1.6	-1.6	-30
1.A	7	-7	-36	7	-7	-30
1.E	-3.9	-10	-36	-3.9	-10	-30
2.B	1.6	-1.6	-72	1.6	-1.6	-60
2.A	7	-7	-72	7	-7	-60
2.E	-3.9	-10	-72	-3.9	-10	-60

Table 6.3. Measured gamma dose rates for Morris Unit 1 and Unit 2 FAs

Detector	Gamma Dose Rate (kR/hr)			
	1A	2A	2B	2D
0.B	10.0	3.75	3.0	12.0
0.A	6.50	2.60	2.15	8.00
0.E	5.80	2.63	2.02	9.60
1.B	33.5	16.0	12.5	37.0
1.A	18.0	7.45	6.00	20.3
1.E	18.0	7.30	5.75	20.8
2.B	34.8	16.8	13.5	40.2
2.A	18.1	7.65	6.15	21.9
2.E	18.0	7.51	5.70	22.0

Figure 6.1. (a) Morris experimental setup, (b) Ion chamber locations relative to the fuel bundle, (c) X-Y cut-view of the experimental setup

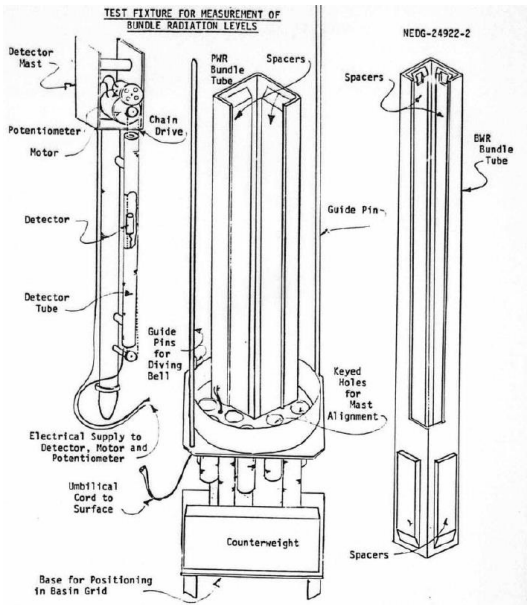

(a)

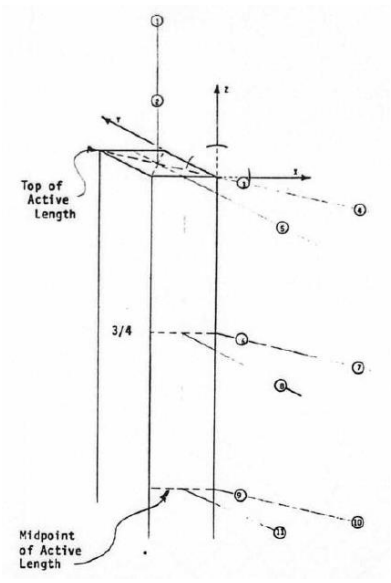

(b)

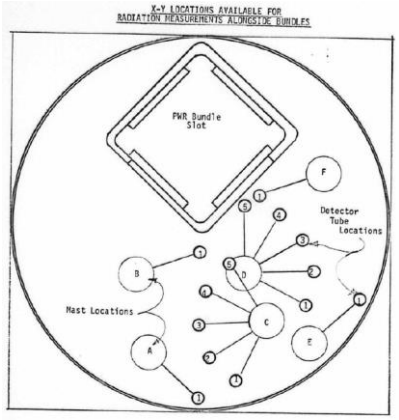

(c)

Source: Strickler, H.R., K.J. Eger, 1981.

6.2. Numerical models and numerical simulations

Numerical simulations of the Morris experiments have been performed by both CEA and ANL. CEA analysed the 1A configuration. ANL analysed all four configurations.

6.2.1. CEA methodology

The calculation scheme is broken down into three steps:

- A first step to perform the neutronic fuel depletion calculation. The TRIPOLI-4® Monte Carlo [3] code and its depletion calculation capability were used. The Euler first-order temporal scheme was used. A calculation was performed with a second-order scheme (MEAN scheme) for the reference case and the observed discrepancy in the main isotope contributors and on gamma dose rate was found to be about a few percent. To note that though TRIPOLI-4® allows performing replica calculations to have a statistical uncertainty on the isotopic balance, this was not set in place here.
- A second step to perform the decay calculation based on the isotopic inventory from the previous step. In this step, the DARWIN-2.4 [4, 5] code package is used.
- A third step to perform the equivalent dose rate calculation based on the gamma and beta source from the previous step using the TRIPOLI-4® Monte Carlo code. Previous benchmark analyses had shown that neutron contribution was negligible and so this was not calculated.
- JEFF-3.1.1 [6] nuclear data are used for neutron transport calculations, EPDL-97 atomic data are used for photon transport calculations and EADL for atomic relaxation data.

TRIPOLI-4® solves the linear Boltzmann equation for neutrons, photons, electrons and positrons, with the Monte Carlo method, in any 3D geometry. TRIPOLI-4® has its own native geometry package, allowing for both a pure surface-based representation and a combinatorial representation with predefined shapes and Boolean operators (any combination of these two kinds of representations can be adopted).

DARWIN is the French reference calculation package for the fuel cycle of all types of reactors, as described in paragraph 3.2.5.

The calculations used a heterogeneous burn-up axial profile from the reference study on UOX PWR assemblies [7]. Both ANS-91 [8] and H*(10) ICRP-74 [9] conversion factors were used in the calculations. The electron contribution to the dose rate (bremsstrahlung) was also assessed independently. It was calculated to be only 2-3% of the total dose rate. This contribution was not accounted for in the final CEA results presented in this report.

Sensitivity studies first showed that the EDR was sensitive to the water albedo. The water and the two experimental vessels were taken into account in the models. Because the experimental setup is not fully detailed in the experimental report, some assumptions were made. These assumptions pertain to dimensions for some parts of the experimental setup or some material properties. They are illustrated in Figures 6.2 and 6.3.

For the lower vessel model, three main assumptions were made. First, the tube and spacer were both assumed to be 0.3 inches thick. Second, the open-cut slot width was assumed to be 4.5 inches, which was half the length of the vessel. Lastly, the steel vessel was assumed to be Stainless Steel 304L.

For the upper vessel model, three main assumptions were also made. First, the side of the diving bell thickness was assumed to be the same thickness as its head (or top cover). Second, the total tube height was deduced from the assembly height and the highest measurement position (38 inches above the top of 120-inch FA) with a 2-inch reservation space assumed above the highest detector. Thirdly, the steel was also assumed to be 304L.

In TRIPOLI-4® calculations, detectors were precisely located in the experimental setup as shown in Figure 6.4. For sensitivity analysis, calculations were performed for three types of assembly environments. The first environment (so-called No Environment) is air only. In this case, no scattering occurs outside the assembly and no gamma can backscatter to the detectors to contribute to the dose rate. The second environment includes all vessels and water (so-called Full Environment). In all the calculations, CEA did not model cobalt activation sources (grid spacers, cladding tubes). The third environment is a water only environment (so-called Water Only Environment). In this last case, the vessels are removed and only water remains at the same boundary as in the second environment model.

Figure 6.2. CEA model of the lower vessel in the Morris experiment

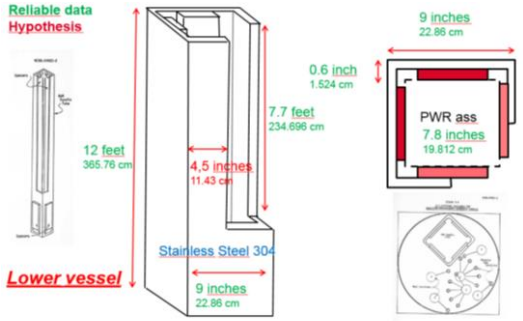

Source: Original data from the NEA EGAFCS, 2020.

Figure 6.3. CEA Model of the upper vessel in the Morris experiment

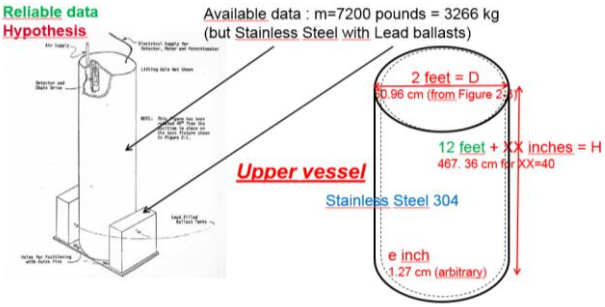

Source: Original data from the NEA EGAFCS, 2020.

Figure 6.4. CEA Model of the detector locations in the Morris – 1A experiment

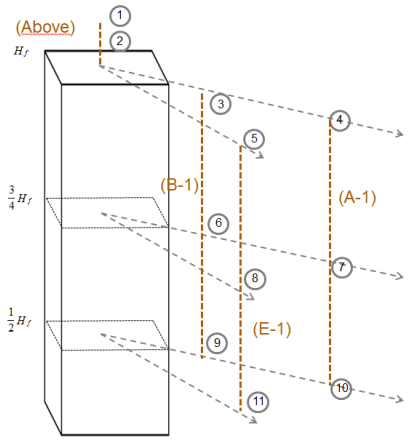

Source: Original data from the NEA EGAFCS, 2020.

The calculated results are provided in Table 6.3 as C/E results. The TRIPOLI-4® statistical uncertainties are provided in parentheses. ANS-91 conversion factor results vary for the full environment configuration from 0.65 to0.75 for radial detectors, whereas they vary from 0.73 to 0.87 for the H*(10) ICRP-74 conversion factors. The ratio between the two conversion factor results is close to 15%. Tables 6.3 and 6.4 show that the water scattering effect is not negligible and that the stainless steel vessels attenuate the gamma propagation. Stainless steel acts more as a shield than as a reflector.

Table 6.4. Morris-1A ANS-91 C/E dose rate results

Detector location (id)	Universal Detector ID	C/E No Environment	C/E Full Environment	C/E Water Only Environment
3	0.B	0.59 (1.1%)	0.65 (1.1%)	0.73 (1.1%)
4	0.A	0.64 (0.5%)	0.68 (0.7%)	0.87 (0.4%)
5	0.E	0.72 (0.5%)	0.75 (0.7%)	1.00 (0.4%)
6	1.B	0.66 (0.6%)	0.70 (0.6%)	0.75 (0.6%)
7	1.A	0.64 (0.3%)	0.68 (0.4%)	0.82 (0.3%)
8	1.E	0.69 (0.3%)	0.71 (0.4%)	0.88 (0.3%)
9	2.B	0.66 (0.6%)	0.69 (0.6%)	0.74 (0.5%)
10	2.A	0.68 (0.3%)	0.69 (0.3%)	0.88 (0.3%)
11	2.E	0.72 (0.3%)	0.73 (0.4%)	0.93 (0.3%)

Table 6.5. Morris-1A H*(10) ICRP-74 C/E dose rate results

Detector location (id)	Universal Detector ID	C/E No Environment	C/E Full Environment	C/E Water Only Environment
3	0.B	0.69 (1.1%)	0.73 (1.0%)	0.85 (1.0%)
4	0.A	0.71 (0.5%)	0.78 (0.5%)	1.00 (0.4%)
5	0.E	0.83 (0.5%)	0.87 (0.7%)	1.15 (0.4%)
6	1.B	0.75 (0.6%)	0.80 (0.6%)	0.85 (0.5%)
7	1.A	0.73 (0.3%)	0.78 (0.4%)	0.95 (0.3%)
8	1.E	0.78 (0.3%)	0.81 (0.4%)	1.01 (0.3%)
9	2.B	0.75 (0.6%)	0.78 (0.6%)	0.85 (0.5%)
10	2.A	0.77 (0.3%)	0.79 (0.4%)	1.01 (0.3%)
11	2.E	0.82 (0.3%)	0.83 (0.4%)	1.07 (0.3%)

A major assumption in these models is the size of the aperture (opening) in the lower vessel. The aperture length is unknown (not specified) and the gamma trajectories may highly depend on the real geometry. To assess the sensitivity of the calculation to this parameter, three calculations were completed with the aperture length equal to half the side length of the lower vessel, three-quarters the total length, or full length. The three models are illustrated in Figure 6.5.

Figure 6.5. Lower vessel aperture configuration of Morris-1A sensitivity study

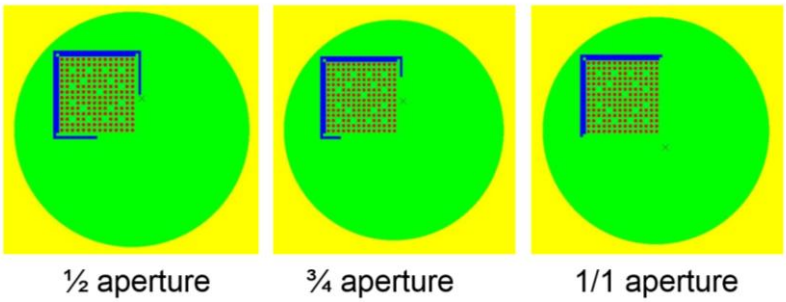

Source: Original data from the NEA EGAFCS, 2020.

The outer vessel is not modelled in this calculation. The results for the three configurations are shown in Table 6.5. The TRIPOLI-4® statistical uncertainties are provided in parentheses and only H*(10) ICRP-74 results are given. The results in Table 6.6 confirm that the main impact of the stainless steel is attenuation rather than reflection. The first column results correspond to the configuration without the outer vessel in the previous section. Additional points that can be underlined here are the relative impact of the aperture size. It is more important for the detector locations 5, 8 and 11 (along the "E" line in the z-direction). This is because these locations are normal to the midpoint of the bottom side shown in Figure 6.4, so any change in the aperture will have the highest impact on gammas detected at these three locations.

Table 6.6. Morris-1A lower vessel aperture impact on C/E dose rate results

Detector location (id)	Universal detector ID	C/E ½ aperture	C/E ¾ aperture	C/E 1/1 aperture
3	0.B	0.77 (0.9%)	0.81 (0.9%)	0.82 (0.9%)
4	0.A	0.85 (0.4%)	0.95 (0.4%)	0.97 (0.4%)
5	0.E	0.94 (0.5%)	1.04 (0.5%)	1.10 (0.4%)
6	1.B	0.81 (0.5%)	0.84 (0.5%)	0.84 (0.6%)
7	1.A	0.83 (0.3%)	0.91 (0.3%)	0.92 (0.3%)
8	1.E	0.86 (0.3%)	0.94 (0.3%)	0.98 (0.3%)
9	2.B	0.81 (0.5%)	0.84 (0.6%)	0.83 (0.5%)
10	2.A	0.84 (0.3%)	0.92 (0.3%)	0.92 (0.3%)
11	2.E	0.88 (0.3%)	0.96 (0.3%)	1.00 (0.3%)

6.2.2. ANL methodology

This section is reproduced courtesy of ANL from Y. Cao and B. Feng (2019), "Validation of Gamma Dose Rate Calculation Methodology using the Morris and Turkey Point Measurements", ANL-19/06.

The ANL numerical studies [17] had a similar three-step approach to simulate the Morris experiments. First, the fuel depletion simulation was performed to calculate the discharged

fuel compositions from the PWR spent nuclear fuel. Secondly, the radioactive decay simulation was performed to calculate the gamma sources from the radioactive isotope decay at the end of the cooling period. Thirdly, the photon transport simulation was performed to calculate the gamma dose rates at the detector locations using the calculated gamma sources from the second step.

MCODE [10], which couples the MCNP6 [11] neutron transport code and the ORIGEN2 [12] fuel burn-up code, was utilised to deplete the fresh fuel bundle. The FAs used in Utility #1 have different fuel lengths than those from Utility #2, but they share the same lattice design. Figure 6.6 shows the Monte Carlo model developed for the fuel lattice.

Figure 6.6. Monte Carlo model of the FAs for the Westinghouse 14X14 FAs

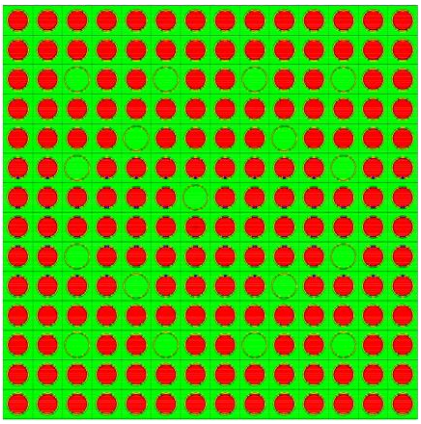

Source: Cao Y., B. Feng, 2019.

The fuel burn-up specified for the fuel bundles was the core average burn-up. Therefore, the Monte Carlo fuel burn-up calculations were performed on the infinite lattice model with reflective boundary conditions applied on all sides of the FA. The ENDF/B-VII.0 library was used in the Monte Carlo transport calculations [13], and the ORIGEN2 library was used for generating the FPs. The MCNP6 code with CINDER90 fuel burn-up code embedded and the SERPENT code [14] were also used to simulate the fuel bundle 1A irradiation for code comparisons. The same ENDF/B-VII.0 data files were used in the transport calculations. In MCNP6 simulations, the tier 3 FPs were used to track FPs in transport calculations. The CINDER90 fission yield libraries are generated from the ENDF/B-VI.0 cross-section libraries [15]. In MCNP6, the fission yield data libraries are old and are based on the ENDF/B-VI.0, and not updated to date. It is a mismatch and there are studies discussing the impacts of using these old libraries in burn-up calculations. The SERPENT code used the ENDF/B-VII.0 cross-section libraries for transport calculations and the fission yield libraries are also generated from the ENDF/B-VII.0 data files.

Figure 6.7 compares the calculated reactivity losses by the three codes with fuel burn-up days to 1 264 days. The reactivity loss ΔK_{eff} calculated by the three codes is very similar to each other with 0.424 by MCODE, 0.425 by MCNP6 and 0.434 by SERPENT. Figure 6.8 shows the calculated amount of actinides in the fuel bundle at the end of the fuel burn-up (see Figure 6.9 for the FPs). Overall, the actinide fuel compositions calculated by MCODE are closer to the compositions obtained from SERPENT. The maximum differences for the U and Pu isotopes are within or around 5% between the MCODE calculation and the SERPENT calculation. The differences for Cm isotopes are slightly larger. About 11% more of ^{242}Cm and 20% less of ^{243}Cm are obtained in the SERPENT

code calculations. The MCNP6 fuel burn-up calculations predict more consumption of ^{235}U and more production of ^{239}Pu at the end of the fuel burn-up as shown in Figure 6.8.

Figure 6.7. Monte Carlo calculated reactivity in the fuel burn-up simulations for the 1A fuel bundle using the MCNP6, MCODE and the SERPENT code respectively

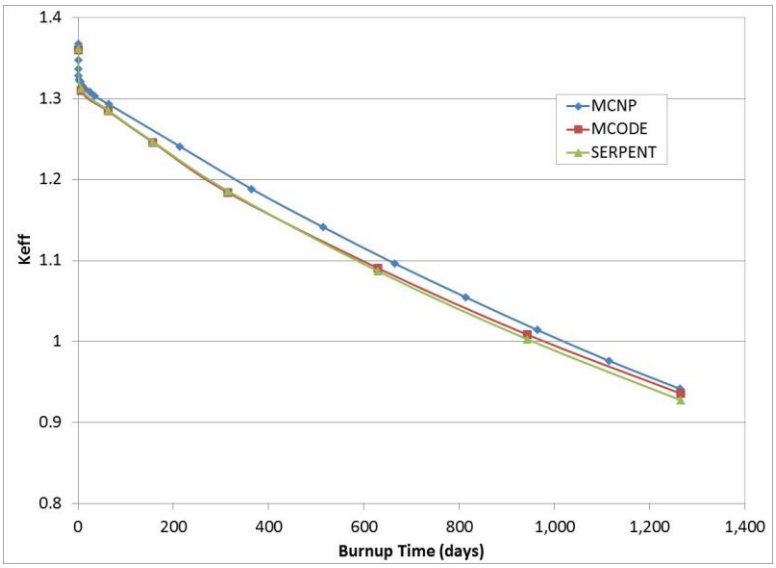

Source: Cao Y. and B. Feng, 2019.

Figure 6.8. Monte Carlo calculated amount of actinide isotope at the end of the fuel burn-up simulations for the 1A fuel bundle using the MCNP6, MCODE and the SERPENT code respectively

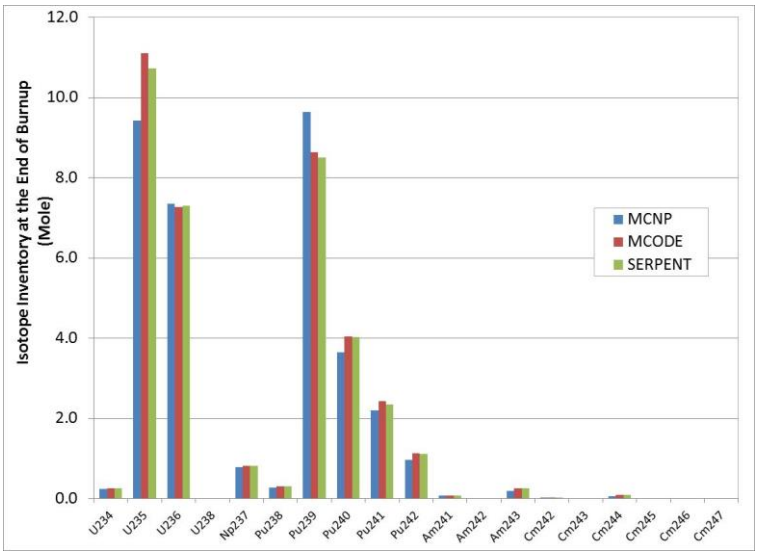

Source: Cao Y. and B. Feng, 2019.

Figure 6.9. Monte Carlo calculated amount of fission isotopes at the end of the fuel burn-up simulations for the 1A fuel bundle using the MCNP6, MCODE and the SERPENT code respectively

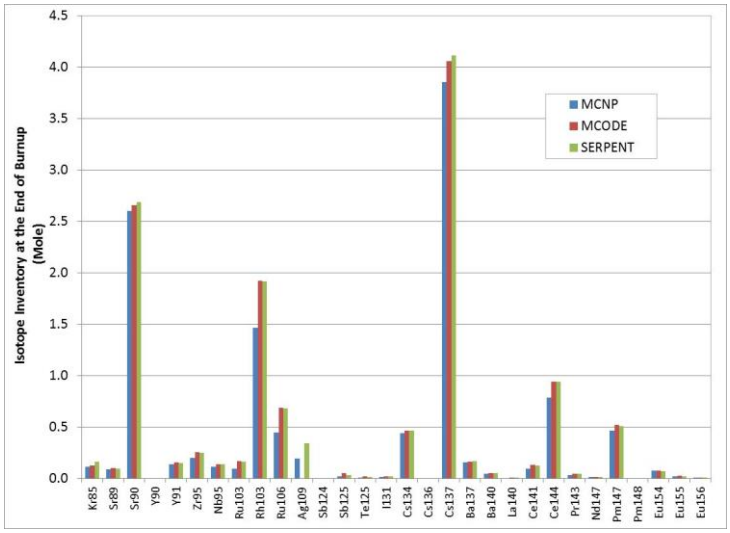

Source: Cao Y. and B. Feng, 2019.

Figure 6.10 compares the calculated amount of FP, which were important gamma ray source emitters from the three codes. Similarly, the SERPENT and MCODE show better agreement on the calculated FP masses. In the MCNP6 fuel burn-up analysis, some of the radioactive isotopes at metastable states, which are important gamma emitters, are not included in the tier three fission product library and cannot be accessed by the users. Therefore, only MCODE was used to perform the fuel burn-up analysis for the Morris experiments. The SERPENT code has been used to simulate the Turkey Point experiments as shown in the later section.

The ORIGEN2 code was used to calculate the gamma source rates of the discharged spent fuel bundle at different cooling stages. The discharged fuel compositions obtained from the fuel depletion calculations were used in the simulations. The gamma ray sources calculated from the code were divided into multiple energy groups. The source rates in each energy group were adjusted to preserve the total amount of gamma source energies released from the FA. In this benchmark analysis, the default 18 energy group structure of the ORIGEN2 was used. For fuel bundle 1A, the total calculated gamma source intensity is 7.81×10^{15} photons/s for the whole assembly, which includes 0.386 tonnes of initial HM and bremsstrahlung from beta particles.

Figure 6.10 compares the multi-energy group gamma sources produced from FP. The discharged fuel compositions are from the SERPENT burn-up simulation or the MCODE depletion calculations for fuel bundle 1A respectively. The calculated gamma source rates agree with each other very well for both cases at all the energy groups.

Figure 6.10. The calculated gamma source energy spectrum of the 1A spent fuel bundle after 4 years of cooling using the SERPENT code and MCODE for fuel burn-up analysis

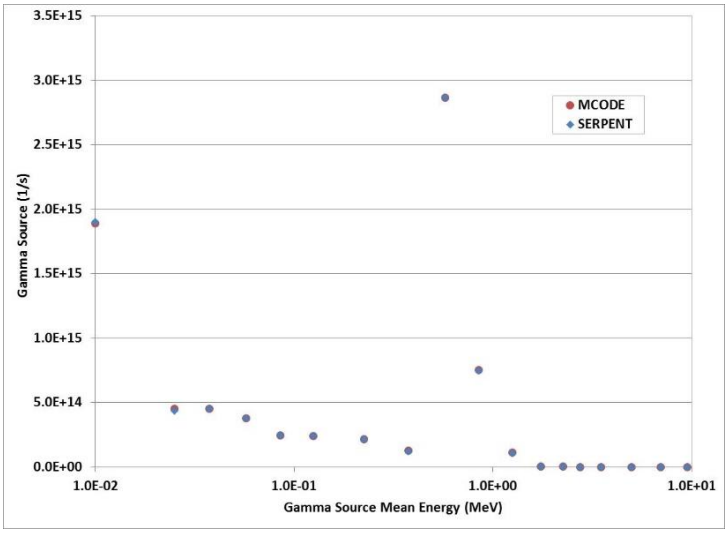

Source: Cao Y. and B. Feng, 2019.

The gamma source rates from a spent FA decrease with a long cooling period. The short-lived radioisotopes only contribute to the gamma sources at short cooling times. As an example, for fuel bundle 1A, Table 6.6 lists the calculated gamma sources originating from each important isotope with contributions larger than 0.1% at different cooling stages. The values in the table are the percentage of gamma rays generated from the particular isotopes to the overall gamma source intensities at that cooling stage. Right after the fuel discharged, the ^{95}Zr, ^{95}Nb, ^{103}Ru, ^{106}Rh, ^{140}La, ^{141}Ce, and ^{144}Pr isotopes contribute more than 71% of gamma sources. After 4 years of cooling, which was at the time of the measurements for assembly 1A, the dominant radioisotopes become ^{90}Y, ^{106}Rh, ^{134}Cs, ^{144}Pr and ^{137M}Ba which generate about 86% of the total gamma sources. For comparison purposes, after a projected 30 total years of cooling, the dominant radioisotopes for gamma ray sources change to ^{90}Y, ^{90}Sr, ^{137}Cs and ^{137M}Ba, which contribute more than 95% of the total gamma sources.

While the FA is irradiated inside the reactor core, the structural material may also be activated by absorbing neutrons. The grid spacer material in the Morris Operation was Inconel-718 which contained a maximum of 1% cobalt as part of its impurities. Other structural materials such as Zircaloy-4 cladding and SS304 structure material also contained some cobalt impurities. ^{59}Co is the only cobalt isotope in nature which can absorb neutrons and turn to ^{60}Co. ^{60}Co releases two gamma rays with energies of 1.17 MeV and 1.33 MeV. To calculate the amount of gamma ray sources from the irradiated spacers, Table 6.8 shows the estimated amount of cobalt mass used in the calculations for all the fuel bundles in the Morris experiments. To simulate the ^{59}Co impurities irradiated in the core, the neutron cross sections for ^{59}Co were tallied as shown in Table 6.9 adopting the neutron flux spectrum inside the guide tubes. The irradiation of ^{59}Co was then simulated using the ORIGEN2 code for different fuel bundles.

Table 6.7. Calculated gamma ray source contributions from the radioisotopes in the Morris discharged FA 1A at discharge and after 4 years or 30 years of cooling

Discharge		4 years of cooling		30 years of cooling	
Isotope	Fraction (%)	Isotope	Fraction (%)	Isotope	Fraction (%)
U237	0.697	PU238	0.101	PU238	0.331
SR 89	2.924	AM241	0.123	AM241	1.852
SR 90	0.153	CM244	0.112	CM244	0.167
Y 90	0.941	KR 85	0.328	KR 85	0.246
Y 91	4.308	SR 90	2.598	**SR 90**	5.641
ZR 95	9.359	**Y 90**	15.950	**Y 90**	34.632
NB 95	11.547	**RH106**	15.551	**CS137**	7.333
RU103	7.804	**CS134**	23.701	EU154	1.110
RH106	12.362	CS137	3.317	**BA137M**	48.086
I131	0.800	CE144	1.842	---	---
XE133	0.327	**PR144**	8.857	---	---
CS134	4.754	PM147	0.455	---	---
CS137	0.195	EU154	2.237	---	---
BA140	2.455	SB125	1.636	---	---
LA140	8.337	TE125M	0.356	---	---
CE141	6.289	**BA137M**	21.748	---	---
PR143	0.894	EU155	0.353	---	---
CE144	3.244	---	---	---	---
PR144	15.596	---	---	---	---
ND147	0.997	---	---	---	---
EU154	0.165	---	---	---	---
EU156	1.068	---	---	---	---
RH103M	0.486	---	---	---	---
SB125	0.234	---	---	---	---
BA137M	1.280	---	---	---	---
CS136	0.279	---	---	---	---
PM148M	0.325	---	---	---	---
Total	97.8	Total	99.3	Total	99.4

Source: Cao Y. and B. Feng, 2019.

Table 6.8. Estimated Co impurities in the Morris FAs

Fuel bundle	1A				2A, 2B, 2D			
	Material	Mass (kg)	Cobalt content (wt%)	Cobalt mass (g)	Material	Mass (kg)	Cobalt content (wt%)	Cobalt mass (g)
Spacer	Inc718	5.9	0.469	27.69	Inc718	5.9	0.469	27.69
Cladding	Zr-4	91.5	0.001	0.92	SS304	89.7	0.08	71.73
Other	SS304	4.6	0.08	3.68	SS304	4.6	0.08	3.68
Total Co (g)	32.29				103.10			

Table 6.9. MCNP tallied neutron cross-sections for ^{59}Co in the Morris Operation at different fuel burn-up steps

Burn-up Step (GWd/MTIHM)	Flux (n/cm^2-s)	Tallied Co-59 cross-sections (barns)			
		(n, gamma)	(n, 2n)	(n, α)	(n, p)
0.2	2.35E+14	5.846	5.69E-5	4.27E-5	3.85E-4
20	2.90E+14	5.409	7.66E-5	4.95E-5	4.23E-4
40.2	3.49E+14	5.416	7.57E-5	5.07E-5	4.34E-4

Figure 6.11 compares the calculated amount of photon sources produced from the actinides and their daughters, from the FP and the ^{60}Co in the irradiated spacers for the Morris FA 1A. The gamma ray sources from the spent nuclear FA are contributed mainly from the decay of the FP. The gamma rays from other actinide isotopes and the activation products are at least one order of magnitude smaller in all energy groups except in the energy group from 1.0 to 1.5 MeV.

The amount of gamma ray sources from the irradiated structural material ^{60}Co is equally important to the gamma sources released from FP in this energy group. The ^{60}Co contributes to about 13% of the total dose rate for assembly 1A (Zircaloy-based cladding and Inconel grid spacers), whereas it contributes between 33% to 42% of the total dose rate for assemblies 2A, 2B and 2D, which use stainless steel cladding. These are quite significant contributions so it is important to document all cobalt impurities in irradiated structural materials in future experiments. Note that the cooling times for these FAs were all relatively short. For dose rates measured at longer cooling times (e.g. 30 years), the contribution of irradiated cobalt is expected to be around only 1% of the total dose rate.

MCNP6 photon transport simulations were performed to calculate the gamma dose rates at the detector locations for the four fuel bundles. The total gamma sources from the ORIGEN2 decay simulations were specified as external sources in the simulation. The gamma sources were correlated to the radioactive isotopes produced in the fuel pin and the structural materials. In the Morris experiment, the gamma dose rates were measured outside and away from the FAs. Thus, in the MCNP6 transport simulation, the gamma sources were assumed to be evenly distributed within the fuel pins in the radial direction. Different axial distributions along the fuel pins were tested. The photon fluxes at the detector locations were tallied. The gamma dose rates were then obtained using the flux-to-dose rate conversion factors recommended by the American Nuclear Standard Institute (ANSI).

Figure 6.14 shows the MCNP model of the Morris experimental setup with the PWR fuel bundle inside the square tube. The ion chambers used in the experiment were modelled as cylinders which were 0.25 inch in diameter and 1 inch long. To develop the numerical model, assumptions were made to the geometry parameters which were not specified in the documents. Table 6.10 lists all these parameters, with different values assigned for each parameter. Sensitivity analyses were performed by comparing the calculated gamma dose rates with different values assigned. Different axial profiles were used.

Figure 6.11. The calculated gamma source energy spectrum from different gamma sources for the 1A spent fuel bundle after 4 years of cooling

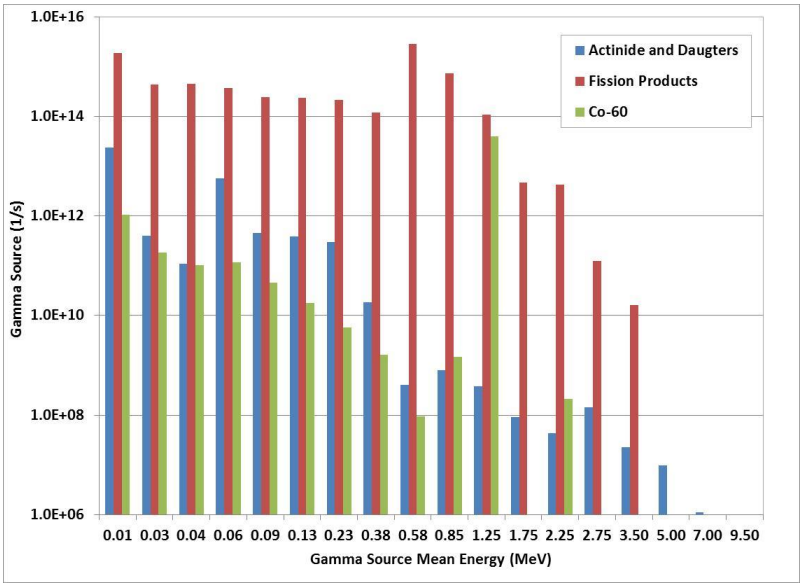

Source: Cao Y. and B. Feng, 2019.

Figure 6.12. MCNP model of the Morris experimental setup with fuel bundle 1A

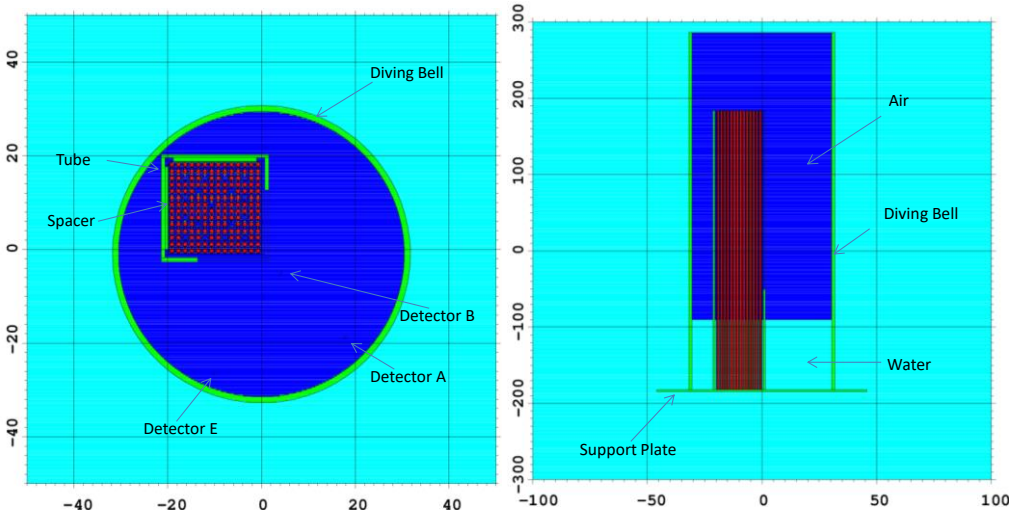

Source: Cao Y. and B. Feng, 2019.

Table 6.10. MCNP model assumptions and parametric studies for fuel bundle 1A

Component	Parameter	Values	Sensitivity analysis
Fuel tube spacer	**Thickness**	0.3 inch	---
	Width	7 inch	---
Fuel tube slot	**Width**	(4.5, **6.0**, 8.0) inch	✓
Support plate	**Radius**	3 feet	---
	Thickness	1 inch	---
Diving bell	**Height**	(**1.0**, 5.0, 10.0) inch above top detector	✓
	Thickness	0.5 inch	---
	Radius	(**1.0**, 1.25) feet	✓
	Air pressure	(0.5, **1.0**, 2.0) atm	✓
Ion chamber	**Radius**	0.125 inch	---
	Length	1 inch	---
Water inside the bell	**---**	(0, **0.25**) height of the tube	✓
Photon source axial distribution	**---**	(tuned, uniform, **Wagner**)	✓

Source: Cao Y. and B. Feng, 2019.

In particular, the width of the tube cut slot determines the open space of the fuel bundle to the ion chambers and was first examined. The tube slot width varied from 4.5 inch, 6.0 inch to 8.0 inch, respectively. Figure 6.13 compares the calculate gamma dose rates with the different open width. The photon flux was tallied at the detector locations with its details not simulated. The 1991 updated flux-to-dose conversion factors by ANSI were used in the calculations [8].

As shown in Figure 6.13, the calculated gamma dose rates are not highly sensitive to the width of the open slot. The calculated gamma dose rates have no significant differences for all detectors located at the fixed B-1 line closer to the open corner. The dose rates are only slightly increased with a wider open slot for detectors at the A-1 and E-1 lines. According to Figure 6.1 (c), the width of the slot can be roughly measured to be about 6 inch based on the relative size in the diagram. Therefore, the width of the slot was selected to be 6 inch in the MCNP model of calculating the gamma dose rates for all the other fuel bundles.

In the Morris experiments, the gamma sources were reflected by the diving bell or were absorbed by the bell. Its impacts on the gamma dose rates were examined by choosing different sizes of the diving bells in the Monte Carlo photon transport simulations. The diving bell was modelled as a cylinder that sits on the bottom support plate. It covered all the FA and all the detectors inside the bell. In the actual experiment, as shown in Figure 6.1 (b), there were two other detectors which were above the fuel tube. Thus, in the MCNP model, to determine the height of the diving bell, an extra manoeuvrable distance of 1 inch, 5 inch and 10 inch above the detector "1" for its operations were assumed respectively. The radius of the diving bell was measured to be around 1 foot according to the diagram in Figure 6.1 (c). Another case with a radius of 1.25 feet was tested to examine its radial reflection impacts. An independent case without the bell but with water presented outside the bell was also tested for comparison.

Figure 6.13. Comparison of the calculated gamma dose rates with different open width of the tube slot for fuel bundle 1A

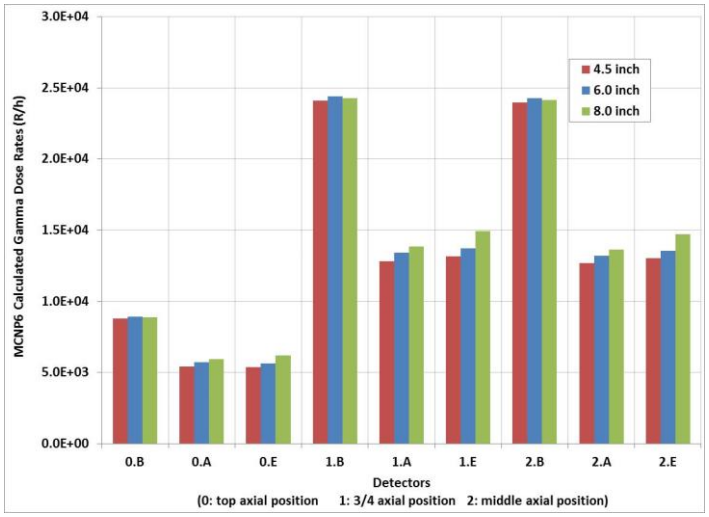

Source: Cao Y. and B. Feng, 2019.

Figure 6.14 shows that the calculated gamma dose rates at all the detector locations were not sensitive to the diving bell geometry. The calculated gamma dose rates all agree with each other for the three cases with different heights and have only slightly smaller values when the diving bell had a larger diameter. The calculated gamma dose rates are only slightly larger with no bell presented, which means the bell absorbed some of the gammas and may also reflect a very small fraction of gammas. Therefore, in the MCNP model, the diving bell was assumed to be a cylinder 1 foot in radius and its top plate 1 cm above the top detector.

To measure the gamma dose rates in the air, the Morris experiments used compressed air to expel water out of the bell. The MCNP photon transport simulations have also been performed with different air pressures inside the bell. Figure 6.15 shows the calculated gamma dose rates with different air pressure. The results show that the air pressure has no impact on the gamma dose rates, thus the normal 1 atm pressure was then assumed in the MCNP model. In all previous trials, the water was assumed to have been completely pushed out of the bell. A case with a water level at ¼ of the active fuel length was also tested. As shown in Figure 6.16 the amount of water left inside the bell has very little impact on the calculated gamma dose rates since the detectors were all far above the water level. In the MCNP model, the water level inside the bell was assumed to be at ¼ of the active fuel length.

Figure 6.14. Comparison of the calculated gamma dose rate with different height and diameter of the diving bell for fuel bundle 1A

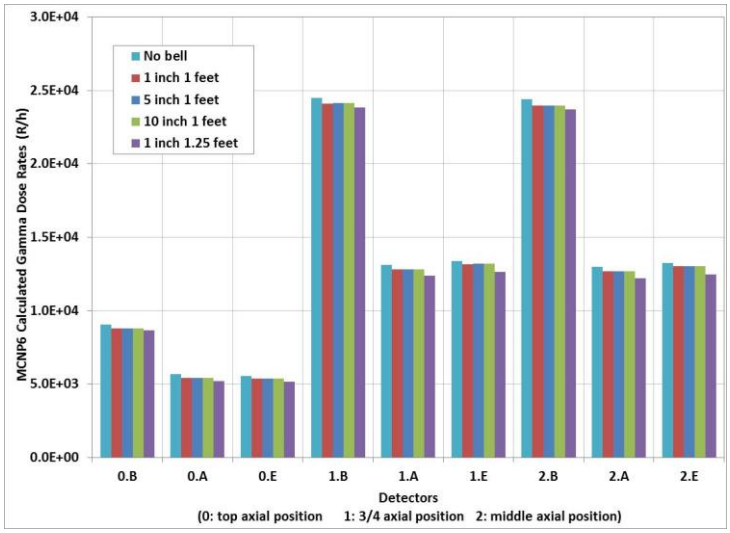

Source: Cao Y. and B. Feng, 2019.

Figure 6.15. Comparison of the calculated gamma dose rate with different air pressure and water level inside the diving bell for fuel bundle 1A

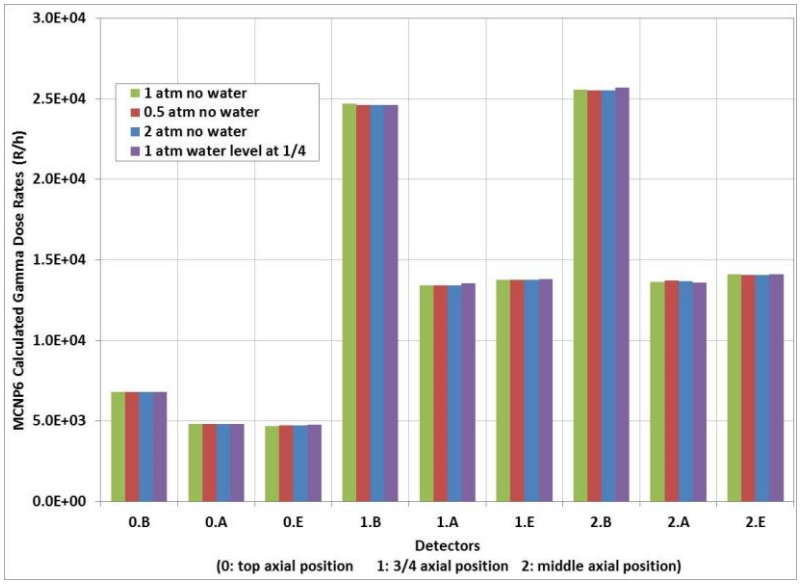

Source: Cao Y. and B. Feng, 2019.

Figure 6.16. Axial gamma source distributions tested in the Monte Carlo transport simulations for fuel bundle 1A

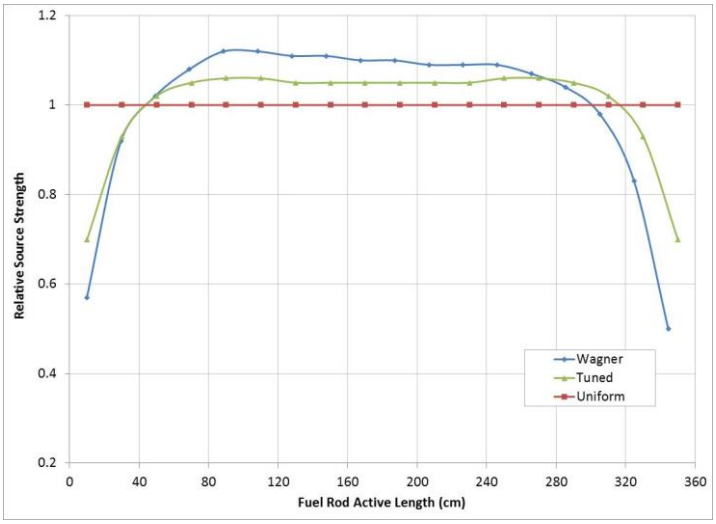

Source: Cao Y. and B. Feng, 2019.

Figure 6.17. Comparison of the calculated gamma dose rate ratios (MCNP model value vs experiment data) with the three axial fuel burn-up distributions for fuel bundle 1A

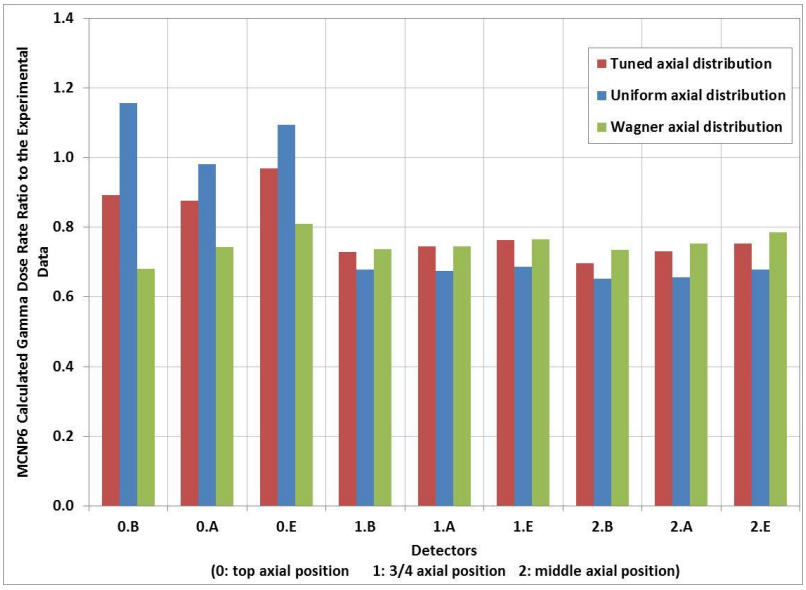

Source: Cao Y. and B. Feng, 2019.

In the MCNP photon transport simulations, the axial distributions of the gamma sources will affect the amount of dose rates calculated for detectors at different heights. In previous trial cases, an axial distribution which was "tuned", or back-estimated, to improve the calculations at the top detector locations was borrowed. For large PWR reactors, the axial power distribution is flatter than a normal cosine shape, and an axial distribution suggested by Wagner is more realistic to represent the axial fuel pin burn-up shape [16]. Thus, a uniform distribution, the previous tuned axial shape and the axial distribution suggested by Wagner were all tested in the Monte Carlo simulations. Figure 6.16 plots these distributions for comparison. Figure 6.17 shows the calculated gamma dose rates using the different

axial source distributions. Compared with the experimental value, the axial uniform distribution distorts the gamma sources at the end of the fuel bundles (top detector locations). The tuned axial distribution has little impact on the detected dose rates at the middle fuel plane and may improve the results at the top detector locations. But to be more consistent and to apply only reasonable assumptions to the numerical simulations, the Wagner distribution which represented a type PWR axial burn-up shape was used in the Monte Carlo burn-up calculations.

In addition, the calculated gamma dose rates are also dependent on the flux-to-dose conversion factors used in the numerical simulations. The most commonly used sets are those by ANSI 6.1.1: ANS-6.1.1 (1977) or the updated standard: ANS-6.1.1 (1991). The gamma dose rates were calculated using both sets and are compared in Figure 6.18. The gamma dose rates using the 1991 updated set obtained lower dose rates. Therefore, the updated 1991 conversion factor set is more conservative to be used in calculating the gamma dose rates for self-guarding nuclear fuels. It has been used in all the later calculations.

Figure 6.18. Comparison of the calculated gamma dose with different flux-to-dose conversion factors for fuel bundle 1A

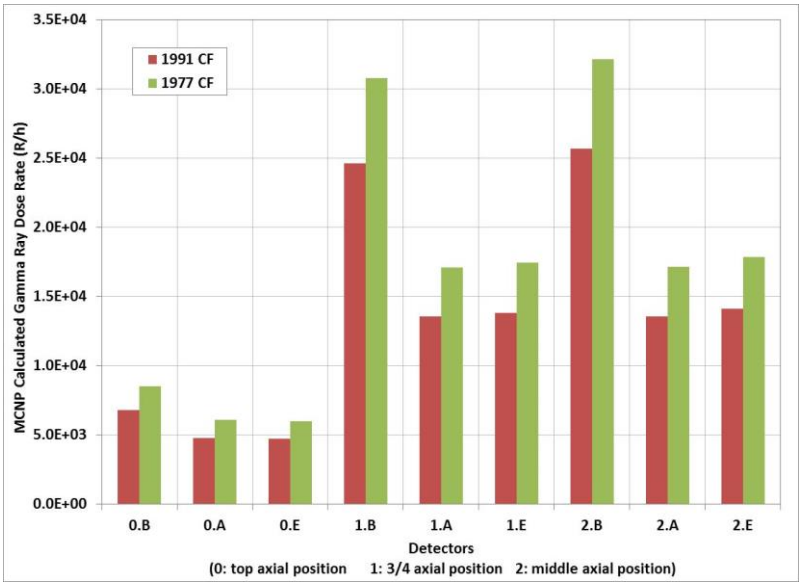

Source: Cao Y. and B. Feng, 2019.

6.3. Results comparison and experimental validations

The CEA results with the full environment modelled for 1A configurations are compared with the ANL numerical results as shown in Table 6.11. The ANL selected geometrical parameters of the Monte Carlo model as bold fonts shown in Table 6.10. Only ANL calculated the gamma dose rates from the other three bundles and the results are listed in Table 6.11 at each detector location. Figure 6.19 plots the ANL gamma dose rate ratios of the calculated values to the measured values.

Overall, compared with the measured gamma dose rates, for assembly 1A, both the CEA and ANL numerical approaches do not overestimate the measured gamma dose rates. Both institutions showed calculated dose rates that are lower than the measured values by about 25-30%. The mean calculation/experiment (C/E) across the nine locations displayed in the

table is about 0.75 for ANL and 0.70 for CEA, which corresponds to ANL's calculated values being about 7% higher than those from CEA. In numerical simulations, CEA and ANL used slightly different assumptions on the experimental setup geometry. They also used slightly different source axial distributions. Another difference is that the CEA calculation did not consider the gamma dose rate contributions from the ^{60}Co impurities, which ANL found to increase the total dose rate by 13% for assembly 1A. Given all these modelling differences, the dose rate from the CEA calculation at each detector location is still very close to the ANL values.

In general, the calculated gamma dose rates agree better with the experimental values for those from detectors at the ¾ height of the FA or the axial mid-plane than for those from detectors located at the top of the FAs. Across all four assemblies, ANL results show that the calculated gamma dose rates are always closer to the experimental values for FAs 2A and 2B than for FAs 1A and 2D.

In particular, in the ANL analysis, for FA 2A and 2B, the average gamma dose rates among the three fixed lines at each axial location are about 10% underestimating the experiment values. For FA 1A, the averaged dose rates at all three axial locations are very consistent and about 25% lower than the experimental values. For FA 2D, the calculated gamma dose rates are about 40% lower at the top detector location, and about 25% lower at the middle plane, and about 18% less at the ¾ height position. The FAs 2A and 2B have similar characteristics. They were irradiated in the core for a similar amount of time, have a similar fuel burn-up, and waited for approximately 83 months before the measurements. However, the FA 1A and 2D have different fuel characteristics. More importantly, the decay time for FA 1A and 2D is much shorter. As shown in Table 6.12, the dominant gamma-ray emitters from the spent FAs change along the FA cooling time as some of the radioisotopes decay quicker than others. Further research work with experimental data covered with all periods of decay time is required to evaluate the different discrepancies from the experimental data shown in this analysis.

The calculated gamma dose rates at the top detector locations are strongly dependent on the axial gamma source distributions used in the simulations. The Wagner axial distribution is an assumption of the FP distributions in the fuel bundles. Bearing these limitations, the calculated gamma dose rates of the Morris experiments still reasonably agree with the experimental data. Both CEA and ANL studies demonstrated that the numerically calculated gamma dose rates from the spent nuclear fuel are on the conservative side to determine the nuclear fuel self-protection.

Table 6.11. CEA and ANL calculated gamma dose rates for the 1A fuel bundle in the Morris experiments with ANS-91 flux-to-dose conversion factors

Detectors	ANL		CEA	
	C/E	Std	C/E	Std
0.B	0.68	0.6%	0.65	1.1%
0.A	0.74	0.7%	0.68	0.7%
0.E	0.81	0.7%	0.75	0.7%
1.B	0.74	0.3%	0.70	0.6%
1.A	0.75	0.4%	0.68	0.4%
1.E	0.77	0.4%	0.71	0.4%
2.B	0.73	0.3%	0.69	0.6%
2.A	0.75	0.4%	0.69	0.3%
2.E	0.79	0.4%	0.73	0.4%

Table 6.12. ANL calculated gamma dose rates for the four fuel bundles in the Morris experiments

Detectors	1A		2A		2B		2D	
	kR/h	C/E	kR/h	C/E	kR/h	C/E	kR/h	C/E
0.B	6.81	0.68	3.16	0.84	2.56	0.85	7.22	0.60
0.A	4.83	0.74	2.42	0.93	1.95	0.91	5.55	0.69
0.E	4.69	0.81	2.35	0.89	1.90	0.94	5.35	0.56
average	---	0.74	---	0.89	---	0.90	---	0.62
1.B	24.7	0.74	13.6	0.85	11.0	0.88	31.1	0.84
1.A	13.4	0.75	7.13	0.96	5.76	0.96	16.4	0.81
1.E	13.8	0.77	7.41	1.02	5.99	1.04	16.9	0.81
average	---	0.75	---	0.94	---	0.96	---	0.82
2.B	25.6	0.73	13.9	0.83	11.2	0.83	31.7	0.79
2.A	13.6	0.75	6.86	0.90	5.54	0.90	15.7	0.71
2.E	14.1	0.79	7.43	0.99	6.01	1.05	17.0	0.77
average	---	0.76	---	0.90	---	0.93	---	0.76

Figure 6.19. Comparison of the calculated gamma dose rate ratios to the measured values for fuel bundles 1A, 2A, 2B and 2D in the Morris experiments

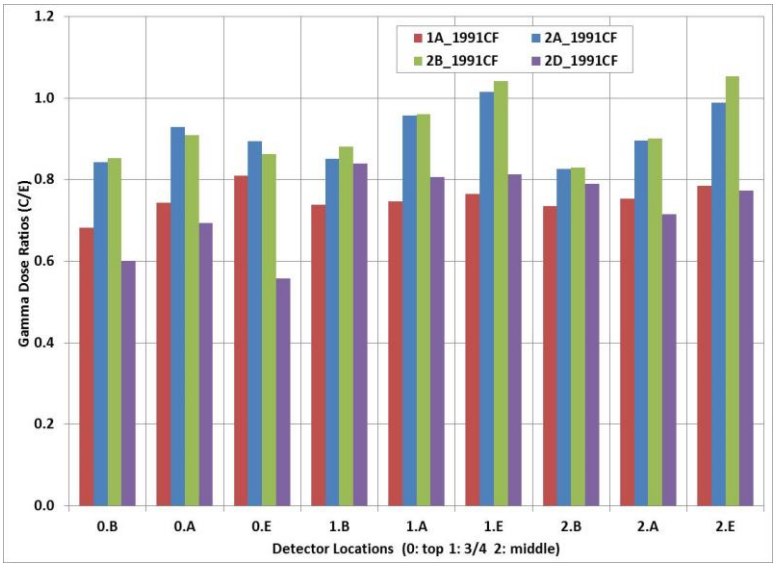

Source: Cao Y. and B. Feng, 2019.

References

[1] Strickler, H.R. and K.J. Eger (1981), *In-Plant Test Measurements for Spent Fuel Storage at Morris Operation, Volume 2, Fuel Bundle Radiation Levels*, NTIS., PC A05/MF A01 as DE82013711, 100 p, NEDG-24922-2, September 1981, DOE, United States, https://doi.org/10.2172/5295958.

[2] Willingham, C.E. (1981), *Radiation Dose Rates from Commercial PWR and BWR Spent Fuel Elements*, PNL-3954/UC-70, Pacific Northwest National Laboratory (PNNL), Richland, WA, United States, https://doi.org/10.2172/6052779.

[3] Brun, E., F. Damian, C.M. Diop, E. Dumonteil, F.X. Hugot, C. Jouanne, Y.K. Lee, F. Malvagi, A. Mazzolo, O. Petit, J.C. Trama, T. Visonneau and A. Zoia (2015), "TRIPOLI-4® CEA, EDF and AREVA reference Monte Carlo code", *Annals of Nuclear Energy*, Vol. 82, pp. 151-160, Elsevier, Amsterdam, http://dx.doi.org/10.1016/j.anucene.2014.07.053.

[4] Tsilanizara, A., et al. (2000), "DARWIN: An evolution code system for a large range of applications", *Journal of Nuclear Science and Technology Supplement*, Sup. 1, pp. 845-849, https://doi.org/10.1080/00223131.2000.10875009.

[5] San-Felice, L., R. Eschbach and P. Bourdot (2013), "Experimental validation of the DARWIN2.3 package for fuel cycle applications", *Nuclear Technology*, Vol. 184, pp. 217-232, https://doi.org/10.13182/NT12-121.

[6] NEA (2009), *The JEFF-3.1.1 Nuclear Data Library, JEFF Report 22*, OECD Publishing, Paris.

[7] Lutier, J. et al. (2015), "Burnup credit implementation for PWR UOX used fuel assemblies in France: From the studies to the practical experience", *Nuclear Science and Engineering*, Vol. 181 (2), pp. 105-136, doi: 10.13182/NSE14-51.

[8] ANS (1991), *American National Standard for Neutron and Gamma-Ray Flux-to-Dose-Rate Factors*, American Nuclear Society, ANSI/ANS-6.1.1 (1991), United States.

[9] ICRP (1996), *Conversion Coefficients for use in Radiological Protection against External Radiation*, ICRP Publication 74, Vol. 26, No. 3-4, Canada.

[10] Xu, Z. and P. Hejzlar (2008), *MCODE, Version 2.2: An MCNP-ORIGEN Depletion Program*, MIT.

[11] Pelowitz, D.B. (2011), *MCNP6-TM User's Manual*, LA-CP-11-01708, December 2011, Los Alamos National Laboratory, United States.

[12] Croff, A.G. (1980), *A User's Manual for the ORIGEN-2 Computer Code*, ORNL/TM-7175, Oak Ridge National Laboratory, United States.

[13] Chadwick, M.B. (2006), "ENDF/B-VII.0: Next generation evaluated nuclear data library for nuclear science and technology", *Nuclear Data Sheets*, Vol. 107, Issue 12, pp. 2931-3060, https://doi.org/10.1016/j.nds.2006.11.001.

[14] Leppanen, J. (2015), *Serpent – A Continuous-energy Monte Carlo Reactor Physics Burnup Calculation Code*, 18 June 2015, VTT, Finland.

[15] Fensin, M.L. and M. Umbel (2015), "Testing actinide fission yield treatment in CINDER90 for use in MCNP6 burnup calculations," *Progress in Nuclear Energy*, Vol. 85, pp. 719-728, https://doi.org/10.1016/j.pnucene.2015.09.001.

[16] Wagner, J.W. and M.D. DeHard (1999), *Review of Axial Burnup Distribution Considerations for Burnup Credit Calculations*, ORNL/Tm-1999/246, Oak Ridge National Laboratory, United States.

[17] Cao Y. and B. Feng (2019), *Validation of Gamma Dose Rate Calculation Methodology using the Morris and Turkey Point Measurements*, ANL-19/06, Argonne National Laboratory, United States.

7. Experimental validation: Turkey Point experiment

This chapter is a summary of the different contributions.

7.1. Introduction

This chapter summarises the outcome of the validation benchmark exercise undertaken by various institutes using their computer tools and approaches for predicting the delayed gamma dose rate distribution around a spent FA. Experimental data on dose rates in the air, carried out in the 1980s using irradiated FA of the Turkey Point Unit 3 reactor, were used for comparison against the calculated dose rates.

The Turkey Point Unit 3 is a conventional 3-loop PWR, designed by Westinghouse Electric Corp. and operated by Florida Power and Light Co. The study focuses on two spent FAs, serial numbers B03 and D04, respectively, discharged from the reactor core after an irradiation period of, respectively, 827 and 851 effective full power days (EFPDs) and under cooling periods of 3.7 and 1.8 years.

Eight institutes have contributed to this study, namely:

- ANL (United States);
- CIEMAT (Spain);
- CEA (France);
- ENEA (Italy);
- KIT(Germany);
- ORANO TN (France);
- SCK CEN (Belgium);
- VTT (Finland).

ANL, CIEMAT, CEA, ORANO-TN, ENEA, KIT and VTT contributed to the case of D04 spent FA while only three (ANL, ENEA and SCK CEN) contributed to the B03 case. This chapter attempts to summarise the contributions from various participants to the computer tools validating exercise based on the above-mentioned cases. It will also highlight the impact of the modelling tools and approaches adopted by participants.

Factors such as the material impurities in the structure materials (mainly cobalt in Inconel-718 spacer grids, in fuel clad and fuel pellet) have been considered. The various components of delayed photon source were also investigated to analyse the calculated result.

7.2. Description of the Turkey Point Unit 3 core and FAs

The design and operating parameters providing the key relevant characteristics of the reactor core, FA and fuel rod configurations have been compiled from the literature [1-3] [6]. The most relevant ones are provided in Table 7.1. Many missing specifications are taken from the documentation on Surry Unit 1 PWR [6], Turkey Point's contemporary reactor having an identical design. The fuel of the Surry Unit 1 and Turkey Point Unit 3 was fabricated at the same time in the same plant. The left-hand picture in Figure 7.1, showing the core configuration and giving the radial dimensions, is of Surry 1.

Each square box in the picture represents an assembly position. The reactor core consists of a 3-batch loading pattern as depicted in the right-hand picture in the figure. In the first reactor cycle, FAs having the highest enrichment are placed in the periphery of the core; those with lower enrichment are mixed in the central region of the core in a checkboard-like pattern, which yields the most uniform power distributions.

Figure 7.1. Turkey Point Unit 3 Core (left) and core loading map (right)

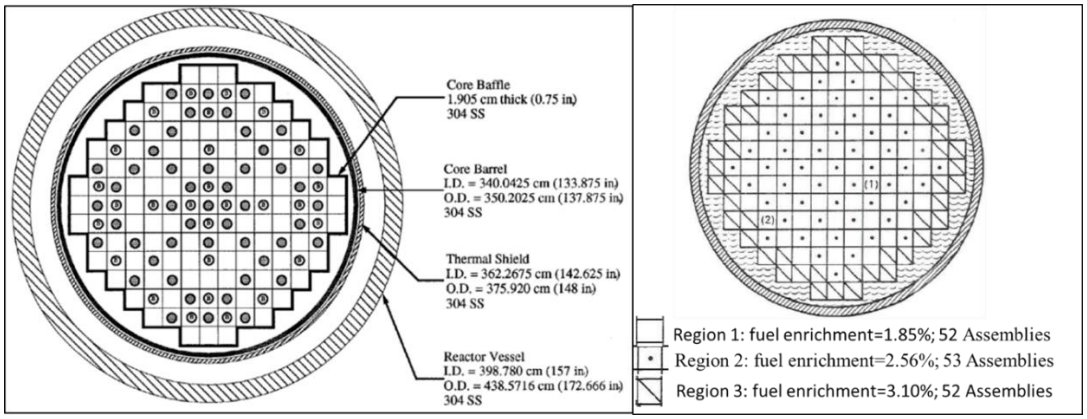

Source: Bowman, S.M. et al., 1995 (left); Radulescu, G.et al., 2010 (right).

A representative FA of the Turkey Point PWR is depicted in Figure 7.2, featuring spacer grid positions and the fuel rod array. The FA design is based on a 15x15 square lattice, with 21 positions containing control rods and instrumentation guide tubes. The radial cut-view (right-side picture) shows the positions of the FA lattice, namely the fuel rod, the guide thimbles and the instrumental tube.

The fuel rods consist of 0.422-inch diameter Zircaloy cladding around uranium oxide pellets. The fuel square lattice pitch (centre-to-centre distance) is 0.563 inches. The active fuel length is nominally 144 inches. The fuel rods are laterally constrained by a series of seven grids located along the length of the rods. The FA is 161.3 inches long (prior to irradiation) with a square cross-section having a maximum distance across flats of 8.426 inches (including grids). The overall length is made up of a top nozzle, the fuel rods and the bottom nozzle. There are only slight differences in the design of the B03 as compared to the D04 FAs, namely the dimensions of the nozzles, the overall length and the initial uranium content.

Figure 7.2. Typical Westinghouse 15x15 fuel assembly

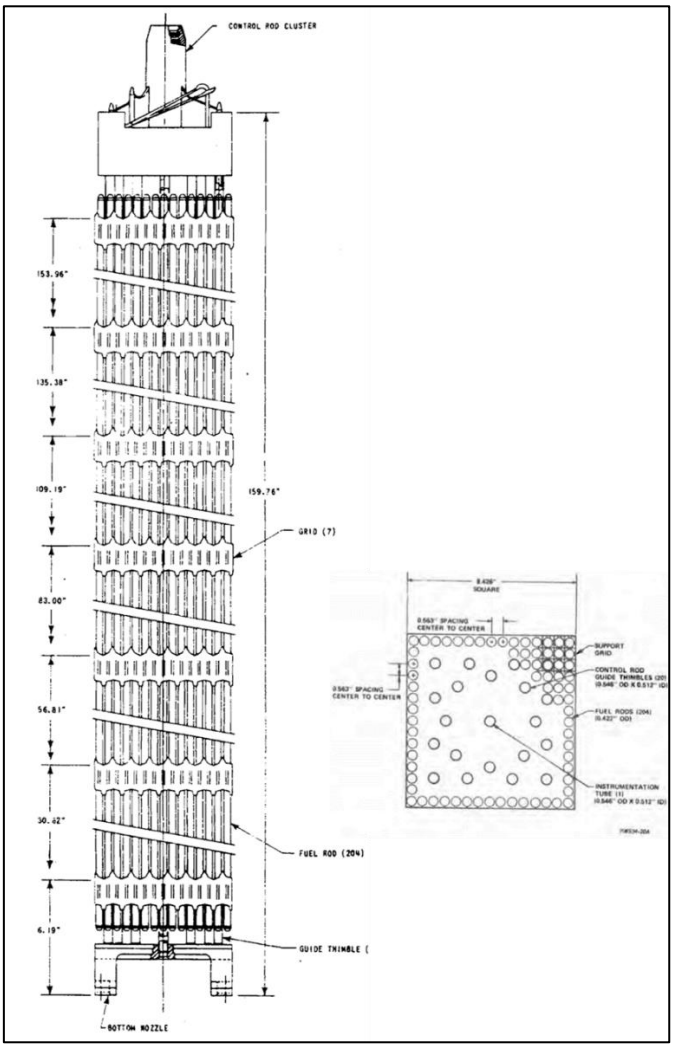

Source: Unterzuber, R. et al., 1982; Weihermiller, W.B. and G.S. Allison, 1979.

Table 7.1. Core and FA design data for Turkey Point Unit 3 PWR

Component	Item (unit)	Data
Core		
	#FAs	157
	Region #1	52
	Region #2	53
	Region #3	52
	Loading pattern	Three fuel-enrichment regions
	Core lattice type	Square
	Core lattice pitch (in.)	8.445
FA		
	Designer	Westinghouse Electric
	Array type	15x15
	EIA assembly code	W1515WL
	Version	LOPAR
	Overall FA length (in.)	159.765
	Transverse dimension (in.)	8.426
Fuel rods		
	Number	204
	Fuel rod pitch (in.)	0.563
	Fuel rod clad thickness (in.)	0.0243
	Fuel rod clad material	Zircaloy-4
	Fuel rod length (in.)	152.06
Fuel pellet		
	Active fuel length (in.)	144
	Material	UO_2
	Region #1	
	Enrichment (^{235}U wt %)	1.85
	Pellet density (% TD)	93.8
	Diametral gap, cold (in.)	0.0075
	Pellet outer diameter (in.)	0.3659
	Region #2	
	Enrichment (^{235}U wt %)	2.56
	Uranium mass per assembly (kg)	448
	Pellet density (% TD)	92.8
	Diametral gap, cold (in.)	0.0075
	Pellet outer diameter (in.)	0.3659
	Region #3	
	Enrichment (^{235}U wt %)	3.1
	Pellet density (% TD)	92

Table 7.1. Core and FA design data for Turkey Point Unit 3 PWR (Continued)

Component	Item (unit)	Data
	Diametrical gap, cold (in.)	0.0085
	Pellet outer diameter (in.)	0.3649
Gas plenum		
	Filling gas	Helium
	Plenum spring volume (in^3)	0.43
	Working length (in.)	6.83
	Spring material (in.)	Inconel-718
Lower end plug	Length (in.)	0.688
Top end plug	Length (in.)	0.688
Spacer grid		
	Grids/Assembly	7
	Spacer height (in.)	1.5
	Spacer weight (gram))	675
	Grid material	Inconel-718
Guide and instrumentation tubes		
	#Guide tubes per assembly	20
	#Instrumentation tubes per assembly	1
	Tube material	Zircaloy-4
	Tube inner diameter (in.)	0.512
	Tube outer diameter (in.)	0.546
FA endings		
	Lower end fitting material	304 SS
	Lower end fitting height (in.)	3.188
	Upper end fitting material	304 SS + Inconel-718 + Inconel-600
	Upper end fitting height (in.)	3.48

7.3. Description of the experimental data

Five FAs (serial numbers B02, B03, B17, B41 and B43) burnt inside Turkey Point Unit 3 core during the first two operation cycles (from 12 January 1972 to 25 November 1975), aggregating 827 EFPDs, while the FA, serial number D04, was irradiated during cycles 2 through 4 (from 12 December 1974 to 24 November 1977), accounting for 851 EFPDs. Figure 7.3 indicates the locations of fuel B's assemblies within the reactor core during the second cycle of operation. The location of the D04 assembly is unknown. The available reactor operating details for the first two cycles are summarised in Table 7.2 [1-3] [5].

Figure 7.3. Irradiation locations of the B's FAs

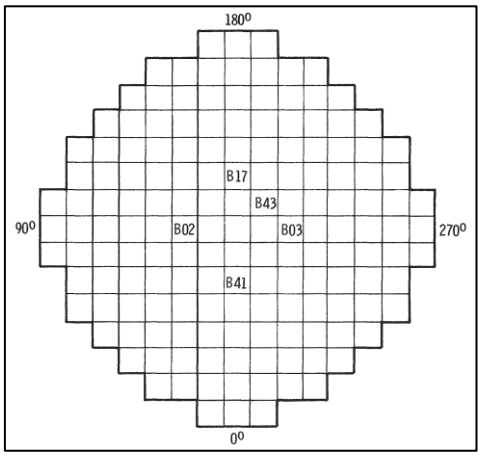

Source: Davis, R.B., 1980.

Table 7.2. Turkey Point Unit 3 core operating data

Reactor operation data	B03	D04
Core average thermal power (MWth/assembly)	13.96	14.26
Irradiation time (EFPD)	827	851
Cooling time (years)	3.7	1.8
(Calculated) Core average burn-up (GWd/MTIHM)	25.665	28.430
(Calculated) Core peak burn-up (GWd/MTIHM)	28.564	-
Initial uranium loading (kg)	448	457
Effective temperature (K)	922	
Clad temperature (K)	595	
Inlet temperature (K)	559	
Outlet temperature (K)	611	
Average moderator temperature (K)	570	
Moderator density (g/cc) at inlet temperature	0.7311	
Soluble boron, cycle average (ppm)	450	

The B03 and D04 spent assemblies have been thoroughly examined (in the air) in a hot cell at Battelle-Columbus Laboratories [1] for gamma activity. Thermoluminescent dosimeters (TLD) were used in this experiment to measure gamma exposure rates. Capsules containing five TLDs were stacked side by side, wrapped in tissue paper and then in foil to minimise contamination. The TLD capsules were divided into four groups of 13 for axial measurements and, for the radial dose rate measurements, a set of eight capsules for B03 assembly and nine capsules for the D04 FA. Each group of capsules was placed inside an aluminium tube with a 30.48 cm (1 foot) distance between adjacent capsules, axially from

the bottom to the top end of the FA active height and radially from the surface of the FA upwards. Figure 7.4 shows the locations of dosimeter tube holders for gamma dose measurements of B03 spent FA. Two of the tubes were exposed within the FA in a guide tube and an instrument tube. Another aluminium tube containing TLDs was exposed resting on the FA surface, and the fourth was exposed 30.48 cm (1 foot) above the FA. The dosimeter holder tubes for radial dose rate measurements were set up perpendicular to the surface at the mid-plane of the FA. The same was done for the D04 assembly, but with dosimeters located only outside. All measurements were carried out inside a hot cell room about which no specifications are provided regarding the size and wall material. The spent FA was resting horizontally on a table. The available experimental dose rates in the air measured through the holder tubes disposed radially above the spent FAs are gathered in Table 7.3 and the data through the tubes disposed axially are in Tables 7.4 and 7.5.

According to [1], experimental data in Tables 7.3, 7.4 and 7.5 are exposure rates in units of Roentgen/h. In a contemporary survey study report [5] on the discrepancies between calculated and measured radiation dose rates in the air from commercial PWR spent fuel elements, the same above experiment data are quoted in units of rad/h and, throughout the document, exposure rates and dose rates are sometimes used interchangeably.

Exposure rate is the amount of ionising radiation per hour in a person's vicinity whereas dose rate is the biological effect on the body from exposure to that radiation. The exposure rate is measured in the US unit of Roentgen per hour (R/h), and the IS unit of Gray (Gy) in air or Rad in tissue. On the other side is the dose rate, in the US unit of Roentgen equivalent man per hour (Rem/h) or the International System unit of sievert per hour (Sv/h), with 1 Rem/h = 0.01 Sv/h. For gamma rays, there is approximately a one-to-one ratio between exposure rate and dose rate, since one roentgen deposits ~0.95 rad in biological soft tissue [51].

Figure 7.4. Live picture showing the B03 FA inside the hot cell and schematic view showing the positions of TLDs holder tubes

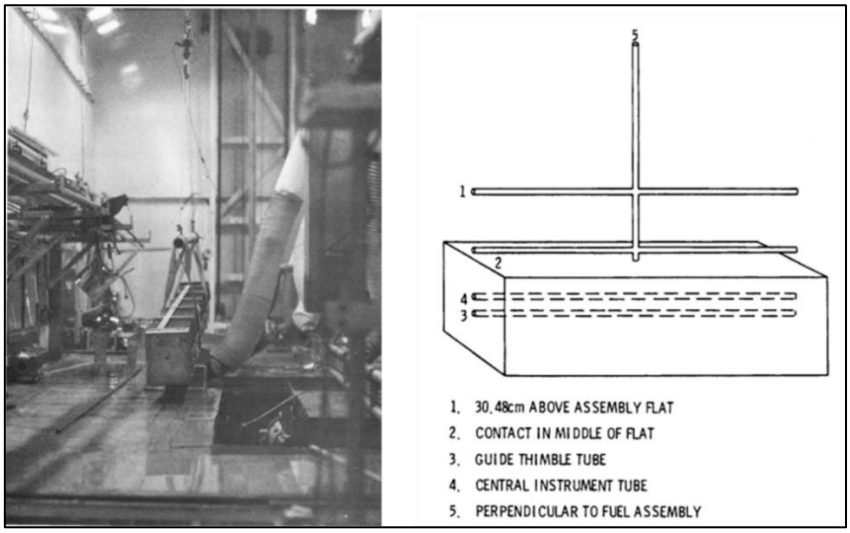

Source: Davis, R.B., 1980.

Table 7.3. B03 FA: dose rates experimental data for TLDs inside the vertical holder tube

	B03		D04	
Vertical distance from assembly surface	Exposure rates	1σ	Exposure rates	1σ
(foot)	(R/h)	(%)	(R/h)	(%)
0	5.88E+04	3	6.30E+04	N/A
1	1.55E+04	7	1.86E+04	
2	7.99E+03	3	9.88E+03	
3	4.62E+03	4	6.81E+03	
4	3.37E+03	5	4.91E+03	
5	2.55E+03	5	3.92E+03	
6	1.90E+03	6	3.34E+03	
7	1.56E+03	4	2.85E+03	
8			2.24E+03	

Table 7.4. B03 FA: dose rates experimental data for TLDs inside axial holder tubes

	Instrumentation tube (holder #4)		Guide tube (holder #3)		On surface (holder #2)		Above surface (holder #1)	
Distance from bottom of fuelled assembly part	Exposure rates	1σ	Exposure rates	1σ	Exposure rates	1σ	Exposure rates	1σ
(foot = 30.48 cm)	(R/h)	(%)	(R/h)	(%)	(R/h)	(%)	(R/h)	(%)
0	3.87E+04	10	1.75E+05	7	1.32E+03	12	1.74E+03	6
1	1.33E+05	3	1.79E+05	4	3.26E+03	3	3.25E+03	4
2	1.74E+05	5	1.69E+05	2	2.24E+04	4	6.02E+03	8
3	1.80E+05	4	1.67E+05	7	3.81E+04	3	8.39E+03	6
4	1.81E+05	4	1.74E+05	4	4.29E+04	3	8.03E+03	9
5	1.71E+05	4	1.65E+05	4	5.67E+04	5	1.18E+04	3
6	1.68E+05	9	1.72E+05	8	5.88E+04	3	1.23E+04	4
7	1.68E+05	8	1.76E+05	5	4.86E+04	5	1.20E+04	5
8	1.72E+05	8	1.65E+05	3	6.33E+04	5	1.24E+04	2
9	1.67E+05	4	1.25E+05	4	6.23E+04	7	1.31E+04	5
10	1.63E+05	2	4.77E+04	6	6.57E+04	4	1.29E+04	8
11	1.27E+05	6	7.18E+03	5	6.26E+04	3	1.17E+04	5
12	6.29E+04	8	1.16E+03	5	5.79E+04	4	1.03E+04	4

Table 7.5. D04 spent FA: Dose rates experimental

	Axial direction distributions			
Distance from bottom of fuelled assembly part	On assembly surface (tube #1)		One foot above surface (tube #2)	
	Exposure rates	1σ	Exposure rates	1σ
(foot)	(R/h)	(%)	(R/h)	(%)
0	8.81E+04	N/A	7.42E+03	N/A
1	8.91E+04		1.21E+04	
2	9.30E+04		1.49E+04	
3	6.57E+04		1.62E+04	
4	9.25E+04		1.62E+04	
5	9.00E+04		1.71E+04	
6	9.52E+04		1.63E+04	
7	9.37E+04		1.58E+04	
8	9.27E+04		1.61E+04	
9	8.25E+04		1.54E+04	
10	5.48E+04		1.42E+04	
11	1.29E+04		1.10E+04	
12	2.75E+03		7.29E+03	

Figure 7.5. Axial power profile in one assembly of the Surry Unit 1 reactor

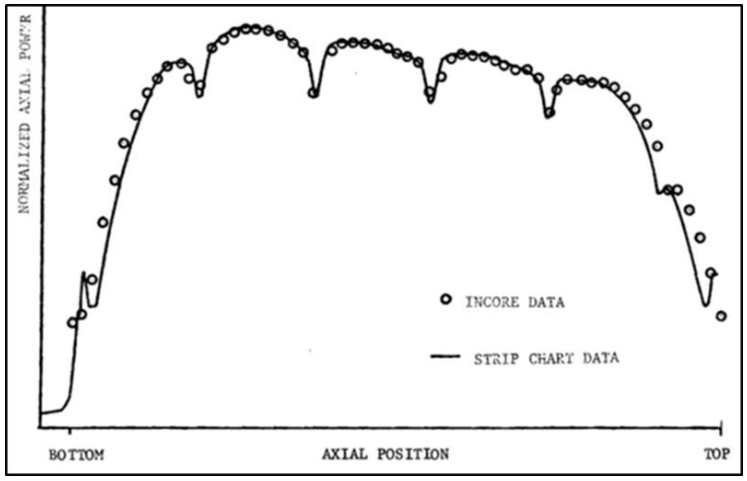

Source: Carlson, R.W., 1979.

The footprint of Inconel-718 spacer grids is visible in Figure 7.5 showing an axial power profile in an irradiated assembly from the Surry Unit 1 PWR. The dotted power profile curve was obtained using a data analysis computer program written by Westinghouse to process data obtained by in-core instrumentation.

In addition, five fuel rods from the B03 spent FA were selected to undergo an axial ^{137}Cs activity gamma scanning. The positions of the investigated fuel rods and the plots of the gamma scanning are shown in Figure 7.6. The latter curves exhibit the expected delayed gamma source axial profile in line with the axial shape fuel rod burn-up, featuring activity depressions at pellet interfaces at spacer grid locations.

Figure 7.6. Location of investigated fuel rods (top left) and replots of gamma scan traces

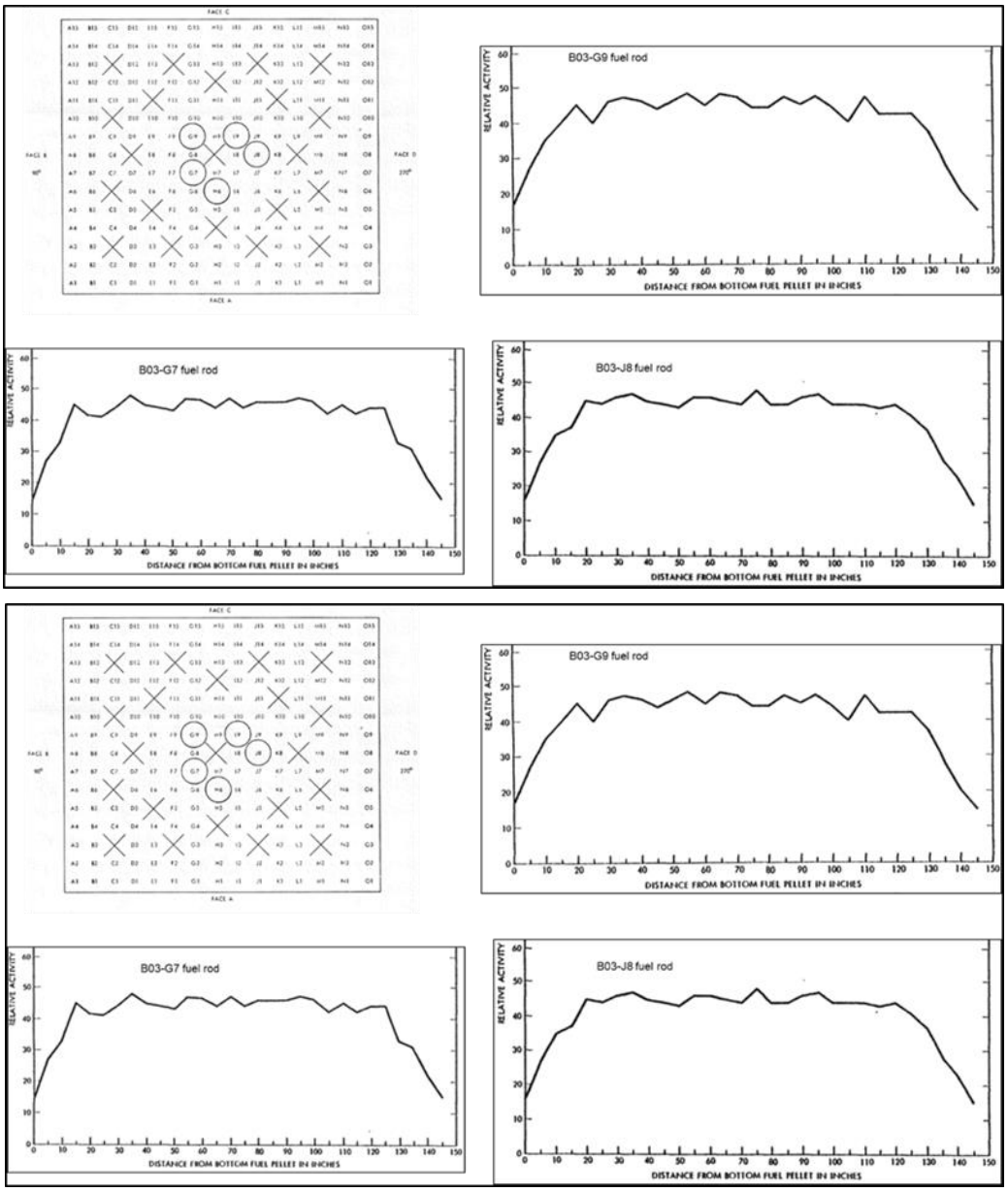

Source: Davis, R.B., 1980.

7.4. Numerical simulation approaches by the various participants

7.4.1. Generic approach

The generic approach to carrying out numerical calculations of dose rates induced by a delayed gamma source has two steps. First is the determination of the delayed radiation source term, which is eventually used in a fixed-source steady-state photon transport simulation using an appropriate computer code along with nuclear data. To this end, a computational model must be built that encompasses the system geometry, the various material zones material specification, the delayed photon source distribution and fluence-to-dose rate conversion functions.

An accurate estimation of the delayed gamma source term should take into account the various reactor core components (fuel pellet and FA hardware) and the different mechanisms of photon-production processes, mainly:

- gamma rays and X-rays from delayed radioactive decay;
- Bremsstrahlung from (beta decay) positron and electron deceleration.

The distance travelled by a photon and the type of interaction that the photon will undergo are determined by its energy and by the material through which it is travelling.

For dose rate calculations, the major characteristics of the delayed photon source are:

- its intensity, which is the normalisation factor for computed tallies;
- its energy distributions (spectrum); and
- its spatial (axial and radial) distribution.

The above characteristics are dependent on parameters such as reactor geometry, material compositions, material temperatures, material cross sections, reactor power level, reactor operating history and problem boundary conditions. Dedicated computer tools, so-called "depletion" or "evolution" or "burn-up" codes, will iterate between a steady-state transport calculation (which uses either deterministic or stochastic methods) and a zone-by-zone material evolution through a deterministic solver of the Bateman equations. In this case, the material compositions in every one of those zones are considered spatially constant when determining the particle flux in the steady-state transport calculation and the particle flux (and the associated spectrum) is assumed constant in space and time during a time step in the evolution calculation.

To accurately calculate the dose rate distribution in the spent FA, the simulation model must include the burn-up-dependent axial variation of the source term. The latter is derived by axially segmenting the calculation model to approximate the axially varying isotopic concentrations, which correspond to the burn-up in each axial segment. The fuel cross sections vary with burn-up because of changes in nuclide concentration and because of the resulting shift in the energy spectrum of the neutron flux. The neutronics-depletion procedure is applied repeatedly to produce cross-section libraries for the irradiation intervals requested by the user.

At the beginning of life, a PWR FA will be exposed to a near-cosine axial-shaped flux, which will deplete fuel near the axial centre at a greater rate than at the ends. As the reactor continues to operate, the cosine flux shape will flatten because of the fuel depletion and FP build-up that occurs near the centre. Near the FA ends, burn-up is suppressed due to leakage. Consequently, the majority of PWR spent FAs have similar axial-burn-up profiles (or shapes) – relatively flat in the axial mid-section (with peak burn-up of ~1.1 times the assembly-averaged burn-up) and significantly under-burnt fuel at the ends (with burn-up of ~0.5 times the assembly-averaged burn-up). PWR axial burn-up profile databases have been developed [16,37], encompassing most of the PWR fuel designs and contain sufficient data to provide reliable statistics. Such databases are often used to avoid modelling complexity.

The computational model should aim at capturing the features relevant to the estimation of the dose rates. Next to the geometry model, one should pay attention to the implementation of the delayed gamma source and the positions of the various detectors.

Another ingredient, at this level, is the fluence-to-dose function. Three sets of fluence-to-dose conversion factors have been proposed since the beginning of the present Taskforce on the Delayed-gamma-induced Dose Rate Calculation, namely: the American National

Standard 6.1.1, 1977, the ANSI/ANS-6.1.1 (1977) [45] and its 1991 update, ANS/ANS-6.1.1 (1991) [46], and one introduced by SCK CEN, the photon ambient dose equivalent H*(10 mm) ICRP (1996) [21], considered the worldwide standard.

Both ANSI/ANS standards dose functions were specified in units of Rem/h/flux. The used ICRP (1996) photon ambient dose equivalent H*(10 mm) coefficients are in units of sievert by photon fluence ($S_v\ cm^2$). The three dose functions are depicted in Figure 7.7, in units of $pS_v\ cm^2$.

Figure 7.7. Fluence-to-dose functions for photons

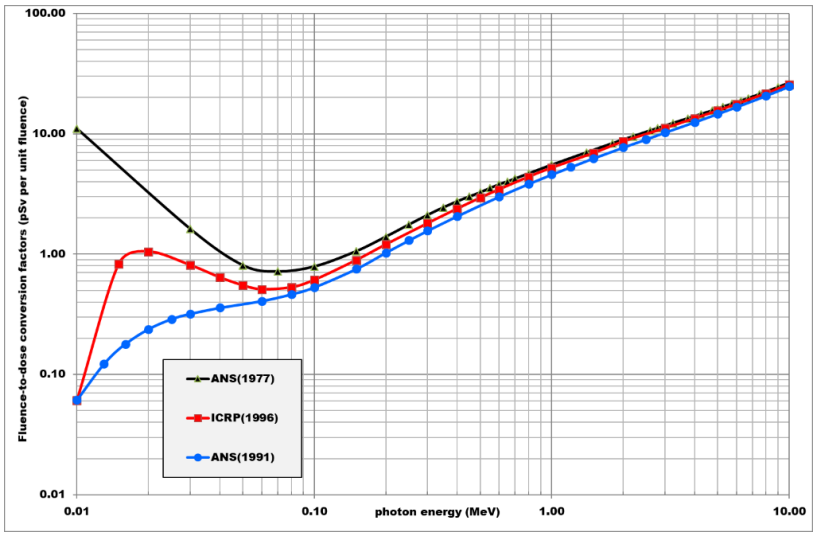

Source: NEA EGAFCS, 2020 – using data from ANSI/ANS (1977), ANSI/ANS (1991) and ICRP (1996).

The 1977 version of the standard was based on the maximum dose equivalent in a 30-cm (diameter) x 60-cm (height) tissue-equivalent cylinder. The ANSI/ANS (1991) version was based on the quantity recommended in the ICRP Publication 26 for the effective dose equivalent. This latter source bases the effective dose equivalent on the sum of weighted organ dose equivalents for an anthropomorphic representation of the human body. The ANSI/ANS-6.1.1 (1977) standard was superseded by its ANSI/ANS-6.1.1 (1991) revision that, however, was formally withdrawn in 2001 and is now designated as a historical standard because the ANS working group failed to issue a revision within 10 years [20]. According to the literature, the two ANSI/ANS standards are known to differ by about 25%, with the 1991 version yielding the lowest dose rate values.

7.4.2. ANL approach

This section is reproduced courtesy of ANL from Y. Cao and B. Feng (2019), "Validation of Gamma Dose Rate Calculation Methodology using the Morris and Turkey Point Measurements", ANL-19/06.

The delayed gamma source characteristics were analysed using the SERPENT 2.1.26 code [23] and the zero-point ORIGEN-S code [38]. The SERPENT Monte Carlo code, along with continuous nuclear data from the ENDF/B-VII.0 library [39], was used to perform the fuel depletion and structural material activation using a 3D FA model assumed to be an element of an infinite lattice (*reflective boundaries conditions being assigned in the lateral directions) to match the average core burn-up specified in the experiments.* A one-metre-thick water layer was assumed as an axial reflector, both at the bottom and the top of the

FA, with vacuum boundary conditions. The full height of the fuel pellet was burnt as a single axial segment yielding an overall spent FA inventory and an assembly-averaged burn-up. The UO_2 fuel and the Zircaloy-4 clad materials were assumed to bear a negligible amount of impurities, contrary to the assembly spacer grid and the gas plenum spring, which both consist of Inconel-718.

Based on [22], the chemical composition of Inconel 718 with cobalt impurity content of 0.91 wt% was used in the present delayed gamma source calculation. The model assumed a 3.81-cm height spacer grid with a total mass of 675 grams [6] at axial positions specified in [13]. *The total mass of the gas plenum spring was assumed to be 11.34 kg (25 lb)* for all the FA. It was smeared with a reduced density of 4.555 g/cm^3 inside the gas plenum chamber.

Monte Carlo fuel burn-up analyses were performed to simulate the fuel depletion and the irradiation of ^{59}Co impurities. Separate burn-up regions were assigned for the seven spacers and the spring, respectively. The Monte Carlo fuel burn-up calculations were performed continuously with no reactor outage time simulated.

The gamma ray sources released from the spent fuel FP, from the activated *spacers and* the activated *spring were all calculated separately using the material compositions generated from the SERPENT code. The default 18 energy group structure in the ORIGEN-S code, as listed* in Table 7.6, *was used to tally the delayed gamma source spectrum. Figure 7.8 shows the calculated gamma ray sources from the fuel zone, from the spacers and the spring, respectively. Overall, the major gamma sources are contributed by the decay of FP,* aggregated mainly within group #8, with a centroid energy value equal to 0.65 MeV. *The ^{60}Co gamma rays, particularly those released from the irradiated spacers, are one of the main contributors* (75%, as shown in Figure 6.16) *to the overall gamma source in the energy range from 0.9 MeV to 1.35 MeV.*

The total gamma source intensity obtained from the calculations is 4.74E+15 photons/s from the B03 FA after about 3.8 years[3] of decay and 1.36E+16 photons/s from the D04 FA after about 1.8 years of decay.

[3] 3.8 years used in the calculation, instead of 3.7 years specified, meaning ~36 days overburning.

Figure 7.8. B03 FA: Calculated gamma source spectra featuring ray-line from ^{60}Co decay

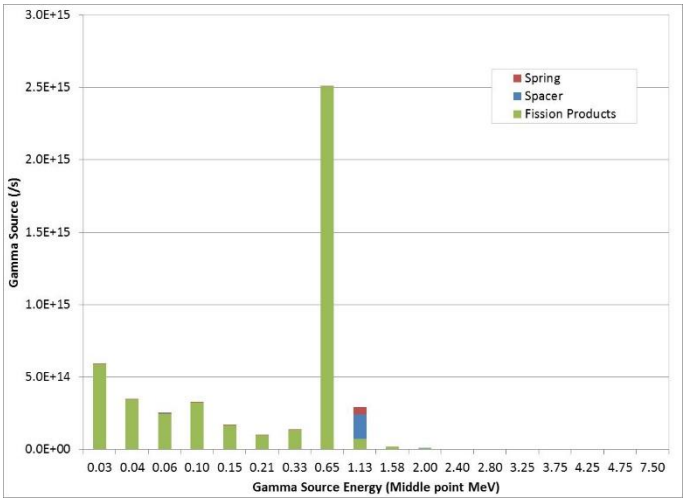

Source: Cao, Y. and B. Feng, 2019.

Table 7.6. Default 18-energy group structures for gamma spectra in ORIGEN-S code

#group	Upper boundary energy (MeV)	Source intensity share (%)	
		D04	B03
1	0.035	15.12	13.0
2	0.050	10.97	7.6
3	0.075	7.53	5.5
4	0.125	9.59	7.2
5	0.175	6.94	3.7
6	0.250	3.12	2.2
7	0.400	4.60	3.0
8	0.900	39.70	55.4
9	1.35	1.54	1.6
10	1.80	0.54	0.5
11	2.20	0.32	0.1
12	2.60	0.03	0.0
13	3.00	0.00	0.0
14	3.50	0.00	0.0
15	4.00	0.00	0.0
16	4.50	0.00	0.0
17	5.00	0.00	0.0
18	10.0	0.00	0.0
Total (photon/s)		1.337E+16	4.520E+15

The gamma sources obtained from ORIGEN-S have been used as external sources in photon steady-state transport simulations using the MCNP6 code. Given the lack of assembly power history, the adopted approach does not provide a problem-dependent axial burn-up profile, meaning no delayed gamma source axial distribution was calculated. To bridge this gap, a PWR burn-up axial profile from the literature database, namely the Wagner fuel burn-up distribution [16], plotted in Figure 6.16 was used for sampling the axial distribution of the gamma source. A single spectrum was used for sampling the delayed gamma source over the full height of the FA. Radially, all fuel pins were assumed to have the same distribution. *The gamma radiation source from the spacer grids was* also *assumed to be uniform* within each of the spacers with total source strength distributed among the seven spacers calculated, based on its axial location, in line with the Wagner burn-up axial distributions. *The gamma sources released from ^{60}Co in the spring zone were assumed to be evenly distributed inside the spring zone for simplicity.*

The geometry setup has considered the spent FA inside a hot cell, which lies down on the 25 cm thick concrete floor as shown in Figure 7.9. *The other concrete walls of the hot cell were two metres away from the FA. The TLD detectors were modelled as LiF cylinders that have the same radius as the fuel pellet and a height of 4.6 cm. The aluminium tubes holding the TLD detectors were modelled with the inner and outer radii equal to those of the fuel pin cladding.* To fit all the aluminium holder tubes within the geometry model, *the vertical aluminium tube was slightly shifted aside to avoid overlapping with the two axial aluminium holder tubes.*

For each of the (B03 and D04) FAs, *three separate radiation transport simulations were performed using the gamma sources from the fuel, the spacer and the spring, respectively.* The calculated contributions to *the gamma dose rates at each detector location* were summed up later on. The dose rates reported hereafter were obtained using conversion factors from the ANSI/ANS (1991).

Figure 7.9. MCNP model of the Turkey Point Unit 3 experiments showing the horizontal aluminium tube and the detectors (right) transversal view (left)

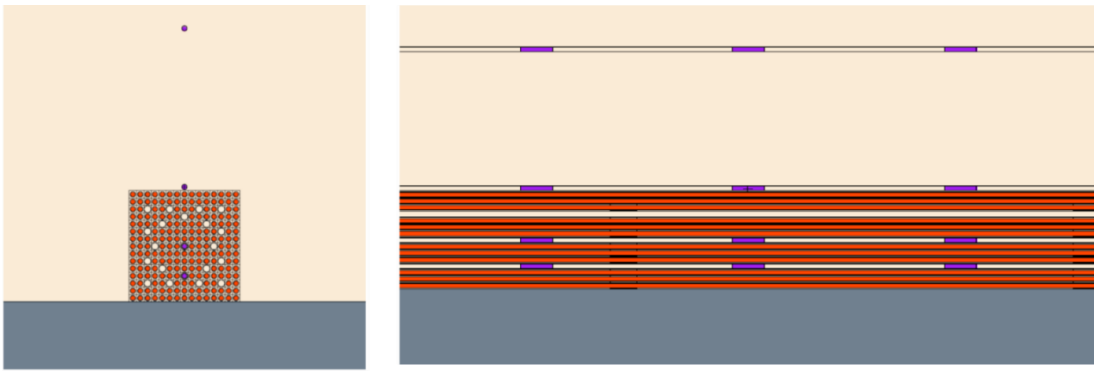

Source: NEA EGAFCS data, 2020.

7.4.3. VTT approach

The fuel depletion and structural material (namely the spacer grid) activation were simulated using the SERPENT Monte Carlo code, version 2.1.29 [23], along with cross-section data from the JEFF-3.1.2 library [40] and fission yield and decay data from the JEFF-3.1.1 libraries. Cut-views of the geometry model are presented in Figure 7.10. All the fuel rods in the assembly were of the same type and the assembly contained 21 water tubes.

The geometry model consisted of a 66.52-cm height segment of the FA applying reflective boundary conditions in the radial direction and black boundary conditions in the axial direction, i.e. the axial segment of the FA was modelled in an infinite lattice in the radial direction. The vertical cut-view in Figure 7.10 features a spacer grid across the assembly segment mid-plane. The spacer grid was modelled as a 5.44-cm height and 3.954-mm thick square wall between the fuel pins with a mass of 780 g, at the mid-plane of the FA segment. Following [22], the chemical composition of Inconel-718 with cobalt impurity content of 0.91 wt% has been used in the present delayed gamma source calculation. An Inconel-718 composition with a lower content in cobalt impurity, namely 0.47 wt% [10] has also been used for the sake of a sensibility study. The UO_2 fuel and the Zircaloy-4 clad materials were assumed to be clean. The gas plenum spring, in Inconel-718, was not considered in the model.

Figure 7.10. Cut-views of 3D assembly segment geometry model for the burn-up calculation

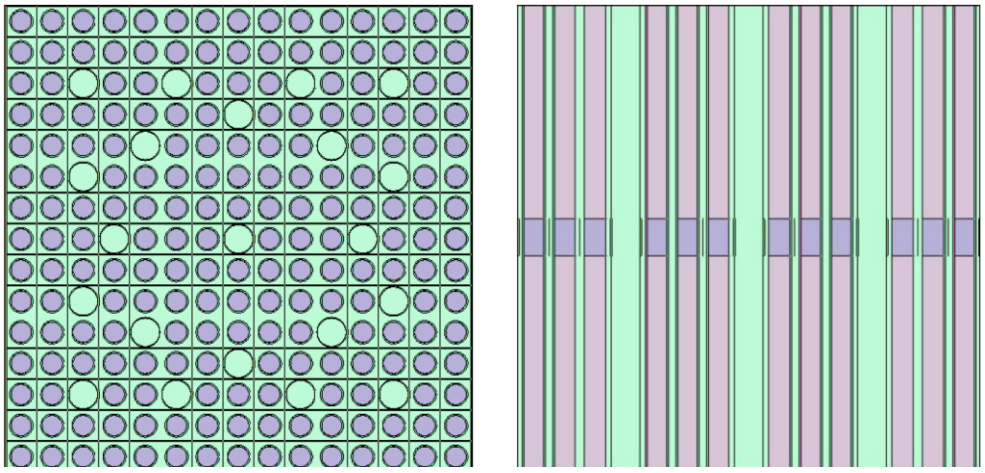

Source: Räty, A. and S. Häkkinen, 2018.

The Monte Carlo fuel burn-up calculations were carried out in 17 burn-up steps to achieve the specified assembly average burn-up of 28.43 GWd/MTIHM. A cooling time of 657 days (1.8 years) following irradiation was considered.

For illustrative purposes, the gamma source energy distribution, in the case with 0.47% cobalt impurity in the Inconel spacers, is described in Table 7.7 using a 19-energy group structure. The top ten radionuclides feeding the source term are also provided.

Table 7.7. Gamma source energy distribution and major contributing radionuclides

	Upper boundary energy (MeV)	Source intensity (%)			
				Radionuclide	Share (%)
1	0.0482	11.07	1	Cs-134	39.39
2	0.0713	0.20	2	Cs-137/Ba-137m	20.59
3	0.106	1.01	3	Ru-106/Rh-106	13.11
4	0.156	6.73	4	Ce-144	12.28
5	0.231	0.15	5	Co-60	5.16
6	0.342	0.10	6	Sb-125	2.62
7	0.507	1.15	7	Eu-154	2.22
8	0.75	57.16	8	Pr-144	1.27
9	1.25	20.60	9	Nb-95	0.62
10	1.75	1.32	10	Te-125m	0.58
11	2.25	0.46	Total		**97.84**
12	2.75	0.03			
13	3.50	0.00			
14	4.50	0.00			
15	5.50	0.00			
16	6.50	0.00			
17	7.50	0.00			
18	8.65	0.00			
19	20.0	0.00			
Total (photon/s)		6.64E+15			

The dose rate distribution around the spent FA was carried out by using the radioactive decay source capability of SERPENT 2.1.29. In this source mode, decay gammas will be created based on unstable nuclides in material inventories, obtained from burn-up or activation calculation, located inside the source cell. Photon emission spectra, read from ENDF format radioactive decay data files, are used to sample the delayed gamma source, including the bremsstrahlung generated by beta radiation from FPs.

In the dose rate calculation, the entire assembly was modelled, namely a Westinghouse 15x15 fuel bundle, which consists of 365.7 cm height active fuel rods and Zircaloy-filled plugs (length 10.2 cm) at the ends of the assembly. The assembly contained seven equally placed 5.44 cm height Inconel spacers. The total length of the assembly was 385.78 cm. The assembly was surrounded by dry air with natural composition. The spent fuel composition corresponding to the average core burn-up was assigned over the entire length, entailing a uniform axial distribution of the delayed gamma source. The same goes for the seven spacer grids.

The photon-induced dose rates were tallied inside 10 cm x 1 cm x 10 cm size vacuum cells representing the TLD detectors at various locations around the spent FA (see Figure 7.11). The photon flux computed using the track-length estimator was converted to dose rates with the ANSI (1977) and ANSI (1991) standard fluence-to-dose rate conversion functions.

Figure 7.11. Geometry model of the spent FA for gamma dose rates calculation

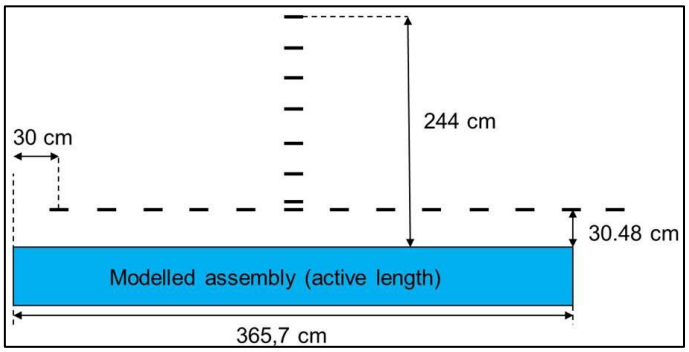

Source: Räty, A. and S. Häkkinen, 2018.

7.4.4. KIT approach

The spent fuel inventory and the photon emission rate (γ/s) after a decay period of 1.8 years were calculated by using the ORIGEN2.2 [25] and ORIGEN-ARP [27] codes. Neither spacer grid/plenum spring nor Zircaloy-4 cladding was considered in this study.

For the B03 FA, the ORIGEN2.2 code was applied using 40 irradiation time steps of 20.67 EFPDs, which yields a delayed gamma radiation source intensity of 6.0E+15 photons/s.

For the D04 spent FA, the intensities of delayed γ source as computed by the ORIGEN2.2 (18 groups) and ORIGEN-ARP (19 groups) codes were 1.6e+16 γ/s and 1.3e+16 γ/s, respectively, including bremsstrahlung gammas. The structure of the energy groups is provided in Table 7.8, alongside the energy distribution obtained using ORIGEN2.2 for the D04 FA. From the data in the latter table and its histogram plot displayed in Figure 7.12, one observes that the first energy group (photons with energy below 20 keV) is the dominant one, with a share of 32.5% of the total source intensity, with photons with energy below 100 keV (i.e. first five energy groups) accounting for ~58% of the total source intensity. For the B03 FA, aggregated group #9 takes the lead with 32.5%, closely followed by group #1 (28.1%), with photons with energy below 100 keV accounting for 50.1%.

The dose rate calculations were investigated using the MCNPX 2.7.0 code version [24], based on a 3D geometry model of the FA located in the air. For the model, the fuel composition and the γ source after decay were uniformly spread axially and radially. The transport of photons and electrons was considered in the calculation, the TENDL-2014 and mcplib04 nuclear data libraries [28] being used.

Finally, the γ flux was tallied for each selected position and the dose rate was computed by using the flux-to-dose rate conversion factors from both the ANSI/ANS-6.1.1 (1977) and ANSI/ANS-6.1.1 (1991).

Figure 7.12. D04 FA: Delayed gamma source spectrum obtained with ORIGEN2.2

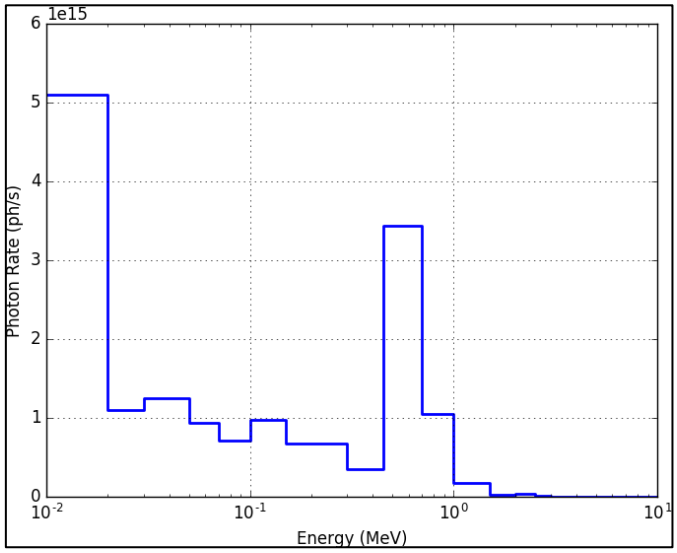

Source: NEA EGAFCS data, 2020.

Table 7.8. Energy group structure for the delayed gammas spectrum description

	ORIGEN2.2	Gamma source for D04 FA		Gamma source for B03 FA	
group #	Upper boundary (MeV)	Photons/s	Share (%)	Photons/s	Share (%)
1	0.02	5.10E+15	32.5	1.69E+15	28.1
2	0.03	1.09E+15	6.9	3.68E+14	6.1
3	0.05	1.24E+15	7.9	3.88E+14	6.4
4	0.07	9.35E+14	6.0	3.43E+14	5.7
5	0.10	7.09E+14	4.5	2.26E+14	3.8
6	0.15	9.70E+14	6.2	2.26E+14	3.8
7	0.30	6.71E+14	4.3	1.95E+14	3.2
8	0.45	3.45E+14	2.2	1.01E+14	1.7
9	0.70	3.37E+15	21.5	1.96E+15	32.5
10	1.00	1.04E+15	6.6	4.44E+14	7.4
11	1.50	1.70E+14	1.1	7.03E+13	1.2
12	2.00	1.99E+13	0.1	4.05E+12	0.1
13	2.50	2.65E+13	0.2	5.32E+12	0.1
14	3.00	5.05E+11	0.0	1.25E+11	0.0
15	4.00	4.57E+10	0.0	1.58E+10	0.0
16	6.00	3.93E+06	0.0	2.53E+06	0.0
17	8.00	4.53E+05	0.0	2.92E+05	0.0
18	11.00	5.21E+04	0.0	3.35E+04	0.0
Total (photons/s)		1.57E+16	100	6.02E+15	100

7.4.5. ENEA approach

The decay and photon emission phase was investigated using the ORIGEN-S point-depletion code [38]. The same code was previously used in the burn-up and depletion phase in which the decay between the intermediate cycles of 58 and 62 days was taken into account. The delayed gamma source spectrum, including bremsstrahlung due to decay only, was obtained using an 18 energy-bins structure (see Table 7.9). Given the importance of the energy-bins structure for a dose rate calculation, this structure was checked through an "optimised" structure in which the most important isotopes with emissions above 0.4 MeV, such as ^{106}Rh, ^{137M}Ba, ^{134}Cs, and ^{144}Pr, are used to create groups narrow and centred on their

main emission energies. Above 0.4 MeV, i.e. at the emission energies relevant to this study, the energy distribution is dominated by photons in groups #9 and #10 representing approximately 29% of the total photon emission.

Table 7.9. Energy group structures for the delayed gammas spectrum description

	ORIGEN2.2	Gamma source for D04 FA	
Group #	Upper boundary [MeV]	Photon/s	Share (%)
1	0.02	5.66E+15	32.15
2	0.03	1.24E+15	7.01
3	0.05	1.74E+15	9.85
4	0.07	6.98E+14	3.96
5	0.10	7.82E+14	4.44
6	0.15	1.06E+15	6.02
7	0.30	7.48E+14	4.25
8	0.45	3.96E+14	2.25
9	0.70	3.86E+15	21.92
10	1.00	1.19E+15	6.73
11	1.50	1.99E+14	1.13
12	2.00	2.29E+13	0.13
13	2.50	2.85E+13	0.16
14	3.00	5.82E+11	0.00
15	4.00	5.28E+10	0.00
16	6.00	5.43E+06	0.00
17	8.00	6.25E+05	0.00
18	11.00	7.19E+04	0.00
Total		1.762E+16	100

The steady-state gamma transport calculation was carried out with the MCNPX 2.7.0 code version [24]. The companion MCLIB04p photon transport cross-section library was used. A non-uniform gamma source within each fuel pin was modelled radially and axially. As for the axial direction, the gamma source was sampled using a PWR's typical burn-up distribution, corresponding to an average burn-up of between 26 and 30 GWd/MTIHM [16]. As for the radial direction, the gamma source was assumed to be proportional to the radial concentration in the fuel pellet of the most relevant gamma emitters above 0.4 MeV, i.e. ^{106}Rh, ^{134}Cs, ^{137M}Ba and ^{144}Pr. As a source, $5 \cdot 10^9$ primary photons, corresponding to one standard deviation on the dose rate of about 3%, are used. Bremsstrahlung due to secondary electrons is included with the Thick-Target Model. The photon flux was computed using MCNP F4 tally type over 5x5x0.5 cm^3 rectangular boxes centred on the measurement points. The applied dose multiplier was of type decontamination factor for flux-to-dose rate conversion. The two conversion factor models used are from the ANSI/ANS (1977) and the ANSI/ANS (1991).

7.4.6. CEA approach

The delayed photon source term was analysed using a computational scheme that couples the APOLLO-2.8 [34] with the DARWIN2.3 [36] codes. APOLLO-2.8 performs the neutron flux calculation in the assembly with a multi-group cross-section library, CEA2005V4, derived from the JEFF3.1.1 [5] evaluation and considering a Pij calculation scheme. The code provides neutronics data (self-shielded cross-sections and neutron spectra) in a dedicated database referred to, internally, as SAPHTOOL.

The calculated geometry is a 2D assembly geometry model and the neutron flux is calculated in a 281 energy group structure, the so-called SHEM scheme [43]. To better take the Rim effect into account, the fuel rod is divided into 4 concentric rings (respectively representing 50%, 80%, 95% and 100% of the total fuel rod volume).

The fuel depletion calculation was performed using the geometry and materials of the 15x15 UOX (used for the verification benchmark) with 208 fuel pins and 17 guide tubes per assembly, except for the ^{234}U and ^{235}U enrichments, which were set to 0.19% and 2.55% respectively. The specific power was also set to 34 W/g. Nevertheless, as the assembly moderation radii are 1.91 and 1.95 for the benchmark assembly and the experiment assembly respectively, it can be considered that neither the neutron flux spectrum nor the macroscopic 1-group cross sections were greatly impacted by this assumption. The depletion calculation is thus considered representative of the real assembly one.

The left-hand picture in Figure 7.13 shows the assembly geometry model used for the source term calculation while the right-hand picture displays the actual design of the D04 assembly used in the TRIPOLI-4® code [35] for the dose rate calculations.

Regarding the depleted fuel inventory calculation, the depletion chain is the standard so-called CEA2005V4 chain including around 160 isotopes. The chain contains 135 FPs and 26 actinides. It is important to note that the irradiation shutdown is not considered in the irradiation history.

DARWIN2.3 is the French reference package for fuel cycle calculations. The code re-calculates the compositions of the discharged FA based on the self-shielded cross-sections in the SAPHTOOL database and with a more detailed depletion chain. The chain includes 3 027 isotopes, with FPs, heavy nuclides and activation isotopes, and is consistent with the CEA2005V4 one.

The depletion calculation was performed until 28.43 GWd/MTIHM and a 1.8-year cooling time was taken into account. DARWIN calculated a 19-group and an explicit ray-by-ray (19 127 rays) delayed gamma source spectrum from this calculation step. The explicit gamma source is used for sensitivity analyses.

Table 7.10 provides the total number of emitted gamma and the gamma spectrum in the 19-group energy structure for an initial mass of 1-tonne uranium. To take into account the bremsstrahlung contribution, DARWIN2.3 provides also a beta-emission spectrum in a 61-group energy structure.

Figure 7.13. 15x15 UOX FA used in APOLLO-2 (left) and in Tripoli-4 (right)

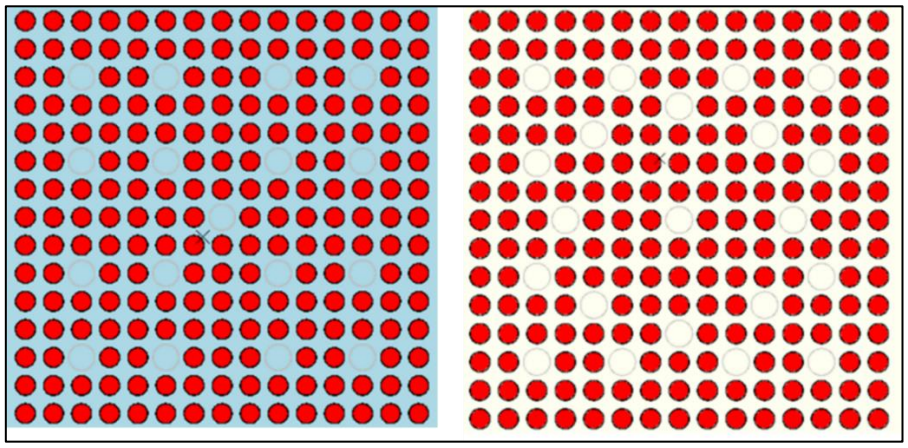

Source: NEA EGAFCS data, 2020.

Table 7.10. Gamma spectrum in a 19-energy group structure

group #	Upper boundary [MeV]	Photon/s	Share (%)
1	0.0482	6.70E+14	10.67
2	0.0713	1.27E+13	0.20
3	0.1055	6.38E+13	1.02
4	0.1562	4.23E+14	6.74
5	0.2312	7.63E+12	0.12
6	0.3423	6.70E+12	0.11
7	0.5066	6.13E+13	0.98
8	0.7500	3.61E+15	57.50
9	1.2500	1.31E+15	20.85
10	1.7500	8.40E+13	1.34
11	2.2500	2.87E+13	0.46
12	2.7500	1.81E+12	0.03
13	3.5000	1.14E+11	0.00
14	4.5000	5.22E+05	0.00
15	5.5000	9.15E+04	0.00
16	6.5000	2.92E+04	0.00
17	7.5000	3.91E+02	0.00
18	8.6538	0.00E+00	0.00
19	20.000	0.00E+00	0.00
	Total	6.28E+15	100

Figure 7.14. Axial burn-up profile used for the dose rate calculation

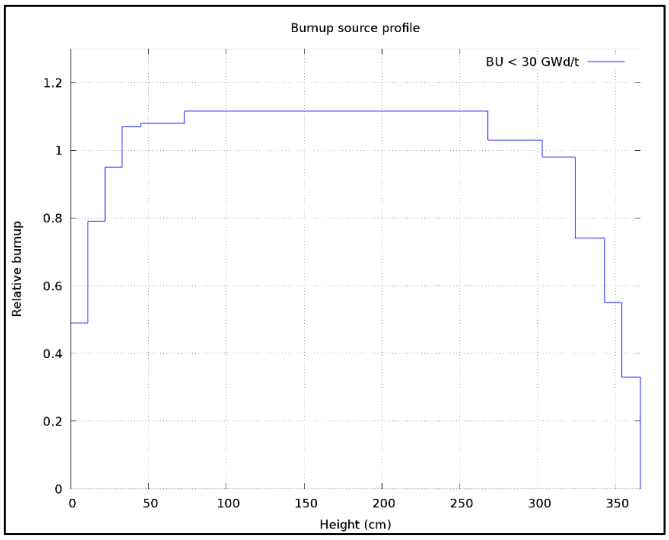

Source: NEA EGAFCS data, 2020.

The dose rate distribution was assessed with the TRIPOLI-4 Monte Carlo code using the EPDL-97 photoatomic data library and the EADL atomic relaxation data. As the gamma source axial profile, a typical PWR burn-up profile [33] was used, as shown in Figure 7.14 and designed for fuel burn-up below 30 GWd/MTIHM.

The fluence-to-dose functions from the ANSI/ANS (1977) report and the ANSI/ANS (1991) were used for this study. For calculations using the TRIPOLI-4® code [35], an additional built-in response function H*(10), based on ICRP-74 recommendations, was used. The dose rates at various detector locations were assessed using point flux estimators.

7.4.7. ORANO TN approach

The delayed gamma source spectrum, including bremsstrahlung due to decay, was obtained with ORIGEN-ARP [41] using a 62 energy-bins structure for the clean fuel pellet and the cladding material. It is detailed in Figure 7.15.

Figure 7.15. D04 total spectrum [γ/s/tHM]

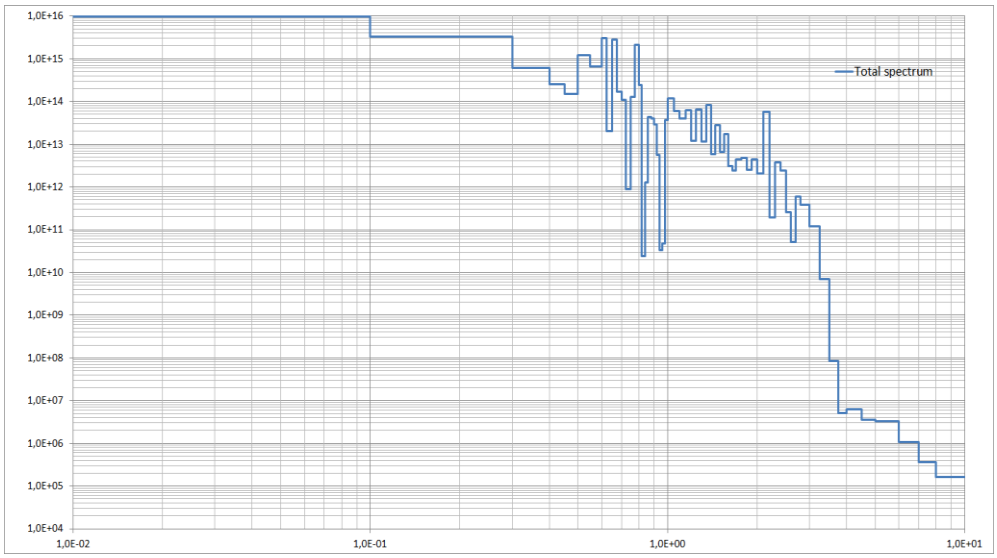

Source: NEA EGAFCS data, 2020.

The dose rate simulation was carried out using the TRIPOLI-4.7 Monte Carlo code [43], based on a 3D homogenised FA model. Photoatomic data from the CEA V5.0 library, mainly based on the JEFF-3.1.1 evaluation, were used.

Figure 7.16 presents also the global 3D TRIPOLI model used to take into account the effect on the dose rates of the gamma backscattering considering the measurement conditions. A built-in six-node axial burn-up profile, shown in Figure 7.17, was used for the axial distribution of the gamma source. The ANSI/ANS (1991) fluence-to-dose conversion factors were used.

Figure 7.16. Schematic view geometry model showing the FA inside the hotcell

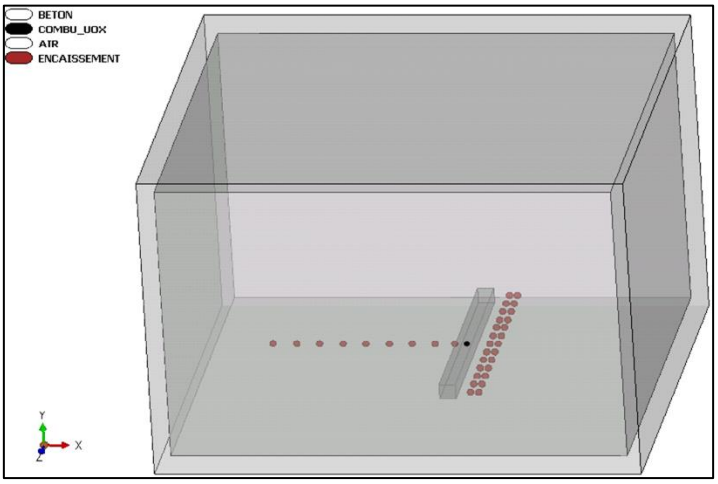

Source: Leger, V. and A. Dalesme, 2020.

Figure 7.17. Burn-up profile used in the TRIPOLI-4 model

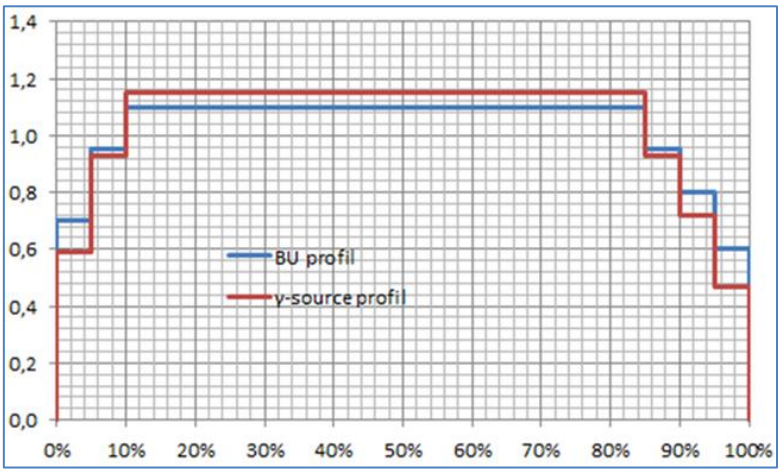

Source: Leger, V. and A. Dalesme, 2020.

7.4.8. CIEMAT approach

The EVOLCODE 2.0 system [29], which is based on the Monte Carlo code MCNP (version 6.1.1b [30]) for the neutron transport simulation and the ACAB code [31] for the Bateman depletion calculations, was used to estimate the burn-up evolution of the FA. A single FA was modelled to represent the whole reactor core. It consisted of an element of an infinite lattice, where reflective boundary conditions were considered for the lateral directions. The model for each rod included concentric geometry for pellet, gap and cladding. The moderator and guide tubes were also taken into account. No spacer grid, plenum spring and axial or radial subdivision of the fuel were considered in this work.

The model for the burn-up considered 19 irradiation steps of constant power, but no intermediate decay periods were taken into account for refuelling purposes. Also, the boron concentration in water was considered a variable for the 19 irradiation steps. The decay period after irradiation was simulated with ACAB. The JEFF-3.2 data library [32] was used for the calculations, making use of decay data, photon production, branching ratios, fission yields and cross-sections. Figure 7.18 shows the gamma line spectrum obtained using a fine energy grid of 1 800 energy intervals, considering the emission of each isotope. In this way, the photon energy from 1 keV until 20 MeV was sampled, yielding a nearly ray-lines spectrum, as depicted in the figure. The top six contributors to the delayed gamma emission, accounting for 96.2% of the total source intensity, are presented in Table 7.11, for the clean UO_2 fuel pellet.

Figure 7.18. Gamma line spectrum of the delayed gamma source

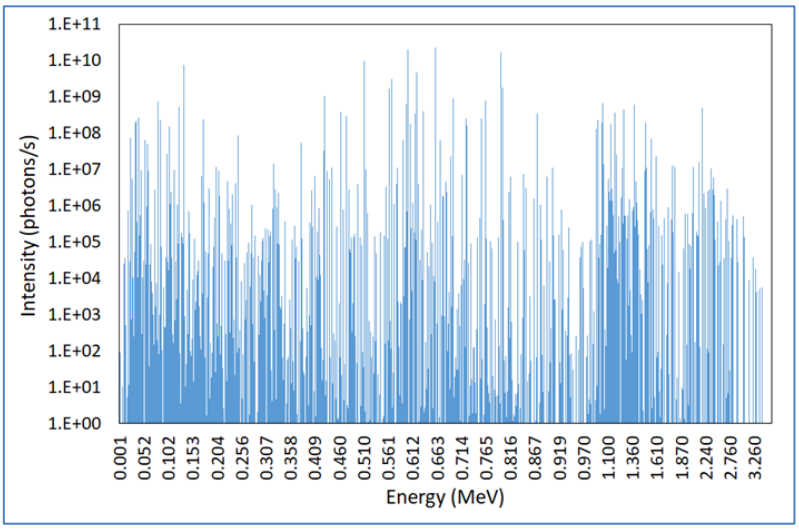

Source: NEA EGAFCS data, 2020.

Table 7.11. Top contributors to delayed gamma source and main gamma lines

Isotope	Share (%) of gamma emission
^{134}Cs	**44.4**
^{137}Cs/^{137M}Ba	22.0
^{106}Ru/^{106}Rh	15.3
^{144}Ce	10.0
^{125}Sb	2.8
^{154}Eu	1.7

Main gamma lines (keV)	Share (%) of gamma emission	Responsible isotope
661.0	**22.3%**	**^{137}Cs/^{137M}Ba**
604.0	19.5%	^{134}Cs
796.0	17.1%	^{134}Cs
512.0	9.4%	^{106}Ru/^{106}Rh
134.0	7.4%	^{144}Ce
622.0	4.6%	^{106}Ru/^{106}Rh
569.0	3.1%	^{134}Cs
801.0	1.7%	^{134}Cs
564.0	1.7%	^{134}Cs
428.0	1.0%	^{125}Sb

The transport of the photon radiation was performed with MCNP code, version 6.1.1b [30]. The FA was considered suspended in the open air, so no water is maintained in the design now. The reflecting boundaries were removed to place the detector cells at the proper distances.

The photon source was randomly generated from the 1 800 different energy groups provided by ACAB. The F4 track-length flux estimator was used to estimate the photon flux at the detector locations. Two flux-to-dose rate conversion factors were used in this

work: the 1977 ANSI/ANS report and its 1991 update, both with a LOGLIN interpolation factor. The detectors were modelled as spheres of a 5-cm radius to calculate the dose rate.

7.4.9. SCK CEN approach

A detailed 3D full-core geometry model was developed for fuel depletion and structural material activation calculation, including the fuel clad and the spacer grids. Figure 7.19 depicts the radial and axial cut-views of the core model. Axially, the B03 FA was divided into 48 axial segments of equal length. The first ring neighbour assemblies are divided into six axial segments while assemblies on the second ring are subdivided into three segments. Assemblies in outer rings are modelled as a single fuel segment. Likewise, the fuel rod cladding of the B03 assembly is divided into 16 axial segments: one segment over the gas plenum and 15 segments of equal length along the active fuel zone.

The fuel rod is modelled radially in three separate zones, namely: the fuel pellet, the gas plenum gap and the clad. As shown in Figure 7.20, the spacer grid elements are modelled as a square wall around every pin, guide and instrumental tube. The wall thickness is determined such as to preserve the grid mass (675 grammes) provided the height is equal to 3.81 cm. The total mass of each grid is shared equally among fuel pins and guide/instrumentation tubes. The plenum gas spring was modelled as a layer on the inner face of the gas plenum room with the thickness calculated to preserve the amount (53.684 g per pin) of the spring material (see Figure 7.21). The seven spacer grids are modelled and irradiated, separately, at their axial actual location alongside the FA, as read in Figure 7.4.

Due to a lack of information concerning control rod insertion, it is assumed that the guide tubes in assemblies were vacant (filled by the coolant). Likewise, the SS 304 sleeves around guide thimble tubes (shown in Figure 7.21 as from [13]) are not modelled. The top end of the guide thimble is fastened to a tubular sleeve by three expansion swages. The sleeve fits into and is welded to the top nozzle adapter plate. The lower end of the guide thimble is fitted with an end plug that is then fastened into the bottom nozzle by a weld-locked screw, which penetrates through the nozzle and mates with an inside fitting in each guide tube.

The bottom nozzle is a box-like structure that serves as a bottom structural element of the FA and directs the coolant flow distribution to the assembly. The square nozzle is fabricated from 304 stainless steel and consists of a perforated plate and four-angle legs with bearing plates. The top nozzle assembly functions as the upper structural element. It consists of an adapter plate, enclosure, top plate, hold-down springs, clamps and pads. The springs are Inconel 718 and the bolts are Inconel-600; the other components are 304 stainless steel. The bottom nozzle zone has been modelled as a mixture of 60 vol% borated cold water and 40% SS-304 (density ~3.64 g/cc) while the top nozzle zone mixture consisted of 70 vol% borated hot water, 20% SS-304 and 10% void (density ~2.0 g/cc). The two zones were not taken into account for the delayed gamma source.

Figure 7.19. Radial and axial cut-view of the core model

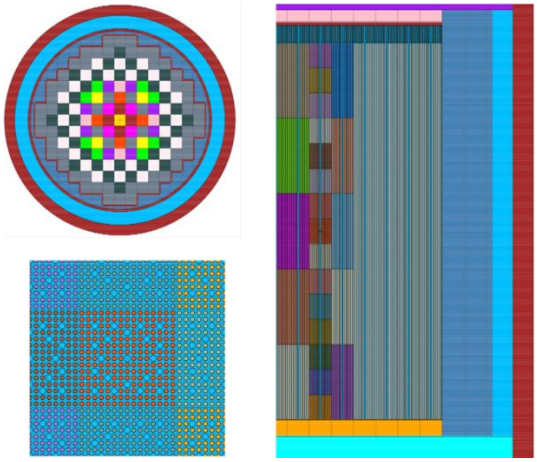

Source: Malambu, E., 2019.

Figure 7.20. Modelling the spacer grids and the gas plenum spring

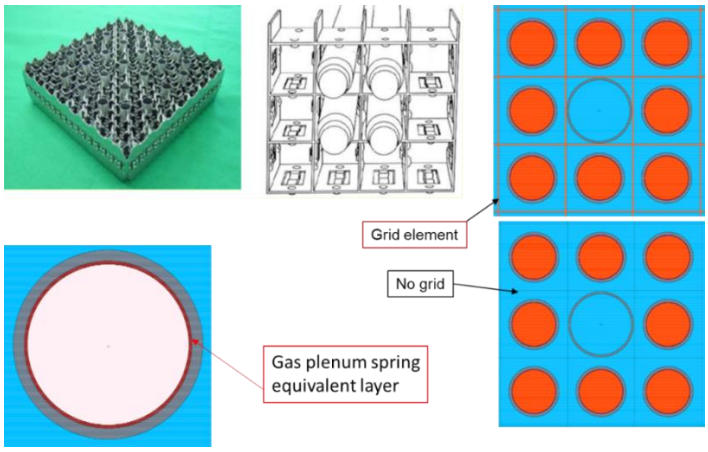

Source: Malambu, E., 2019.

Figure 7.21. Not modelled guide thimble-to-grid bulge joint

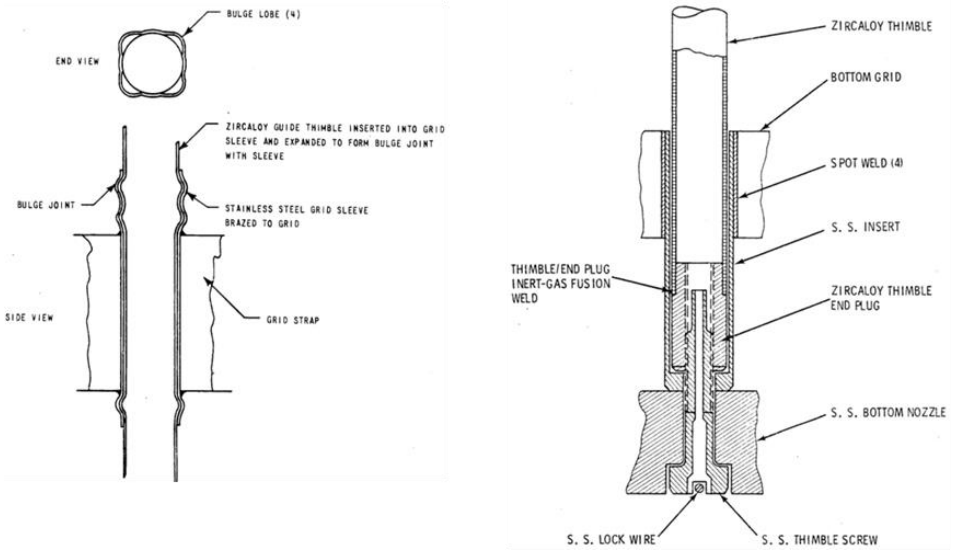

Source: Weihermiller, W.B. and G.S. Allison, 1979.

The fuel depletion and structural material activation were carried out using the ALEPH2 depletion code [18], which has been under development at SCK CEN since 2004. ALEPH v2 couples a steady-state MCNP/MCNPX particle transport with a "deterministic" depletion equations' solver employing Radau IIA implicit Runge-Kutta method (three stages, accuracy order 5) as implemented in RADAU5 solver [19]. A typical step of the ALEPH2 simulation consists of an MCNP steady-state calculation to obtain the transported particle fluxes and spectra that are used to prepare spectrum-average data to be eventually used in a deterministic depletion solver to update the material compositions for the next irradiation step. For the present study, the steady-state calculations were carried out using the MCNP 6.2 code version [17]. Amongst the key features of the ALEPH2 is the full data consistency between steady-state Monte Carlo and time-dependent depletion calculations. The continuous pointwise nuclear data from JEFF-3.3 [44] were used, not only for the steady-state calculation yielding the neutron spectrum but also to prepare the spectrum-averaged cross-sections used in the material evolution routine.

The nuclide depletion calculation was carried out in a once-through job run for the various core zones (89 fuel zones, including 48 axial segments for the B03 FA, 16 clad zones, 7 spacer grids and for the gas plenum spring) at constant core full power of 2191.726 MW (13.96 MW/FA x 157 FAs), continuously during an irradiation period of 827 EFPDs. To reduce the number of zones, all FAs loaded in symmetric positions were burnt as a single zone. Such was the case for the assemblies B03, B02, B17 and B41 (see Figure 7.5). The irradiation history was subdivided into time steps of 30 or 35 EFPDs, updating the neutron spectrum (steady-state MCNP run), to take into account the change flux profile due to fuel depletion. A partial core reshuffling was simulated generically after 367 EFPDs and 587 EFPDs irradiation times, to keep the core critical. The output of the calculation includes, at various irradiation and decay time steps and for various depleted materials, among others:

- the radionuclide inventory (in g/cm^3 and in atom/barn*cm);
- various delayed radiation activity inventory;
- the power released in each material zone.

The normalisation factor of the radiation source for subsequent calculations was determined using only the above data (i.e. irradiation time, 827 EFPDs and operation power, 2191.726 MWth).

A part of the raw output of the ALEPH2 depletion calculation is the burn-up in GWd/MTIHMM for every burnt fuel zone as a function of irradiation time (the time bins being defined by the time steps used to model the irradiation history). Collecting and averaging over the full core yields an average burn-up of 25.367 GWd/MTIHM for the full core, which is very close to 25.665 GWd/MTIHM, the specified "calculated" core average burn-up. The calculation yields an average burn-up of 27.85 GWd/MTIHM for B03 assembly and its companions (B02, B17 and B41).

Figure 7.22. Calculated burn-up and gamma source axial profile along the B03 assembly

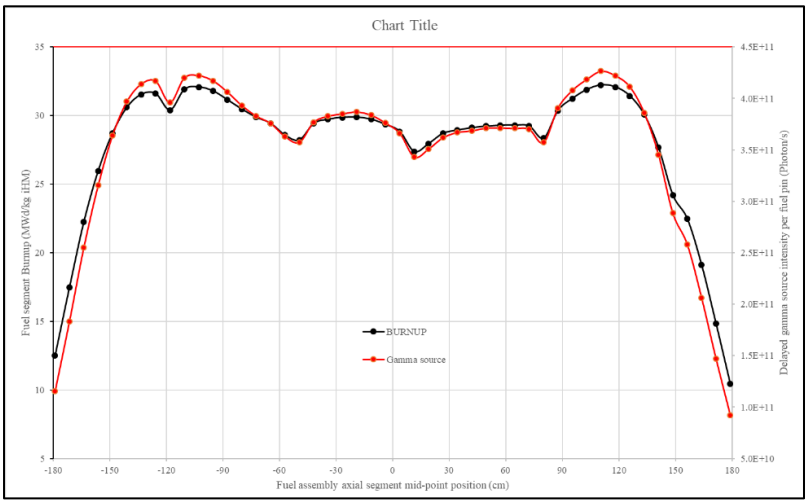

Source: NEA EGAFCS data, 2020.

The axial distribution of the fuel pellet burn-up is plotted in Figure 7.22 alongside the axial distribution of the gamma source from fuel, featuring the characteristic flat shape with dips at the spacer grid locations, in good agreement with the experimental shapes shown in Figure 7.5.

The intensities of the delayed photon source due to various components investigated in this study are summarised in Table 7.13. As regards the intensity, the spent fuel pellet (FP and actinides) dominates the source term: both the spacer grid (Inconel-718 material with 0.47 wt% cobalt impurity) and the cladding (Zircaloy-4 with 10-ppm-weight cobalt impurity) account for only ~5%.

As can be noticed in Table 7.12 only seven radionuclides deliver more than one percent to the source intensity, the leading contributors being the ^{134}Cs nuclide and ^{137}Cs/^{137M}Ba generator with, respectively ~41% and ~38%. The 75-ppm-weight ^{59}Co impurity content in the UO_2 fuel pellet makes ^{60}Co become the fourth major contributor with a share of 5%.

The ALEPH2 burn-up code retrieves photon spectra from the basic radioactive decay library and aggregates the individual (discrete) gamma lines and the continuous spectra, if available, using an energy-grid structure consisting of 1-keV gap from 1 keV to 1 MeV and a 5 keV gap above 1 MeV. Such fine grid structure allows identifying discrete gamma lines of most decaying nuclides yielding gamma line-by-line spectrum as is depicted in Figure 7.23, assigning to ray lines the energy of the group centroids, shown to be so close

to the actual line energy from literature or MCNP database, as highlighted in Table 7.12 (bottom part, column #2 and #3).

Figure 7.23. Delayed gamma spectrum of clean UO_2 spent fuel in B03 assembly

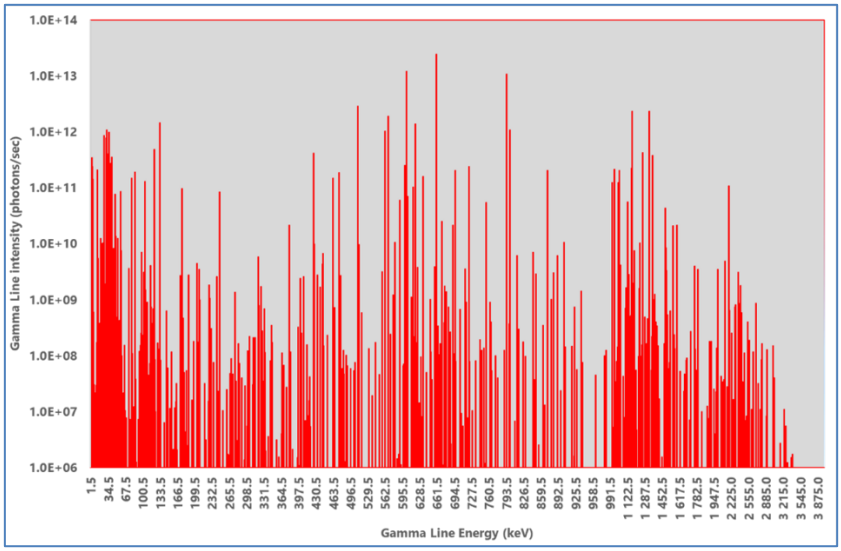

Source: Malambu, E., 2019.

The source term spectrum is dominated by the 661.7 keV gamma-line from the $^{137}Cs/^{137M}Ba$ generator, 34% of the overall intensity, followed by two ^{134}Cs signature ray lines at 604.7 keV and 796 keV, with ~18% and ~16% share respectively. ^{60}Co, an activation product of the ^{59}Co impurity, plays a non-negligible role due to its two high-energy rays at 1.1725 and 1.3325 MeV, respectively.

Table 7.12. Major radionuclides and gamma lines feeding the source term

	Radionuclide	Intensity share (%)	
		UO_2 with 75 ppm Co-60 impurity	Clean UO_2
1	^{134}Cs	38.64	40.90
2	$^{137}Cs/^{137m}Ba$	35.51	37.60
3	$^{106}Ru/^{106}Rh$	6.82	7.23
4	^{60}Co	5.44	
5	^{144}Ce	4.19	4.43
6	^{154}Eu	3.79	4.01
7	^{125}Sb	2.80	2.93
8	^{155}Eu	0.84	0.89
9	^{125m}Te	0.66	0.69
10	^{144}Pr	0.46	0.48
11	^{241}Am	0.27	0.28
12	^{110m}Ag	0.12	0.11
13	^{238}Pu	0.12	0.12
14	^{144m}Pr	0.09	0.09

Table 7.12. Major radionuclides and gamma lines feeding the source term (Continued)

	Radionuclide	Intensity share (%)	
		UO_2 with 75 ppm Co-60 impurity	Clean UO_2
15	^{244}Cm	0.08	0.08
16	^{119m}Sn	0.06	0.05
Total		**99.87**	**99.90**

	Gamma line energy (keV)		Nuclide ID	UO_2 with impurities	Clean UO_2
	E-bin centroid	actual		Intensity share (%)	
1	661.50	661.66	$^{137}Cs/^{137m}Ba$	32.51	34.42
2	604.50	604.70	^{134}Cs	16.86	17.85
3	795.50	795.85	^{134}Cs	14.76	15.62
4	511.50	511.84	$^{106}Ru/^{106}Rh$	4.09	4.33
5	1 332.50	1 332.50	^{60}Co	2.72	
6	1 172.50	1 173.20	^{60}Co	2.72	
7	569.50	569.31	^{134}Cs	2.65	2.81
8	133.50	133.54	^{144}Ce	2.01	2.13
9	621.50	621.94	$^{106}Ru/^{106}Rh$	1.97	2.08
10	801.50	801.93	^{134}Cs	1.50	1.59
11	32.50			1.45	1.54
12	563.50	563.24	^{134}Cs	1.44	1.52
13	36.50			1.35	1.43
14	27.50			1.19	1.25
15	31.50			1.06	1.12
16	123.50	123.07	^{154}Eu	0.77	0.82
17	1 272.50	1 274.43	^{154}Eu	0.67	0.70
18	427.50	427.00	^{125}Sb	0.58	0.61
19	42.50			0.57	0.60
20	35.50	35.80	^{154}Eu	0.56	0.60
21	1 367.50			0.52	0.55
			Total	91.95	91.57

Table 7.13. Delayed gamma source for various material compositions

Material	Source intensity (photon/s)
Spent fuel (clean UO_2)	3.27E+15
Spent fuel (+metallic impurities; 75 ppm-weight cobalt)	3.44E+15
Spacer grid+spring (0.91 wt% Cobalt)	2.76E+14
Spacer grid+spring (0.47 wt% Cobalt)	1.39E+14
Clad (with impurities; 10 ppm-weight cobalt)	1.95E+13

The dose rate distributions around the B03 spent FA were analysed using the MCNP6.2 code [17] version along with the state-of-the art EPRDATA14 photoatomic data library, released within the MCNP6.2 package. The B03 assembly, isolated in open dry air, was modelled with the same level of detail as for the depletion calculation step. As displayed in Figure 7.24, the assembly is modelled lying on a 20 cm thick concrete table inside a 510 cm x 500 cm x 500 cm hot cell room with a wall consisting of a 10 cm thick layer of lead and a 30 cm thick layer of concrete. Figure 7.25 shows the dosimeter holders in aluminium, explicitly modelled by 1-mm-thick, 5-mm-inner radius tubes with TLD detectors modelled as air-filled 0.8-cm-diameter, 1-cm-height cylindrical cells. The vertical dosimeter can stand up in the middle of the assembly's flat surface while the axial cans (at flat and one foot above the flat) are slightly shifted laterally, 1.5 cm away, to avoid overlapping with the vertical can.

Simulations were carried out separately for each component of the delayed gamma source term described in Table 7.13. For each component, the delayed photon source was sampled in the same volume where it had been obtained in the previous calculation step. For instance, the delayed gamma source due to the spent fuel was sampled inside each one of the 48-pin pellet axial segments, thereby accounting for the self-shielding effect of the pellet and the shielding due to the fuel pin clad, with a different spectrum for each segment. Radially the source is the same for all fuel pins of a given assembly segment.

The gamma radiation sources from the spacer grids and plenum spring were also sampled using different spectra in the seven spacers and plenum chamber. The same went for the 16 axial segments along the Zircaloy-4 clad.

Figure 7.24. Geometry model for dose rates calculation

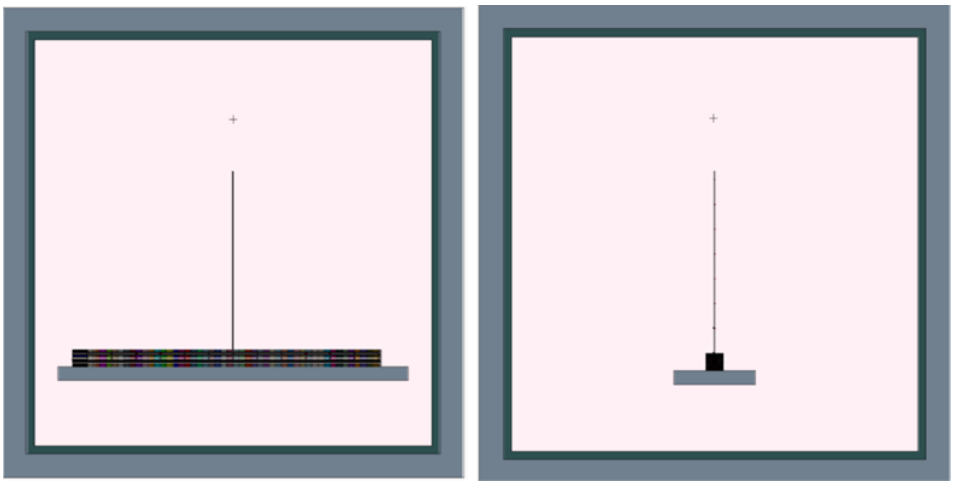

Source: Malambu, E., 2019.

The dose rate due to bremsstrahlung gammas was carried out only for the fuel pellet, using the spontaneous beta-decay source capability of the MCNP6.2 code. The code samples each beta-emitter radionuclide contained in the source cell, using a 100-bin beta-decay spectrum from a specific companion library.

For each code run, 10^{10} (per batch of 10^{9}) source particles were tracked to achieve low statistical errors (< 3%) in all tallying cells. The MCNP F4 track-length flux estimator was used to tally the cell-averaged photon flux at the various dosimeter locations. The stochastic dose rate distributions were obtained by folding the above gamma flux with an energy-dependent flux-to-dose response function.

Hence, the MCNP track-length tally yields a result in units of sievert per photon source particle. Upon multiplication by the photon source intensity (normalisation factor), by 3 600 s/h and by 100 rad/sievert, a dose rate in Rad/h (or Rem/h since one rad is equal to one rem for photon) is found. The ANSI/ANS dose conversion factors being in units of Rem/hr/Flux, the MCNP raw tally value needs only to be folded by the photon source intensity.

Figure 7.25. Modelling details featuring dosimeter tube holders and tallying cells

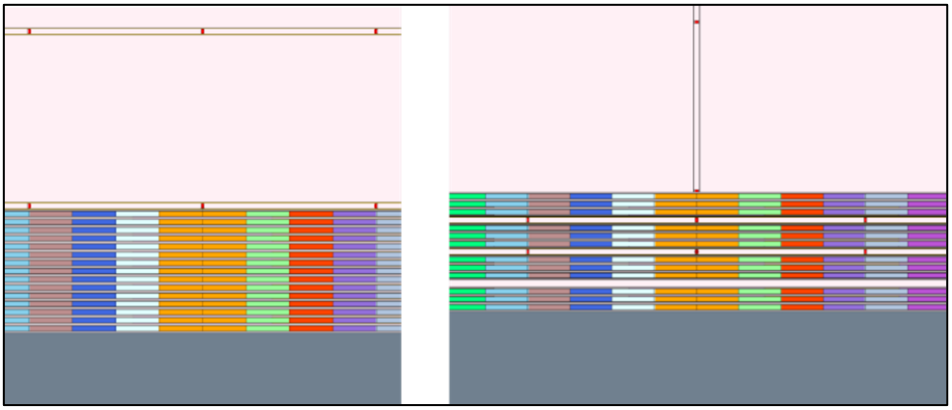

Source: Malambu, E., 2019.

7.5. Results analysis

7.5.1. Analysis of key features used for calculating the dose rates

Influence of the fluence-to-dose response function

The photon fluence-to-dose conversion tables (ICRP or ANSI) are used to calculate the biological dose (equivalent or effective). Since this involves biological weight factors yielding different dose rate values, Table 7.14 highlights the discrepancy in dose rates, as calculated by SCK CEN for the B03 FA at the various detector locations, using simultaneously in the same MCNP simulation dose conversion factors from ANS-6.1.1 (1977), ANS-6.1.1 (1991) and ICRP (1996). The $100 \times (C - E)/E$-like metric is used, where E stands for ANS-6.1.1 (1991) and C for either ANS-6.1.1 (1977) or ICRP (1996).

The dose rate values calculated using the ANS-6.1.1 (1977) conversion function are 24-25% higher compared to values obtained with the ANS-6.1.1(1991). The dose rates calculations by ENEA, for the D04 assembly, exhibit a discrepancy of 24.7% between values derived by ANS-6.1.1 (1977), in perfect agreement with SCK CEN for B03, which confirms the statement quoted from the literature. The H*(10 mm) ICRP (1996) dose function yields values about 14% higher compared to ANS-6.1.1 (1991) and, hence, about 9% lower compared to the ANS-6.1.1 (1977).

In Figure 7.26, the shares of the total dose rate at a given location, calculated by SCK CEN for the B03 FA, have been plotted as a function of scoring photon energy intervals. It is worth noting that dose rates induced by photons at an energy below 100 keV barely reach 0.4% for ICRP (1996) and ANSI/ANS (1991) and 0.5% for ANSI/ANS (1977), which is roughly half of the 1-σ uncertainty on the peak value (with a share of ~55%) occurring in the energy range from 600 keV to 800 keV wherein are the major contributors to the gamma source. Hence, the difference in dose function curves at low energy has no impact.

Table 7.14. Percentage discrepancy in dose rates: ICRP (1996) and ANSI/ANS (1977) vs. ANSI/ANS (1991)

	Axial distribution								Vertical distribution	
	Instrumental tube		Guide tube		On the surface		1 foot above surface			
Detector position	ICRP(1996) Vs. ANS(1991)	ANS(1977) Vs. ANS(1991)	ICRP(1996) Vs. ANS(1991)	ANS(1977) Vs. ANS(1991)	ICRP(1996) Vs. ANS(1991)	ANS(1977) Vs. ANS(1991)	ICRP(1996) Vs. ANS(1991)	ANS(1977) Vs. ANS(1991)	ICRP(1996) Vs. ANS(1991)	ANS(1977) Vs. ANS(1991)
0	14.1	24.5	14.1	24.4	14.0	24.0	14.1	24.3	14.0	23.6
1	14.1	24.0	14.1	24.1	14.0	23.7	14.1	24.1	14.1	24.2
2	14.1	23.9	14.1	24.0	14.0	23.6	14.1	24.0	14.1	24.4
3	14.1	23.9	14.1	24.0	14.0	23.6	14.1	24.1	14.2	24.8
4	14.1	24.0	14.1	24.1	14.0	23.7	14.1	24.2	14.2	24.7
5	14.1	24.0	14.1	24.1	14.0	23.7	14.1	24.1	14.2	24.8
6	14.1	24.0	14.1	24.1	14.0	23.7	14.1	24.2	14.2	25.4
7	14.1	24.0	14.1	24.0	14.0	23.7	14.1	24.3	14.2	25.1
8	14.1	24.0	14.1	24.1	14.0	23.7	14.1	24.1		
9	14.1	24.0	14.1	24.0	14.0	23.6	14.1	24.1		
10	14.1	23.9	14.1	24.0	14.0	23.6	14.1	24.2		
11	14.1	24.0	14.1	24.0	14.0	23.6	14.1	24.2		
12	14.1	24.3	14.1	24.3	14.0	23.8	14.1	24.3		

Figure 7.26. Dose rates fraction as a function of the photon energy

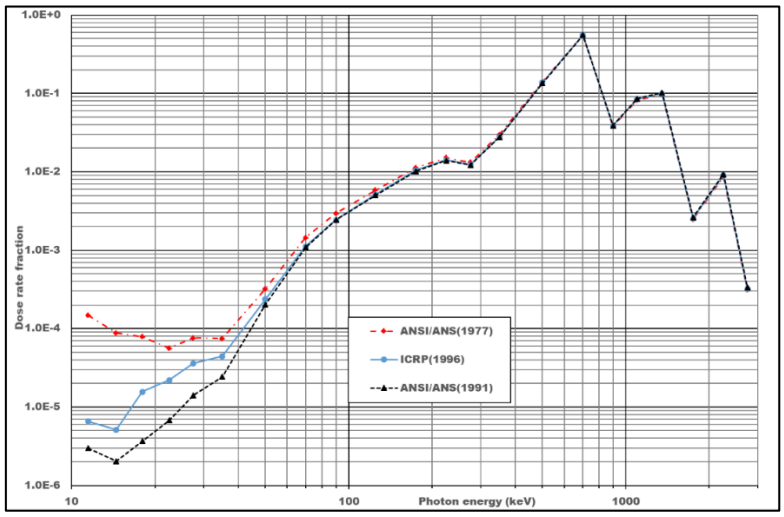

Source: NEA EGAFCS data, 2020.

Influence of the hotcell wall backscattering

Another item likely to influence the dose rate calculation is the radiation backscattering due to various structural materials surrounding the experimental setup, mainly the hotcell

wall and the FA support table. Calculations were carried out by some participants, namely ORANO TN for D04 and SCK CEN for B03 FAs. The results obtained for the B03 FA are reported in Table 7.15 in terms of the (C-E)/E-like metrics, where E stands for the model accounting for the backscattering. The impact of backscattering increases noticeably moving away from the spent fuel surface and getting closer to the hotcell walls. The backscattering contribution varies from 2.5% to 7%.

Table 7.15. Impact of radiation backscattering inside the assumed B03 hotcell

Detector position	$\left(\frac{No\ backscattering}{backscattering} - 1\right) \times 100$				
	Axial dosimetry tubes				Vertical
	Instrumental tube	Guide tube	On assembly surface	Above surface	
0	-0.2	-0.1	-0.2	-3.6	0.0
1	0.0	0.0	0.0	-2.2	-2.5
2	0.0	0.0	0.0	-2.1	-4.3
3	0.0	0.0	0.0	-2.4	-5.4
4	0.0	0.0	0.0	-2.4	-5.5
5	0.0	0.0	0.0	-2.4	-6.4
6	0.0	0.0	-0.1	-2.7	-7.3
7	0.0	0.0	0.0	-2.7	-6.7
8	0.0	0.0	0.0	-2.5	
9	0.0	0.0	0.0	-2.3	
10	0.0	0.0	0.0	-2.1	
11	0.0	0.0	0.0	-2.7	
12	0.0	0.0	-0.1	-3.5	

Dose rate induced by the various source term components

Three components were thoroughly investigated by the participants of this validating benchmark exercise regarding the delayed gamma source term, namely the UO_2 fuel pellet, the Zircaloy-4 cladding and the Inconel-718 spacer grids/plenum springs. The contribution of the above source term components was compiled in Table 7.16 by SCK CEN for the B03 spent FA, considering metallic impurities including cobalt (75 ppm-weight in the UO_2, 10 ppmw in the Zircaloy-4 and 0.47 wt% in the Inconel-718, respectively). The share of the cladding to the dose rates is constant at all detector locations, amounting to ~0.6%.

For the spacer grids, the contribution to the dose rates depends much more on the distance to the detectors: below 6% for detectors close to the FA, but with spikes for detectors near the core active height, up to 58% at the bottom and up to 80% at the top with the contribution from the spring. Away from the FA surface, the contribution of the spacer grids and spring reaches values up to 14% of the total detector dose rate. Inside and on the surface of the FA, the delayed gamma radiation from the spent fuel pellet is responsible for

up to 99% of the dose rates. Outside the assembly and near spacer grids the share of the spent fuel pellet decreases.

Table 7.16. Share of various components of the dose rate

Detector position	Share of total dose rate from the various gamma source components (%)														
	Axial distribution												Vertical distribution		
	Instrumental tube			Guide tube			On the surface			1 foot above surface					
	Fuel	Clad	Grids/ spring	Fuel	Clad	Grids/ spring	Fuel	Clad	Grids/ spring	Fuel	Clad	Grids/ spring	Fuel	Clad	Grids/ spring
0	42.0	0.5	57.5	41.5	0.4	58.0	51.8	0.5	47.7	89.4	0.6	10.1	97.6	0.5	1.9
1	99.2	0.6	0.2	99.2	0.6	0.2	99.2	0.5	0.3	93.2	0.5	6.3	92.0	0.5	7.5
2	76.6	0.5	22.9	76.5	0.4	23.1	79.9	0.4	19.7	91.4	0.5	8.1	90.7	0.6	8.7
3	99.2	0.6	0.2	99.2	0.6	0.3	99.1	0.5	0.4	93.1	0.5	6.4	89.5	0.6	10.0
4	93.4	0.6	6.0	93.4	0.5	6.1	93.3	0.5	6.2	91.7	0.5	7.8	88.4	0.6	11.0
5	99.0	0.6	0.4	99.0	0.6	0.4	98.9	0.5	0.6	92.8	0.5	6.7	87.4	0.6	12.0
6	97.7	0.6	1.7	97.7	0.6	1.8	97.5	0.5	2.0	92.1	0.5	7.4	86.7	0.6	12.7
7	98.4	0.6	1.0	98.4	0.6	1.1	98.2	0.5	1.3	92.1	0.5	7.4	85.2	0.6	14.2
8	98.8	0.6	0.6	98.7	0.6	0.7	98.6	0.5	0.9	92.2	0.5	7.3			
9	96.4	0.6	3.0	96.3	0.6	3.1	96.1	0.5	3.3	91.3	0.5	8.2			
10	99.2	0.6	0.2	99.2	0.6	0.3	99.1	0.5	0.4	91.1	0.5	8.4			
11	86.0	0.6	13.4	85.9	0.6	13.6	86.7	0.5	12.8	81.4	0.5	18.1			
12	19.0	0.3	80.7	19.5	0.3	80.2	20.5	0.3	79.2	53.7	0.4	45.9			

Figure 7.27. Axial profiles of dose rates induced by gammas from fuel and clad in B03 assembly

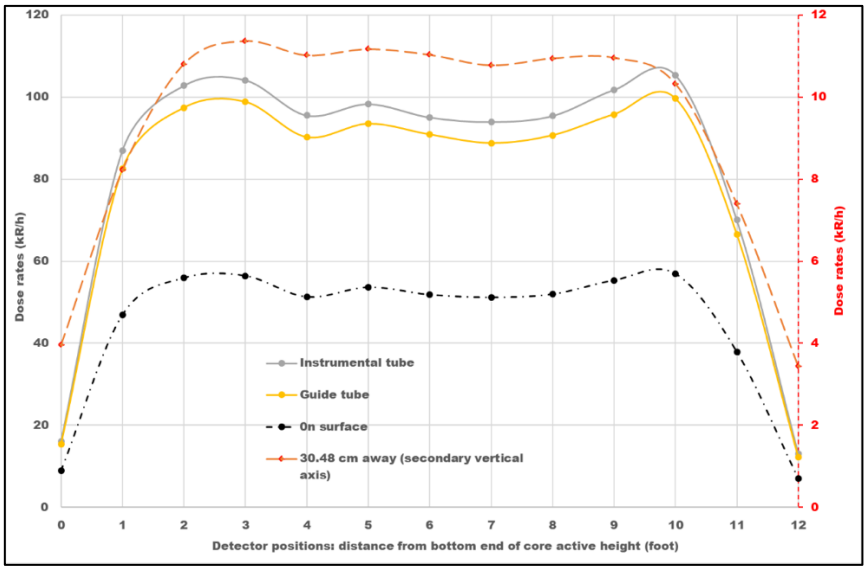

Source: NEA EGAFCS data, 2020

Figure 7.28. Axial profiles of dose rates including gammas from spacer grids/spring in B03 assembly

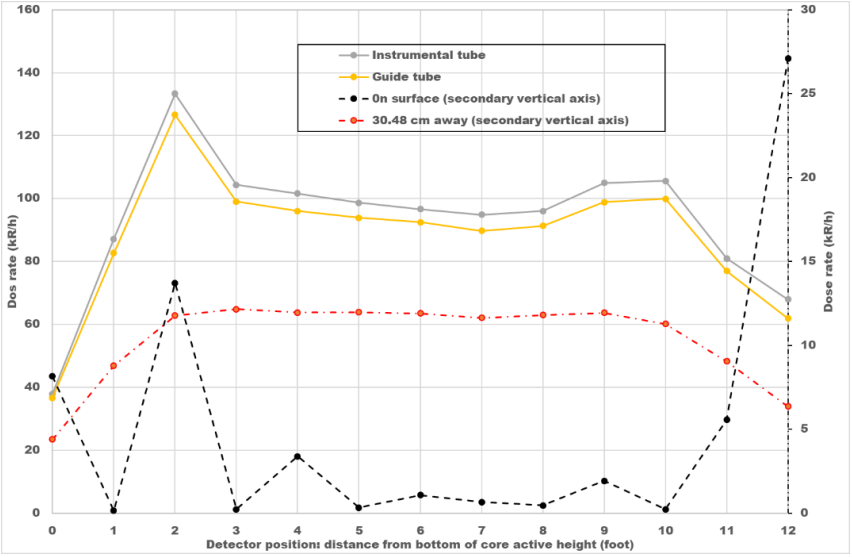

Source: NEA EGAFCS data, 2020.

The axial profiles of the dose rates, aggregating the contributions from the pellet and the cladding, are featured in Figure 7.27. They exhibit a smooth shape, in line with the shape of the source term shown in Figure 7.22. The shapes of the dose rate curves, including the contribution of gamma from the spacer grids and plenum spring, are shown in Figure 7.28, featuring the eddies due to located grids source term.

7.5.2. Dose rate curves comparison

A critical review of the experimental data

Figure 7.29 shows the experimental data plotted from Table 7.4 regarding the B03 spent FA from Turkey Point Unit 3. At first glance, the strange shapes of three of the dose rate distribution curves can be noticed. They are presented in the figure. Only the dose rates through the instrumental (central) tube exhibits the expected profile, in line with both the experimental burn-up and the gamma source scan profiles in Figure 7.6 and Figure 7.5, respectively. While the instrumental tube and the guide tube are only ~6 cm apart and have the same structure, the shape of the dose rate curves through the two tubes looks very different.

Figure 7.30 shows the axial dose rates on the surface (left picture) and 1-foot away (right picture) for both B03 and D04 FAs. The two assemblies are similar in design and were irradiated inside the same core in nearly similar conditions. Here again, the axial dose rate profiles are significantly different. For the D04 assembly, the dose rate curve 1-foot away from the surface exhibits the expected shape. However, there is a lack of consistency between the shapes of the various axial curves either for curves of the same FAs (B03 or D04), at different tube positions, or for the homologous curves from B03 and D04, at a similar position. Surprisingly, these oddities are not mentioned in the found literature reporting on these experimental. As an exception to the concern raised above, the radial distribution curves of dose rates around both B03 and D04 FAs are consistent, as can be seen in Figure 7.31.

Figure 7.29. Experimental axial distributions of the dose rates for the B03 FA

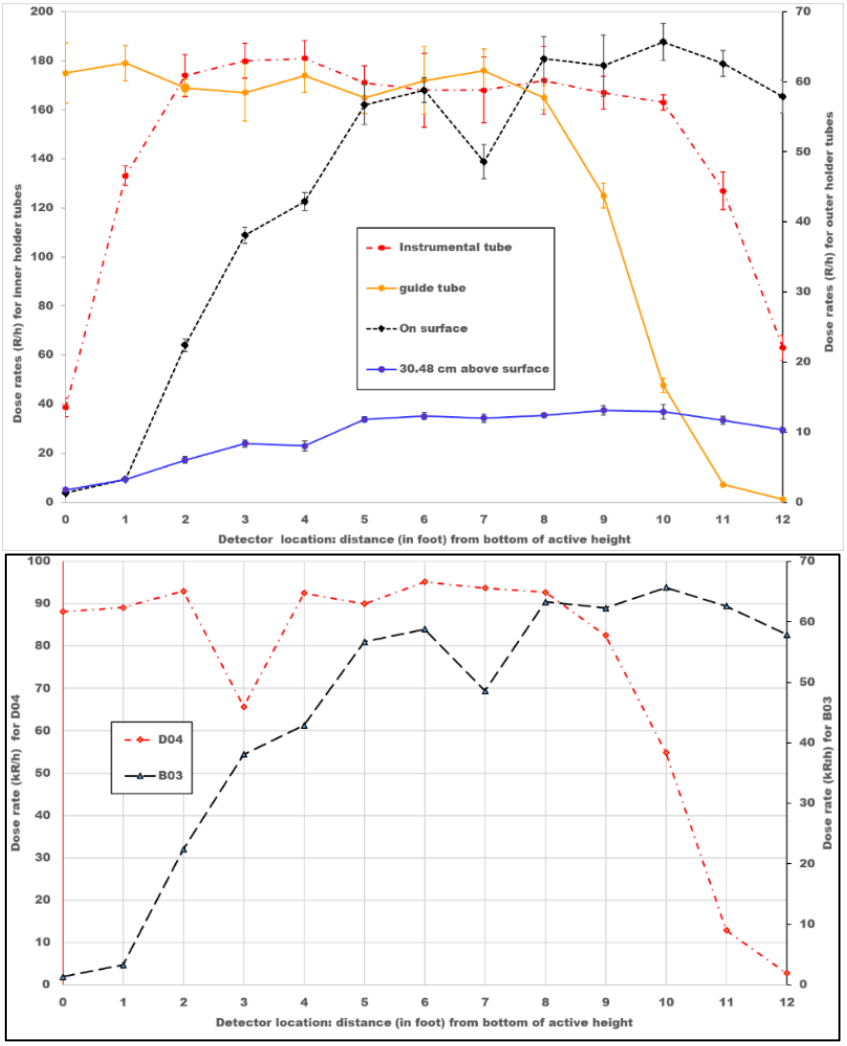

Source: NEA EGAFCS data, 2020.

Figure 7.30. Experimental dose rate curves on and away from the surface: D04 versus B03 FAs

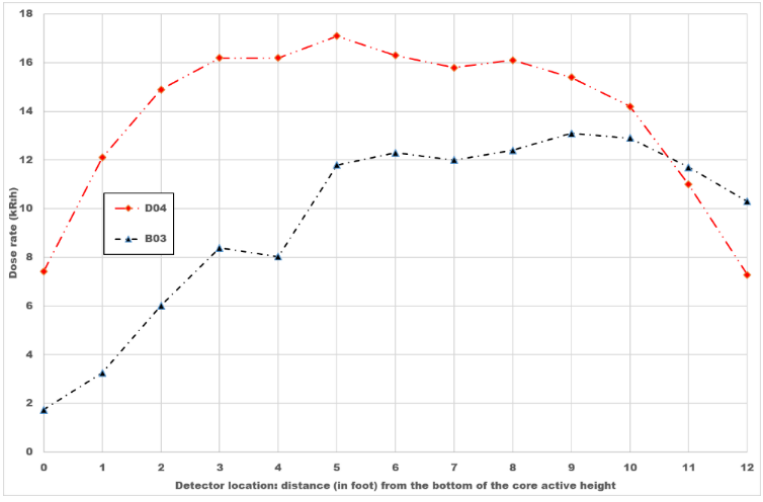

Source: NEA EGAFCS data, 2020.

Figure 7.31. Radial distribution at the FA mid-plane

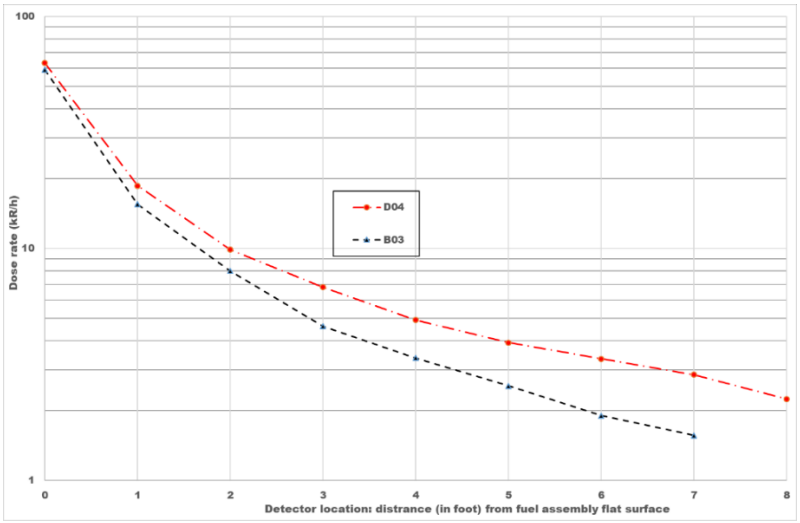

Source: NEA EGAFCS data, 2020.

Outcome of the validation benchmark exercise

Figures 7.32, 7.34 and 7.36 show the dose rate distributions computed by the various participants to the D04 validation case, while the discrepancy trends between calculation and experiment data are depicted in Figures 7.33 and 7.35.

Figure 7.32. Calculated versus experimental dose rates inside the vertical holder tube at the mid-plane of the D04 assembly

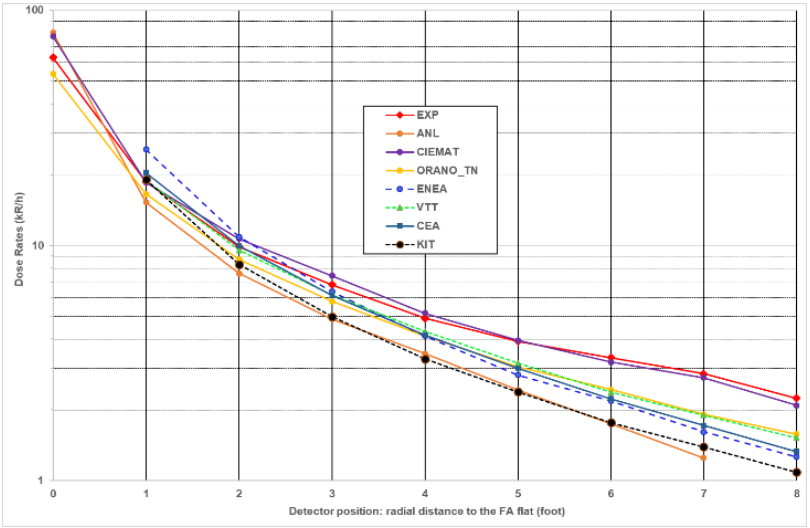

Source: NEA EGAFCS data, 2020.

Figure 7.33. Calculated-to-experiment data discrepancy along the vertical axis for the D04 assembly

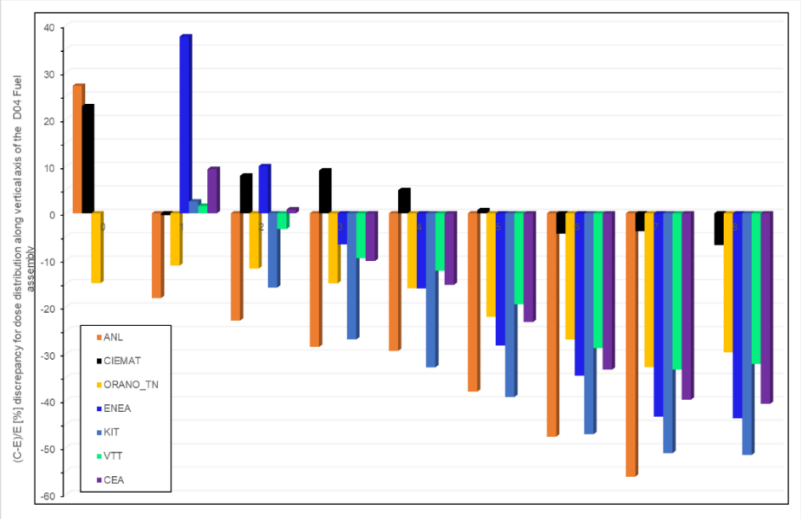

Source: NEA EGAFCS data, 2020.

Figure 7.34. Calculated versus experimental dose rates inside the axial holder tube 1 foot away from the surface of the D04 assembly

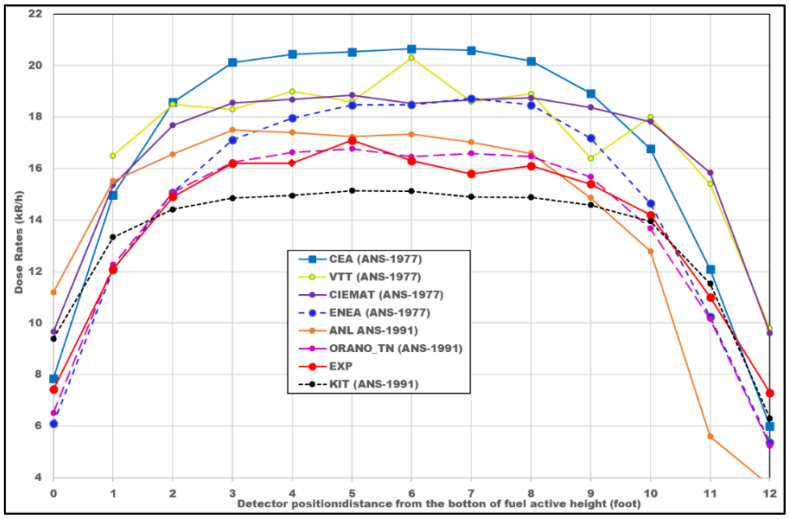

Source: NEA EGAFCS data, 2020.

Figure 7.35. Calculated-to-experiment data discrepancy through the axial tube 30.48 cm away from the D04 FA

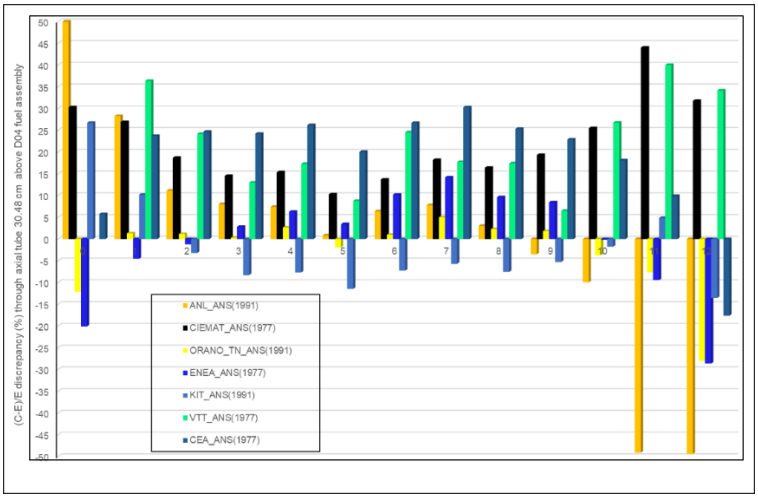

Source: NEA EGAFCS data, 2020.

Figure 7.36. Calculated versus experimental dose rates inside the axial holder tube on the surface of the D04 assembly

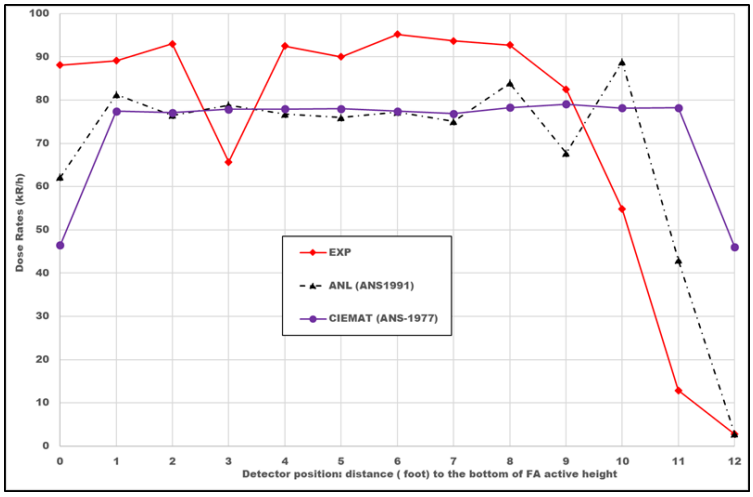

Source: NEA EGAFCS data, 2020.

In the following, as an additional metric, the mean discrepancy defined below will be used:

$$\langle \sigma \rangle = \sqrt{\frac{1}{N}\sum_{i=1}^{N}\left(\frac{C_i - E_i}{E_i}\right)^2}$$

Where

- C_i stands for the calculated dose rate at a given detector location;
- E_i, the experimental data;
- N the number of point values.

Considering the case of D04 FA, the experimental data roughly exhibit the expected shape for the detector along the vertical holder tube and the axial holder tube 30.48 cm (1 foot) away from the surface. For dose rate distribution through the vertical axis, the calculated values from CIEMAT, using the ANS-6.1.1 (1977) dose function, are in better agreement with the experimental data, with an average discrepancy of 6% at detector locations away from the assembly surface. Yet, for the axial distribution, the data from CIEMAT overestimate the experiment data by 26% on average, less well than ENEA with 12% or CEA with 22%. Regarding the axial distribution, the dose rates calculated by ORANO TN and KIT, using ANS-6.1.1 (1977), appear closer to the experimental data. Yet, at the same time, the data calculated by both institutes for the vertical axis underestimate the experiment by ~30%, on average.

For the B03 assembly, the computed dose rate distributions are plotted in Figures 7.37, 7.39, 7.41, 7.42 and 7.43. The discrepancy trends are depicted in Figure 7.38 for the dose rate radial distribution and in Figure 7.40 for the axial distribution away from the fuel. Considering the vertical axis dose distribution, where the experimental curve sounds correct, the calculated dose curves from all participants seem to match the experimental curves: the calculation has underestimated the dose rate at all detector locations with a discrepancy not varying much from one location to the neighbour. The average discrepancy in the dose rate values calculated by SCK CEN, using 0.47wt% cobalt impurity in the Inconel-718 is ~19% ANS-6.1.1 (1977) and ~26% ICRP (1996), respectively. Both ANL and KIT used the ANSI/ANS-6.1.1 (1991) dose function and the average discrepancies are 56% and 59%, respectively. The same trend is observed in the cases of axial distributions for detection locations where the comparison is relevant between experimental and calculated data.

Figure 7.37. Calculated versus experimental dose rates inside the vertical holder tube at the mid-plane of the B03 assembly

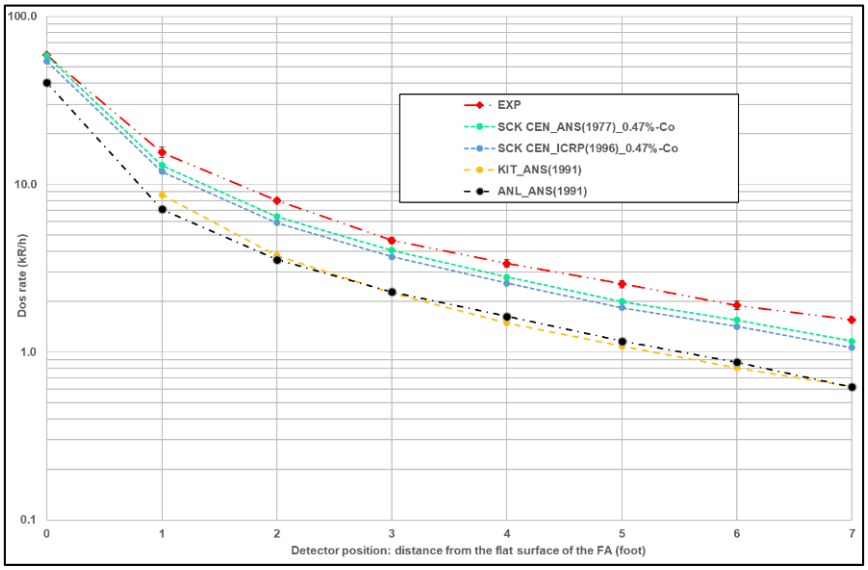

Source: NEA EGAFCS data, 2020.

Figure 7.38. Calculated-to-experiment data discrepancy along the vertical axis for B03 assembly

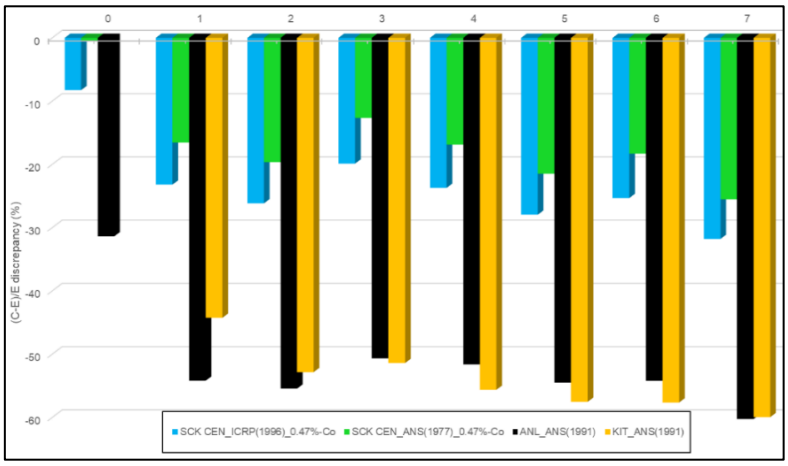

Source: NEA EGAFCS data, 2020.

Figure 7.39. Calculated versus experimental dose rates inside the axial holder tube 30.48 cm away from the surface of the B03 assembly

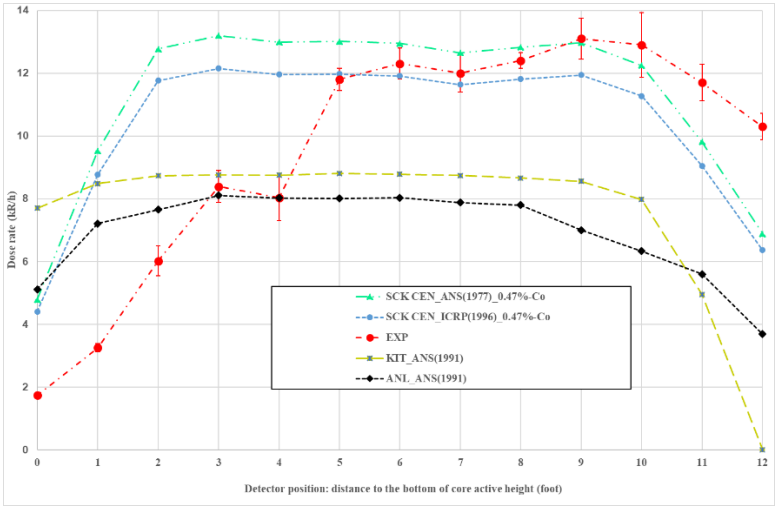

Source: NEA EGAFCS data, 2020.

Figure 7.40. Calculated-to-experiment data discrepancy inside the axial holder tube 30.48 cm above the B03 assembly

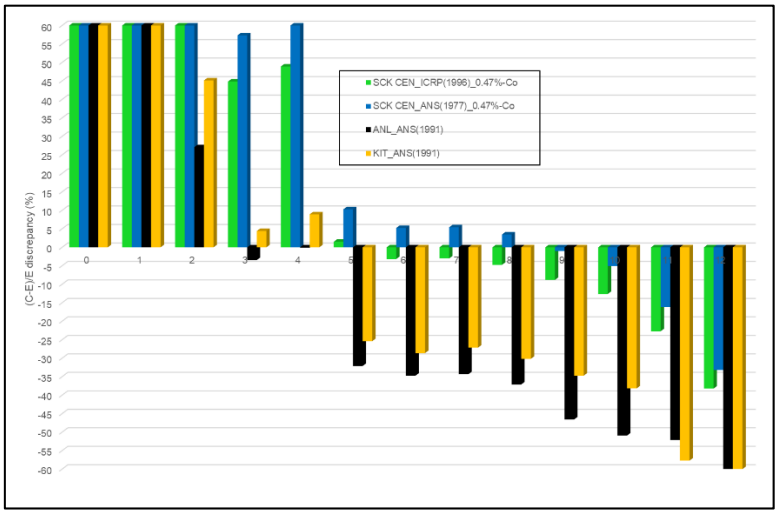

Source: NEA EGAFCS data, 2020.

Figure 7.41. Calculated versus experimental dose rates inside the axial holder tube on the surface of the B03 assembly

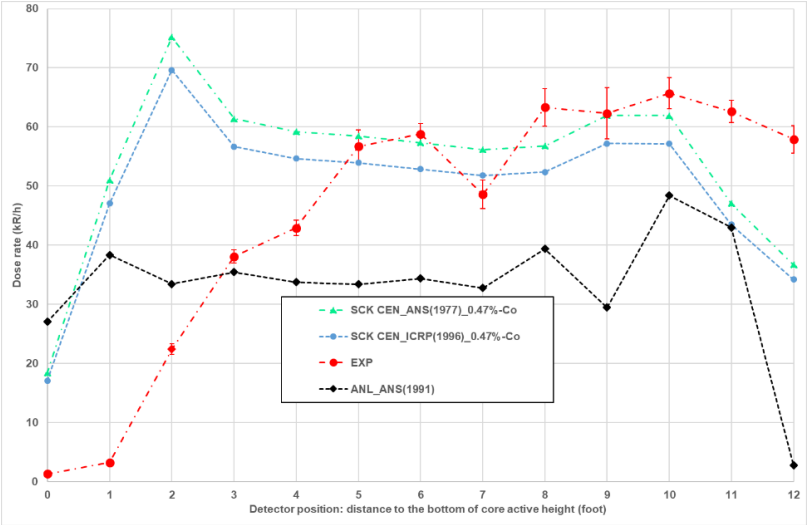

Source: NEA EGAFCS data, 2020.

Figure 7.42. Calculated versus experimental dose rates inside a guide tube of the B03 assembly

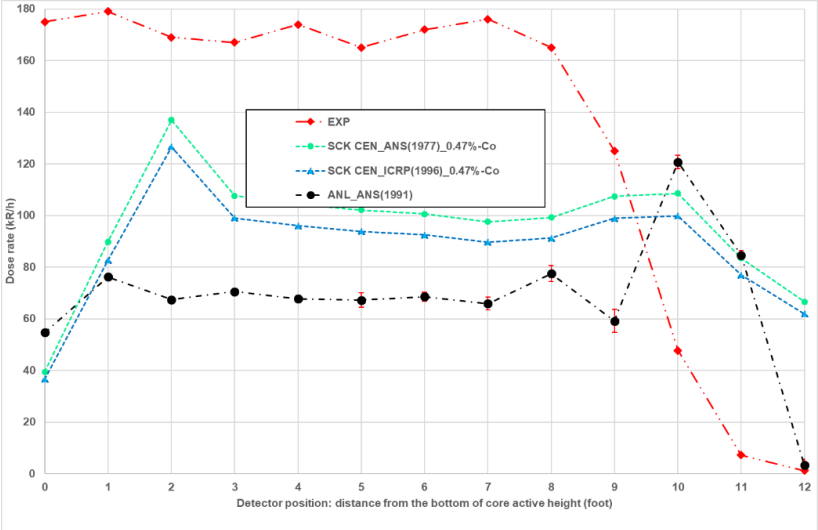

Source: NEA EGAFCS data, 2020.

Figure 7.43. Calculated versus experimental dose rates inside the axial holder tube through the instrumentation (central) tube of the B03 assembly

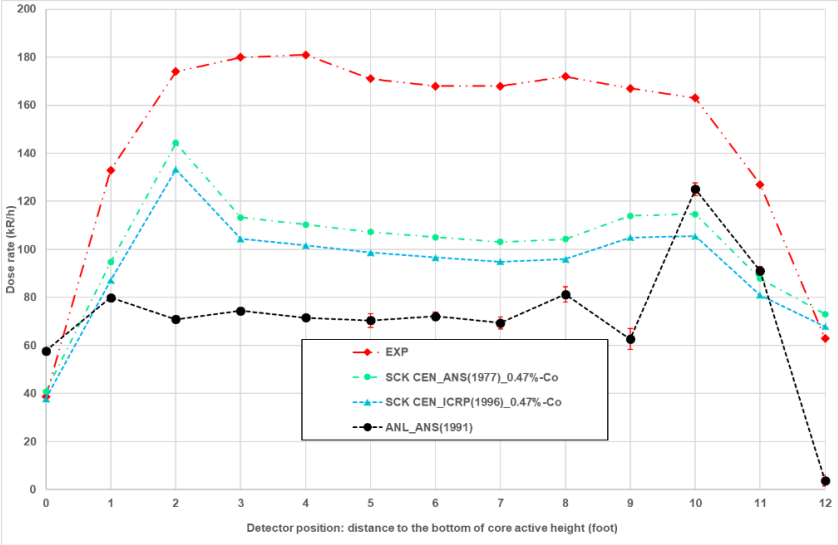

Source: NEA EGAFCS data, 2020.

7.6. Conclusion

The present study has shown that the delayed gammas source term of a UO_2 spent FA irradiated inside a PWR at an average burn-up between 25 and 30 GWd/MTIHM and cooled during 1.8 to 3.7 years is dominated by the signature gammas-rays from a few FP, namely ^{134}Cs, $^{137}Cs/^{137M}Ba$ generator, $^{106}Ru/^{106}Rh$ generator, ^{144}Ce, ^{154}Eu and ^{125}Sb. The above FPs bring along 97% of the total gamma source intensity. In addition, there are the two signature gamma rays of ^{60}Co, an activation product of ^{59}Co, found as an impurity component of the spacer grids and gas plenum spring, both consisting of Inconel-718 alloy.

The major contribution to the dose rates is due to the delayed gamma source from the fuel pellet. For the spacer grids, the contribution to the dose rates depends much more on the distance to the detectors: below 6% for detectors close to the FA, but with spikes for detectors located near spacer grids or gas plenum spring. Away from the FA surface, the contribution of the spacer grids and spring reaches values up to 14% of the total detector dose rate.

The calculated dose rate value is very dependent on the photon-fluence–to-dose conversion function. The dose rate values calculated using the ANS-6.1.1 (1977) conversion function are 24-25% higher compared to values obtained with the ANS-6.1.1 (1991), in agreement with the statement quoted from the literature. The H*(10 mm) ICRP (1996) dose function, considered the worldwide standard, yields values about 14% higher compared to ANS-6.1.1 (1991) and, hence about 9% lower compared to the ANS-6.1.1 (1977).

A critical review of the experimental data has highlighted the disagreement between some of the dose rate distribution curves and the available experimental burn-up and the gamma source scan profiles. This questions the relevancy of using such data for computer tool validation exercises.

For the D04 spent FA, the calculated dose rates obtained using the ANS-6.1.1 (1977) dose function appear to overestimate the dose distribution through the axial detector holder tube 30.48 cm above the spent fuel, the dose rates calculated with the ANS-6.1.1 (1991) giving less discrepancy concerning the experimental data. However, the situation is reversed for the dose rates through the vertical axis wherein the dose rates calculated using ANS-6.1.1 (1977) yield a better agreement, the better agreement being achieved by CIEMAT.

For the B03 spent fuel, the detail modelling approach adopted by SCK CEN has been proven to be effective in achieving the lower discrepancy where the experiment dose rate curves sound reliable.

References

[1] Davis, R.B. (1980), *Data Report for the Nondestructive Examination of Turkey Point Spent Fuel Assemblies B02, B03, B17, B41 AND B43*, HEDL-TME 79-&8 UC-70, April 1980, Hanford Engineering Development Laboratory, Richland, WA, United States, https://doi.org/10.2172/5445903.

[2] Davis, R.B. (1981), *Pre-Test Nondestructive Examination Data Summary Report on Turkey Point Spent Fuel Assemblies D01, D04 and D06 for the Climax-Spent Fuel Test*, HEDL-TME 80-83, January 1981, Hanford Engineering Development Laboratory, Richland, WA, United States.

[3] Davis, R.B. and V. Pasupathi (1981), *Data Summary Report for the Destructive Examination of Rods G7, G9, J8, I9, and H6 from Turkey Point Fuel Assembly B17*, HEDL-TME 80-85 UC-70, April 1981, Hanford Engineering Development Laboratory, Richland, WA, United States.

[4] Davis, R.B., R.L. Fish, V. Pasupathi and D.E. Stellrecht (1980), *Remote Characterization of Spent LWR Fuel for Geologic Disposal Demonstrations*, HEDL-8-2055, 1980, Hanford Engineering Development Laboratory, Richland, WA, United States.

[5] Willingham, C.E. (1981), *Radiation Dose Rates from Commercial PWR and BWR Spent Fuel Elements*, PNL-3954 UC-70, 1981, United States, https://doi.org/10.2172/6052779.

[6] Carlson, R.W. (1979), *Reactor Core Physics Design and Operating data for Cycles 1, 2, and 3 of Surry Unit 1 PWR Power Plant*, EPRI NP-79-2-LD, Project 519, Final report, March 1979, United States.

[7] Unterzuber, R. R.D. Milnes, B.A. Marinkovich and G.M. Kubancsek (1982), *Spent Fuel Dry Storage Testing at E-MAD (March 1978 Through March 1982)*, PNL-4533, 1982, United States.

[8] Hermann, O.W., C.V. Parks and J.P. Renier (1994), *Technical Support for a Proposed Decay Heat Guide Using SAS2H/ORIGEN-S Data*, NUREG/CR-5625 ORNL-6698, 1994, United States.

[9] Gauld, I.C., G. Ilas, B.D. Murphy and C.F. Weber (2010), *Validation of SCALE 5 Decay Heat Predictions for LWR Spent Nuclear Fuel*, NUREG/CR-6972 ORNL/TM-2008/015, February 2010, United States.

[10] Croff, A.G., M.A. Bjerke, G.W. Morrison and L.M. Petrie (1978), *Revised Uranium-Plutonium Cycle PWR and BWR Models for the ORIGEN Computer Code*, ORNL/TM-6051, 1978, Oak Ridge National Laboratory, United States, https://doi.org/10.2172/6787757.

[11] Hermann, O.W. and C.W. Alexander (1986), *A Review of Spent-Fuel Photon and Neutron Source Spectra*, ORNL/CSD/TM-205, 1986, United States.

[12] Van Konynenburg, R.A. (1994), "Behavior of carbon-14 in waste packages for spent fuel in a tuff repository", *Waste Management*, Vol. 14, pp. 363-383, UCRL-90855-Rev. 1, United States, https://doi.org/10.1016/0956-053X(94)90042-6.

[13] Weihermiller, W.B. and G.S. Allison (1979), *LWR Nuclear Fuel Bundle Data for Use in Fuel Bundle Handling*, PNL-2575 UC-85, Topical report, 1979.

[14] Radulescu, G., I.C. Gauld and G. Ilas (2010), *SCALE 5.1 Predictions of PWR Spent Nuclear Fuel Isotopic Compositions*, ORNL/TM-2010/44, 2010, Oak Ridge National Laboratory, United States.

[15] Dahlheimer, J.A. and D. Testa (1984), *The Westinghouse Pressurized Water Reactor Nuclear Power Plant*, Westinghouse Electric Corporation, Water Reactor Division, 1984.

[16] Wagner, J.W. and M.D. De Hart (1999), *Review of Axial Burnup Distribution Considerations for Burnup Credit Calculations*, ORNL/TM-1999/246, 1999, United States.

[17] LANL (2017), *MCNP Users Manual - Code Version 6.2*, LA-UR-17-29981, Los Alamos National Laboratory, United States.

[18] Stankovskiy, A. and G. Van den Eynde (2012), "Advanced method for calculations of core burn-up, activation of structural materials, and spallation products accumulation in accelerator-driven systems", *Science and Technology of Nuclear Installations*, Vol. 2012, pp.1-12, doi:10.1155/2012/545103.

[19] Hairer, E. and G. Wanner (1996), "Solving ordinary differential equations. stiff and differential-algebraic problems", *Springer Series in Computational Mathematics*, Vol. 14, 2nd edition, 1996.

[20] ANS (2004), "American Nuclear Society ANS Issues Clarification on ANSI/ANS-6.1.1 (1991), 'Neutron and gamma-ray fluence-to-dose factors'", *Nuclear News*, Vol. 47(11), October 2004.

[21] Shultis, J.K. and R.E. Faw (2000), *Radiation Shielding*, American Nuclear Society, La Grange Park, IL, United States.

[22] McConn, R.J., G.J. Gesh, R.T. Pagh, R.A. Rucker and R.G. Williams III (2011), *Compendium of Material Composition Data for Radiation Transport Modelling*, PIET-43741-TMN-963/PNNL-15870 (2011).

[23] Leppänen, J., M. Pusa, T. Viitanen, V. Valtavirta and T. Kaltiaisenaho (2014), "The Serpent Monte Carlo code: Status, development and applications in 2013", *Annals of Nuclear Energy*, Vol. 82, pp. 142-150, Elsevier, Amsterdam, doi:10.1051/snamc/201406021.

[24] Pelowitz, D.B. (2011), *MCNPX User's Manual, Version 2.7.0*, LANL report LA-CP-11-00438, 2011, Los Alamos National Laboratory, United States.

[25] Croff, A.G. (1983), "ORIGEN2: A versatile computer code for calculating the nuclide compositions and characteristics of nuclear materials", *Nuclear Technol*ogy, Vol. 62, pp. 335-352, https://doi.org/10.13182/NT83-1.

[26] NEA (2006), *The JEFF-3.1 Nuclear Data Library, JEFF Report 21*, OECD Publishing, Paris.

[27] Rearden, B.T. and M.A. Jessee (2016), *SCALE Code System*, ORNL/TM-2005/39, Oak Ridge National Laboratory, United States.

[28] Koning, A.J. and D. Rochman (2012), "Modern nuclear data evaluation with the TALYS code system", *Nuclear Data Sheets*, Vol.113, pp. 2841-2934, https://doi.org/10.1016/j.nds.2012.11.002.

[29] Álvarez-Velarde, F., E.M. González-Romero and I.M. Rodríguez (2014), "Validation of the burn-up code EVOLCODE 2.0 with PWR experimental data and with a sensitivity/uncertainty analysis", *Annals of Nuclear Energy*, Vol. 73, pp. 175-188, Elsevier, Amsterdam, http://dx.doi.org/10.1016/j.anucene.2014.06.049.

[30] Pelowitz, D.B. (2014), *MCNP6 User's Manual, Code Version 6.1.1beta*, LA-CP-14-00745, Los Alamos National Laboratory, United States.

[31] NEA (2008), *ACAB-2008: Activation Abacus Code V2008*, NEA Data Bank NEA-1839.

[32] NEA (2014), *Data Bank, JEFF-3.2 Evaluated Data Library - Neutron data* (2014), www.oecd-nea.org/dbforms/data/eva/evatapes/jeff_32.

[33] Lutier, J. et al. (2015), "Burnup credit implementation for PWR UOX used fuel assemblies in France: From the studies to the practical experience", *Nuclear Science and Engineering*, Vol. 181 (2), pp. 105-136, doi: 10.13182/NSE14-51.

[34] Santamarina, A., D. Bernard, P. Blaise and P. Leconte (2009), "APOLLO-2.8: A validated code package for PWR neutronics calculations", *Proceedings Of the International Conference on Advances in Fuel Management ANFM-IV*, Hilton Head Island, United States.

[35] Brun, E. et al. (2015), "TRIPOLI-4® CEA, EDF and AREVA reference Monte Carlo code", *Annals of Nuclear Energy*, Vol. 82, pp. 151-160, Elsevier, Amsterdam, https://doi.org/10.1016/j.anucene.2014.07.053.

[36] San-Felice, L., R. Eschbach and P. Bourdot (2013), "Experimental validation of the DARWIN2.3 package for fuel cycle applications", *Nuclear Technology*, Vol. 184, pp. 217-232, https://doi.org/10.13182/NT12-121.

[37] Wagner, J.C., M.D. DeHart and C.V. Parks (2003), *Recommendations for Addressing Axial Burnup in PWR Burnup Credit Analyses*, NUREG/CR-6801ORNL/TM-2001/273, Oak Ridge National Laboratory, United States.

[38] Gauld, I.C. (2011), *ORIGEN-S: Depletion Module to Calculate Neutron Activation, Actinide Transmutation, Fission Product Generation and Radiation Source Terms*, ORNL/TM-2005/39, ORNL, United States.

[39] Chadwick, M.B. et al. (2006), "ENDF/B-VII.0: Next generation evaluated nuclear data library for nuclear science and technology", *Nuclear Data Sheets*, Vol. 107, pp. 2931-3060, https://doi.org/10.1016/j.nds.2006.11.001.

[40] NEA (2012), *JEFF 312 - Joint Evaluated Nuclear Data Library for Fission and Fusion Applications* (DVD), www.oecd-nea.org/jcms/c_12798/joint-evaluated-fission-and-fusion-jeff-nuclear-data-library.

[41] Gauld, I.C., S.M. Bowman and J.E. Horwedel (2011), *ORIGEN-ARP: Automatic Rapid Processing for Spent Fuel Depletion, Decay, and Source Term Analysis*, SCALE 6.1 Manual, Sect. D1, ORNL/TM-2005/39, Oak Ridge National Laboratory, United States.

[42] Hfaiedh, N. and A. Santamarina (2005), "Determination of the optimized SHEM mesh for neutron transport calculation", *Proc. Int. Conf. on Mathematics and Computation M&C2005*, Avignon, France, 12-15 September 2005.

[43] CEA (2021), *TRIPOLI-4. Version 7: Manuel de l'utilisateur*, Rapport DM2S SERMA/LTSD/RT/10-4941/A, France.

[44] Plompen, A.J.M. et al. (2020), "The joint evaluated fission and fusion nuclear data library, JEFF-3.3", *European Physical Journal A*, Vol. 56, Springer, Berlin, https://doi.org/10.1140/epja/s10050-020-00141-9.

[45] ANS (1977), *American National Standard for Neutron and Gamma-Ray Flux-to-Dose-Rate Factors*, ANSI/ANS-6.1.1 (1977), American Nuclear Society, United States.

[46] ANS (1991), *American National Standard for Neutron and Gamma-Ray Flux-to-Dose-Rate Factors*, ANSI/ANS-6.1.1 (1991), American Nuclear Society, United States.

[47] Cao, Y. and B. Feng (2019), *Validation of Gamma Dose Rate Calculation Methodology using the Morris and Turkey Point Measurements*, ANL-19/06, Argonne National Laboratory, United States.

[48] Álvarez-Velarde, F. and A.V. Skarbeli (2019), *Dose Rate Calculations Involving Irradiated PWR Fuel Assemblies: Verification and Validation Benchmark*, CIEMAT internal report DFN/IN-01/II-19, December 2019.

[49] Leger, V. and A. Dalesme (2020), *OCDE/NEA Dose Rate Benchmark – ORANO TN Contribution to the Validation Step*, NTE-20-032401-000-1.02020, Orano TN, France.

[50] Räty, A. and S. Häkkinen (2018), WPFC/AFCS Expert Group Benchmark on Dose Rate Calculations with Serpent, VTT Technical Research Centre of Finland, VTT Research Report (internal), No. VTT-R-02506-18.

[51] Vanderbilt University Medical Center (n.d.), *Radiation Safety Reference Manual*, www.vumc.org/safety/sites/vumc.org.safety/files/public_files/radiation-safety-reference-manual.pdf (last accessed in June 2023).

[52] Malambu, E. (2019), *SCK CEN Contribution to OECD/NEA Computer Tools Validating Exercise on the Dose Rates Calculation for a PWR Spent Fuel Assembly*, Internal report, ER-0519, SCK CEN/32649230, 13-08-2019, Belgium.

[53] Bowman, S.M. and O.W. Hermann (1995), *SCALE-4 Analysis of Pressurized Water Reactor Critical Configurations: Volume 3 Surry Unit 1 Cycle 2*, ORNL/TM-12294/V3, Oak Ridge National Laboratory, United States.

[54] Pergreffi, R., F. Rocchi and A. Guglielmelli (2020), *WPFC/AFCS Expert Group Benchmark on Dose Rate Calculations*, ENEA report, SICNUC-P000-026, Rev.1, 2020, https://hdl.handle.net/20.500.12079/55061.

8. Conclusions

Under the auspices of the NEA EGAFCS, an international benchmark on dose rate calculations for PWR spent FA was conducted. The objectives of the benchmark were to verify updated dose rate calculation procedures (new modelling approaches, new nuclear data, new versions of codes) and to share the benchmark results at the international level. The benchmark was divided into two parts: verification (comparison of results with different codes/methodologies, sensitivity studies) and validation (comparison of results with experimental data). The participants of the benchmark were: ANL, CEA, CIEMAT, CNL, ENEA, KIT, ORANO TN, SCK CEN and VTT.

The participants conducted a code-to-code benchmark comparing nuclide masses, photon release rates and gamma dose rates at 1 m distance from a PWR UOX and PWR MOX FA (a 15x15 PWR UOX FA at 33 GWd/MTIHM burn-up and a 17x17 PWR MOX FA at 60 GWd/MTIHM burn-up). Gamma dose rates were calculated at 3.7 and 30 years after discharge using two different photon flux-to-dose rate conversion factors (the time of 3.7 years was considered, as it corresponds to the experimental measurements; see Chapter 7). The agreement between participants was good, with RSD from 7 to 15%. The calculated dose rate for PWR MOX is two times greater than that for PWR UOX, in accordance with a higher gamma release rate. For the ANSI (1977) conversion factor and 30 years of cooling, the average dose rates are 5.8 Sv/h (UOX) and 11.1 Sv/h (MOX). It should be noted that these dose rates are 20 to 25% lower with the ANSI (1991) conversion factor because of the differences in the weighting factors.

Various sensitivity studies were carried out to assess the impact of the calculation scheme on the calculated dose rate, leading to some recommendations for dose rate calculation models.

These reference calculations were validated by comparison with two experiments (Morris and Turkey Point). The experimental validation exercise showed the need for accurate and complete measurements (knowledge of the level of impurities in the components in particular).

To conclude, this benchmark made it possible to establish recommendations for the calculation of dose rates in the air for PWR UOX and MOX spent FAs.

In the future, the dose rate could be an additional relevant parameter for the scenario studies, in particular in the framework of proliferation resistance evaluations, by comparing the self-protection capabilities of different reactors or fuel cycles. Thus, it would be interesting to complete the calculations carried out here on PWR UOX and MOX with calculations on other types of reactors (PWR, BWR, fast reactor…), and to complete or consolidate the experimental validation with quality measurements, subject to availability.

Appendix A. Verification step and contributions

KIT contribution

Introduction

The Karlsruhe Institute of Technology (KIT) participated in the verification and validation benchmarks on the evaluation of the γ dose rate of light water reactor (LWR) (UOX and MOX) spent fuel assemblies (FAs), which were proposed within the framework of the NEA Expert Group on Advanced Fuel Cycle Scenarios (EGAFCS) [1,2].

In the following, the description of the assessed calculation route is provided as well as related codes and nuclear data. Finally, the KIT results for the verification and validation benchmarks will be shown.

Calculation procedure and codes

To evaluate the γ dose rate for a FA, the calculation procedure shown in Figure A.1 was employed. The procedure consists of three steps: depletion, decay and radiation analyses.

Figure A.1. Flow chart of the calculation procedure for γ dose rate evaluation

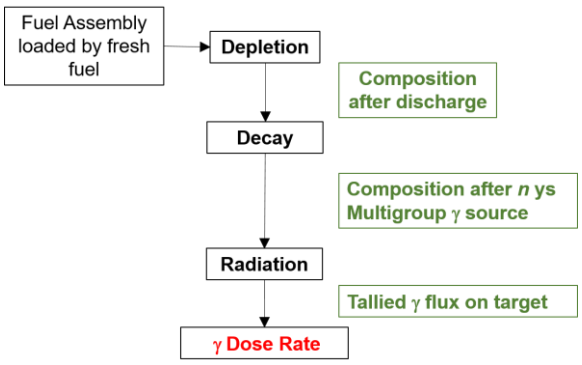

Source: NEA EGAFCS data, 2020.

The depletion calculation was performed by employing ECCO [3] and ERANOS [4] to evaluate the composition at the discharge of the FA. The ECCO code was used for processing the 172 multi-group (XMAS standard energy structure) effective neutron cross-sections for the FA model (real geometry). The JEFF3.1 reference data library [5] was employed for such calculations. Note that a different procedure was employed for the MOX FA analysis, as it will be described later. The burn-up calculation was performed by employing the BISTRO code [6,7] as a neutron transport solver (P_0S_{16}), the effective neutron XSs being recalculated by ECCO at each burn-up step up. For the UOX FA analyses, a 1D (R) model totally reflected was assessed in BISTRO. On the contrary, a 2D (XY) model was assessed for the MOX FA analyses. The irradiation history provided in the benchmark specifications was employed. In the burn-up model, a decay chain taking into account 250 isotopes was assessed.

The fuel composition after depletion was employed for the next decay calculation. It was performed by using the ORIGEN2.2 [8] and the ORIGEN-ARP [9] codes, the gxuo2brm.lib photon library being employed. The calculation aims at evaluating the multi-group γ source after *n* yr, where *n* is provided by the benchmark specifications. In particular, the

ORIGEN2.2 and ORIGEN-ARP calculations were performed to evaluate the 18 and 19 energy groups γ source, the employed discretisation being shown in Table A.1.

Table A.1. Energy discretisation of the γ source employed in the procedure

ORIGEN2.2			ORIGEN-ARP	
Lower boundary [MeV]	Upper boundary [MeV]		Lower boundary [MeV]	Upper boundary [MeV]
0.00	0.02		0.00	0.05
0.02	0.03		0.05	0.07
0.03	0.05		0.07	0.11
0.05	0.07		0.11	0.16
0.07	0.10		0.16	0.23
0.10	0.15		0.23	0.34
0.15	0.30		0.34	0.51
0.30	0.45		0.51	0.75
0.45	0.70		0.75	1.25
0.70	1.00		1.25	1.75
1.00	1.50		1.75	2.25
1.50	2.00		2.25	2.75
2.00	2.50		2.75	3.50
2.50	3.00		3.50	4.50
3.00	4.00		4.50	5.50
4.00	6.00		5.50	6.50
6.00	8.00		6.50	7.50
8.00	11.00		7.50	8.65
			8.65	20.00

The fuel composition and the γ source after decay were employed for the radiation calculation, which aims at evaluating the γ dose rate in selected positions around the FA. For such analyses, the 3D actual model of the FA located in the air was assessed in the MCNPX2.7 code [10]. For the model, the fuel composition and the γ source after decay were uniformly spread axially and radially. The transport of photons and electrons was considered in the calculation, with the TENDL-2014 and mcplib04 nuclear data libraries [11] being used. Finally, the γ flux was tallied for each selected position and the dose rate was computed by using the flux-to-dose rate conversion factors from ANSI/ANS-6.1.1 (1977) and the ANSI/ANS-6.1.1 (1991).

Verification phase

The verification phase aimed at benchmarking the KIT calculation procedure for the UOX and the MOX FA described in the verification benchmark (UOX and MOX). In the following, the calculation models and the results for each of the benchmark problems are shown.

The UOX FA model

The ECCO and ERANOS models as well as a detailed description of the depletion calculation are shown in Figure A.2. In the calculation, the effective neutron XSs are recalculated by ECCO with a burn-up step of ~1.5 GWd/MTIHM.

Figure A.2. Depletion calculation scheme for the analysis of the UOX FA

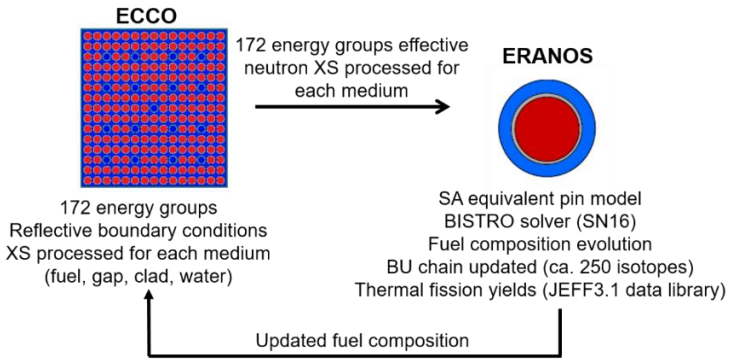

Source: NEA EGAFCS data, 2020.

The main parameters of the burn-up calculation are shown in Table A.2, where the burn-up value was assessed assuming the ^{148}Nd as an indicator.

Table A.2. Parameters employed in the burn-up calculation

Parameter	Value
Power density [W/g]	51
Power [W]	319.01
Efpd [d]	687
N_{step} x efpd/step	68 x 10.1
Burn-up [GWd/MTIHM)	35.4

As a result, the HM and the FP isotope-wise masses at the discharge were obtained and employed for the decay calculation. The fuel composition and the photon emission rate (γ/s) after a decay period of 30 and 3.7 years were calculated by using the ORIGEN2.2 code. Note that the discharged composition from depletion calculation was scaled to 469 kg of initial HM as indicated in the benchmark. Furthermore, only the isotopes (HM and FP) included in the summary tables requested by the benchmark were considered.

The computed total γ source was 9.68e+15 γ/s and 1.98e+15 γ/s after a decay of 3.7 years and 30 years, respectively. The energy dependence of the γ source is shown in Figure A.3.

Figure A.3. UOX FA: γ source after 30 years and 3.7 years of decay vs. energy

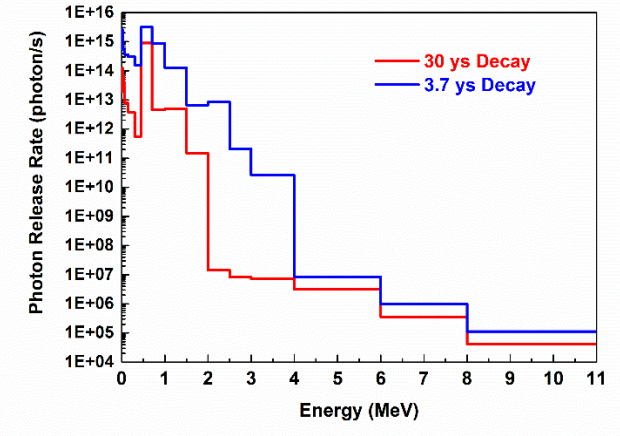

Source: NEA EGAFCS data, 2020.

The dose rate was computed by evaluating the flux averaged over a surface tallied (tally F2) at 1 m from the flat edge and axially at the core mid-plane. The results after a decay period of 30 and 3.7 years are shown in Table A.3.

Table A.3. Dose rate at 1 m from the flat edge and axially at core mid-plane

Conversion factor	Dose rate (Sv/h) after 3.7 years of decay	Dose rate (Sv/h) after 30 years of decay
1977	30.8	5.47
1991	24.6	4.31

Parametric analysis

A large parametric analysis was performed to evaluate the impact of the modelling assumptions on the final results concerning:

- the surface of the tally (Tally F2 – 400/100 cm^2);
- the tally type (Tally F4 vs. F2);
- the TENDL distribution (TENDL-2012 vs. TENDL 2014);
- the fuel density;
- the distances from the FA centre at which the dose rate is evaluated.

The effect on the dose rate of the surface of the tally is shown in Table A.4. Here the Tally F2 was employed and the effect of three different surfaces was studied. In the reference case, a 100 cm^2 was employed. The reference is compared with case 1 (4 surfaces of 400 cm^2) and case 2 (16 surfaces surrounding the FA of 400 cm^2 each).

Table A.4. Effect of the surface of the tally on the dose rate result

Parameter	KIT - REF	Case 1	Case 2
Tally type	F2	F2	F2
Surface of the tally	4 x 100 cm^2	4 x 400 cm^2	16 x 400 cm^2 (cyl)
Standard	Dose rate (Sv/h)	Dose rate (Sv/h)	Dose rate (Sv/h)
ANSI/ANS-6.1.1 (1977)	5.47	5.07	6.28
ANSI/ANS-6.1.1 (1991)	4.31	3.99	-

The results of the effect on the dose rate of using a different TENDL distribution and of employing the F4 tally instead of the F2 tally are shown in Table A.5.

Table A.5. Effect of using a different TENDL set of data on the dose rate result

Parameter	KIT - REF	Case 1	Case 2
Tally type	F2	F2	F4
Surface of the tally	4 x 100 cm	4 x 400 cm	4 x 400 cm
Distribution	TENDL 2014	TENDL 2014	TENDL 2012
Standard	Dose rate (Sv/h)	Dose rate (Sv/h)	Dose rate (Sv/h)
ANSI/ANS-6.1.1 (1977)	5.47	5.07	5.07
ANSI/ANS-6.1.1 (1991)	4.31	3.99	3.99

The results of effect on the dose rate of using a different fuel density are shown in Table A.6.

Table A.6. Effect of the fuel density on the dose rate result

Parameter	KIT - REF	Case 1	Case 1 + density 1	Case 1 + density 2
Tally type	F2	F2	F2	F2
Surface of the tally	4 x 100 cm	4 x 400 cm	4 x 400 cm	4 x 400 cm
Fuel density (g/cm^3)	10.412	10.412	10.301	9.683
Standard	Dose rate (Sv/h)	Dose rate (Sv/h)	Dose rate (Sv/h)	Dose rate (Sv/h)
ANSI/ANS-6.1.1 (1977)	5.47	5.07	5.11	5.44
ANSI/ANS-6.1.1 (1991)	4.31	3.99	4.02	4.28

The results of effect on the dose rate of the position of the tally are shown in Table A.7.

Table A.7. Effect of the fuel density on the dose rate result

Parameter	KIT - REF	Case 1	Case 1 + distance	Case 2 + distance
Tally type	F2	F2	F2	F2
Surface of the tally	4 x 100 cm	4 x 400 cm	4 x 400 cm	16 x 400 cm^2 (cyl)
Distance from the centre of the FA (m)	~1.11	~1.11	1.0	1.0
Standard	Dose rate (Sv/h)	Dose rate (Sv/h)	Dose rate (Sv/h)	Dose rate (Sv/h)
ANSI/ANS-6.1.1 (1977)	5.47	5.07	5.91	7.11 (6.28)
ANSI/ANS-6.1.1 (1991)	4.31	3.99	4.65	-

The MOX FA model

The analysis of the MOX FA needed the assessment of the actual model in the BISTRO calculation because three sets of MOX pins with different enrichments are loaded in the FA. With this in mind, a 2D (XY) Cartesian model of the MOX FA was assessed for the depletion calculation.

Because of the large number of calculation meshes in the BISTRO model, effective neutron XSs at 12 energy groups were processed by condensation, generated from an ultra-fine-group data library (1 968 energy groups). A calculation benchmark was performed to investigate the performance of the 2D (XY) against the reference 1D (R) models, shown in Figure A.4, as well as the effect of the group discretisation (172 vs. 12).

Since the results provided a satisfactory agreement, as shown in Figure A.5, the depletion calculation was performed according to the scheme in Figure A.4. In the calculation, the effective neutron XSs are recalculated by ECCO with a burn-up step of ~1.5 GWd/MTIHM.

Figure A.4. 1D (R) and 2D (XY) models of the MOX FA

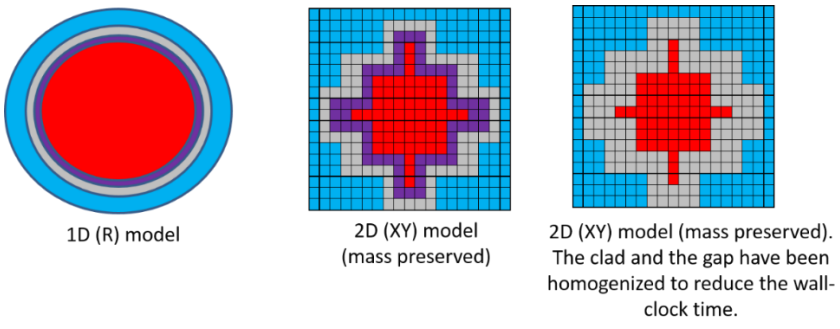

Source: NEA EGAFCS data, 2020.

Figure A.5. Verification of the Cartesian and 12 energy groups effective XSs option for the MOX FA

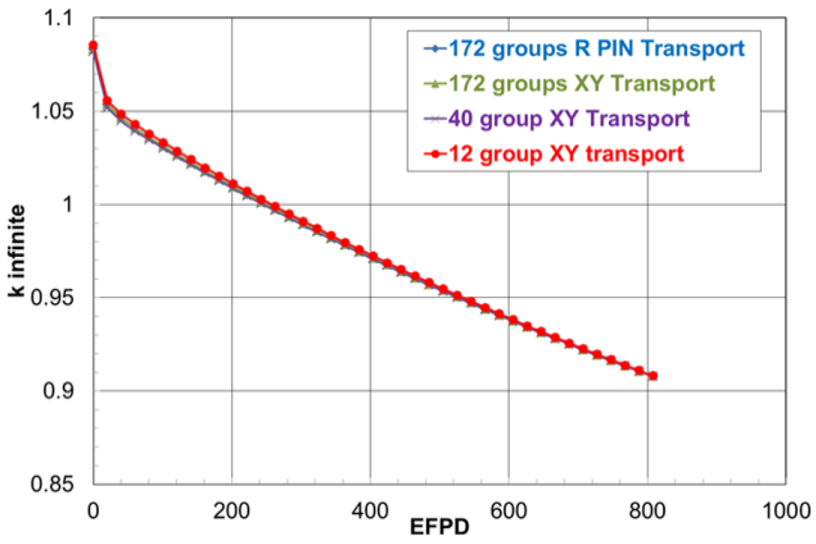

Source: NEA EGAFCS data, 2020.

Figure A.6. Depletion calculation scheme for the analysis of the MOX FA

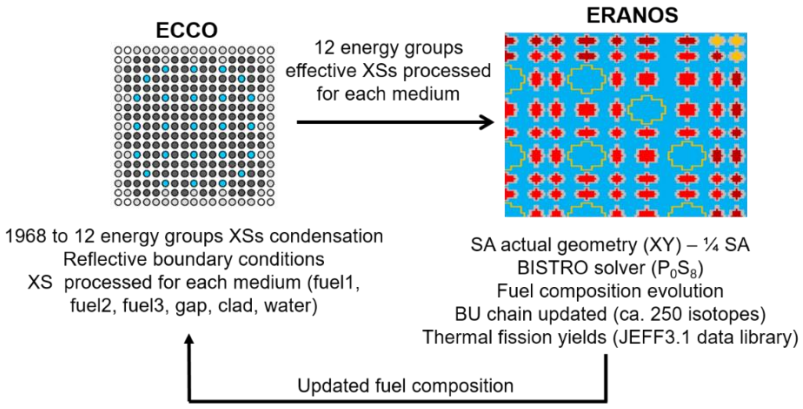

Source: NEA EGAFCS data, 2020.

The main parameters of the burn-up calculation are shown in Table , where the burn-up value was assessed assuming the ^{148}Nd as indicator.

Table A.8. Parameters employed in the burn-up calculation

Parameter	Value
Power density [W/g]	48
Power [W]	14 970
Efpd [d]	1 290
N_{step} x efpd/step	43 x 30
Burn-up [GWd/MTIHM)	60

As a result, the HM and FP isotope-wise masses at the discharge were obtained and employed for the decay calculation. The fuel composition and the photon emission rate (γ/s) after a decay period of 30 years were calculated by using the ORIGEN2.2 code. Only

the isotopes (HM and FPs) included in the summary tables requested by the benchmark were considered.

The computed total γ source was 1.72e+16 γ/s and 3.32e+15 γ/s after a decay of 3.7 years and 30 years, respectively. The energy dependence of the γ source is shown in Figure A.7.

Figure A.7. UOX FA: γ source after 30 years and 3.7 years of decay vs. energy

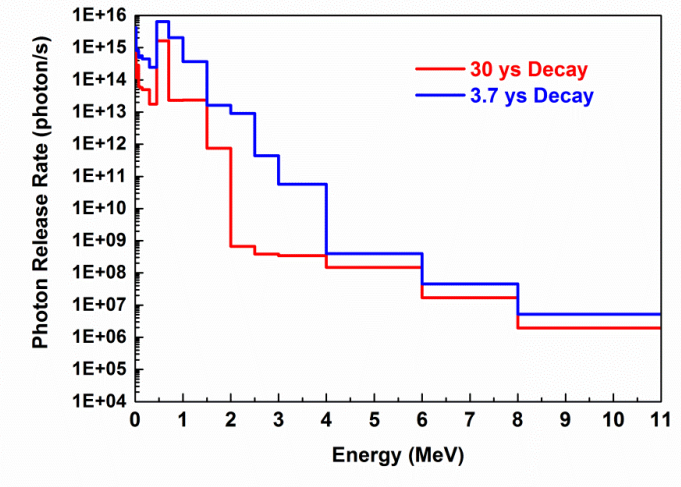

Source: NEA EGAFCS data, 2020.

The dose rate was computed by evaluating the flux average over a surface tallied (tally F2) at 1 m from the flat edge and axially at core mid plane. The results after a decay of 30 years and 3.7 years are shown in Table A.9.

Table A.9. Dose rate at 1 m from the flat edge and axially at core mid-plane

Conversion factor	Dose rate (Sv/h) after 3.7 years of decay	Dose rate (Sv/h) after 30 years of decay
1977	69.8	11.49
1991	55.9	9.12

References

[1] Eschbach, R. et al. (2017), "Verification of dose rate calculations for PWR spent fuel assemblies", *Proc. of GLOBAL 2017*, 24-29 September, Seoul, Korea.

[2] Eschbach, R., R. Girieud, B. Feng and R. Hill (2015), "Proposal for a benchmark on dose rate calculations for irradiated assemblies by the WPFC/AFCS Expert Group*", proposed by CEA/Nuclear Energy Division (DEN) and DOE (ANL)*". (internal document)

[3] Rimpault, R. (1995), "Algorithmic features of the ECCO cell code for treating heterogeneous reactor subassemblies", Proceedings of the International Topical Meeting on Reactor Physics and Computations, 30 April-4 May, Portland, OR, United States.

[4] Doriath, J.Y., C.W. McCallien, E. Kiefhaber, U. Wehmann and J.M. Rieunier (1993), "ERANOS1: The advanced European system of codes for reactor physics analysis", Proceedings of the International Conference on Mathematical Methods and Supercomputing for Nuclear Application, Karlsruhe, Germany.

[5] NEA (2006), *The JEFF-3.1 Nuclear Data Library*, JEFF Report 21, OECD Publishing, Paris.

[6] Gho, C. and G. Palmiotti, (1984), *BISTRO: Bidimensionnel Sn Transport Optimise - Un Programme Bidimensionnel de Transport Sn aux Differences Finies*, Note No.1 Definition Des Algorithmes Pour La Geometrie X-Y, CEA Technical Note NT-SPRC-LEPh-84-270.

[7] Palmiotti, G., J.M. Rieunier, C. Gho and M. Salvatores (1990), "Optimized two-dimensional Sn transport (BISTRO)", *Nuclear Science and Engineering*, Vol. 104:1, pp. 26-33, https://doi.org/10.13182/NSE90-1.

[8] Croff, A.G. (1983), "ORIGEN2: A versatile computer code for calculating the nuclide compositions and characteristics of nuclear materials", *Nuclear Technology*, Vol. 62, pp. 335-352, https://doi.org/10.13182/NT83-1.

[9] ORNL (2016), *SCALE Code System*, ORNL/TM-2005/39, Oak Ridge National Laboratory, United States.

[10] Pelowitz, D.B. (2011), *MCNPX User's Manual, Version 2.7.0*, LANL report LA-CP-11-00438, Los Alamos National Laboratory, United States.

[11] Koning, A.J. and D. Rochman, (2012), "Modern nuclear data evaluation with the TALYS code system", *Nuclear Data Sheets*, Vol. 113, pp. 2841-2934, https://doi.org/10.1016/j.nds.2012.11.002.

VTT contribution

SERPENT model in the depletion calculations

The verification phase studies the photon dose rates of two irradiated PWR assemblies: The first one is a 15x15 UOX FA and the second one is a 17x17 type MOX assembly [1].

Both depletion calculations were performed in two dimensions applying reflective boundary conditions. SERPENT models are presented in Figure A.8 and Figure A.9. One burn-up zone was applied in all fuel rods. The UOX assembly was irradiated for 33 GWd/MTIHM with a specific power of 48 W/g in 19 burn-up steps and the 17x17 MOX assembly was irradiated for 60 GWd/MTIHM with a specific power of 41 W/g in 28 burn-up steps. After the irradiation, both assemblies were cooled for 30 years with an intermediate time point of 3.7 years.

In both models, five million source neutrons were sampled to irradiate the assembly. Doppler broadening rejection correction (DBRC) was also used to enhance the modelling of elastic scattering and absorption near resonances [2].

Figure A.8. Modelled 15x15 UOX assembly

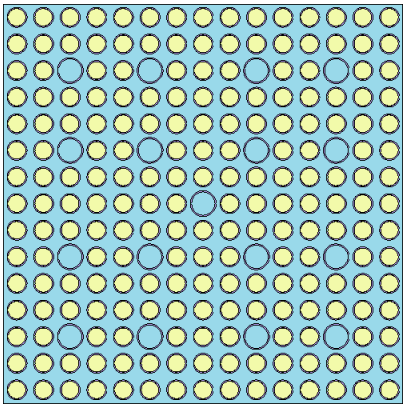

Source: Räty, A. and S. Häkkinen, 2018.

Figure A.9. Modelled 17x17 MOX assembly

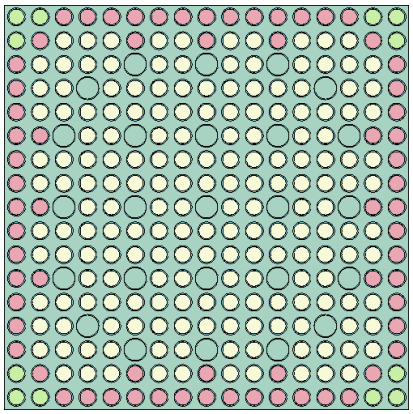

Source: Räty, A. and S. Häkkinen, 2018.

Photon dose rate calculation

The irradiated assembly was used as the source in a separate photon transport calculation using the restart feature of SERPENT after the depletion and decay calculations. The model had the same geometrical data as the depletion calculation, but the assembly was modelled in three dimensions with a length of 365.8 cm. The assembly was surrounded by dry air.

Altogether 20 000 000 000 source photons in 20 000 source batches were modelled. Photon transport was performed with analogue source sampling or sampling the source randomly and accepting with probability relative to the ratio of local to maximum emission rate.

Photon dose rates from the irradiated assembly were calculated by placing a 10x1x10 cm void cuboid detector at a 1 m distance from the surface of the assembly at its axial midpoint. Track-length estimator feature in the detector was also used to enhance the collision data. Results were finally scaled with the detector volume and multiplied with ANSI standard dose rate conversion factors with a log-log interpolation feature in the code. Multiplication was repeated with both ANSI (1977) [3] and ANSI (1991) [4] conversion factors.

Results

According to the benchmark specification, one aim in the verification step is to provide nuclide inventories of certain specified HM and FP in irradiated UOX and MOX PWR assemblies after 3.7 and 30 years of cooling. Only the inventories in the fuel are listed, neglecting all cladding and spacer materials.

Calculated nuclide inventories for 15x15 UOX assembly are listed in Table A.10 and for 17x17 MOX assembly in Table A.11. Inventory masses for the UOX and MOX assemblies were scaled to HM mass of 469 kg and 454 kg, respectively. The list of required nuclides in the two-time points is different and only the required nuclides are listed.

Fuel inventories were also converted to a photon source to calculate the dose rates at 1 m distance from the surface of the assembly. The aim was to test if the photon dose rates from the assemblies exceed the self-protection limit of 1 Sv/h at a 1 m distance. Dose rates for a 10x1x10 cm detector are listed in Table A.12 and Table A.13. Calculated dose rates exceed the self-protection limit of 1 Sv/h at a 1 m from the FA.

Table A.10. Calculated HM and FP masses (g) in the UOX assembly after 3.7 and 30 years of cooling

HM Nuclide	Mass (g) after 3.7 years	Mass (g) after 30 years	Fission product nuclide	Mass (g) after 3.7 years	Mass (g) after 30 years
U-234	9.55E+01	1.08E+02	**Kr-83**	1.93E+01	
U-235	3.81E+03	3.81E+03	**Rh-103**	2.37E+02	
U-236	1.80E+03	1.80E+03	**Rh-105**	0.00E+00	
U-237	1.68E-05	4.72E-06	**Ag-109**	4.18E+01	
U-238	4.43E+05	4.43E+05	**I-135**	0.00E+00	
Np-236	5.84E-04		**Xe-131**	2.02E+02	
Np-236m	0.00E+00		**Xe-135**	0.00E+00	
Np-237	1.94E+02	2.08E+02	**Cs-133**	5.22E+02	
Np-238	2.77E-08		**Cs-134**	1.79E+01	
Np-239	3.90E-05		**Cs-135**	1.29E+02	
Pu-236	1.34E-06		**Cs-137**	5.26E+02	2.87E+02
Pu-237	1.50E-13		**Ba-137m**	8.03E-05	4.38E-05
Pu-238	6.61E+01	5.37E+01	**Ba-140**	0.00E+00	
Pu-239	2.69E+03	2.68E+03	**La-140**	0.00E+00	
Pu-240	1.11E+03	1.11E+03	**Nd-143**	3.74E+02	
Pu-241	5.39E+02	1.51E+02	**Nd-145**	3.15E+02	
Pu-242	2.42E+02	2.42E+02	**Nd-148**	1.75E+02	
Pu-243	2.26E-14		**Pm-147**	3.75E+01	
Pu-244	1.47E-02		**Pm-148**	7.21E-13	
Am-241	1.17E+02	4.91E+02	**Pm-149**	0.00E+00	
Am-242	1.91E-06	1.68E-06	**Sm-147**	8.55E+01	
Am-242m	1.48E-01	1.30E-01	**Sm-149**	1.90E+00	
Am-243	4.53E+01	4.51E+01	**Sm-150**	1.39E+02	
Am-244	0.00E+00	0.00E+00	**Sm-151**	5.56E+00	
Cm-242	1.90E-02		**Sm-152**	5.04E+01	
Cm-243	1.06E-01		**Sm-154**		1.86E+01
Cm-244	1.17E+01	4.28E+00	**Eu-153**	5.50E+01	5.50E+01
Cm-245	7.07E-01	7.08E-01	**Eu-154**	8.35E+00	1.00E+00
Cm-246	5.86E-02		**Eu-155**	2.16E+00	4.68E-02
Cm-247	6.50E-04		**Eu-156**	4.58E-27	
Cm-248	3.36E-05		**Gd-155**	1.56E+00	
Bk-249	3.26E-08		**Sr-90**		1.19E+02
Cf-249	6.51E-07		**Y-90**		3.02E-02
Cf-250	0.00E+00				
Cf-251	0.00E+00	0.00E+00			
Cf-252	0.00E+00	0.00E+00			

Table A.11. Calculated HM and FP masses (g) in the MOX assembly after 3.7 and 30 years of cooling

HM Nuclide	Mass (g) after 3.7 years	Mass (g) after 30 years	Fission product nuclide	Mass (g) after 3.7 years	Mass (g) after 30 years
U-234	5.51E+01	2.62E+02	**Kr-83**	2.21E+01	
U-235	4.27E+02	4.34E+02	**Rh-103**	5.85E+02	
U-236	1.35E+02	1.55E+02	**Ag-109**	1.59E+02	
U-237	1.25E-04	3.47E-05	**I-135**	0.00E+00	
U-238	3.95E+05	3.84E+05	**Xe-131**	3.55E+02	
Np-236	1.02E-03		**Xe-135**	0.00E+00	
Np-236M	0.00E+00		**Cs-133**	8.68E+02	
Np-237	1.00E+02	2.17E+02	**Cs-134**	3.62E+01	
Np-238	1.54E-06		**Cs-135**	6.56E+02	
Np-239	8.55E-04		**Cs-137**	9.03E+02	4.79E+02
Pu-236	8.63E-05		**Ba-137m**	1.38E-04	7.30E-05
Pu-237	3.61E-12		**Ba-140**	0.00E+00	
Pu-238	1.14E+03	9.15E+02	**La-140**	0.00E+00	
Pu-239	9.30E+03	9.41E+03	**Nd-143**	6.22E+02	
Pu-240	8.15E+03	8.38E+03	**Nd-145**	4.64E+02	
Pu-241	4.00E+03	1.11E+03	**Nd-148**	3.02E+02	
Pu-242	3.67E+03	3.51E+03	**Pm-147**	4.48E+01	
Pu-243	7.86E-12		**Pm-148**	1.68E-12	
Pu-244	4.58E-01		**Pm-149**	0.00E+00	
Am-241	1.20E+03	3.93E+03	**Sm-147**	1.32E+02	
Am-242	1.06E-04	9.38E-05	**Sm-149**	4.55E+00	
Am-242M	8.24E+00	7.27E+00	**Sm-150**	2.52E+02	
Am-243	9.93E+02	9.72E+02	**Sm-151**	2.06E+01	
Am-244	0.00E+00	0.00E+00	**Sm-152**	9.17E+01	
Cm-242	4.11E-01		**Sm-154**		5.29E+01
Cm-243	5.85E+00		**Eu-153**	1.27E+02	1.24E+02
Cm-244	6.03E+02	2.15E+02	**Eu-154**	3.42E+01	3.87E+00
Cm-245	9.37E+01	9.07E+01	**Eu-155**	6.19E+00	1.29E-01
Cm-246	8.54E+00		**Eu-156**	5.52E-27	
Cm-247	2.26E-01		**Gd-155**	4.72E+00	
Cm-248	1.74E-02		**Sr-90**		9.57E+01
Bk-249	3.37E-05		**Y-90**		2.43E-02
Cf-249	8.47E-04				
Cf-250	0.00E+00				
Cf-251	2.46E-10	0.00E+00			
Cf-252	0.00E+00	0.00E+00			

Table A.12. Calculated dose rates for the 15x15 UOX assembly

Conversion factor	3.7 years of cooling (Sv/h)	30 years of cooling (Sv/h)
ANSI (1977)	29.35	5.71
ANSI (1991)	23.15	4.47

Table A.13. Calculated dose rates for the 17x17 MOX assembly

Conversion factor	3.7 years of cooling (Sv/h)	30 years of cooling (Sv/h)
ANSI (1977)	57.13	10.06
ANSI (1991)	47.48	7.94

References

[1] Eschbach, R., R. Girieud, B. Feng and R. Hill (2015), "Proposal for a benchmark on dose rate calculations for irradiated assemblies by the WPFC/AFCS Expert Group*", proposed by CEA/Nuclear Energy Division (DEN) and DOE (ANL)*". (internal document)

[2] Viitanen T. (2009), *Implementing a Doppler-preprocessor of Cross section Libraries in Reactor Physics Code Serpent*, M.Sc. Thesis, Helsinki University of Technology.

[3] ANS (1977), *American National Standard for Neutron and Gamma-Ray Flux-to-Dose-Rate Factors*, ANSI/ANS-6.1.1 (1977), American Nuclear Society, United States.

[4] ANS (1991), American National Standard for Neutron and Gamma-Ray Flux-to-Dose-Rate Factors, ANSI/ANS-6.1.1(1991), American Nuclear Society, United States.

[5] Räty, A. and S. Häkkinen (2018), *WPFC/AFCS Expert Group Benchmark on Dose Rate Calculations with Serpent*, VTT Technical Research Centre of Finland, VTT Research Report, No. VTT-R-02506-18.

ENEA contribution

The gamma dose rate calculation is divided into three phases: burn-up and depletion; decay and photon emission; photon transport and gamma dose rate. To this end, five different calculation strategies are simultaneously used to compare the performance of the codes [1]. In particular, five different neutronics codes are used in the first phase: APOLLO2, NEWT, SERPENT, KENO-VI and ORIGEN-ARP. The second and third phases are performed using, respectively, ORIGEN-S/ORIGEN-ARP and MCNPX.

The main results of this part are presented below, distinguishing between the two types of FA. More in detail, Table A.14 to Table A.19 refer to the irradiated UOX PWR assembly while Table A.20 to Table A.25 refer to irradiated MOX PWR assembly. It can be noted that there is a good agreement in each phase between the five calculation strategies.

Results for UOX PWR FA

Calculated HM masses at end of life (EoL) are shown in Table A.14.

Table A.14. Calculated HM masses [g] in UOX assembly at discharge

	APOLLO2	NEWT	SERPENT	KENO-VI	ORIGEN-ARP
U-234	8.14E+01	8.38E+01	8.31E+01	8.26E+01	8.19E+01
U-235	3.69E+03	3.83E+03	3.64E+03	3.93E+03	3.66E+03
U-236	1.80E+03	1.81E+03	1.81E+03	1.80E+03	1.83E+03
U-237	5.49E+00	5.77E+00	5.81E+00	5.90E+00	6.04E+00
U-238	4.43E+05	4.42E+05	4.43E+05	4.42E+05	4.43E+05
Np-236	5.24E-04	1.62E-04	6.88E-04	1.76E-04	7.91E-05
Np-236m	-	1.06E-05	2.86E-09	1.11E-05	4.05E-06
Np-237	1.75E+02	1.85E+02	1.84E+02	1.90E+02	1.88E+02
Np-238	7.83E-01	7.80E-01	7.78E-01	8.00E-01	8.42E-01
Np-239	5.92E+01	6.01E+01	5.94E+01	6.11E+01	5.90E+01
Pu-236	4.50E-04	6.96E-04	1.12E-05	7.31E-04	2.67E-04
Pu-237	1.29E-04	1.79E-04	1.56E-04	1.93E-04	1.55E-04
Pu-238	5.80E+01	5.73E+01	5.49E+01	5.97E+01	6.00E+01
Pu-239	2.51E+03	2.65E+03	2.45E+03	2.80E+03	2.52E+03
Pu-240	1.10E+03	1.11E+03	1.11E+03	1.13E+03	1.10E+03
Pu-241	6.32E+02	6.44E+02	5.98E+02	6.71E+02	6.06E+02
Pu-242	2.49E+02	2.35E+02	2.33E+02	2.33E+02	2.41E+02
Pu-243	8.77E-02	9.74E-02	9.29E-02	9.78E-02	9.88E-02
Pu-244	8.99E-03	1.52E-02	1.40E-02	1.54E-02	9.72E-03
Am-241	1.17E+01	1.31E+01	1.20E+01	1.37E+01	1.22E+01
Am-242	5.06E-02	4.90E-02	4.73E-02	5.00E-02	4.36E-02
Am-242m	2.36E-01	1.82E-01	1.24E-01	1.96E-01	2.44E-01
Am-243	4.48E+01	4.94E+01	4.62E+01	4.97E+01	5.08E+01
Am-244	5.84E-02	4.05E-03	3.69E-03	4.12E-03	6.18E-02
Cm-242	5.60E+00	5.26E+00	5.03E+00	5.36E+00	4.63E+00
Cm-243	1.15E-01	1.08E-01	1.00E-01	1.12E-01	1.16E-01
Cm-244	1.36E+01	1.49E+01	1.32E+01	1.53E+01	1.44E+01
Cm-245	6.94E-01	8.38E-01	7.26E-01	8.99E-01	5.37E-01
Cm-246	6.05E-02	7.03E-02	6.39E-02	7.19E-02	4.70E-02
Cm-247	6.52E-04	7.50E-04	6.49E-04	7.94E-04	4.45E-04
Cm-248	3.41E-05	4.14E-05	3.47E-05	4.44E-05	2.40E-05
Bk-249	3.42E-07	4.20E-07	3.25E-07	4.74E-07	2.44E-07
Cf-249	3.09E-08	3.82E-08	2.78E-08	4.37E-08	2.17E-08
Cf-250	1.84E-07	1.73E-07	1.46E-07	1.86E-07	5.54E-08
Cf-251	4.03E-08	6.67E-08	5.26E-08	7.39E-08	2.96E-08
Cf-252	2.07E-08	3.33E-08	2.73E-08	3.53E-08	1.53E-08
Total	4.53E+05	4.53E+05	4.53E+05	4.53E+05	4.53E+05

The calculated FP masses at end of life (EoL) are listed in Table A.15.

Table A.15. Calculated FP masses [g] in UOX assembly at discharge

	APOLLO2	NEWT	SERPENT	KENO-VI	ORIGEN-ARP
Kr-83	1.87E+01	1.92E+01	1.94E+01	1.92E+01	1.92E+01
Rh-103	2.05E+02	2.05E+02	2.03E+02	2.05E+02	2.04E+02
Rh-105	8.45E-01	7.66E-01	7.91E-01	7.67E-01	7.55E-01
Ag-109	3.67E+01	3.76E+01	3.70E+01	3.76E+01	3.67E+01
I-135	3.29E-01	3.36E-01	3.38E-01	3.36E-01	3.38E-01
Xe-131	1.92E+02	2.00E+02	2.01E+02	2.00E+02	1.96E+02
Xe-135	8.68E-02	9.22E-02	8.47E-02	9.26E-02	8.83E-02
Cs-133	5.15E+02	5.24E+02	5.22E+02	5.24E+02	5.28E+02
Cs-134	6.13E+01	6.15E+01	6.08E+01	6.15E+01	5.57E+01
Cs-135	1.26E+02	1.31E+02	1.23E+02	1.30E+02	1.33E+02
Cs-137	5.67E+02	5.72E+02	5.74E+02	5.72E+02	5.78E+02
Ba-137m	-	8.82E-05	8.82E-05	8.82E-05	8.91E-05
Ba-140	-	1.42E+01	1.43E+01	1.42E+01	1.43E+01
La-140	1.93E+00	1.92E+00	1.94E+00	1.92E+00	1.94E+00
Nd-143	3.58E+02	3.63E+02	3.58E+02	3.63E+02	3.62E+02
Nd-145	3.15E+02	3.10E+02	3.11E+02	3.10E+02	3.15E+02
Nd-148	1.77E+02	1.75E+02	1.74E+02	1.75E+02	1.73E+02
Pm-147	9.53E+01	9.22E+01	9.38E+01	9.42E+01	8.95E+01
Pm-148	7.75E-01	8.02E-01	7.92E-01	7.80E-01	6.53E-01
Pm-149	8.63E-01	8.51E-01	8.66E-01	8.43E-01	9.67E-01
Sm-147	2.39E+01	2.34E+01	2.37E+01	2.37E+01	2.31E+01
Sm-149	9.70E-01	1.08E+00	9.78E-01	1.07E+00	1.13E+00
Sm-150	1.39E+02	1.38E+02	1.39E+02	1.39E+02	1.45E+02
Sm-151	5.29E+00	5.61E+00	5.09E+00	5.45E+00	7.05E+00
Sm-152	5.13E+01	5.13E+01	5.05E+01	5.02E+01	6.11E+01
Eu-153	5.43E+01	5.49E+01	5.37E+01	5.42E+01	5.38E+01
Eu-154	1.11E+01	1.14E+01	1.07E+01	1.14E+01	1.06E+01
Eu-155	3.71E+00	3.75E+00	3.84E+00	3.74E+00	2.56E+00
Eu-156	2.61E+00	2.65E+00	2.69E+00	2.64E+00	2.59E+00
Gd-155	1.81E-02	1.88E-02	1.74E-02	1.88E-02	1.32E-02
Total	2.96E+03	3.00E+03	2.99E+03	3.00E+03	3.01E+03

The calculated masses of HM and FP after 30 years of cooling are shown in Table A.16 and Table A.17, respectively.

Table A.16. Calculated HM masses [g] in UOX assembly after 30 years

	APOLLO2 ORIGEN-S	NEWT ORIGEN-S	SERPENT ORIGEN-S	KENO-VI ORIGEN-S	ORIGEN-ARP
U-234	9.48E+01	9.69E+01	9.57E+01	9.57E+01	9.55E+01
U-235	3.70E+03	3.84E+03	3.65E+03	3.83E+03	3.66E+03
U-236	1.80E+03	1.81E+03	1.82E+03	1.81E+03	1.83E+03
U-237	4.60E-06	4.69E-06	4.35E-06	4.71E-06	4.31E-06
U-238	4.43E+05	4.42E+05	4.43E+05	4.42E+05	4.43E+05
Np-237	1.94E+02	2.06E+02	2.03E+02	2.06E+02	2.08E+02
Pu-238	5.08E+01	5.00E+01	4.79E+01	4.79E+01	5.17E+01
Pu-239	2.57E+03	2.71E+03	2.51E+03	2.73E+03	2.58E+03
Pu-240	1.10E+03	1.12E+03	1.11E+03	1.12E+03	1.11E+03
Pu-241	1.48E+02	1.50E+02	1.40E+02	1.51E+02	1.42E+02
Pu-242	2.49E+02	2.35E+02	2.33E+02	2.34E+02	2.41E+02
Am-241	4.82E+02	4.92E+02	4.57E+02	4.95E+02	4.62E+02
Am-242	2.63E-06	2.03E-06	1.34E-06	2.04E-06	2.72E-06
Am-242m	2.04E-01	1.57E-01	1.04E-01	1.58E-01	2.11E-01
Am-243	4.48E+01	4.93E+01	4.62E+01	4.85E+01	5.07E+01
Am-244	0.00E+00	0.00E+00	0.00E+00	0.00E+00	0.00E+00
Cm-244	4.32E+00	4.71E+00	4.18E+00	2.21E+00	4.59E+00
Cm-245	6.92E-01	8.36E-01	7.24E-01	3.99E-01	5.36E-01
Cf-251	3.94E-08	6.52E-08	5.18E-08	6.20E-08	2.89E-08
Cf-252	7.98E-12	1.28E-11	1.05E-11	1.20E-11	5.87E-12
Total	4.53E+05	4.53E+05	4.53E+05	4.53E+05	4.53E+05

Table A.17. Calculated FP masses [g] in UOX assembly after 30 years

	APOLLO2 ORIGEN-S	NEWT ORIGEN-S	SERPENT ORIGEN-S	KENO-VI ORIGEN-S	ORIGEN-ARP
Sr-90	1.19E+02	1.21E+02	1.22E+02	1.21E+02	1.20E+02
Y-90	3.01E-02	3.07E-02	3.10E-02	3.08E-02	3.12E-02
Cs-137	2.84E+02	2.86E+02	2.87E+02	2.86E+02	2.89E+02
Ba-137m	4.34E-05	4.37E-05	4.39E-05	4.37E-05	4.41E-05
Sm-154	1.79E+01	1.79E+01	1.77E+01	1.79E+01	1.72E+01
Eu-153	5.43E+01	5.49E+01	5.37E+01	5.42E+01	5.45E+01
Eu-154	9.89E-01	1.02E+00	9.53E-01	1.01E+00	9.38E-01
Eu-155	4.67E-02	4.72E-02	4.83E-02	4.70E-02	3.01E-02
Total	4.76E+02	4.81E+02	4.82E+02	4.81E+02	4.82E+02

The calculated 30-year gamma release rates and contribution from each energy group for each are listed in Table A.18.

Table A.18. Calculated 30-year gamma release rates and contribution from each energy group for UOX assembly

E_{low} [MeV]	E_{high} [MeV]	APOLLO2 Origen-S		NEWT Origen-S		Serpent Origen-S		KENO-VI Origen-S		Origen-ARP	
		Gamma release rate [photons/s]	Fraction of total gammas	Gamma release rate [photons/s]	Fraction of total gammas	Gamma release rate [photons/s]	Fraction of total gammas	Gamma release rate [photons/s]	Fraction of total gammas	Gamma release rate [photons/s]	Fraction of total gammas
0	0.02	5.19E+14	2.66E-01	5.29E+14	2.68E-01	5.31E+14	2.68E-01	5.28E+14	2.67E-01	5.38E+14	2.69E-01
0.02	0.03	1.01E+14	5.19E-02	1.03E+14	5.22E-02	1.04E+14	5.24E-02	1.03E+14	5.22E-02	1.05E+14	5.26E-02
0.03	0.05	1.34E+14	6.86E-02	1.36E+14	6.87E-02	1.36E+14	6.88E-02	1.36E+14	6.87E-02	1.38E+14	6.88E-02
0.05	0.07	1.04E+14	5.35E-02	1.06E+14	5.39E-02	1.05E+14	5.32E-02	1.07E+14	5.39E-02	1.07E+14	5.33E-02
0.07	0.1	5.52E+13	2.84E-02	5.64E+13	2.85E-02	5.69E+13	2.87E-02	5.64E+13	2.86E-02	5.74E+13	2.87E-02
0.1	0.15	4.81E+13	2.47E-02	4.92E+13	2.49E-02	4.93E+13	2.49E-02	4.91E+13	2.49E-02	4.96E+13	2.48E-02
0.15	0.3	4.78E+13	2.46E-02	4.89E+13	2.47E-02	4.92E+13	2.48E-02	4.89E+13	2.48E-02	4.96E+13	2.48E-02
0.3	0.45	2.00E+13	1.03E-02	2.05E+13	1.04E-02	2.06E+13	1.04E-02	2.05E+13	1.04E-02	2.08E+13	1.04E-02
0.45	0.7	9.03E+14	4.64E-01	9.11E+14	4.61E-01	9.14E+14	4.61E-01	9.11E+14	4.61E-01	9.19E+14	4.60E-01
0.7	1	9.15E+12	4.70E-03	9.38E+12	4.75E-03	9.08E+12	4.58E-03	9.36E+12	4.74E-03	9.02E+12	4.51E-03
1	1.5	6.14E+12	3.15E-03	6.30E+12	3.19E-03	6.00E+12	3.03E-03	6.28E+12	3.18E-03	5.94E+12	2.97E-03
1.5	2	3.07E+11	1.58E-04	3.15E+11	1.59E-04	3.03E+11	1.53E-04	3.14E+11	1.59E-04	3.01E+11	1.51E-04
2	2.5	2.06E+09	1.06E-06	2.11E+09	1.07E-06	2.12E+09	1.07E-06	2.10E+09	1.06E-06	2.13E+09	1.07E-06
2.5	3	1.05E+08	5.38E-08	1.60E+08	8.11E-08	8.16E+06	4.12E-09	1.57E+08	7.97E-08	8.44E+07	4.22E-08
3	4	5.30E+06	2.72E-09	5.76E+06	2.92E-09	5.12E+06	2.58E-09	2.83E+06	1.44E-09	5.59E+06	2.80E-09
4	6	2.27E+06	1.16E-09	2.46E+06	1.25E-09	2.19E+06	1.11E-09	1.21E+06	6.12E-10	2.39E+06	1.20E-09
6	8	2.61E+05	1.34E-10	2.84E+05	1.43E-10	2.52E+05	1.27E-10	1.39E+05	7.03E-11	2.75E+05	1.38E-10
8	11	3.00E+04	1.54E-11	3.26E+04	1.65E-11	2.90E+04	1.46E-11	1.60E+04	8.08E-12	3.17E+04	1.58E-11
Total		1.95E+15	1.00E+00	1.98E+15	1.00E+00	1.98E+15	1.00E+00	1.97E+15	1.00E+00	2.00E+15	1.00E+00

The most relevant contributors in terms of photon emission are, in descending order of importance: ^{137M}Ba, ^{90}Y, ^{137}Cs, ^{90}Sr, ^{241}Am, ^{154}Eu, ^{208}Tl, ^{244}Cm and ^{240}Pu. In this regard, it is worth noting that the isotope ^{208}Tl, which is the most important contributor of group 14, was not included in the benchmark specifications. However, it should be noted that these isotopes are not necessarily the most important also in terms of gamma dose rate. The gamma dose rate also depends on two non-proportional contributions, such as the photon attenuation due mostly to the fuel matrix and the flux-to-dose conversion, both strongly variable with energy. Combining these contributions, the most relevant isotopes in terms of gamma dose rate are those that emit above 0.4 MeV.

The results of the gamma dose rate at 1 m from the midpoint after 30 years of decay are shown in Table A.19. The following can be noted:

- the five calculation strategies show a very good agreement in each phase, i.e. nuclide inventory, gamma source and gamma dose rate;
- the gamma dose rates calculated with the ANSI/ANS-6.1.1 (1991) conversion factor are about 20% lower than those calculated with the 1977 version;
- bremsstrahlung of the secondary electrons is slightly relevant;
- ICRP60 standard provides a value, calculated only according to strategy 5, which is 5.6% and 26% lower than those calculated with the ANSI/ANS-6.1.1 (1991) and ANSI/ANS-6.1.1 (1977) conversion factors, respectively.

Compared to the dose rates at 1 m from the centre of FA in perpendicular direction estimated by [2] for two PWR UOx FAs irradiated up to 30 and 35 GWd/MTIHM after a cooling time of 30 years, i.e. 13.0 and 15.2 Sv/h respectively, these values are between two and three times lower.

With regard to the values obtained with the ANSI/ANS-6.1.1 (1991) conversion factor according to strategy 5, 98.8% of the total gamma dose rate is due to three energy groups, namely 9 (0.45-0.70 MeV), 10 (0.70-1.00 MeV), and 11 (1.00-1.50 MeV) and 93.9% to the only group 9 i.e. to the photon contribution of ^{137M}Ba. ^{90}Y and ^{154}Eu contribute almost 5% to the total dose rate, a small but not negligible contribution. It is therefore confirmed that, in this study, the most important energy range for the dose rate calculation is between 0.45 and 1.5 MeV.

Table A.19. Calculated 30-year gamma dose rates [Sv/h] at 1 m from the midpoint for UOX FA

Conversion factors	APOLLO2 ORIGEN-S MCNPX	NEWT ORIGEN-S MCNPX	Serpent ORIGEN-S MCNPX	KENO-VI ORIGEN-S MCNPX	ORIGEN-ARP MCNPX	Average
ANSI/ANS-6.1.1 (1977)	5.25	5.34	5.21	5.22	5.20	5.24
ANSI/ANS-6.1.1 (1991)	4.13	4.21	4.11	4.11	4.09	4.13
ICRP60	-	-	-	-	3.86	3.86

Results for MOX PWR FA

Calculated HM masses at EoL are shown in Table A.20.

Table A.20. Calculated HM masses [g] in MOX assembly at discharge

	APOLLO2	NEWT	SERPENT	KENO-VI	ORIGEN-ARP
U-234	2.19E+01	2.23E+01	2.21E+01	2.23E+01	2.11E+01
U-235	4.33E+02	4.29E+02	4.25E+02	4.31E+02	4.38E+02
U-236	1.31E+02	1.32E+02	1.33E+02	1.32E+02	1.31E+02
U-237	1.13E+00	1.19E+00	1.21E+00	1.19E+00	1.15E+00
U-238	3.97E+05	3.96E+05	3.96E+05	3.96E+05	3.96E+05
Np-236	9.77E-04	2.93E-04	1.38E-03	2.95E-04	3.66E-04
Np-236M	-	5.37E-06	1.69E-09	5.38E-06	1.95E-06
Np-237	9.25E+01	1.00E+02	1.02E+02	1.00E+02	9.44E+01
Np-238	2.10E-01	2.18E-01	2.19E-01	2.18E-01	2.11E-01
Np-239	3.82E+01	3.81E+01	3.93E+01	3.82E+01	3.88E+01
Pu-236	4.76E-04	1.54E-03	8.27E-04	1.55E-03	1.10E-03
Pu-237	3.24E-03	4.19E-03	4.24E-03	4.21E-03	3.72E-03
Pu-238	1.03E+03	1.02E+03	1.02E+03	1.02E+03	1.00E+03
Pu-239	9.20E+03	9.30E+03	9.43E+03	9.35E+03	9.77E+03
Pu-240	8.18E+03	8.21E+03	8.23E+03	8.17E+03	8.10E+03
Pu-241	4.69E+03	4.68E+03	4.73E+03	4.71E+03	4.83E+03
Pu-242	3.84E+03	3.64E+03	3.59E+03	3.63E+03	3.65E+03
Pu-243	4.20E-01	4.53E-01	4.63E-01	4.56E-01	4.67E-01
Pu-244	1.14E-01	4.11E-01	4.24E-01	4.14E-01	1.28E-01
Am-241	4.14E+02	4.68E+02	4.75E+02	4.71E+02	4.71E+02
Am-242	5.97E-01	5.97E-01	6.12E-01	5.99E-01	5.60E-01
Am-242M	1.32E+01	1.06E+01	8.04E+00	1.08E+01	1.57E+01
Am-243	9.06E+02	1.00E+03	1.03E+03	1.01E+03	1.03E+03

Table A.20. Calculated HM masses [g] in MOX assembly at discharge (Continued)

	APOLLO2	NEWT	SERPENT	KENO-VI	ORIGEN-ARP
Am-244	6.11E-01	4.16E-02	4.24E-02	4.19E-02	6.97E-01
Cm-242	1.14E+02	1.13E+02	1.16E+02	1.13E+02	1.05E+02
Cm-243	6.06E+00	5.84E+00	6.13E+00	5.87E+00	6.32E+00
Cm-244	6.23E+02	6.81E+02	6.95E+02	6.85E+02	7.32E+02
Cm-245	8.01E+01	9.82E+01	1.02E+02	9.94E+01	9.47E+01
Cm-246	7.42E+00	9.28E+00	9.47E+00	9.30E+00	8.35E+00
Cm-247	1.89E-01	2.35E-01	2.33E-01	2.36E-01	1.99E-01
Cm-248	1.48E-02	2.12E-02	2.04E-02	2.12E-02	1.41E-02
Bk-249	3.38E-04	4.59E-04	4.73E-04	4.61E-04	3.08E-04
Cf-249	9.38E-05	1.30E-04	1.31E-04	1.31E-04	8.86E-05
Cf-250	1.56E-04	1.39E-04	1.44E-04	1.39E-04	7.51E-05
Cf-251	3.04E-05	7.78E-05	7.83E-05	7.80E-05	6.37E-05
Cf-252	1.15E-05	3.03E-05	2.92E-05	3.00E-05	2.26E-05
Total	4.26E+05	4.26E+05	4.26E+05	4.26E+05	4.26E+05

Calculated FP masses at EoL are listed in Table A.21.

Table A.21. Calculated FP masses [g] in MOX assembly at discharge

	APOLLO2	NEWT	Serpent	KENO-VI	ORIGEN-ARP
Kr-83	2.13E+01	2.28E+01	2.33E+01	2.29E+01	2.24E+01
Rh-103	5.49E+02	5.56E+02	5.65E+02	5.56E+02	5.30E+02
Ag-109	1.43E+02	1.43E+02	1.44E+02	1.43E+02	1.33E+02
I-135	2.76E-01	2.78E-01	2.81E-01	2.78E-01	2.70E-01
Xe-131	3.38E+02	3.59E+02	3.61E+02	3.58E+02	3.22E+02
Xe-135	2.15E-01	2.18E-01	2.21E-01	2.20E-01	2.26E-01
Cs-133	8.56E+02	8.69E+02	8.71E+02	8.69E+02	8.54E+02
Cs-134	1.22E+02	1.21E+02	1.24E+02	1.21E+02	1.06E+02
Cs-135	6.40E+02	6.59E+02	6.64E+02	6.62E+02	6.78E+02
Cs-137	9.75E+02	9.92E+02	1.00E+03	9.92E+02	9.96E+02
Ba-137m	-	1.53E-04	1.53E-04	1.53E-04	1.53E-04
Ba-140	-	1.12E+01	1.13E+01	1.12E+01	1.14E+01
La-140	1.54E+00	1.51E+00	1.52E+00	1.51E+00	1.54E+00
Nd-143	6.07E+02	6.10E+02	6.16E+02	6.10E+02	6.08E+02
Nd-145	4.60E+02	4.57E+02	4.60E+02	4.57E+02	4.51E+02
Nd-148	6.54E-01	3.01E+02	3.03E+02	3.01E+02	2.94E+02
Pm-147	1.16E+02	1.12E+02	1.13E+02	1.12E+02	1.07E+02
Pm-148	6.54E-01	6.50E-01	6.55E-01	6.50E-01	5.79E-01
Pm-149	6.90E-01	6.60E-01	6.73E-01	6.60E-01	6.91E-01
Sm-147	5.82E+01	5.79E+01	5.76E+01	5.79E+01	5.62E+01

Table A.21. Calculated FP masses [g] in MOX assembly at discharge (Continued)

	APOLLO2	NEWT	Serpent	KENO-VI	ORIGEN-ARP
Sm-149	3.73E+00	3.89E+00	3.96E+00	3.95E+00	4.47E+00
Sm-150	2.50E+02	2.40E+02	2.50E+02	2.40E+02	2.46E+02
Sm-151	2.03E+01	2.08E+01	2.04E+01	2.10E+01	2.69E+01
Sm-152	9.29E+01	9.15E+01	9.10E+01	9.14E+01	9.46E+01
Eu-153	1.25E+02	1.30E+02	1.27E+02	1.30E+02	1.26E+02
Eu-154	4.52E+01	4.65E+01	4.65E+01	4.66E+01	4.61E+01
Eu-155	1.05E+01	1.09E+01	1.14E+01	1.09E+01	7.34E+00
Eu-156	3.17E+00	3.23E+00	3.24E+00	3.22E+00	3.10E+00
Gd-155	2.79E-01	2.82E-01	2.99E-01	2.87E-01	2.44E-01
Total	5.44E+03	5.82E+03	5.87E+03	5.82E+03	5.73E+03

The calculated masses of HM and FM after 30 years of cooling are shown in Table A.22 and Table A.23, respectively.

Table A.22. Calculated HM masses [g] in MOX assembly after 30 years

	APOLLO2 ORIGEN-S	NEWT ORIGEN-S	SERPENT ORIGEN-S	KENO-VI ORIGEN-S	ORIGEN-ARP
U-234	2.59E+02	2.57E+02	2.57E+02	2.52E+02	2.51E+02
U-235	4.41E+02	4.37E+02	4.33E+02	4.46E+02	4.46E+02
U-236	1.57E+02	1.58E+02	1.59E+02	2.00E+02	1.57E+02
U-237	3.41E-05	3.41E-05	3.45E-05	3.51E-05	3.43E-05
U-238	3.97E+05	3.96E+05	3.96E+05	3.96E+05	3.96E+05
Np-237	2.16E+02	2.26E+02	2.29E+02	1.29E+02	2.23E+02
Pu-238	9.03E+02	8.94E+02	8.97E+02	8.76E+02	8.76E+02
Pu-239	9.24E+03	9.34E+03	9.47E+03	9.80E+03	9.81E+03
Pu-240	8.57E+03	8.64E+03	8.67E+03	8.56E+03	8.56E+03
Pu-241	1.09E+03	1.09E+03	1.10E+03	1.13E+03	1.13E+03
Pu-242	3.84E+03	3.64E+03	3.59E+03	3.65E+03	3.65E+03
Am-241	3.89E+03	3.93E+03	3.98E+03	4.04E+03	4.03E+03
Am-242	1.47E-04	1.18E-04	8.95E-05	1.75E-04	1.75E-04
Am-242m	1.14E+01	9.15E+00	6.94E+00	1.36E+01	1.36E+01
Am-243	9.04E+02	9.98E+02	1.03E+03	5.78E-01	1.03E+03
Am-244	0.00E+00	0.00E+00	0.00E+00	0.00E+00	0.00E+00
Cm-244	1.98E+02	2.16E+02	2.20E+02	2.32E+02	2.32E+02
Cm-245	7.99E+01	9.80E+01	1.02E+02	9.45E+01	9.45E+01
Cf-251	2.97E-05	7.60E-05	7.66E-05	6.22E-05	6.22E-05
Cf-252	4.43E-09	1.17E-08	1.12E-08	8.71E-09	8.71E-09
Total	4.27E+05	4.26E+05	4.26E+05	4.25E+05	4.26E+05

Table A.23. Calculated FP masses [g] in MOX assembly after 30 years

	APOLLO2 ORIGEN-S	NEWT ORIGEN-S	SERPENT ORIGEN-S	KENO-VI ORIGEN-S	ORIGEN-ARP
Sr-90	9.74E+01	1.01E+02	1.02E+02	1.01E+02	9.78E+01
Y-90	2.47E-02	2.56E-02	2.59E-02	2.56E-02	2.54E-02
Cs-137	4.88E+02	4.97E+02	5.01E+02	4.97E+02	4.98E+02
Ba-137	4.87E+02	5.43E+02	5.47E+02	5.43E+02	5.46E+02
Ba-137m	7.46E-05	7.59E-05	7.66E-05	7.59E-05	7.60E-05
Sm-154	5.29E+01	5.25E+01	5.29E+01	5.25E+01	5.17E+01
Eu-153	1.25E+02	1.30E+02	1.27E+02	1.30E+02	1.27E+02
Eu-154	4.03E+00	4.14E+00	4.14E+00	4.16E+00	4.09E+00
Eu-155	1.32E-01	1.37E-01	1.43E-01	1.37E-01	8.64E-02
Total	1.25E+03	1.33E+03	1.34E+03	1.33E+03	1.32E+03

Calculated 30-year gamma release rates and contributions from each energy group are listed in Table A.24.

Table A.24. Calculated 30-year gamma release rates and contributions from each energy group for MOX FA

E_{low} [MeV]	E_{high} [MeV]	APOLLO2 Origen-S		NEWT Origen-S		Serpent Origen-S		KENO-VI Origen-S		Origen-ARP	
		Gamma release rate [photons/s]	Fraction of total gammas	Gamma release rate [photons/s]	Fraction of total gammas	Gamma release rate [photons/s]	Fraction of total gammas	Gamma release rate [photons/s]	Fraction of total gammas	Gamma release rate [photons/s]	Fraction of total gammas
0	0.02	8.83E+14	2.73E-01	9.07E+14	2.74E-01	9.16E+14	2.74E-01	1.20E+15	3.19E-01	9.15E+14	2.75E-01
0.02	0.03	1.30E+14	4.01E-02	1.33E+14	4.03E-02	1.35E+14	4.03E-02	1.50E+14	3.98E-02	1.33E+14	4.01E-02
0.03	0.05	1.80E+14	5.56E-02	1.84E+14	5.57E-02	1.86E+14	5.57E-02	1.84E+14	4.90E-02	1.84E+14	5.53E-02
0.05	0.07	2.63E+14	8.13E-02	2.68E+14	8.09E-02	2.71E+14	8.10E-02	2.73E+14	7.25E-02	2.72E+14	8.19E-02
0.07	0.1	5.73E+13	1.77E-02	5.95E+13	1.80E-02	6.03E+13	1.80E-02	1.39E+14	3.69E-02	5.89E+13	1.77E-02
0.1	0.15	6.29E+13	1.94E-02	6.50E+13	1.97E-02	6.56E+13	1.97E-02	8.93E+13	2.37E-02	6.46E+13	1.94E-02
0.15	0.3	4.86E+13	1.50E-02	5.04E+13	1.52E-02	5.10E+13	1.53E-02	8.45E+13	2.24E-02	5.00E+13	1.50E-02
0.3	0.45	1.75E+13	5.40E-03	1.81E+13	5.48E-03	1.83E+13	5.49E-03	1.81E+13	4.80E-02	1.79E+13	5.38E-03
0.45	0.7	1.55E+15	4.78E-01	1.58E+15	4.76E-01	1.59E+15	4.76E-01	1.58E+15	4.19E-01	1.58E+15	4.76E-01
0.7	1	2.48E+13	7.68E-03	2.56E+13	7.73E-03	2.56E+13	7.66E-03	2.64E+13	7.02E-03	2.53E+13	7.60E-03
1	1.5	2.09E+13	6.45E-03	2.15E+13	6.49E-03	2.15E+13	6.43E-03	2.16E+13	5.73E-03	2.13E+13	6.39E-03
1.5	2	8.95E+11	2.77E-04	9.21E+11	2.78E-04	9.22E+11	2.76E-04	9.93E+11	2.64E-04	9.12E+11	2.74E-04
2	2.5	2.14E+09	6.61E-07	2.25E+09	6.79E-07	2.28E+09	6.81E-07	2.28E+09	6.07E-07	2.25E+09	6.78E-07
2.5	3	3.69E+08	1.14E-07	6.28E+08	1.90E-07	4.77E+08	1.43E-07	1.44E+12	3.84E-04	5.51E+08	1.66E-07
3	4	2.37E+08	7.34E-08	2.60E+08	7.86E-08	2.65E+08	7.93E-08	4.07E+08	1.08E-07	2.78E+08	8.36E-08
4	6	1.02E+08	3.15E-08	1.12E+08	3.37E-08	1.14E+08	3.40E-08	1.19E+08	3.17E-08	1.19E+08	3.59E-08
6	8	1.17E+07	3.62E-09	1.28E+07	3.88E-09	1.31E+07	3.92E-09	1.37E+07	3.65E-09	1.37E+07	4.13E-09
8	11	1.35E+06	4.17E-10	1.48E+06	4.46E-10	1.51E+06	4.51E-10	1.58E+06	4.20E-10	1.58E+06	4.75E-10
Total		3.24E+15	1.00E+00	3.31E+15	1.00E+00	3.34E+15	1.00E+00	3.76E+15	1.00E+00	3.32E+15	1.00E+00

The results of the gamma dose rate at 1 m from the midpoint after 30 years of decay are shown in Table A.25**.** For both ANSI conversion factors, a very good agreement can be observed between the values obtained with the five calculation strategies. The values for the ANSI/ANS-6.1.1(1991) conversion factor are about 21% lower than those for the 1977 version, regardless of the strategy used.

Table A.25. Gamma dose rate at 1 m after 30 years of decay

Conversion factors	APOLLO2 ORIGEN-S MCNPX	NEWT ORIGEN-S MCNPX	Serpent ORIGEN-S MCNPX	KENO-VI ORIGEN-S MCNPX	ORIGEN-ARP MCNPX	Average
ANSI/ANS-6.1.1 (1977)	11.40	11.62	11.72	11.75	11.65	11.63
ANSI/ANS-6.1.1 (1991)	9.01	9.18	9.26	9.30	9.21	9.19

References

[1] Pergreffi, R., F. Rocchi and A. Guglielmelli (2020), *WPFC/AFCS Expert Group Benchmark on Dose Rate Calculations*, ENEA report, SICNUC-P000-026, Rev.1, 2020, https://hdl.handle.net/20.500.12079/55061.

[2] Lloyd, W.R., M.K. Sheaffer and W.G. Sutcliffe (1994), *Dose Rate Estimates from irradiated Light-Water-Reactor Fuel Assembly in Air*, Lawrence Livermore National Laboratory, Livermore, CA, United States, https://doi.org/10.2172/10137382.

ORANO TN contribution

The objectives of the benchmark are to verify updated dose rate calculation procedures (new modelling approaches, new nuclear data, new versions of the codes) and to share the benchmark results at the international level [1].

The verification part is divided into three calculation steps:

- Depletion: given the FA description and power conditions, simulate the depletion (burn-up) of a FA to obtain the discharge composition.
- Decay: simulate 30 years of decay for this discharge composition and calculate the isotopic photon release rates that are discretised into multiple gamma energy groups.
- Radiation: apply the multi-group gamma source uniformly (axially and radially) to a heterogeneous 3D transport model of the FA and tally the gamma flux at 1 m away from the midpoint. Calculate the corresponding dose rate using flux-to-dose rate conversion factors.

Calculation cases

This benchmark involves two reference cases:

- a 15x15 PWR spent FA with UOX fuel at 33 GWd/MTIHM burn-up;
- a 17x17 PWR spent FA with MOX fuel at 60 GWd/MTIHM burn-up.

Two different cooling times were chosen: 30 years and 3.7 years to differentiate the short-lived and long-lived fission product contributions to the dose rate.

The dose rate from a spent FA decreases with time after discharge due to the radioactive decay of the gamma-emitting isotopes. Calculated neutron, gamma, and total dose rates from standard PWR spent FAs at 1 m away through the air show that the gamma dose rate is 3-4 orders of magnitude higher than the neutron dose rate. So, for this study, the total dose rate is approximated by just the gamma dose rate.

Model description

The gamma emissions of the active length of the FAs are calculated by the ORIGEN-ARP code of the SCALE6 code package [2].

The dose rate calculations are performed with TRIPOLI-4.7 code [3], which solves the linear Boltzmann equation for neutrons and photons, with the Monte Carlo method, in any 3D geometry. The code uses the CEA V5.0 nuclear data library, mainly based on the JEFF-3.1.1 evaluation and continuous energy cross-sections. The dose rates are provided with a standard deviation of some percent.

The responses function is the personal dose equivalent called H*(10). Conversion factors of flux-to-dose are issued from:

- ICRP74 evaluation, recommendation ICRP 60 [4];
- ANSI/ANS 1991 evaluation [5];
- ANSI/ANS 1977 evaluation [6].

Figure A.10 presents the models used in the case of the 15x15 PWR UOX FA.

Figure A.10. Models for 15x15 PWR UOX FA

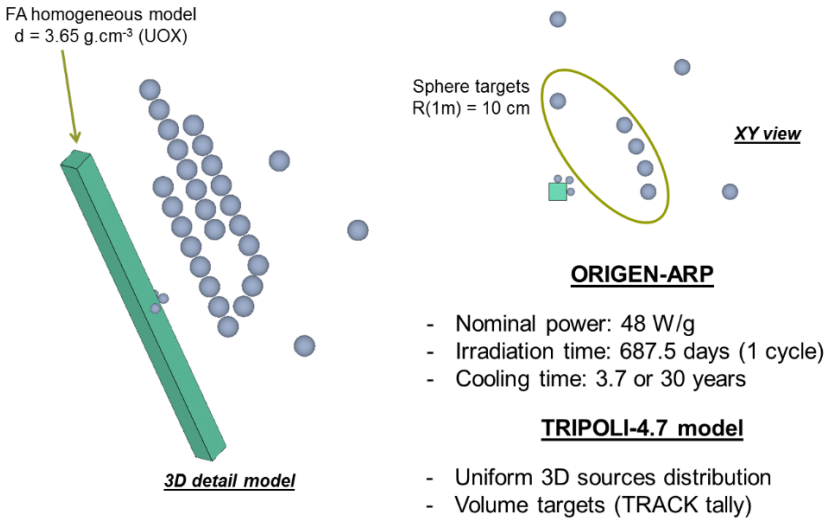

Source: Leger, V. and A. Dalesme, 2020.

The chemical compositions of the used materials in the radiation model (TRIPOLI4.7) are given in Table A.26.

Table A.26. Chemical compositions for the FA

Materials	Density (g/cm³)	Chemical composition (% in weight)	
FA	3.65	Zr U Pu ^{16}O	15.99 66.74 7.35 9.92
Air	1.29×10^{-3}	^{14}N ^{16}O	80 20

Results

The dose rates calculated with the calculation sequence ORIGEN-ARP/TRIPOLI4.7 are presented in Table A.27. Two gamma energy group structures have been considered.

Table A.27. Calculated dose rates with ORIGEN-ARP/TRIPOLI4.7

FA Type (burn-up – cooling time)	Conversion factors	Average EDR*[Sv/h] – CEAV5 library	
		62 γ-energy groups	18 γ-energy groups
UOX (33 GWd/MTIHM – 3.7 years)	ANSI/ANS 1977	35.18	33.88
	ANSI/ANS 1991	28.28	27.17
	IRCP60	32.36	31.06
MOX (60 GWd/MTIHM – 3.7 years)	ANSI/ANS 1977	69.10	67.18
	ANSI/ANS 1991	55.66	54.05
	IRCP60	63.64	61.76
UOX (33 GWd/MTIHM – 30 years)	ANSI/ANS 1977	6.64	5.80
	ANSI/ANS 1991	5.30	4.57
	IRCP60	6.12	5.26
MOX (60 GWd/MTIHM – 30 years)	ANSI/ANS 1977	11.70	10.23
	ANSI/ANS 1991	9.36	8.09
	IRCP60	10.73	9.28

*Average dose rate at 1 m around the FA mid-height.

The results show that, in the case of FAs:

- with small cooling time, the use of a reduced gamma energy group structure leads to an average overestimation of up to 4.2% of the dose rates;
- with large cooling time, the use of a reduced gamma energy group structure leads to an average overestimation of up to 16.4% of the dose rates.

Furthermore, the above results show that the conversion factors of flux-to-dose issued from:

- the ANSI/ANS 1977 evaluation lead to an average overestimation of up to 25% of the dose rates generated with the conversion factors of flux-to-dose issued from the ANSI/ANS 1991 evaluation;
- ICRP60 recommendations lead to an average overestimation of up to 15% of the dose rates generated with the conversion factors of flux-to-dose issued from the ANSI/ANS 1991 evaluation.

Sensitivity studies

Detector size effect

Figure A.11 presents the sensitivity study performed regarding a potential effect on the dose rates of the size detectors used for the radiation calculation.

Figure A.11. Sensitivity studies performed

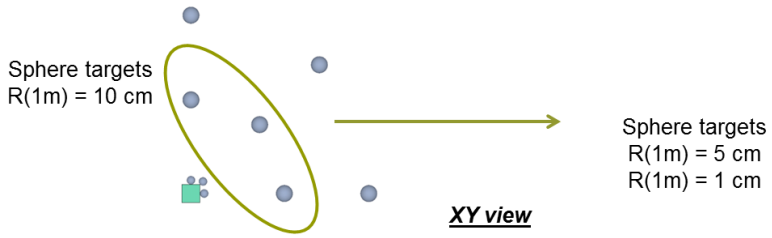

Source: Leger, V. and A. Dalesme, 2020.

The dose rates calculated with the calculation sequence ORIGEN-ARP/TRIPOLI4.7 are presented in Table A.28.

Table A.28. Calculated dose rates versus Sphere radius

FA Type (burn-up – cooling time)	Sphere radius (R)	Average EDR [Sv/h]	Radius effect vs. R = 10 cm
		62 γ-energy groups	
UOX (33 GWd/MTIHM – 3.7 years)	10 cm	32.36	
	5 cm	31.96	- 1.2%
	1 cm	32.27	- 0.3%

The results show that the size detector has no significant effect on the dose rates at 1 m around the FA.

Cross-section library effect

A sensitivity study has been performed to assess a potential effect on the dose rates of the cross-section library used for the radiation calculation.

The dose rates calculated with the calculation sequence ORIGEN-ARP/TRIPOLI4.7 are presented in Table A.29.

Table A.29. Calculated dose rates versus cross-section library

FA Type (burn-up – cooling time)	Cross-section library	Average EDR [Sv/h]	Cross-section effect vs. CEA V5 library
		62 γ-energy groups	
MOX (60 GWd/MTIHM – 3.7 years)	CEA V5	63.64	
	ENDF/B-VI.4	63.24	- 0.1%
	JEF2.2	63.15	- 0.8%

The results show that the cross-section library has no significant effect on the dose rates at 1 m around the FA.

Interpolation model of conversion factors

A sensitivity study has been performed to assess a potential effect on the dose rates of the interpolation model of the conversion factors used for the radiation calculation.

The dose rates calculated with the calculation sequence ORIGEN-ARP/TRIPOLI4.7 are presented in Table A.30.

Table A.30. Calculated dose rates versus interpolation model of conversion factors

UOX (33 GWd/MTIHM – 30 years)	Interpolation model of conversion factors (IRCP60)			
	LIN-LIN	LOG-LIN	LIN-LOG	LOG-LOG
EDR (Sv/h)	6.12	6.06	6.14	6.11
Relative dev. vs LIN-LIN model		-0.86%	0.46%	-0.16%

The results show that the interpolation model of the conversion factors has no significant effect on the dose rates at 1 m around the FA.

References

[1] Eschbach, R. et al. (2017), "Verification of dose rate calculations for PWR spent fuel assemblies", Paper A-081, *GLOBAL2017*, Seoul, Korea, 24-29 September 2017.

[2] Bowman, S.M. and L. C. Leal (2000), *ORIGEN ARP Automatic Rapid Process for Spent Fuel Depletion, Decay, and Source Term Analysis*, Oakland Ridge National Laboratory Report, Tennessee, United States.

[3] CEA (2021), *TRIPOLI-4. Version 7: Manuel de l'utilisateur*, Rapport DM2S SERMA/LTSD/RT/10-4941/A, France.

[4] ICRP (1991), *1990 Recommendations of the International Commission on Radiological Protection*, ICRP Publication 60, Vol. 21 (1-3), Canada, https://doi.org/10.1007/bf00184120.

[5] ANS (1977), *American National Standard for Neutron and Gamma-Ray Flux-to-Dose-Rate Factors*, ANSI/ANS-6.1.1 (1977), American Nuclear Society, United States.

[6] ANS (1991), *American National Standard for Neutron and Gamma-Ray Flux-to-Dose-Rate Factors*, ANSI/ANS-6.1.1 (1991), American Nuclear Society, United Sates.

[7] Leger, V. and A. Dalesme (2020), *NTE-20-032401-001-1.0, OCDE/NEA Dose Rate Benchmark – ORANO TN Contribution to the Verification Step* (internal document), Orano TN, France.

CIEMAT contribution

15x15 UO_2 PWR FA

The isotopic vectors after the irradiation and decay can be seen in Table A.31 for the actinides and in Table A.32 for the fission products. Two different decay periods can be seen in these tables, 3.7 years and 30 years, corresponding to the moments when the dose rate has to be estimated according to the benchmark specifications. Also, according to specifications, both tables include the isotopes of the fuel only.

Table A.31. Isotopic composition of the 15x15 UO_2 PWR FA after irradiation and decay – Actinides

Isotope	Mass after 3.7-year decay (g)	Mass after 30-year decay (g)	Isotope	Mass after 3.7-year decay (g)	Mass after 30-year decay (g)
U-234	8.51E+01	9.75E+01	Pu-244	7.32E-03	
U-235	3.71E+03	3.71E+03	Am-241	1.13E+02	4.68E+02
U-236	1.80E+03	1.81E+03	Am-242	3.41E-06	2.99E-06
U-237	1.60E-05	4.49E-06	Am-242m	2.64E-01	2.32E-01
U-238	4.43E+05	4.43E+05	Am-243	4.44E+01	4.43E+01
Np-236	5.49E-04		Am-244	1.11E-16	1.47E-17
Np-236m	0.00E+00		Cm-242	2.05E-02	
Np-237	1.92E+02	2.05E+02	Cm-243	1.44E-01	
Np-238	4.94E-08		Cm-244	1.13E+01	4.09E+00
Np-239	3.82E-05		Cm-245	7.26E-01	7.25E-01
Pu-236	1.15E-06		Cm-246	5.93E-02	
Pu-237	1.29E-13		Cm-247	6.05E-04	
Pu-238	6.71E+01	5.45E+01	Cm-248	3.06E-05	
Pu-239	2.55E+03	2.55E+03	Bk-249	1.67E-08	
Pu-240	1.09E+03	1.09E+03	Cf-249	3.27E-07	
Pu-241	5.13E+02	1.44E+02	Cf-250	1.40E-07	
Pu-242	2.40E+02	2.40E+02	Cf-251	3.70E-08	3.63E-08
Pu-243	2.10E-14		Cf-252	7.11E-09	7.22E-12

The photon release for the FA is shown in Figure A.12 at the moment of the dose rate estimation. The total values are:

- $3.95 \cdot 10^{15}$ photons/s for the case of 3.7-year decay;
- $8.08 \cdot 10^{14}$ photons/s for the case of 30-year decay.

The dose rate at 1 m from the FA has been calculated by simulating a detector using a 5-cm radius sphere. The 1977 ANSI/ANS and the 1991 ANSI/ANS flux-to-dose rate conversion factors have been used for both decay periods to calculate the dose rate. The results are:

For the 1977 ANSI/ANS conversion factor, the dose rate is equal to 29.87 Sv/h after 3.7-year decay and 5.21 Sv/h after a 30-year decay.

For the 1991 ANSI/ANS conversion factor, the dose rate is equal to 24.04 Sv/h after 3.7-year decay and 4.17 Sv/h after a 30-year decay.

These results show that the 1977 ANSI/ANS flux-to-dose rate conversion factor provides a larger value of the dose rate because the energy range between 10^{-2} and 1 MeV includes larger conversion factors. This means that a more conservative result can be obtained using the 1991 ANSI/ANS flux-to-dose rate conversion factor when a proliferation resistance point of view is pursued. Results also show that both conversion factors verify the "self-protection" definition since all the calculated dose rates beat the limit of 1 Sv/h at 1 m from the FA.

Table A.32. Isotopic composition of the 15x15 UO_2 PWR FA after irradiation and decay – FPs

Isotope	Mass after 3.7-year decay (g)	Mass after 30-year decay (g)	Isotope	Mass after 3.7-year decay (g)	Mass after 30-year decay (g)
Sr-90		1.19E+02	Nd-145	3.12E+02	
Y-90		3.03E-02	Nd-148	1.70E+02	
Kr-83	2.04E+01		Pm-147	3.57E+01	
Rh-103	2.30E+02		Pm-148	5.79E-18	
Rh-105	0.00E+00		Pm-149	0.00E+00	
Ag-109	4.41E+01		Sm-147	8.68E+01	
I-135	0.00E+00		Sm-149	1.20E+00	
Xe-131	2.03E+02		Sm-150	1.09E+02	
Xe-135	0.00E+00		Sm-151	4.91E+00	
Cs-133	5.19E+02		Sm-152	4.92E+01	
Cs-134	1.71E+01		Sm-154		1.83E+01
Cs-135	1.45E+02		Eu-153	5.39E+01	5.39E+01
Cs-137	5.16E+02	2.81E+02	Eu-154	8.00E+00	9.59E-01
Ba-137m	7.86E-05	4.29E-05	Eu-155	2.13E+00	4.60E-02
Ba-140	1.60E-31		Eu-156	3.64E-27	
La-140	0.00E+00		Gd-155	1.54E+00	
Nd-143	3.68E+02				

Figure A.12. Photon release for the UO_2 assembly after decay – The integrated value is equal to $3.95 \cdot 10^{15}$ photons/s in the case of 3.7-year decay and $8.08 \cdot 10^{14}$ photons/s for 30-year decay

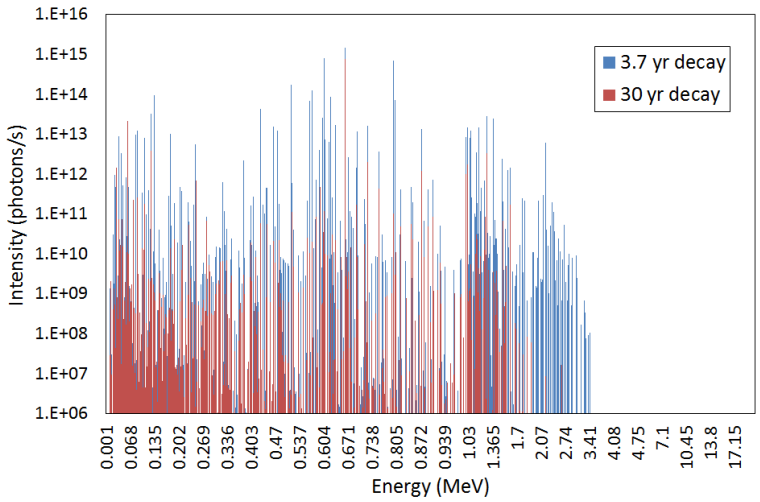

Source: Álvarez-Velarde, F. and A.V. Skarbeli, 2019.

17x17 MOX PWR FA

The isotopic vectors after the irradiation and decay for the 17x17 MOX PWR FA can be seen in Table A.33, after the 30-year decay. It has to be reminded that the isotopic composition has been taken from the specifications. Thus, only the differences coming from the radiation transport simulation are considered.

The photon release for the FA is shown in Figure A.13 at the moment of the dose rate estimation, having a total integrated value of $1.60 \cdot 10^{15}$ photons/s.

The dose rate at 1 m from the MOX PWR FA has been calculated simulating a detector again by means of a 5-cm radius sphere. Results for flux-to-dose rate conversion factors are shown in Table A.34. These results show that again the 1977 ANSI/ANS flux-to-dose

rate conversion factor provides a larger value of the dose rate for the same above-mentioned reason. This means that a more conservative result can be obtained using the 1991 ANSI/ANS flux-to-dose rate conversion factor when a proliferation resistance point of view is pursued. Results also show that for the MOX PWR FA both conversion factors verify the "self-protection" definition, since the values exceed the limit of 1 Sv/h at 1 m from the FA.

Figure A.13. Photon release for the MOX assembly after 30-year decay – The integrated value is equal to $1.60 \cdot 10^{15}$ photons/s

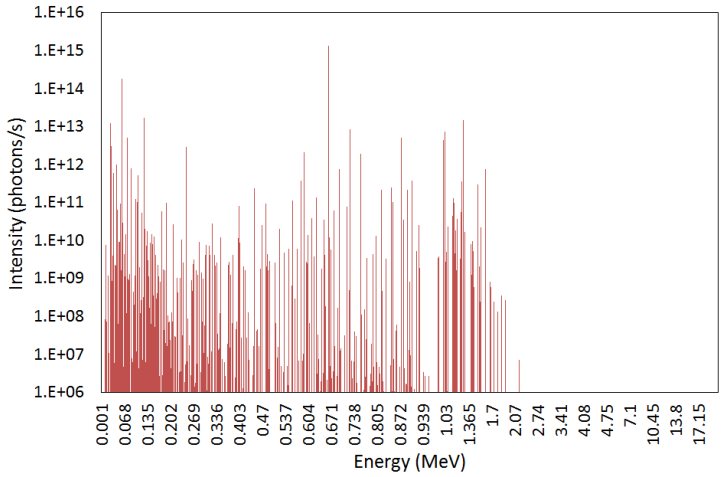

Source: Álvarez-Velarde, F. and A.V. Skarbeli, 2019.

Table A.33. Isotopic composition of the 17x17 MOX PWR FA after irradiation and decay

Isotope	Mass after 30-year decay (g)	Isotope	Mass after 30-year decay (g)
U-234	2.61E+02	Sr-90	9.74E+01
U-235	4.39E+02	Y-90	2.47E-02
U-236	1.59E+02	Cs-137	4.88E+02
U-237	3.41E-05	Ba-137	5.34E+02
U-238	3.96E+05	Ba-137m	7.43E-05
Np-237	2.17E+02	Sm-154	5.29E+01
Pu-238	9.09E+02	Eu-153	1.26E+02
Pu-239	9.42E+03	Eu-154	4.11E+00
Pu-240	8.68E+03	Eu-155	1.33E-01
Pu-241	1.09E+03		
Pu-242	3.64E+03		
Am-241	3.87E+03		
Am-242	1.54E-04		
Am-242m	1.20E+01		
Am-243	9.83E+02		
Am-244	3.97E-14		
Cm-244	2.18E+02		
Cm-245	9.35E+01		
Cf-251	3.66E-05		
Cf-252	5.01E-09		

Table A.34. MOX assembly dose rate after decay at 1 m

Conversion factor	Dose rate after 30-year decay (Sv/h)
1977	9.25
1991	7.41

Reference

[1] Álvarez-Velarde, F. and A.V. Skarbeli (2019), *Dose Rate Calculations Involving Irradiated PWR Fuel Assemblies: Verification and Validation Benchmark*, CIEMAT internal report DFN/IN-01/II-19, December 2019, Spain.

Appendix B. Sensitivity studies – Contributions

CIEMAT contribution

This work also includes a series of sensitivity analyses to evaluate the different hypotheses used in the calculations to obtain results as accurately as possible. These sensitivity analyses are described in the following:

- The reference depletion calculation included no radial or axial subdivision of the pin. To take into account possible distributions of photon-emitting isotopes after burn-up and decay, a pin subdivision (10 axial and 5 radial subdivisions) has been considered. Although a very similar average photon emission (spectrum and integrated value) has been found, the dose rate at 1 m shows an increase of approximately 10% for both conversion factors. This behaviour is a consequence of a redistribution of the photon-emitting isotopes. When the FA is divided into cells, the larger amount of fissions at the middle region of the assembly (due to a larger neutron flux in that area) makes them more concentrated there than in the reference scenario, where they are uniformly distributed in height. When the photon-emitting isotopes are more concentrated in the middle height, they are closer to the detector on average, so the probability of the emitted photons reaching the detector is larger.
- A simple irradiation history has been tested to check the impact of intermediate decay periods during irradiation. Using this irradiation history, the isotopic inventory shows some differences regarding the reference calculation, mainly for those isotopes being generated via decay from their radioactive parents, such as ^{241}Am, ^{242}Am, ^{242M}Am, ^{242}Cm and ^{243}Cm. This sensitivity calculation also provides a value of the photon emission 2% larger than the reference calculation, providing values of the dose rate of 2% larger for both conversion factors.
- A LINLIN interpolation factor for the flux-to-dose rate conversion factors has been considered. Different interpolation schemes for the flux-to-dose factors provide only a 1% difference in the final values of the dose rate, for both ANSI/ANS conversion factors [1,2].
- A set of calculations has been performed to study the impact of the statistics in the radiation transport calculation, by means of different detector sizes (spheres with radius of 1 cm, 2 cm, 5 cm -reference- and 10 cm, centred at 1 m of the FA at mid-plane). The different values of the dose rate obtained for different detector sizes vary within a relatively small range of 3% with no clear tendency. These differences are probably caused by the statistical uncertainty of the different Monte Carlo calculations.

CEA contribution

Different sensitivity studies were carried out by CEA to assess the impact of the calculation scheme on calculated EDRs. They have been focused on conversion factor impact, flux estimation impact, axial burn-up profile impact, particle source contributions and gamma source structure impact.

Conversion factors

Two conversion factor models were used for this study: one from the 1977 ANSI/ANS report [1] and the other from the 1991 ANSI/ANS report [2]. These factors were given as reference data for the benchmark. For TRIPOLI-4® calculations (CEA), an additional predefined response function H*(10) is used, based on ICRP-74 [3] recommendations. The ICRP-74 factors are between the ANS-77 ones and ANS-91 ones. Figure B.1 compares the different flux-to-dose conversion factors.

Figure B.1. Flux-to-dose conversion factors comparison

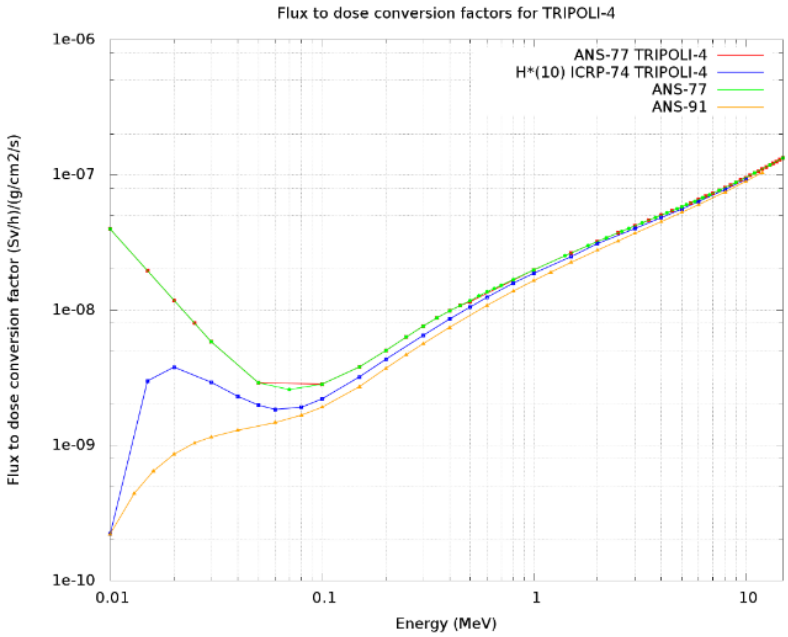

Source: NEA EGAFCS data, 2020.

Moreover, different interpolation schemes were tested to assess the impact of the conversion function representation on the equivalent dose rate. The interpolation schemes in energy E for the conversion factor C are: NO_INTERPOLATION, LINEAR in E LINEAR in C, LINEAR in E LOGARITHMIC in C, LOGARITHMIC in E LINEAR in C, and LOGARITHMIC in E LOGARITHMIC in C.

TRIPOLI-4® uses predefined conversion factors, so-called ANS_77 and H*(10). These conversion factors are based on functional expressions:

- ANS_77: polynomial interpolation of log(C):

$$C = e^{a \times E^3 + b \times E^2 + c \times E + d}$$

- H*(10): cubic Lagrange interpolation.

In Tables B.1 and B.2 for UOX and 30 years cooling time, the reference ANS-77 and ICRP-74 calculations were obtained with these predefined conversion functions and with tabulated values. Interpolation scheme results are obtained for the reference tabulated data provided for the benchmark.

Table B.1. ANS-77 reference results compared to ANS-77 results with different interpolation types

Conversion factor	Sv/h	St. dev. (%)	Difference
ANS-77	5.106	0.19	
ANS-77 IN_NO_INTERPOLATION	4.915	0.21	**-3.74%**
ANS-77 IN_LIN_LIN	5.091	0.19	-0.29%
ANS-77 IN_LIN_LOG	5.106	0.19	0.00%
ANS-77 IN_LOG_LIN	5.084	0.18	-0.43%
ANS-77 IN_LOG_LOG	5.121	0.21	0.29%

Table B.2. ICRP-74 reference results compared to ANS-91 with different interpolation types

Conversion factor	Sv/h	St. dev. (%)	Difference
ICRP-74	4.670	0.20	
ANS-91 IN_NO_INTERPOLATION	3.473	0.18	**-25.63%**
ANS-91 IN_LIN_LIN	4.067	0.21	-12.91%
ANS-91 IN_LIN_LOG	4.099	0.20	-12.23%
ANS-91 IN_LOG_LIN	4.019	0.20	-13.94%
ANS-91 IN_LOG_LOG	4.076	0.21	-12.72%

The results show that the ANS-77 predefined TRIPOLI-4® conversion factors are consistent with the ANS-77 ones given as benchmark data whereas a difference remains between ANS-91 benchmark data and the predefined H*(10) in TRIPOLI-4®. The other conclusion is that ANS-77 provides the highest results, ICRP-74 provides intermediate results (about -9% with ANS-77) and ANS-91 provides the lowest results (about -20%). Finally, the LINEAR in E LINEAR in C interpolation scheme provides accurate enough results for this benchmark.

Flux estimation

Another important issue in the Monte Carlo calculation is the flux estimator that is used. The participants of the benchmark used very different estimators for the estimator type (track length, surface, point), for the detector geometry (box, ring) and for the size of the detector.

In this section, TRIPOLI-4® was used to assess the impact of the different options. Four configurations were tested:

- a point estimation at (110.7, 0, 0) for UOX or (110.86, 0, 0) for MOX;
- a track-length estimation for a 10 cm x 10 cm x 10 cm box whose centre is located at (110.7, 0, 0) for UOX or (110.86, 0, 0) for MOX;
- a track-length estimation for a 1 cm x 100 cm x 200 cm large box whose centre is located at (110.7, 0, 0) for UOX or (110.86, 0, 0) for MOX;
- a surface estimator with a ring at X=0 plane with 10 cm height or 2 cm height, which inner radius is 110.7 cm for UOX and 110.86 cm for MOX.

Figure B.2. Tally volumes and surfaces for Monte Carlo estimators in the benchmark geometry

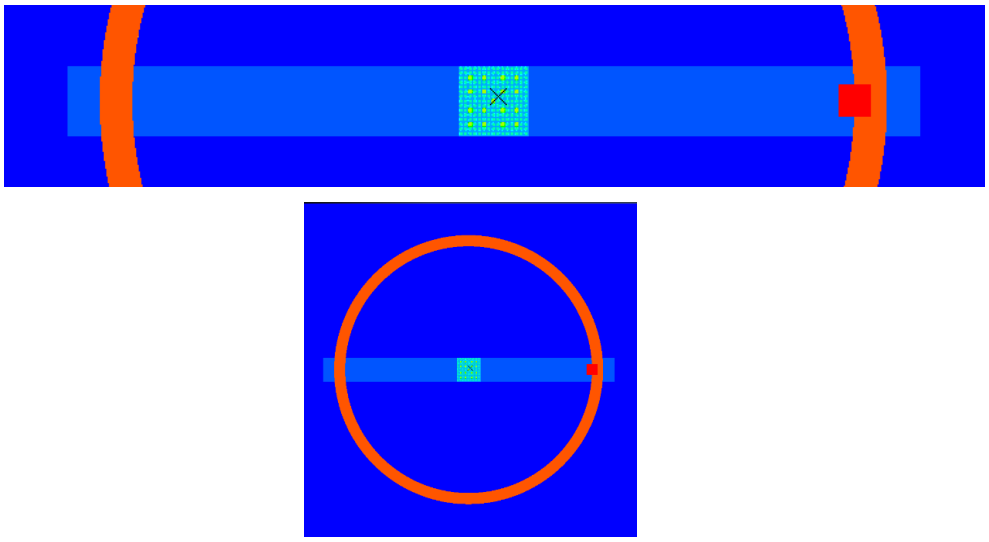

Source: NEA EGAFCS data, 2020.

Calculations were performed both for ANS-77 and ICRP-74 conversion factors and for UOX and MOX fuels.

Table B.3. ANS-77 conversion factors dose rate with different flux estimators

UOX	Sv/h	St. Dev. (%)	Difference	MOX	Sv/h	St. Dev. (%)	Difference
Point	5.116	0.01		Point	9.411	0.01	
Surface 10 cm	6.158	0.03	20.37%	Surface 10 cm	11.18	0.03	18.80%
Surface 2 cm	6.229	0.06	**21.76%**	Surface 2 cm	11.31	0.07	**20.18%**
Volume 10 cm	5.133	0.22	0.33%	Volume 10 cm	9.494	0.25	0.88%
Volume large	5.405	0.02	**5.65%**	Volume large	9.893	0.02	**5.12%**

Table B.4. ICRP-74 conversion factors dose rate with different flux estimators

UOX	Sv/h	St. Dev. (%)	Difference	MOX	Sv/h	St. Dev. (%)	Difference
Point	4.669	0.01		Point	8.604	0.01	
Surface 10 cm	5.628	0.03	18.80%	Surface 10 cm	10.23	0.03	18.90%
Surface 2 cm	5.693	0.06	**20.18%**	Surface 2 cm	10.35	0.07	**20.29%**
Volume 10 cm	4.683	0.22	0.88%	Volume 10 cm	8.678	0.25	0.86%
Volume large	4.938	0.02	**5.12%**	Volume large	9.052	0.02	**5.21%**

The results show that the detector behaviour does not depend on the conversion factors. For the ring detector and the surface estimator, one can notice a 20% difference compared to the reference point estimator value whatever the size of the ring is. The large volume also induces a discrepancy, less important in magnitude by approximately 5%.

The ring differences can be explained by the mean distance of the ring to the side of the assembly. For points close to the corners of the ring, the distance to the assembly is lower than at the point estimation. A point-by-point dose rate estimation is shown in Figure B.3 and proves that globally the dose rate is higher when the point reaches the corner of the assembly. The 0° point is the point at X=110.7 cm.

It should be noted here that the results are a little different from the reference calculations for the gamma contribution. The difference cannot be explained by the statistical uncertainties only. This origin of the difference is probably the TRIPOLI-4® versions that

were used in the two calculations: TRIPOLI-4.10® in the current paragraph versus TRIPOLI-4.9® in the other analyses.

Figure B.3. Dose rate angular distribution at 110.7 cm far from the centre of the assembly

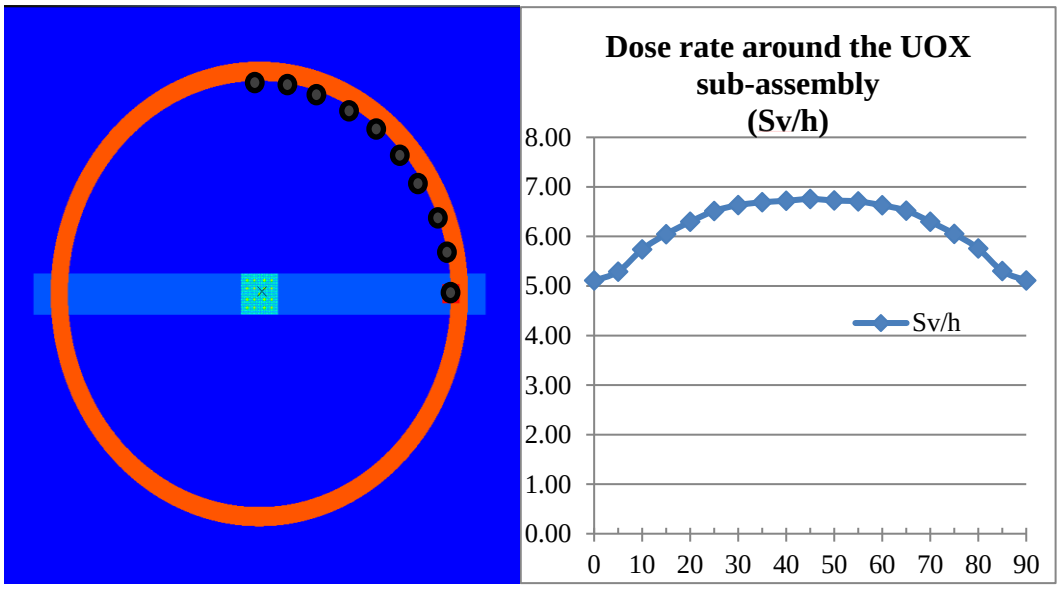

Source: NEA EGAFCS data, 2020.

Burn-up axial profile

The burn-up axial profile comes from the reference study performed on UOX PWR assemblies. Calculations were performed with gamma contribution only.

Table B.5. Relative gamma source intensity axial profile

min (cm)	max (cm)		> 30 GWd/t	< 30 GWd/t
0	11		0.52	0.49
11	22		0.79	0.79
22	33		0.96	0.95
33	45		1.04	1.07
45	73		1.05	1.08
73	268		1.089	1.116
268	303		1.05	1.03
303	324		1.01	0.98
324	343		0.83	0.74
343	354		0.66	0.55
354	365.76		0.48	0.33

Figure B.4. UOX reference burn-up axial profile in assembly

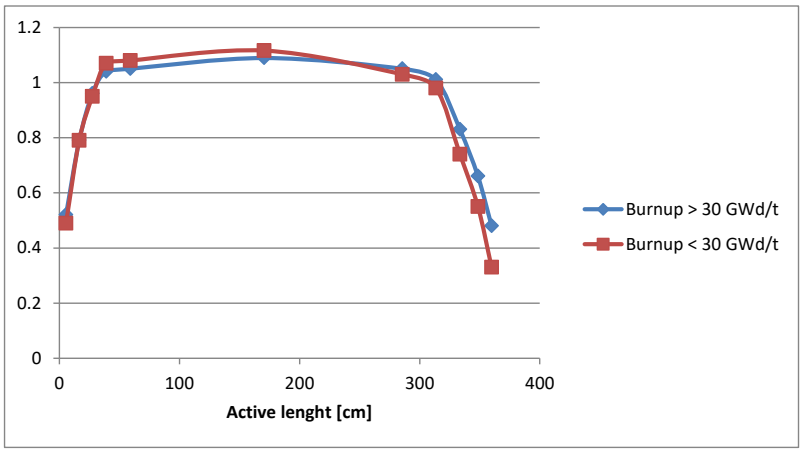

Source: NEA EGAFCS data, 2020.

The equivalent dose rates are provided in Sv/h (statistical uncertainties are provided between brackets):

Table B.6. Burn-up axial profile impact on dose rate for UOX assembly

Gamma source	UOX 33 GWd/MTIHM 30 years	UOX 33 GWd/MTIHM 3.7 years	MOX 60 GWd/MTIHM 30 years
Non uniform 19 groups	4.925 (0.06%)	32.26 (0.06%)	9.374 (0.08%)
Uniform 19 groups	4.646 (0.05%)	30.46 (0.05%)	8.550 (0.05%)
Difference (%)	+6%	+6%	+10%

The burn-up axial profile impact is positive and varies from 6% to 10%.

Beta and neutron contributions

The main contribution to the equivalent dose rate is the gamma contribution. Nevertheless, neutron and X-rays produced through the bremsstrahlung process by beta particles also contribute to the total dose rate.

The beta particle contribution is assessed by performing an electromagnetic shower calculation where electrons, positrons and photons are transported. The calculation source is the beta particle source (electron source) provided by the DARWIN-2.3 depletion-activation code package.

The equivalent dose rates are provided in Sv/h (statistical uncertainties are provided between brackets):

Table B.7. Relative source particle contribution to total dose rate

Particle source contribution (Sv/h)	UOX 33 GWd/MTIHM 30 years	MOX 60 GWd/MTIHM 30 years
Neutron	0.00024 (0.13%)	0.012 (0.07%)
Neutron fraction	0.005%	0.14%
Beta	0.135 (3.4%)	0.111 (3.4%)
Beta fraction	2.8%	1.3%
Gamma	4.620 (0.05%)	8.519 (0.05%)
Gamma fraction	97.2%	98.6%

It should be noted that results differ slightly from the reference calculations for the gamma contribution presented in Table 2.19. The difference cannot be explained by the statistical uncertainties only. The origin of the difference is probably the TRIPOLI-4® versions that were used in the two calculations: TRIPOLI-4.7® in the current paragraph versus TRIPOLI-4.9® in the other analyses.

The neutron contribution is negligible. The beta emissions contribute a few % to the total dose rate. The main contribution is the gamma one.

Gamma source group structure

Activation computational tools provide the gamma source. Generally, the source is given on an energy mesh that the user can specify. In DARWIN-2, a default 19-group energy mesh is used. The intensity in a group can be calculated either considering that it is the number of gammas whose ray is in the group or considering that it is an equivalent number of gamma for which the total energy is consistent with the total energy delivered in the group. Either way, this leads to some assumptions about gamma production.

To assess the impact of this parameter on the calculations, three different source representations have been tested with DARWIN-2.3:

- the standard 19-group structure;
- the 315-group structure;
- the ray-by-ray source.

The calculations were performed with gamma contribution only and with the H*(10) ICRP-74 conversion factors.

Table B.8. Gamma source energetic structure impact on dose rate

Source structure	UOX 30 years	UOX 3.7 years	MOX 30 years
19 groups	4.646 (0.06%)	30.46 (0.05%)	8.550 (0.06%)
315 groups	5.021 (0.06%)	25.97 (0.07%)	9.160 (0.05%)
19 127 rays	5.117 (0.05%)	26.33 (0.04%)	9.339 (0.04%)
19 127 rays/19 groups	1.10	0.86	1.09

The dose rates are about 10% different when using ray-by-ray structure for 30 years old fuels.

References

[1] ANS (1977), *American National Standard for Neutron and Gamma-Ray Flux-to-Dose-Rate Factors*, ANSI/ANS-6.1.1 (1977), American Nuclear Society, United States.

[2] ANS (1991), *American National Standard for Neutron and Gamma-Ray Flux-to-Dose-Rate Factors*, ANSI/ANS-6.1.1 (1991), American Nuclear Society, United States.

[3] ICRP (1996), *Conversion Coefficients for use in Radiological Protection against External Radiation*, ICRP Publication 74, Canada, https://doi.org/10.1016/S0146-6453(96)90001-9.